Nucleotide analogs as rigid spin labels for DNA and RNA

Dissertation zur Erlangung des wissenschaftlichen Doktorgrades der
Julius-Maximilians-Universität Würzburg

vorgelegt von

Aaron Siewert

aus Gronau (Leine)

Würzburg 2021

Eingereicht bei der Fakultät für Chemie und Pharmazie am

23.08.2021
_____

Gutachter der schriftlichen Arbeit

1. Gutachter: Prof. Dr. Claudia Höbartner

2. Gutachter: Jun.-Prof. Dr. Ann-Christin Pöppler

Prüfer des öffentlichen Promotionskolloquiums

1. Prüfer: Prof. Dr. Claudia Höbartner

2. Prüfer: Jun.-Prof. Dr. Ann-Christin Pöppler

3. Prüfer: Prof. Dr. Holger Helten

Datum des öffentlichen Promotionskolloquiums

18.10.2021
_____

Doktorurkunde ausgehändigt am

_____

Die vorliegende Arbeit wurde unter Anleitung von Prof. Dr. Claudia Höbartner in der Zeit vom Juli 2016 bis Juli 2017 am Institut für Organische und Biomolekulare Chemie der Georg-August-Universität Göttingen und vom August 2017 bis August 2021 am Institut für Organische Chemie der Julius-Maximilians-Universität Würzburg angefertigt.

Acknowledgements

First of all I would like to thank my supervisor, Prof. Dr. Claudia Höbartner, for providing me with the opportunity to work in an interesting field of research, on a challenging subject and for supporting me from the beginning all the way to the end.

Furthermore, I would like to thank Jun.-Prof. Dr. Ann-Christin Pöppler for taking the time to review my thesis.

I am also very grateful to Dr. Ivo Krummenacher from the group of Prof. Dr. Holger Braunschweig for performing the EPR measurements and simulations.

The analytics departments of the universities of Göttingen and Würzburg deserve credit for their services regarding the characterization of compounds by NMR and MS.

All the students who decided to contribute to the project by doing an internship or their bachelor thesis under my supervision should also not go unmentioned. Though many of them where only in our lab for a short time, they nonetheless did a lot of synthetic work which took some of the workload off my shoulders.

Many thanks to my colleagues from the lab, for providing an enjoyable atmosphere to work in and introducing me to techniques which go beyond what chemistry students usually encounter. I can look back on many fruitful discussions, funny moments and enjoyable activities during my time in the lab. Special thanks to Julia, Florian and Carina for proofreading my thesis and providing many helpful comments.

Finally, I would like to thank my parents, without whom I would not be where I am today. Their decision to send me to high school in spite of the costs involved and their continued support during my time as a student is what allowed me to come this far.

List of publications

1. T. P. Hoernes, K. Faserl, M. A. Juen, J. Kremser, C. Gasser, E. Fuchs, X. Shi, A. Siewert, H. Lindner, C. Kreutz, R. Micura, S. Joseph, C. Höbartner, E. Westhof, A. Hüttenhofer, M. D. Erlacher, *Nat. Commun.* **2018**, *9*, 4865-4877.

2. G. Kokic, H. S. Hillen, D. Tegunov, C. Dienemann, F. Seitz, J. Schmitzova, L. Farnung, A. Siewert, C. Höbartner, P. Cramer, *Nat. Commun.* **2021**, *12*, 279-286.

Table of contents

Abstract

Nucleic acids are one of the important classes of biomolecules together with carbohydrates, proteins and lipids. Both deoxyribonucleic acid (DNA) and ribonucleic acid (RNA) are most well known for their respective roles in the storage and expression of genetic information.

Over the course of the last decades, nucleic acids with a variety of other functions have been discovered in biological organisms or created artificially. Examples of these functional nucleic acids are riboswitches, aptamers and ribozymes. In order to gain information regarding their function, several analytical methods can be used.

Electron paramagnetic resonance (EPR) spectroscopy is one of several techniques which can be used to study nucleic acid structure and dynamics. However, EPR spectroscopy requires unpaired electrons and because nucleic acids themselves are not paramagnetic, the incorporation of spin labels which carry a radical is necessary.

Here, three new spin labels for the analysis of nucleic acids by EPR spectroscopy are presented. All of them share two important design features. First, the paramagnetic center is located at a nitroxide, flanked by ethyl groups to prevent nitroxide degradation, for example during solid phase synthesis. Furthermore, they were designed with rigidity as an important quality, in order to be useful for applications like pulsed electron double resonance (PELDOR) spectroscopy, where independent motion of the spin labels relative to the macromolecule has a noticeable negative effect on the precision of the measurements.

Benzi-spin (**1**) is a spin label which differs from most previous examples of rigid spin labels in that rather than being based on a canonical nucleoside, with a specific base pairing partner, it is supposed to be a universal nucleoside which is sufficiently rigid for EPR measurements when placed opposite to a number of different nucleosides. Benzi-spin was successfully incorporated into a 20 nt oligonucleotide and its base pairing behavior with seven different nucleosides was examined by UV/VIS thermal denaturation and continuous wave (CW) EPR experiments. The results show only minor differences between the different nucleosides, thus confirming the ability of benzi-spin to act as a universally applicable spin label.

Lumi-spin (**2**) is derived from lumichrome. It features a rigid scaffold, as well as a free 2'-hydroxy group, which should make it well suited for PELDOR experiments once it is incorporated into RNA oligonucleotides.

EÇr (**3**) is based on the Ç family of spin labels, which contains the most well known rigid spin labels for nucleic acids to this day. It is essentially a version of EÇm with a free 2'-hydroxy group. It was converted to triphosphate EÇrTP (**55**) and used for primer extension experiments to test the viability of enzymatic incorporation of rigid spin labels into oligonucleotides as an alternative to solid-phase synthesis. Incorporation into DNA by Therminator III DNA polymerase in both single-nucleotide and full-length primer extensions was achieved.

All three of these spin labels represent further additions to the expanding toolbox of EPR spectroscopy on nucleic acids and might prove valuable for future research.

Zusammenfassung

Nukleinsäuren sind neben den Kohlenhydraten, Proteinen und Lipiden eine der wichtigen Klassen von Biomolekülen. Sowohl Deoxyribonukleinsäure (DNA) und Ribonukleinsäure (RNA) sind am besten für ihre Funktionen bei der Speicherung und Expression der genetischen Informationen bekannt.

Während der letzten Jahrzehnte wurden Nukleinsäuren mit einer Vielzahl von Funktionen in biologischen Organismen entdeckt oder künstlich hergestellt. Beispiele für diese funktionellen Nukleinsäuren sind Riboswitches, Aptamere und Ribozyme. Um Informationen über ihre Funktionsweisen zu erhalten, können verschiedene analytische Methoden verwendet werden.

Elektronenspinresonanzspektroscopie (ESR) ist eine Analysetechnik, die Aufschluss über Struktur und Dynamik von Nukleinsäuren geben kann. Für ESR Messungen werden ungepaarte Elektronen benötigt, sodass nicht paramagnetische Verbindungen mit einem Spinmarker modifiziert werden müssen, der ein Radikal trägt.

In dieser Arbeit werden drei neue Spinmarker für die ESR Analyse von Nukleinsäuren vorgestellt. Allen liegen zwei Designprinzipien zugrunde. Erstens wird als paramagnetische Verbindung ein Nitroxid verwendet, welches von Ethylgruppen flankiert wird um das Radikal zu stabilisieren, zum Beispiel gegen Reagenzien, die in der Festphasensynthese verwendet werden. Zweitens sind die Nitroxide Teil starrer Ringsysteme. Dies ist besonders wichtig für Anwendungen wie Abstandsmessungen mittels Pulselektronendoppelresonanzspektroskopie (PELDOR), wo die Genauigkeit der Messung von Bewegungen der Spinmarker relativ zum Makromolekül beeinträchtigt wird.

Benzi-spin (**1**) unterscheidet sich von vielen anderen starren Spinmarkern dadurch, dass es nicht auf einem kanonischen Nukleosid mit einem spezifischen Bindungspartner basiert. Stattdessen handelt es sich um ein universelles Nukleosid, das unabhängig vom gegenüberliegenden Nukleosid starr genug für ESR Messungen ist. Benzi-spin wurde erfolgreich in ein Oligonucleotid eingebaut und seine Basenpaarung mit sieben verschiedenen Nukleosiden mittels UV/VIS Schmelzkurven und Continuous Wave (CW) ESR Experimenten untersucht. Die Ergebnisse zeigen nur geringe Unterschiede zwischen den verschiedenen Nukleosiden, was die Einsetzbarkeit von Benzi-spin als universeller Spinmarker bestätigt.

Lumi-spin (**2**) ist vom Lumichrom abgeleitet. Es zeichnet sich durch ein starres Gerüst und eine freie 2'-Hydroxygruppe aus, wodurch es gut für PELDOR Messungen in RNA geeignet sein sollte.

EÇr (**3**) gehört zur Ç Familie, welche die am besten bekannten starren Spinmarker für Nukleinsäuren enthält. Es handelt sich um eine Version von EÇm mit einer freien 2'-Hydroxygruppe. EÇr wurde zum Triphosphat EÇrTP (**55**) konvertiert und für Primer Extension Experimente verwendet um die Möglichkeit des enzymatischen Einbaus starrer Spinmarker in Oligonukleotide als Alternative zur Festphasensynthese zu prüfen. Der Einbau in DNA mit Therminator III DNA Polymerase in Primer Extensions war erfolgreich.

Alle drei Spinmarker erweitern die Möglichkeiten der ESR-spektroskopischen Untersuchung von Nukleinsäuren und können sich für zukünftige Forschung als nützlich erweisen.

1 Introduction

1.1 Nucleic acids

Nucleic acids are an essential part of living organisms. Their genetic information is stored in the deoxyribonucleic acid (DNA). In order for the genetic information to be expressed into proteins, ribonucleic acid (RNA) is required to fulfill several important roles. A template of DNA, which contains the necessary information for the desired protein, is first transcribed into messenger RNA (mRNA). The mRNA is then translated into the protein by the ribosome, which is made of both proteins and ribosomal RNA (rRNA). This requires transfer RNA (tRNA), which is used for delivering specific amino acids to the ribosome, where they are incorporated into the protein.

In addition to these well known examples, nucleic acids can also fulfill other functions, like binding of certain molecules or catalysis of chemical reactions. The following chapters will provide an introduction to three classes of functional nucleic acids, namely riboswitches, aptamers and ribozymes.

1.2 Functional nucleic acids

1.2.1 Riboswitches

Riboswitches are a class of functional nucleic acids first discovered in the year 2002[1-4], which perform a regulatory function, mostly in bacteria. Most riboswitches act in one of two different ways, by aborting transcription or preventing translation (Fig. 1). In the first case, the riboswitch is transcribed ahead of the part of the gene which codes for the protein and can, as a response to an outside stimulus, adopt a terminator structure which inhibits the RNA polymerase, causing transcription to end (Fig. 1A). In the second case, the riboswitch can, again in response to a certain stimulus, adopt a conformation called sequestrator, which makes the Shine-Dalgarno sequence, the binding site of the ribosome, inaccessible, thus preventing the ribosome from binding to the mRNA for translation (Fig. 1B).
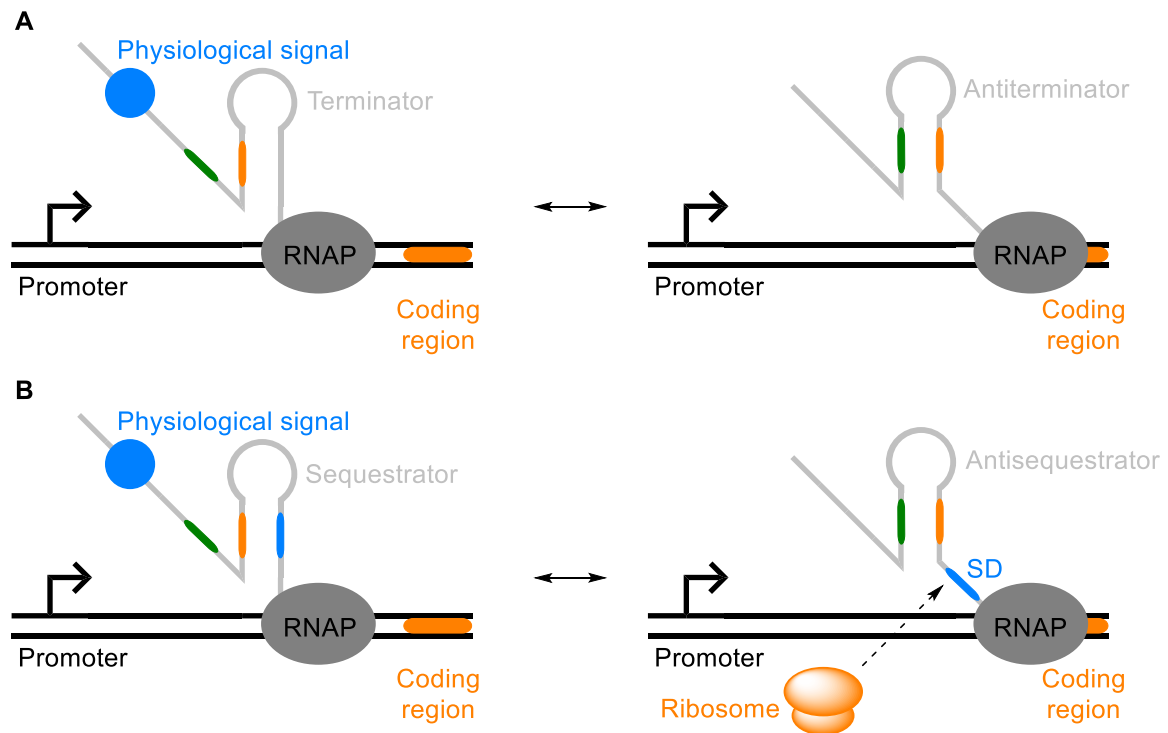
Fig. 1: Regulation of gene expression by riboswitches by transcription attenuation (A) and translation initiation (B). (A) The physiological signal causes a terminator structure to form, which prevents the RNA polymerase (RNAP) from continuing transcription (left). In absence of the physiological signal, an antiterminator structure is formed and the transcription can proceed (right). (B) The physiological signal causes a sequestrator structure to form which prevents the ribosome from binding to the Shine-Dalgarno (SD) sequence (left). In absence of the physiological signal, an antisequestrator structure is formed, the ribosome can bind to the SD-sequence and the translation can take place (right). The figure was reproduced based on [5].

To perform their function, riboswitches need two parts, one for recognition of the stimulus triggering the structural change and one for interfering with the gene expression, called the expression platform[5, 6]. As far as the stimuli are concerned, there are different factors which can trigger the structural change of the riboswitches, but most riboswitches are triggered by binding of a target molecule. There is a wide range of substrates for riboswitches, but the majority of riboswitches identified to date are triggered by small molecules, usually the products of synthetic pathways. The riboswitches prevent overproduction of these molecules by downregulation of the expression of proteins involved in their synthesis. There are about 40 classes of riboswitches[7], which target many different substances.

With riboswitches performing important functions in living organisms, it was seen as desirable to also use them for various other applications, which requires engineering[8], for example by adapting the recognition domain of a riboswitch to recognize a different compound than the original. Hereby it was possible to create artificial riboswitches that recognize different non-natural molecules[9]. Another approach is to engineer the expression platform, which was done to generate a riboswitch which can regulate gene expression in vivo based on the presence or absence of theophylline[10].

1.2.2 Aptamers

Aptamers are short oligonucleotides which can bind a specific target by folding into a certain tertiary structure. Most aptamers are generated by a process called systematic evolution of ligands by exponential enrichment (SELEX)[11]. A library of oligonucleotides containing a region of random nucleotides is incubated with the target, non-binding oligonucleotides are removed and binding oligonucleotides amplified by PCR. This process has to be repeated multiple times and thus requires a lot of time and effort, so improvements are desirable. Recently, an automated version of this process was developed, which can perform the selection without manual interference[12]. Aptamers hold great promise for therapeutic uses, as they perform a similar function as antibodies, while offering several advantages like faster preparation, larger scope of possible targets and modifiability[13]. The first aptamer, pegaptanib, has been approved for use against ocular vascular disease in the United States in 2004[14]. Some clinical aptamers can have a direct therapeutic effect but most are used as drug transporters or recognition units to deliver drugs to cells where they are needed[15].

Another important class are fluorogenic aptamers. These can bind a chromophore which will then become fluorescent upon being bound while showing little to no fluorescence when being in solution, which is useful for fluorescence imaging of RNA in cells. In most cases the fluorescence turn-on is achieved by rigidification of the chromophore by the aptamer, which prevents the relaxation of the excited chromophore by conformational changes or vibrations[16]. Early examples of aptamers selected for binding of chromophores go back to the 1990s[17, 18], with the crystal structure of the malachite green (Fig. 2) aptamer being successfully solved in the year 2000[19], which enabled the first insights into how the fluorescence activation by aptamers works. One prominent recent example for fluorogenic aptamers is the Mango family, of which there are four members, numbered I-IV. Mango I was the result of in vitro selection against the thiazole orange-derived dye TO1-Biotin[20] (Fig. 2). The pool from the selection was later subjected to a microfluidics-based selection, which resulted in the other three Mango aptamers[21]. Another important example of fluorogenic aptamers are those which bind various derivatives of 4-hydroxybenzylidene imidazolone (HBI) (Fig. 2), which is the chromophore used by the green fluorescent protein (GFP). The first example of these is the Spinach aptamer, which was selected for binding DFHBI, a difluorinated derivative of HBI[22]. More examples of aptamers which bind HBI derivatives were developed since then[23], including Chili, which got its name because of its ability to generate fluorescence of different colors with different fluorophores, which are derivatives of 3,5-dimethoxy-4-hydroxybenzylidene imidazolone (DMHBI) (Fig. 2)[24, 25].
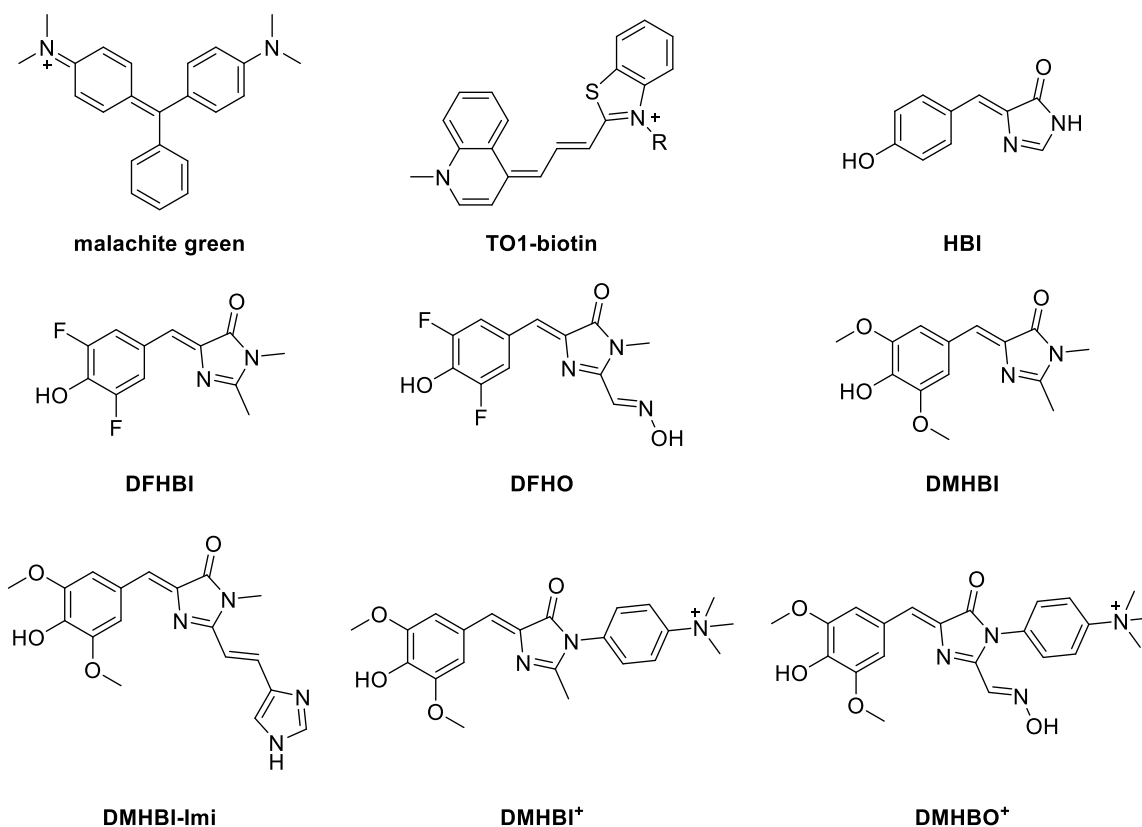
Fig. 2: Fluorescent dyes bound and activated by different fluorogenic aptamers. R = 3PEG-biotin.

1.2.3 Ribozymes and deoxyribozymes

For a long time it was thought that only proteins are responsible for catalyzing reactions in living organisms. However, during the 1980s the first examples of catalytically active RNA were discovered[26, 27]. The class of catalytic RNAs was named ribozymes. There are also catalytically active DNA sequences, which are called deoxyribozymes (DNAzymes), but they are so far purely artificial[28]. In nature, the scope of reactions catalyzed by ribozymes is fairly limited. One example is the synthesis of peptide bonds by the ribosome. It was discovered in the year 2000 that, while the ribosome contains proteins, the peptide bond formation during protein biosynthesis is actually catalyzed by the ribosomal RNA which makes it an example of a ribozyme[29, 30]. Besides the ribosome, natural ribozymes usually catalyze either RNA cleavage, like the small self-cleaving ribozymes[31-33], or ligation[34, 35]. Figure 3 illustrates different catalytic strategies for RNA cleavage employed by ribozymes.
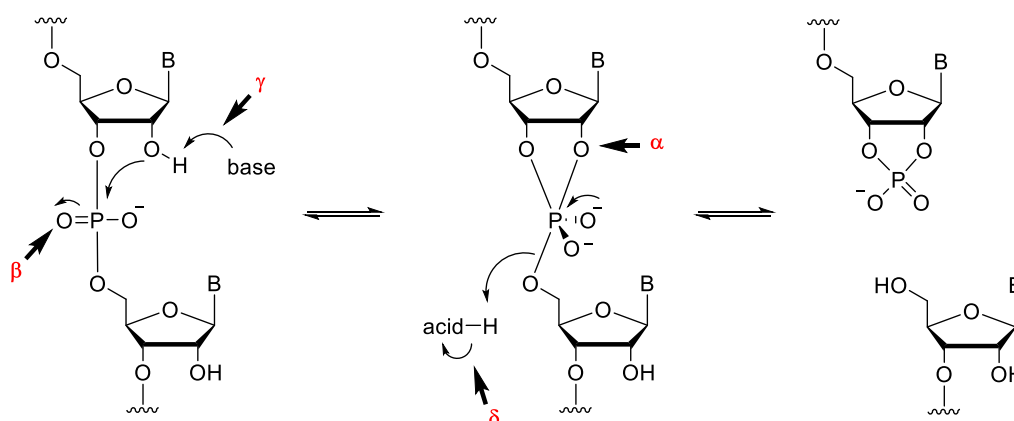
Fig. 3: RNA cleavage catalyzed by small self-cleaving ribozymes resulting in a cyclic 2'-3'-phosphate. Greek letters correspond to different catalytic strategies: α = in-line nucleophilic attack, β = neutralization of the phosphate, γ = deprotonation of 2'-OH, δ = protonation of 5'-oxygen. B = nucleobase. The figure was reproduced based on [36].

When it comes to RNA-cleaving DNAzymes, many examples can be brought up, the earliest one being reported in 1994[37]. Early DNAzymes were incapable of cleaving targets made up entirely of RNA, instead using a single ribonucleotide in a DNA sequence. Further in vitro selection experiments resulted in the 8-17 and 10-23 deoxyribozymes which can cleave RNA substrates[38]. Recently, DNAzymes which can discriminate for or against the modified nucleosides N^6-methyladenosine (m^{6}A)[39] and N^6-isopentenyladenosine (i^{6}A)[40], have been developed.

In addition to cleavage, ligation of nucleic acids is another important reaction catalyzed by ribozymes and DNAzymes. A well-known DNAzyme for RNA ligation is 9DB1[41]. Labeling of RNA by ligation is another goal which can be achieved, by attaching a 5'-triphosphate to a 2'-OH group. The deoxyribozyme 10DM24 was used for this purpose[42].
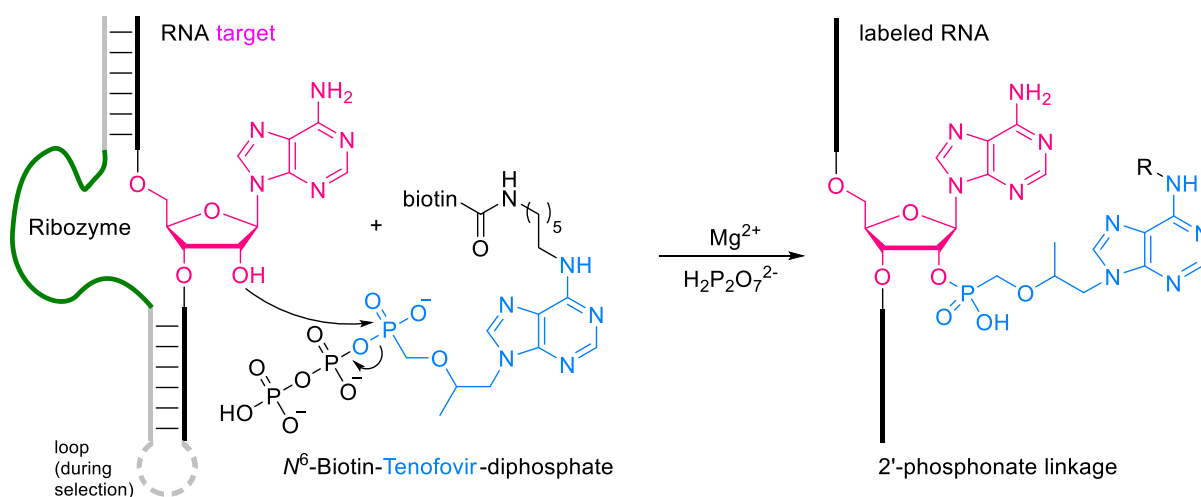

Fig. 4: Labeling of RNA by ribozyme-catalyzed nucleophilic attack of a 2'-OH group on a biotin-labeled Tenofovir derivative forming a phosphonate ester linkage. The figure was reproduced based on [43].

5

Recently, ribozymes for RNA labeling were generated from in vitro selection which are capable of attaching small molecules derived from the antiviral drug Tenofovir at specific positions of an RNA strand[43] (Fig. 4), as well as others which attach N^6-modified ATP derivatives[44].

1.2.4 Structure determination

All classes of functional nucleic acids presented above depend on their ability to fold into specific three-dimensional structures to carry out their functions. In order to understand the mechanisms by which they work or to make improvements to them by engineering it is helpful to determine the structures they adopt. One method for this is x-ray crystallography. Obtaining a crystal structure is often a highly desired goal, as it allows for fairly precise determination of each atom's position. Another advantage of x-ray crystallography is that modifications of the nucleic acid to be investigated are not necessary. Crystallization of nucleic acids can be challenging and time-consuming, so in some cases no crystal structure could be obtained so far. Also, for ribozymes, often only crystals of the post-catalytic state can be obtained. For fluorogenic aptamers, as mentioned above, the crystal structure of the malachite green aptamer[19] was the first to be solved. More followed later, like the different versions of Mango[45, 46], Spinach[47] and Corn (Fig. 5)[48].
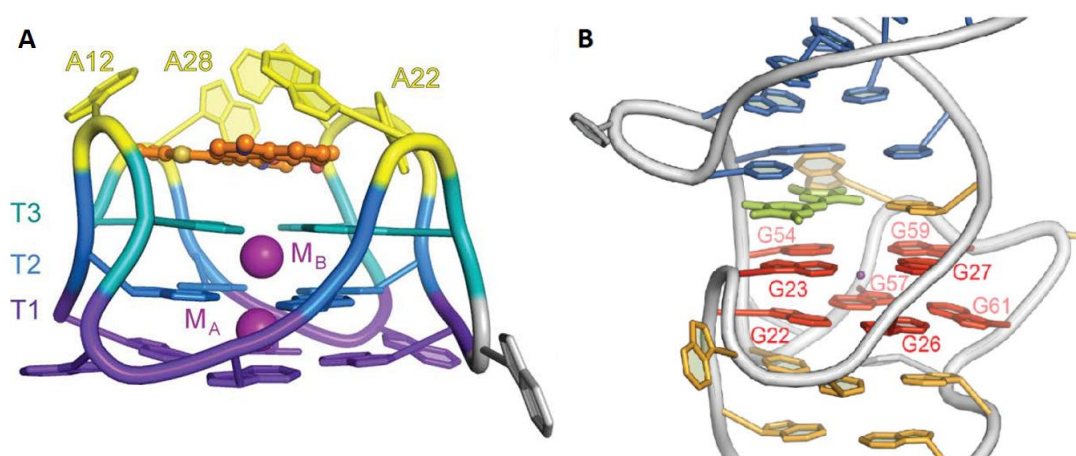
Fig. 5: Crystal structures of the binding pockets of (A) Mango-II with TO1-biotin (orange) and (B) Spinach with DFHBI (green). T1-3 are different tiers of the Mango-II G-quadruplex, the Spinach G-quadruplex is marked in red. Purple spheres represent potassium ions in both structures. The figures were taken from [45] and [47].

These structures reveal the presence of a guanine quadruplex which plays a significant role in binding and fluorescence activation. Thus, the G-quadruplex seems to be a structure which is advantageous for this purpose, possibly because their stable planar structure is well suited for restricting the conformation of the chromophores[23].

Many crystal structures of ribozymes and DNAzymes could also be obtained. One recent example is the structure of the RNA-ligating deoxyribozyme 9DBI, published in 2016[49]. It was crystallized in the post-catalytic state with the product RNA still in complex with the catalyst (Fig. 6).

Fig. 6: Visual representation of the deoxyribozyme 9DB1 (blue) in complex with a ligated RNA product (orange) in the post-catalytic state. The brown sphere on the RNA marks the ligation site. The figure was taken from [50].
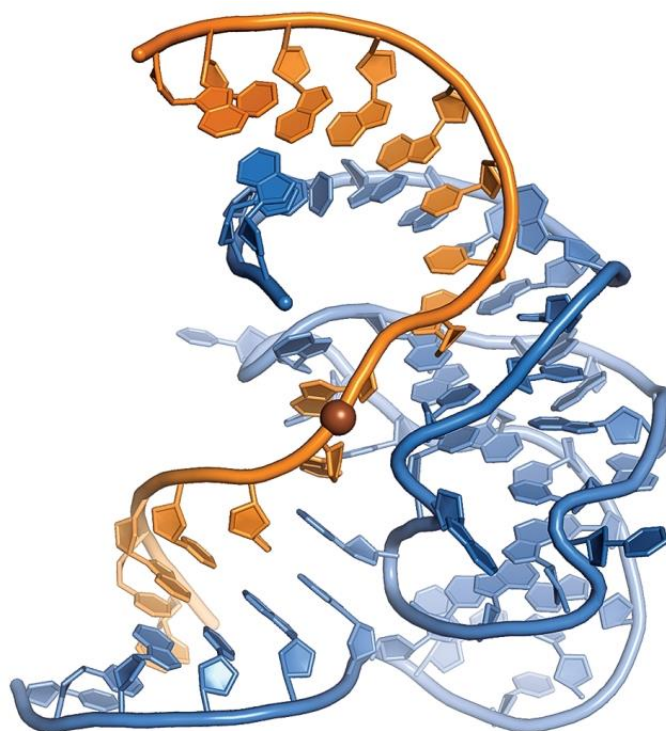
Fluorescence spectroscopy can also reveal information about nucleic acid structures. If two different fluorescent labels are close together, between 15-90 Å, and the emission spectrum of the first dye overlaps with the excitation spectrum of the other, fluorescence of the second dye can be detected even though the first one was excited. This is called fluorescence resonance energy transfer (FRET), also called Förster resonance energy transfer. The extent of the FRET effect is dependent on the distance between the fluorophores, allowing for determination of this distance[51, 52]. The advantage of this technique is that it can be measured in solution and requires only a relatively small amount of sample. FRET experiments can be done with external dyes that are connected to the oligonucleotides in question by alkyl linkers. However, those linkers provide a certain degree of flexibility which reduces accuracy of the distance measurements and causes information about the relative orientation of the dyes to be lost. To overcome this problem, fluorescent nucleobase analogs can be used[53-56]. A number of fluorescent nucleobase analogs are presented below (Fig. 7). FRET is also well suited for use in fluorogenic aptamers, because the bound dye can act as fluorescence donor or acceptor. This was done with different versions of the Chili aptamer which were modified with the fluorescent nucleobase 4-cyanoindole (4CI) in different positions[57].
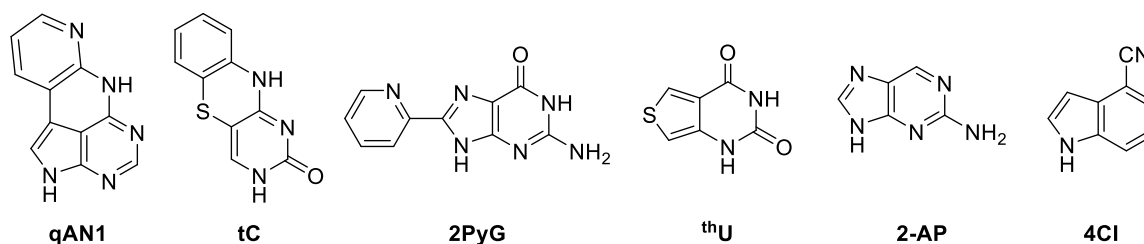
Fig. 7: Various fluorescent nucleobase analogs: quadracyclic adenine qAN1, tricyclic cytosine tC, 8-(2-pyridyl)-guanine (2PyG), thienouracil (thU), 2-aminopurine (2-AP) and 4-cyanoindole (4CI).

Another important method for nucleic acid structure determination is nuclear magnetic resonance (NMR) spectroscopy. NMR provides signals for individual atoms while not requiring crystals, which is a significant advantage over x-ray crystallography. However, nucleic acid NMR spectroscopy is not without challenges either, the amount of sample required is fairly large compared to other methods. Also, the proton density is fairly low and there is only a small number of different monomers, thus causing signal overlap, especially in longer sequences, where the slow tumbling also causes signal broadening[58]. To overcome these problems, isotopic labeling is commonly used[59-62]. Using ^{13}C- or ^{15}N-labeled nucleotides gives stronger signals because of the low natural abundance of these isotopes. Partial deuteration can also be helpful to make proton spectra, including nuclear Overhauser enhancement and exchange spectroscopy (NOESY), easier to interpret because undesired signals and correlations that would crowd the spectra can be eliminated in this way. A different approach for isotopic labeling is the introduction of fluorine. ^{19}F-NMR is very sensitive and fluorine is rarely present in biomolecules, making it a very attractive label[63]. A promising fluorine label, 2'-OCF$_3$ has been tested recently[64].

NMR spectroscopy on nucleic acids is usually done with the sample dissolved in different buffers, but this is not a good representation of the conditions present inside living cells, where nucleic acid structure and dynamics can be different. It is thus desirable to measure nucleic acid NMR in cells[65]. This has been done for some time, but was limited to *Xenopus laevis* oocytes[66], due to problems with introducing suitable amounts of nucleic acids into other cells. Recently, the first NMR measurements of nucleic acids in living human cells were reported, after using the bacterial toxin streptolysin O to form pores in the cell membranes (Fig. 8)[67]. Several other reports followed, such as studies on human telomeric DNA G-quadruplex structures by ^{19}F-NMR[68], DNA-ligand interactions in cells[69] and DNA i-motifs, where it was shown that i-motifs are more stable in vivo than in vitro[70].
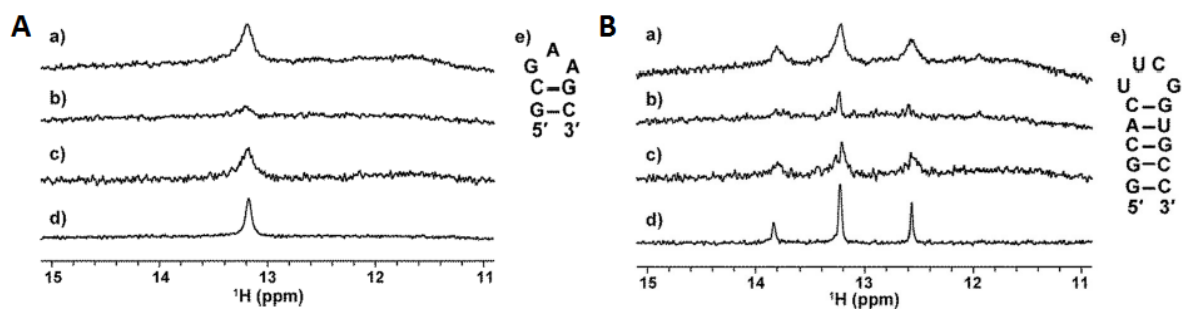
Fig. 8: Parts of in-cell ¹H-NMR spectra of (A) DNA and (B) RNA. (a) spectra of HeLa cells into which the nucleic acids were introduced, (b) spectra of the outer solution of the cell suspension, (c) difference spectra between (a-b), and (d) in vitro spectra. The figure was taken from [67].

A different NMR technique which is being used to study nucleic acids is solid-state NMR (ssNMR)[71, 72]. While also working with solid samples, the advantage of ssNMR over x-ray crystallography is that crystals are not required. Other solid samples, like powders or frozen solutions, can be measured as well. Recently, frozen human cells have been used to study an antisense oligonucleotide (ASO) drug in cells[73]. In-cell solution-state ³¹P-NMR did not result in any detectable signal for the ASO, likely because it formed complexes with its target mRNA and certain proteins, leading to signal broadening, so the cells had to be lysed and the proteins digested for the signal to become visible. But when the cells were frozen, the ASO could be detected by ssNMR in intact cells. Another approach used RNA microcrystals to measure ssNMR spectra which revealed information about hydrogen bonds from Watson-Crick base pairs[74]. This allowed distinguishing between kissing loop and extended duplex structures of RNA dimers. A recent ssNMR study on nucleotide-protein interactions demonstrated the ability of solid state NMR experiments to provide information about nucleotide binding modes[75].

Another method for structure determination is electron paramagnetic resonance (EPR) spectroscopy, which is the focus of this thesis.

1.3 Spin labels for nucleic acids

1.3.1 Paramagnetic compounds

EPR spectroscopy works in a similar way to NMR[76]. The sample is put into a magnetic field, causing a split in energy between parallel and antiparallel spin orientations of magnetic dipoles with respect to the magnetic field, which allows for spins to be excited by radiation. Unlike NMR, which works with nuclear spins, in EPR spectroscopy, unpaired electrons are excited. The energy difference between electron spin states is significantly larger than between nuclear spin states, so microwave irradiation is required. Contrary to NMR, the irradiation frequency is usually kept constant in EPR while the magnetic field strength is varied. In the EPR spectrum, the field strength at which the signal is

observed depends on the *g*-factor. For a free electron this is approximately 2.0023, but like the chemical shift of nuclear spins, the *g*-factor of a compound depends on the environment of the electron. The *g*-factor is also orientation dependent, with three different factors g_x, g_y and g_z being observable, but when small molecules are measured in solution, fast tumbling averages the *g*-factors to the isotropic *g*-factor g_{iso}, which leads to a single signal (Fig. 9).

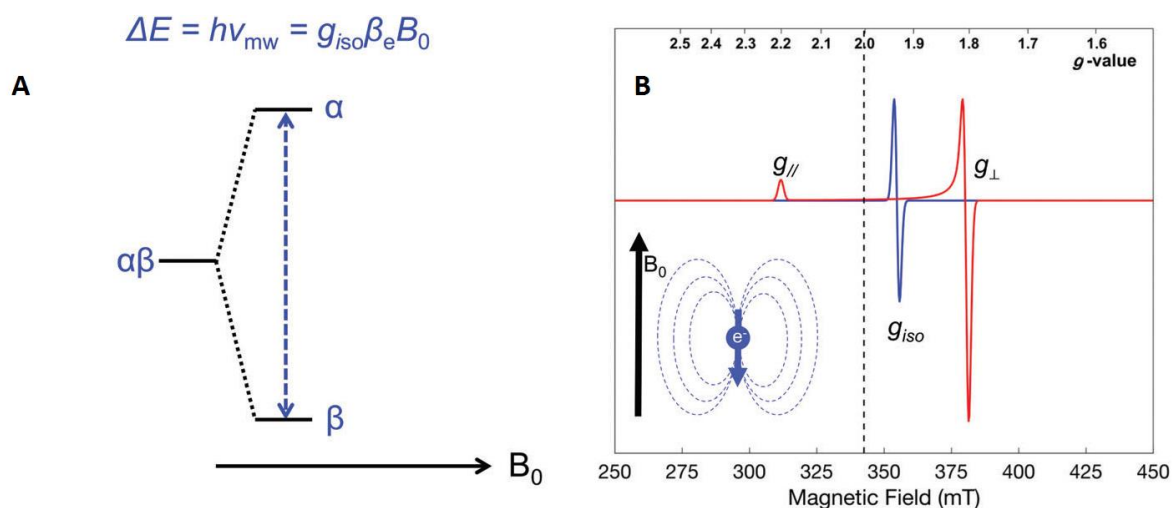$$\Delta E = h\nu_{mw} = g_{iso}\beta_e B_0$$

Fig. 9: Energy level diagram (A) and simulated field-swept EPR spectra (B) of an unpaired electron without hyperfine interactions. The isotropic energy transition between antiparallel (β) and parallel (α) spin states shown in A leads to the blue isotropic spectrum in B. The dotted line in B shows the *g*-factor of a free electron (2.0023). The red spectrum shows an anisotropic spectrum for a compound with axial symmetry, where two signals are observed for $g_z = g_\parallel$ and $g_x = g_y = g_\perp$, where $(2g_\perp + g_\parallel)/3 = g_{iso}$. The inset in B illustrates the magnetic interaction between electron spin and magnetic field. ΔE is the energy difference between α and β, h is the Planck constant, ν_{mw} is the microwave frequency, β_e is the Bohr magneton and B_0 the external magnetic field. The figure was adapted from [76].

$$\Delta E = h\nu_{mw} = g_{iso}\beta_e B_0 \pm a_{iso}/2$$
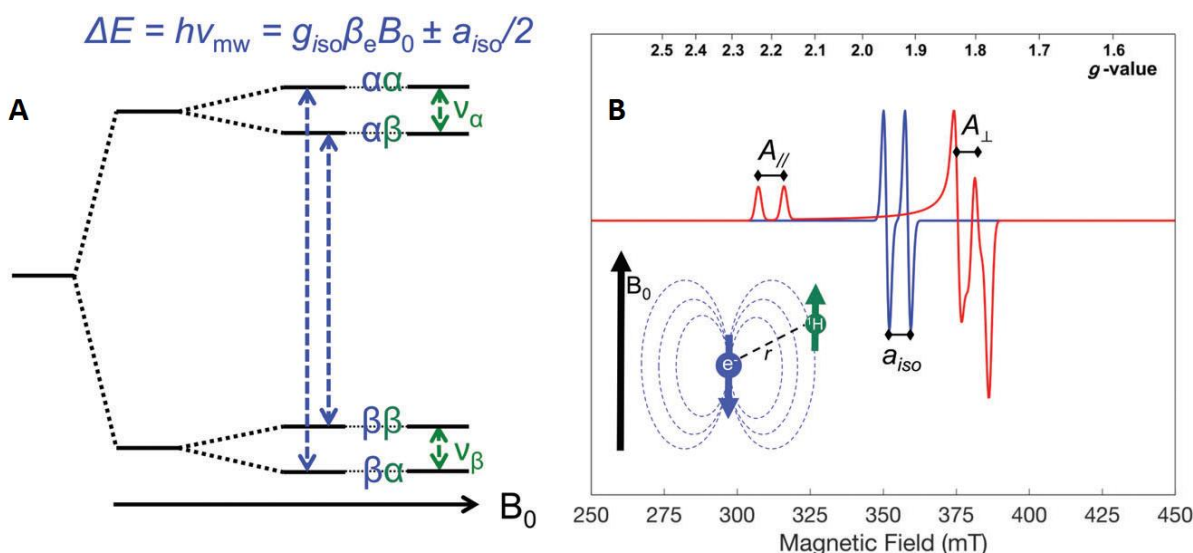
Fig. 10: Energy level diagram (A) and simulated field-swept EPR spectra (B) of an unpaired electron with hyperfine interaction with a nucleus with nuclear spin $I = 1/2$. The NMR transitions are marked by green arrows in A. The isotropic energy transitions between antiparallel (β) and parallel (α) spin states shown in A lead to the blue isotropic spectrum in B, where two lines separated by the isotropic hyperfine interaction a_{iso} are visible. The red spectrum shows an anisotropic spectrum for a compound with axial symmetry, where two signals are observed for $g_z = g_\parallel$ and $g_x = g_y = g_\perp$, where anisotropic hyperfine splitting $A_\parallel$ and $A_\perp$ is observed. The inset in B illustrates the magnetic interaction between electron spin, nuclear spin and magnetic field. ΔE is the energy difference between α and β, h is the Planck constant, ν_{mw}

Electron spins can also interact with nuclear spins, which leads to hyperfine splitting of the EPR signals analogous to the coupling between nuclei in NMR spectroscopy. The hyperfine interactions are also anisotropic, but with fast tumbling in solution only the isotropic part a_{iso} is observed (Fig. 10).

Since nucleic acids are not paramagnetic by nature, a paramagnetic spin label needs to be introduced for EPR measurements. There are three kinds of compounds that are used for EPR on nucleic acids on a regular basis. One category are gadolinium labels. Gd(III) has an electron spin of $S = 7/2$, and offers high sensitivity for EPR measurements[77].
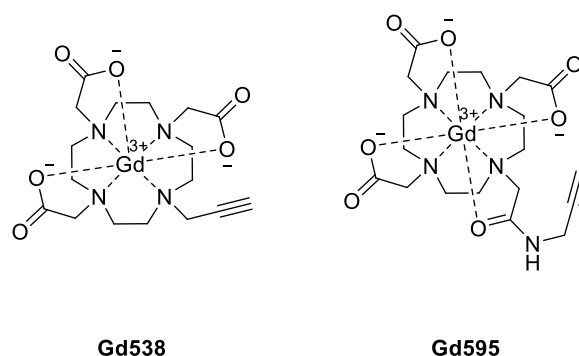

Gd538   **Gd595**

Fig. 11: Gadolinium spin labels Gd538 and Gd595, which were used on nucleic acids.

One of the reasons for the development of gadolinium labels were in-cell measurements. Organic radicals are often reduced in cells fairly quickly, which limits their usefulness for EPR measurements under biologically relevant conditions[78]. Gadolinium offers a better chemical stability by comparison, and is more sensitive, which reduces the amount of sample required, another advantage for in-cell measurements where the concentration of specific biomolecules is low[79]. Gadolinium spin labels consist of a complex, where the ligand is attached to the biomolecule in question, in the case of nucleic acids often by copper(I)-catalyzed azide-alkyne cycloaddition (CuAAC). Gadolinium labels have been used for distance determination in cells by pulsed EPR techniques. Most Gd(III) labels are designed for proteins[80-82], but a few examples for nucleic acids also exist, like Gd538 and Gd595 (Fig. 11)[83].

Another class of spin labels are the tetrathiatriarylmethyl (TAM) radicals. They are characterized both by a lack of hyperfine coupling, resulting in simple spectra, as well as a slow relaxation with a relatively long phase memory time T_m[84-86]. This can be helpful for pulsed EPR measurements, where a sufficiently long T_m is required (see chapter 1.3.2)[87].
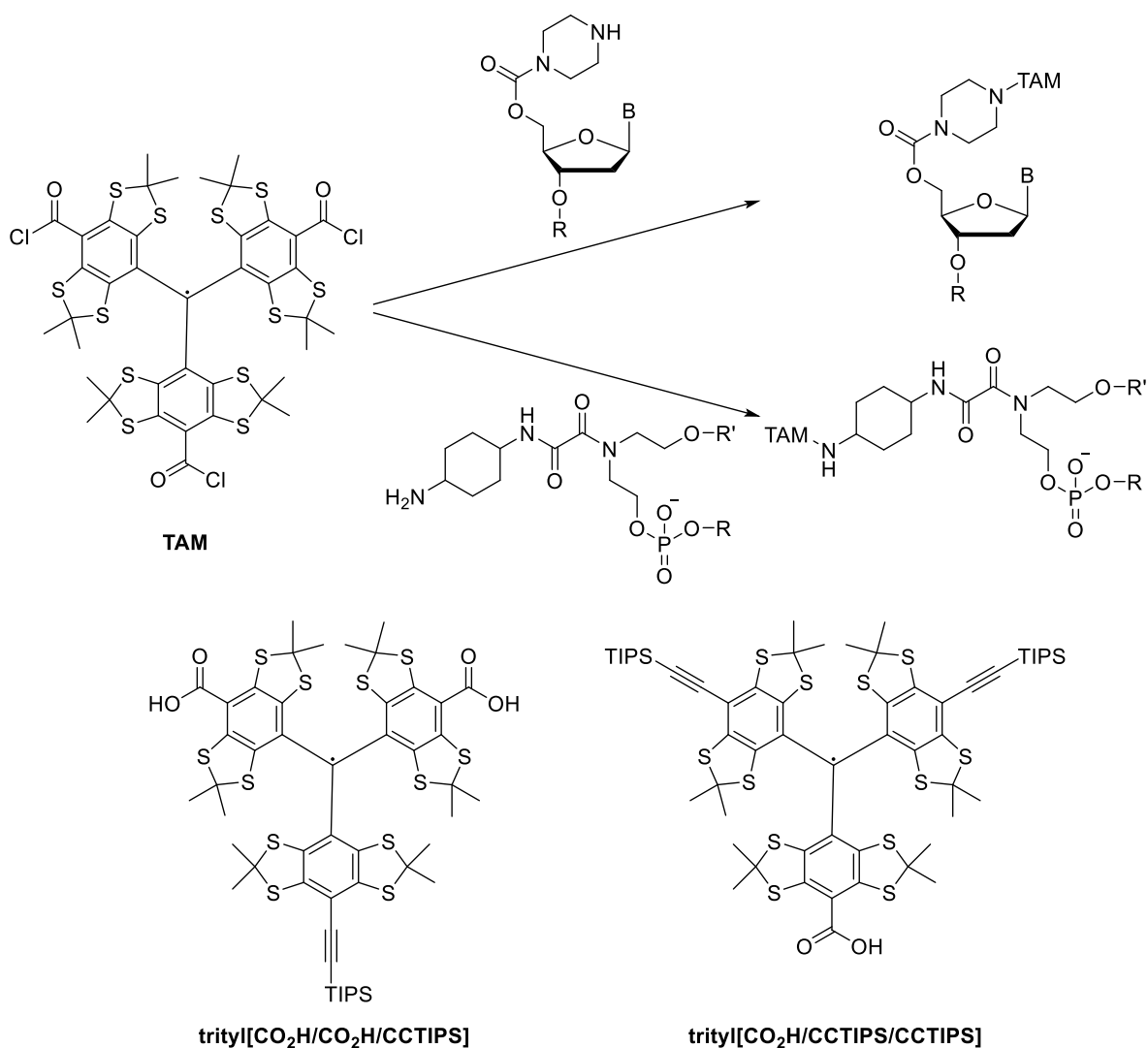
Fig. 12: Postsynthetic labeling of DNA with TAM (top) and trityl labels with orthogonal functional groups (bottom). B = nucleobase. R = oligonucleotide. R' = H/oligonucleotide.

As a result, TAMs were used in the first distance measurement by EPR on nucleic acids at physiological temperature, while previously only frozen samples could be measured[88]. Trityl labels are generally introduced to nucleic acids after solid phase synthesis, by reaction between a nucleophile on a modified building block in the oligonucleotide with an activated carboxyl group on the label, like an acyl chloride[88, 89] (Fig. 12 top). However, because TAM contains three carboxyl groups, reaction with more than one nucleophile is possible, resulting in a mixture containing undesired side-products. Recently, the synthesis of new trityl labels with ethyne as well as carboxyl was published[90]. When labeling by nucleophilic attack is desired, a label with only one carboxyl and two ethyne groups can be used, while a label with two carboxyl groups and one ethyne group can be used for labeling by cycloaddition (Fig. 12 bottom).

Nitroxides, like 2,2,6,6-tetramethylpiperidin-1-yloxyl (TEMPO), are probably the most well known example of stable organic radicals. Even though gadolinium and trityl labels have been shown to

possess certain advantages which can be desirable, nitroxides are still the most commonly used type of spin label for nucleic acids. This is because nitroxides also offer some advantages. Simple nitroxide labels, or the building blocks for their attachment to oligonucleotides, are easy to synthesize, although this is not true for more advanced rigid labels. Also, compared to the bulky gadolinium complexes or trityl compounds, nitroxide labels are comparatively small and it is possible to design them in such a way that they are analogs of canonical nucleosides, allowing rigid spin labels to be incorporated into oligonucleotides with only minimal detrimental effects on duplex stability. The following chapters will focus on design, incorporation and applications of nitroxide spin labels.

1.3.2 Nitroxide spin label design

One important concern when it comes to spin label design is stability of the radical. The decomposition of nitroxides has been studied extensively[91, 92]. Nitroxides will decompose by disproportionation, particularly in the presence of strong acids. Reducing agents are also detrimental to nitroxides, as they can reduce the nitroxide to the corresponding hydroxylamine or amine. The degradation by disproportionation can be suppressed by introducing four substituents next to the nitroxide so there is no hydrogen in the α-positions, as in the case of TEMPO. Another study determined the effect of different α-substituents on nitroxide reduction[93].
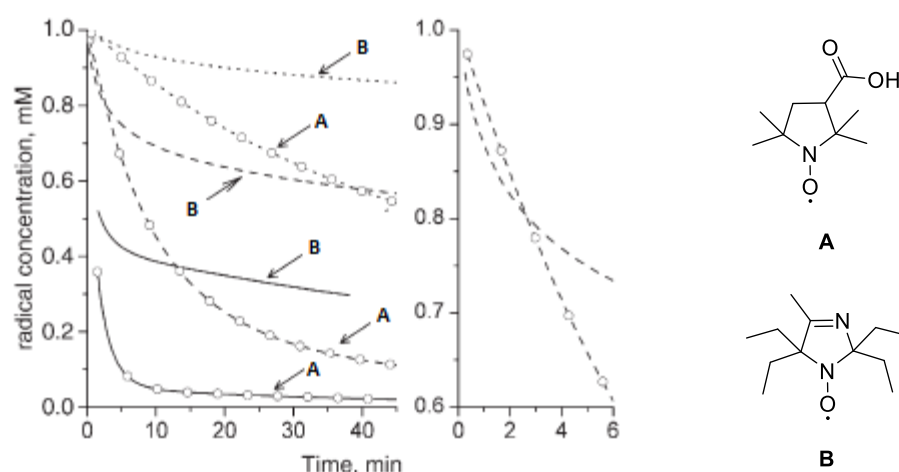
Fig. 13: Reduction of nitroxide radicals A and B by ascorbate measured by EPR. Initial nitroxide concentration is 1 mM, ascorbate concentration is 2 mM (dotted lines), 20 mM (dashed lines) and 100 mM (solid lines). The initial time for 20 mM ascorbate is shown enlarged to the right. The figure was taken from [93].

It showed that ethyl groups are significantly more beneficial for nitroxide stability (Fig. 13). This is most likely due to the increased steric bulk of the ethyl groups, as a later study showed that spirocyclohexyl groups, which are between methyl and ethyl groups in their steric demand, have an intermediate effect[94]. It has also been shown that the size of the ring, which the nitroxide is part of, has an influence on stability, with five-membered rings being more stable than six-membered rings against reduction by ascorbate[93].

The substituents can also have a direct effect on the EPR measurements by influencing relaxation[95]. In case of methyl groups, which are most commonly used, the rotation of the methyl groups reduces the phase memory time T_m, which limits pulsed EPR techniques to low temperatures (see chapter 1.3.2)[96]. Using substituents which do not rotate or which have no hydrogen next to the radical significantly increases T_m, which allows for pulsed EPR measurements at higher temperatures[97, 98].

The second important part about spin label design next to the nitroxide itself is the way in which it is attached to the nucleic acid in question. When a modified nucleoside is incorporated into an oligonucleotide, a spin label can be attached to it later by a number of different reactions. Nucleophilic substitutions were often used, and they can be performed in two ways. The nucleophile can be a modified nucleoside attacking the spin label, or if a suitable leaving group is introduced, the spin label can be the nucleophile. In the first case, sulfur has been used quite often, as it can be easily introduced into the phosphate backbone during solid-phase synthesis, which allows for labeling of the backbone by attaching the spin label to either one[99] or two[100] thiophosphates (Fig. 14 **A,B**). The latter option prevents rotation of the label, thus reducing movement of the label with respect to the entire molecule, which can be helpful for EPR measurements, at the cost of distorting the local structure. Another modification which carries sulfur is 4-thiouridine, which also appears naturally in tRNA, allowing for labeling without the need for artificially introduced modifications (Fig. 14 **C**)[101]. Instead of sulfur, amino groups have also been used as nucleophiles, for example on the 2'-position of the ribose, to allow for sugar labeling for example (Fig. 14 **D**)[102-104].
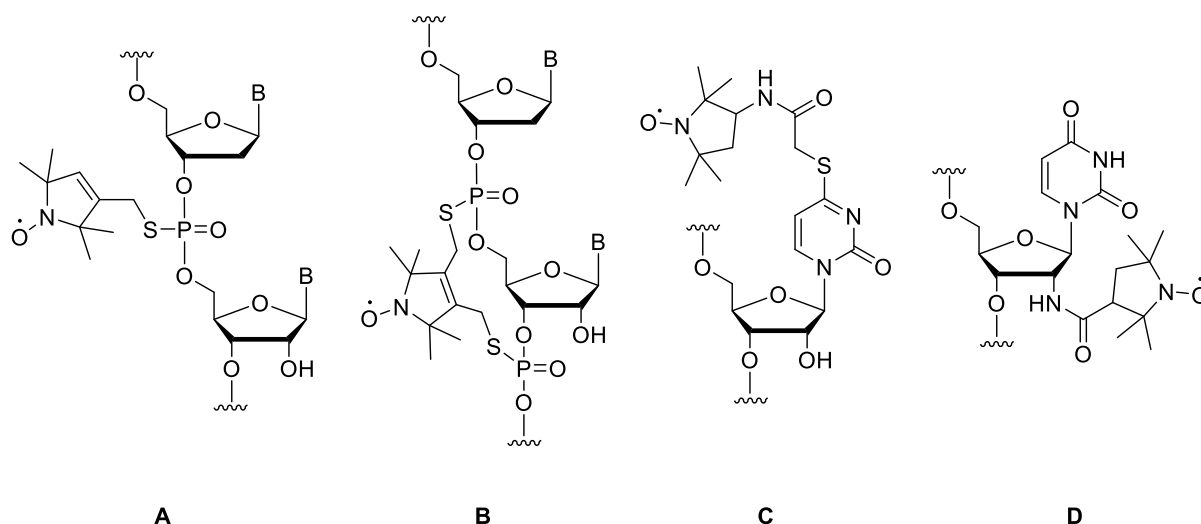
Fig. 14: Various spin labels introduced by nucleophilic attack of the oligonucleotide on the spin label, by a phosphothioate (A and B), 4-thiouridine (C) or a 2'-amino group.

If the spin label is supposed to work as the nucleophile, like 4-amino-TEMPO, one possibility is to activate the terminal phosphate of a nucleic acid, which does not require the prior incorporation of a modification (Fig. 15 **A,B**)[105]. However, this approach is limited to terminal phosphates. Internal

labeling with 4-amino-TEMPO is possible by using convertible nucleosides which are modified with a leaving group like 4-chlorophenyl or fluorine (Fig. 15 **C-E**)[106].
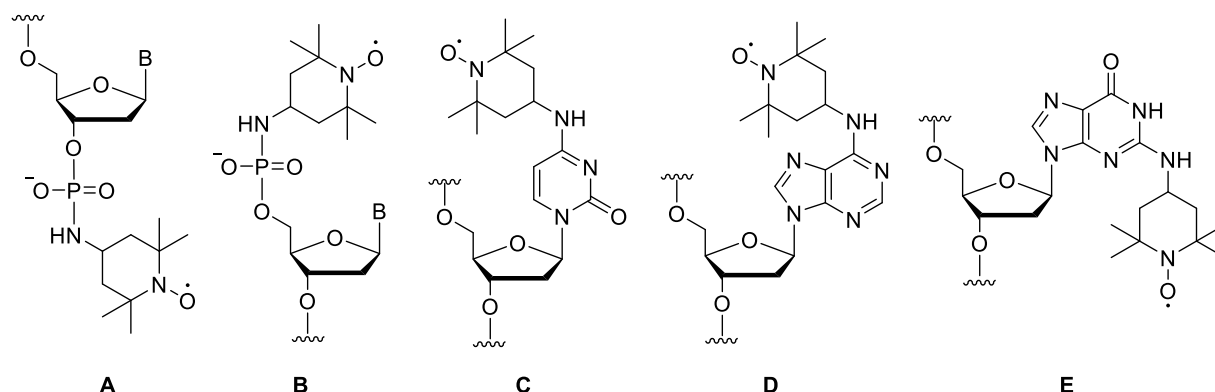

Fig. 15: Various spin labels introduced by nucleophilic attack of the spin label on the oligonucleotide on an activated terminal phosphate (A and B) or a convertible nucleoside (C-D).

Another reaction which has been used for spin labeling is the copper(I)-catalyzed azide-alkyne cycloaddition (CuAAC), which is widely used as a bioorthogonal labeling method. It allows for labeling of an alkyne-modified oligonucleotide with an azide-containing spin label. This has been used for sugar (Fig. 16 **A**)[107] as well as base labeling (Fig. 16 **B,C**)[108, 109]. Sonogashira coupling with an iodo-modified nucleoside and a spin label carrying an alkyne has also been done (Fig. 16 **D**)[110].
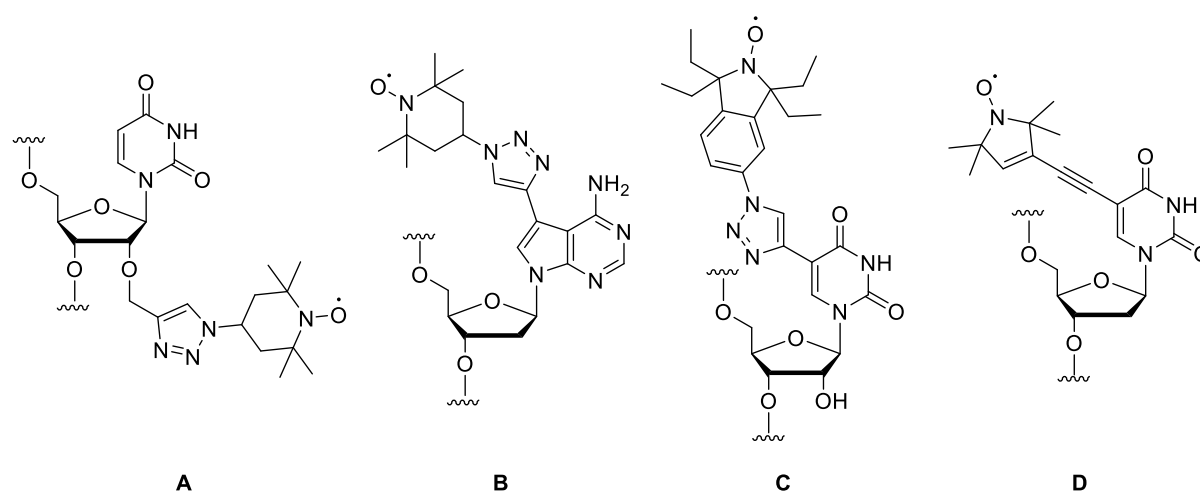
Fig. 16: Various spin labels introduced by copper-catalyzed azide-alkyne-cycloaddition (CuAAC) and Sonogashira coupling.

The advantage of the spin labels presented so far is that they are introduced postsynthetically, so the nitroxide does not need to be subjected to the conditions of solid-phase synthesis. Their disadvantage is that they are connected to the oligonucleotide by more or less flexible linkers. This allows for independent movement of the label, which is detrimental for measurements, especially when trying to determine distances between labels. Developing spin labels where such movement is prevented is therefore a desirable goal. One class of such labels are the conformationally

15

unambiguous labels (Fig 17)[111-113]. They do not prevent rotation of the nitroxide, but having the nitroxide N-O-bond aligned with the linker means that rotation does not change the position of the nitroxide relative to the oligonucleotide. Furthermore, in the labels [Im]U and [Im]Um, a hydrogen bond between the amino group of the imidazole ring and the O4 of the uridine can restrict the rotation. This is not the case in [ExIm]U, the first conformationally unambiguous label used for distance measurements in nucleic acids. Its free rotation means there is no fixed orientation of the labels relative to each other, but it makes distance determination easier.
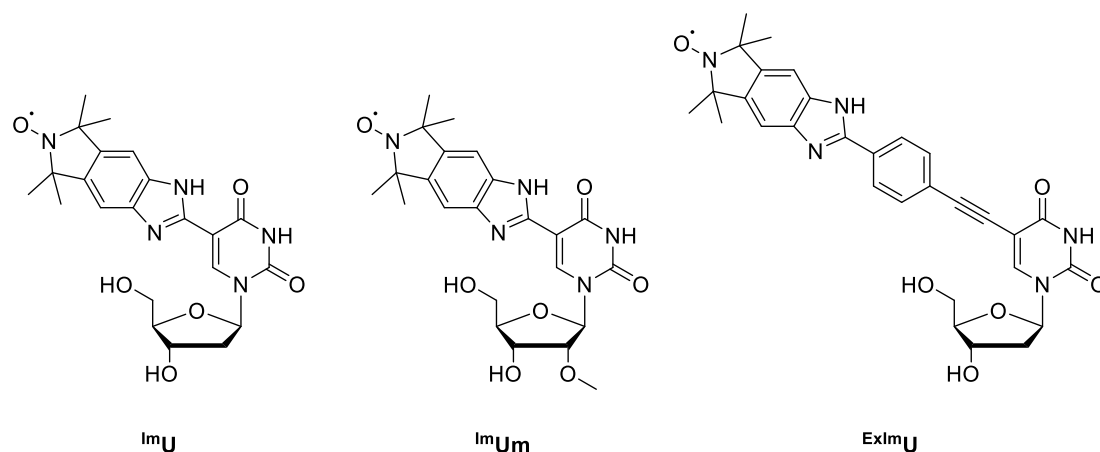

Fig. 17: Conformationally unambiguous spin labels [Im]U, [Im]Um and [ExIm]U.

One additional step in the direction of restricted mobility leads to rigid spin labels, where the nitroxide is an extension of the ring system of the nucleobase. Thus, the rotation of the nitroxide is prevented completely, which can allow for the determination of relative orientation of two spin labels by pulsed EPR spectroscopy. This was first achieved in a spin label called Q (Fig. 18), although it came with the drawback of requiring the artificial 2-aminopurine as its partner for proper base pairing[114]. Later, the development of Ç (C-spin) represented the next big step forward in spin label development[115, 116]. It is rigid, retains all functional groups of cytidine required to form base pairs with guanosine, while minimizing perturbation of the nucleic acid secondary structure by having the extension point towards the major groove, a quality it shares with the conformationally unambiguous labels and Q. A version of Ç for labeling of RNA, called Çm, was also developed, which carries a 2'-OMe group[117]. Recently, further improvements have been made by using ethyl groups to flank the nitroxide, which increases stability of the radical as discussed above (Fig. 18)[118].
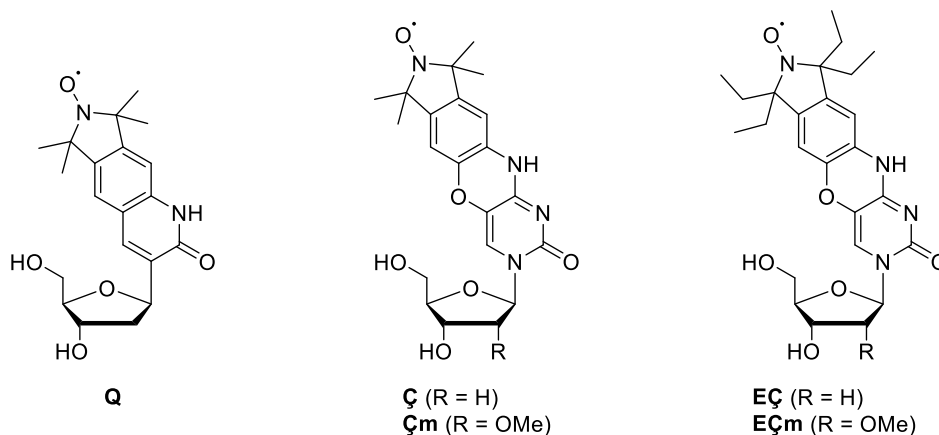
Fig. 18: Rigid spin labels Q and different versions of Ç.

The concept of rigid spin labels has also been expanded to purine nucleosides[119]. Isoxyl-A is a spin label based on adenosine, which is able to form base-pairs with uridine (Fig. 19). It was also designed with the nitroxide pointing into the major groove to keep structure perturbation to a minimum.
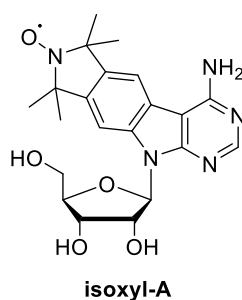
Fig. 19: Rigid spin label isoxyl-A.

The effect of spin label rigidity is illustrated in Fig. 20, where the CW EPR spectra of the rigid spin labels isoxyl-A and Çm compared to 4-TEMPO-cytidine (C^{TEMPO}), when the labels where incorporated into an RNA duplex or a hairpin motif. For the rigid labels, the peaks are broader, and sometimes even split, which is the result of a larger rotational correlation time as a result of the label not moving independently from the RNA, while the TEMPO of C^{TEMPO} can still rotate. This makes rigid labels more sensitive to the structural context in which they are placed, as can be seen in Fig. 20 when comparing the spectra of the hairpin and duplex.

Fig. 20: Comparison of the CW EPR spectra of isoxyl-A, TEMPO-modified cytidine, and Çm, when incorporated into RNA hairpin (top) or duplex (bottom) structures. Blue dots in the schemes represent the location of the spin label. The figure was adapted from [119]. Spectra of C^{TEMPO} and Çm modified oligonucleotides are originally from [117].

1.3.3 Incorporation of spin labels

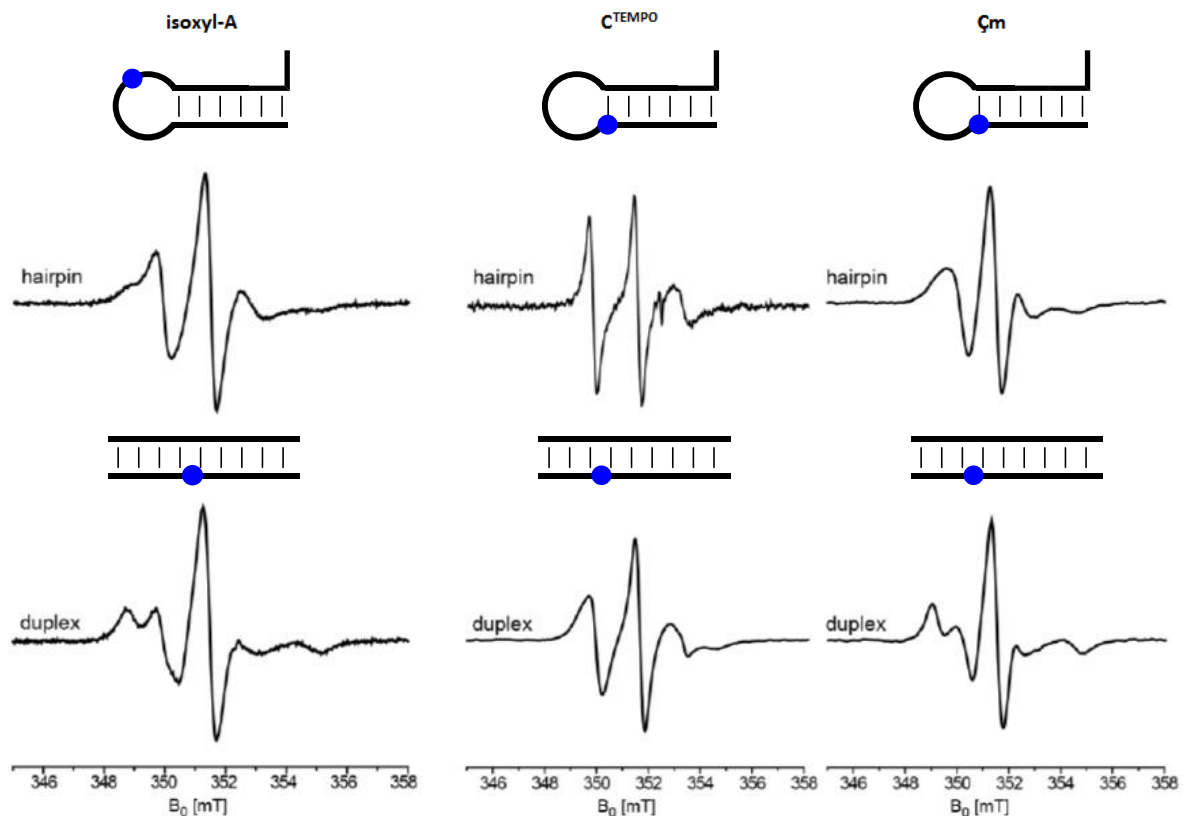If a spin label is supposed to be introduced into an oligonucleotide, some kind of modified nucleoside has to be introduced during oligonucleotide synthesis, regardless of whether the nitroxide is already present on the nucleoside or to be introduced postsynthetically on a nucleotide carrying some functional group. The standard method for synthesizing modified nucleic acids is solid-phase synthesis (SPS)[120]. An overview of this process is given in Fig. 21. SPS starts with the first nucleoside, which will be the 3'-end of the desired oligonucleotide, on a solid support, usually controlled pore glass (CPG) or polystyrene. To this first nucleoside, the following ones are sequentially attached one after the other. This requires those nucleosides to be used as 3'-phosphoramidites modified with certain protecting groups[121]. The phosphorus usually carries a β-cyanoethyl group for protection and a diisopropylamino group as a leaving group.
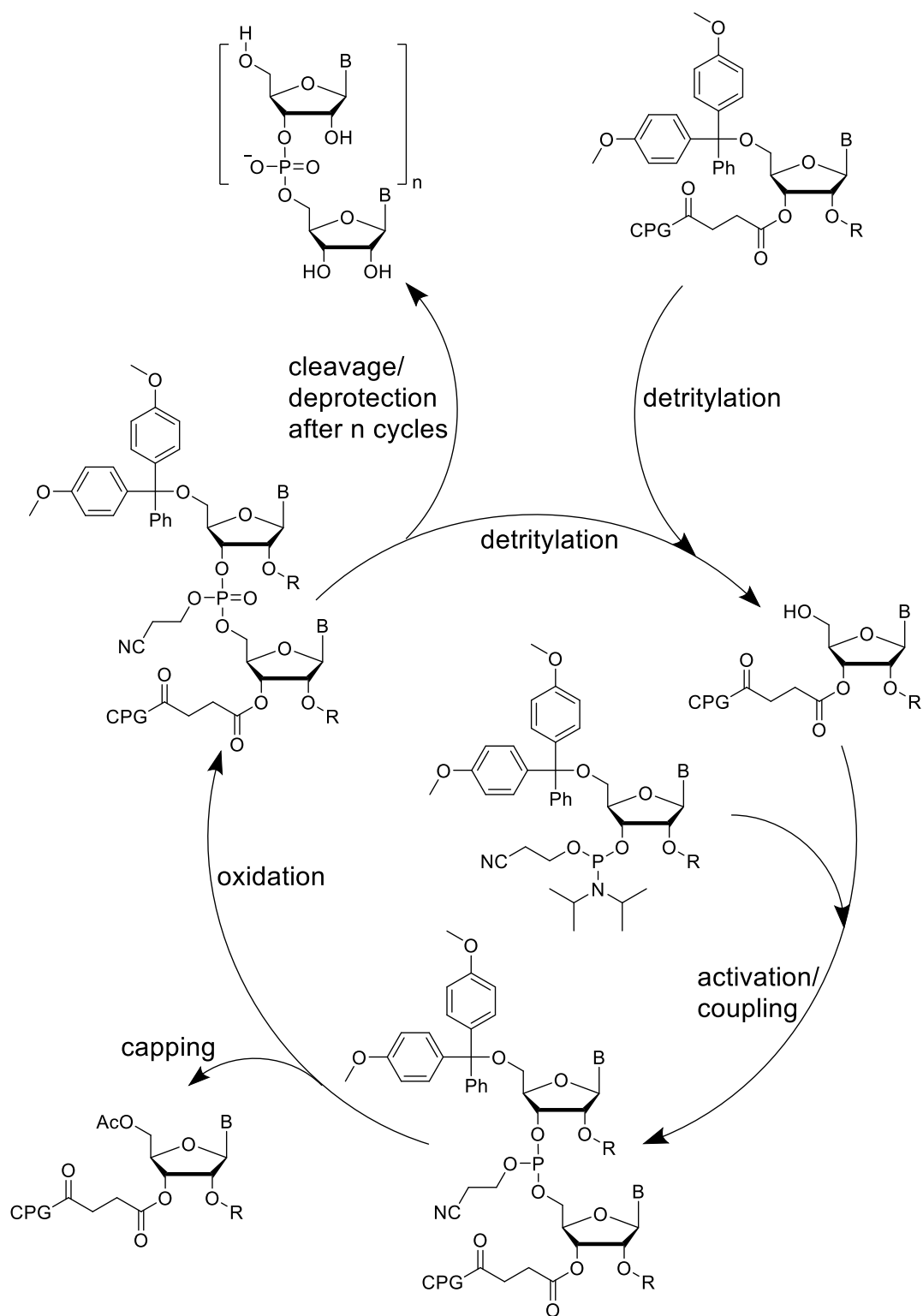
Fig. 21: Solid-phase synthesis of RNA with the phosphoramidite method. B = nucleobase, R = 2'-silyl protecting group, CPG = controlled pore glass solid support.

The 5'-OH is protected with a 4,4'-dimethoxytrityl (DMT) group and amino groups on the nucleobases are protected with different groups, usually acetyl or benzoyl for adenosine, acetyl or dimethylformamidine for guanosine[122] and either acetyl or benzoyl for cytidine. In case of RNA synthesis, the 2'-OH also needs to be protected, usually with a silyl group like *tert*-butyldimethylsilyl

(TBDMS)[123] or tri-*iso*propylsilyl-oxymethyl (TOM)[124]. Each step of solid-phase synthesis starts with the deprotection of the 5'-OH. The acid-labile DMT can be removed with acid, often trichloroacetic acid (TCA). The absorption of the cleaved DMT$^+$ cation can be used to monitor the synthesis efficiency at each step. Then, the next phosphoramidite is activated by some tetrazole compound, like 5-ethylthio-(1*H*)-tetrazole (ETT) or 5-benzylthio-(1*H*)-tetrazole (BTT), which replaces the diisopropylamino group on the phosphorus as a leaving group. The phosphoramidite is then attacked by the 5'-hydroxy group of the oligonucleotide chain to form the new 3'-5'-linkage. After a capping step where unreacted 5'-OH groups are acetylated with acetic anhydride to prevent them from reacting further, the phosphorus is oxidized to obtain a phosphotriester. Iodine is usually used as an oxidant. This cycle continues until the desired oligonucleotide has been finished[125]. After removal of the terminal DMT group, the oligonucleotide is cleaved from the solid support, usually with ammonia or methylamine. This also removes the β-cyanoethyl groups, resulting in the natural phosphodiester bond, and the protecting groups on the amines. If RNA was synthesized, the 2'-silyl group then has to be removed separately, usually with tetrabutylammonium fluoride (TBAF).

Solid-phase synthesis is a powerful tool for the synthesis of nucleic acids because it allows for the site specific incorporation of a vast number of different modifications. However, incorporation of spin labels by SPS comes with an additional challenge, namely nitroxide stability. The iodine used for oxidation of the phosphorus under standard SPS conditions as well as the TCA used for DMT cleavage can cause degradation of the nitroxide to the corresponding amine, which reduces the yield of the spin labeled oligonucleotide[116]. One way to prevent this is to change the conditions. Using *tert*-butyl hydroperoxide as the oxidant and dichloroacetic acid (DCA) for 5'-deprotection can reduce the extent of degradation. Another way of reducing the extent of nitroxide degradation during SPS without using a protecting group is to use ethyl groups instead of the commonly used methyl groups next to the nitroxide (see chapter 1.2.1). It was shown that the ethyl group carrying analogs of Ç and Çm, called EÇ and EÇm, are reasonably stable during SPS as long as *tert*-butyl hydroperoxide is used as the oxidant[118]. Another way to prevent degradation is to not have the nitroxide present during SPS by protecting it. This has the additional advantage during synthesis of the phosphoramidite of resulting in a diamagnetic compound, which can be characterized more easily by NMR, which is challenging for paramagnetic compounds. Several protecting groups have been tried, one of the most promising classes being photolabile groups, like a coumarin-based protecting group (Fig. 22 **A**) or a nitrobenzyloxymethyl group (Fig. 22 **B** and **C**)[126-128].
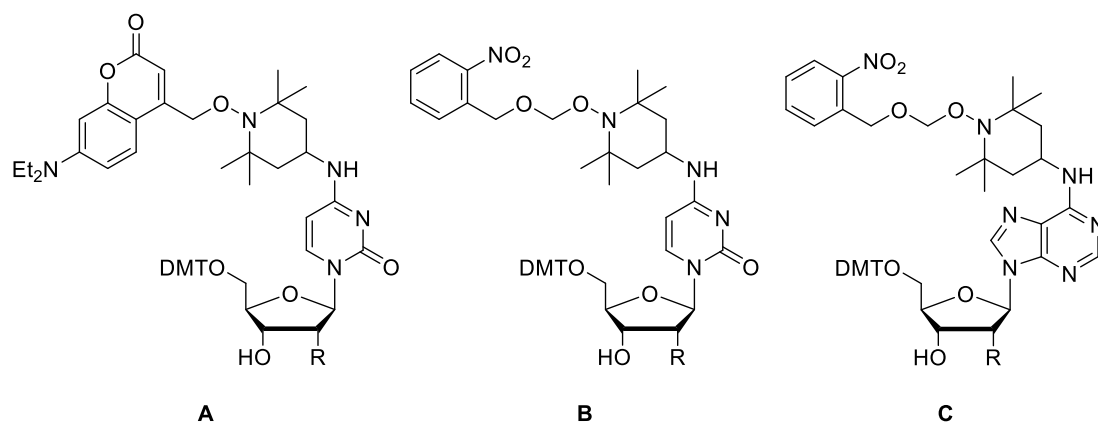
Fig. 22: Spin labeled nucleosides protected with photolabile protecting groups. R = H or OTOM.

These groups can be removed by irradiation with light at relatively long wavelengths which does not harm the oligonucleotide, and the hydroxylamine generated by this is then oxidized to the nitroxide under air without extra effort. However, preparation of the protecting group requires additional synthetic steps. Recently, a procedure was published, by which a nitroxide can be protected with a simple benzoyl group, which is cleaved during the regular oligonucleotide deprotection procedure after solid-phase synthesis with ammonia or methylamine (Fig. 23)[118, 129].

Ç-Bz (R = H)
Çm-Bz (R = OMe)

EÇm-Bz (R = OMe)
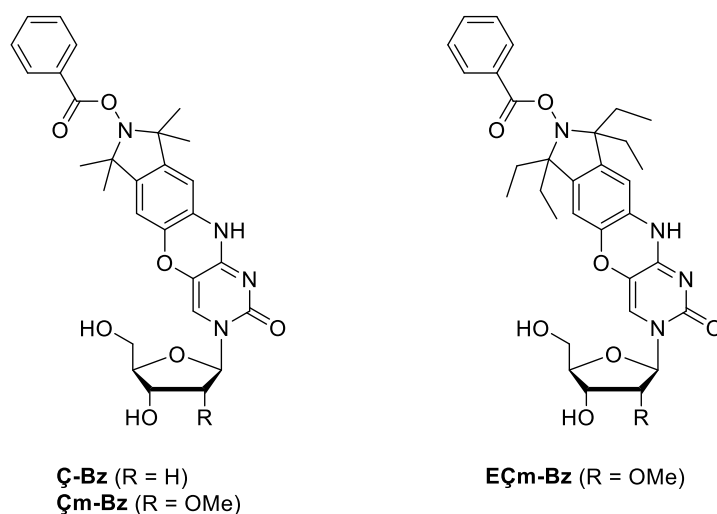
Fig. 23: Rigid spin labels from the Ç family with a benzoyl-protected nitroxide.

Another limit of solid-phase synthesis is the length of the oligonucleotides that can be synthesized. Most functional nucleic acids are too long to be synthesized in one piece. One solution to this problem has been to synthesize smaller pieces and ligate them to obtain the full-length product. This has been done to obtain spin labeled versions of the 53-nucleotide (nt) SAM-III and the 118-nt SAM-I riboswitches by ligation with 9DBI*, a shortened version of the 9DBI deoxyribozyme[130]. Recently, a double-labeled version of the 81 nt TPP (thiamine pyrophosphate) riboswitch aptamer was synthesized by enzymatic ligation of two smaller spin-labeled pieces[131].

An alternative to SPS which can be used to obtain nucleic acids is enzymatic synthesis, where the desired oligonucleotide is built up from nucleoside triphosphates by a polymerase enzyme according to a template strand. Some attempts to use this method for the synthesis of spin-labeled oligonucleotides have been made. It has been shown for example, that Therminator DNA polymerase is able to incorporate spin labels like the 5'-triphosphate of the deoxyuridine spin label shown in Fig. 16 **D**[132, 133].
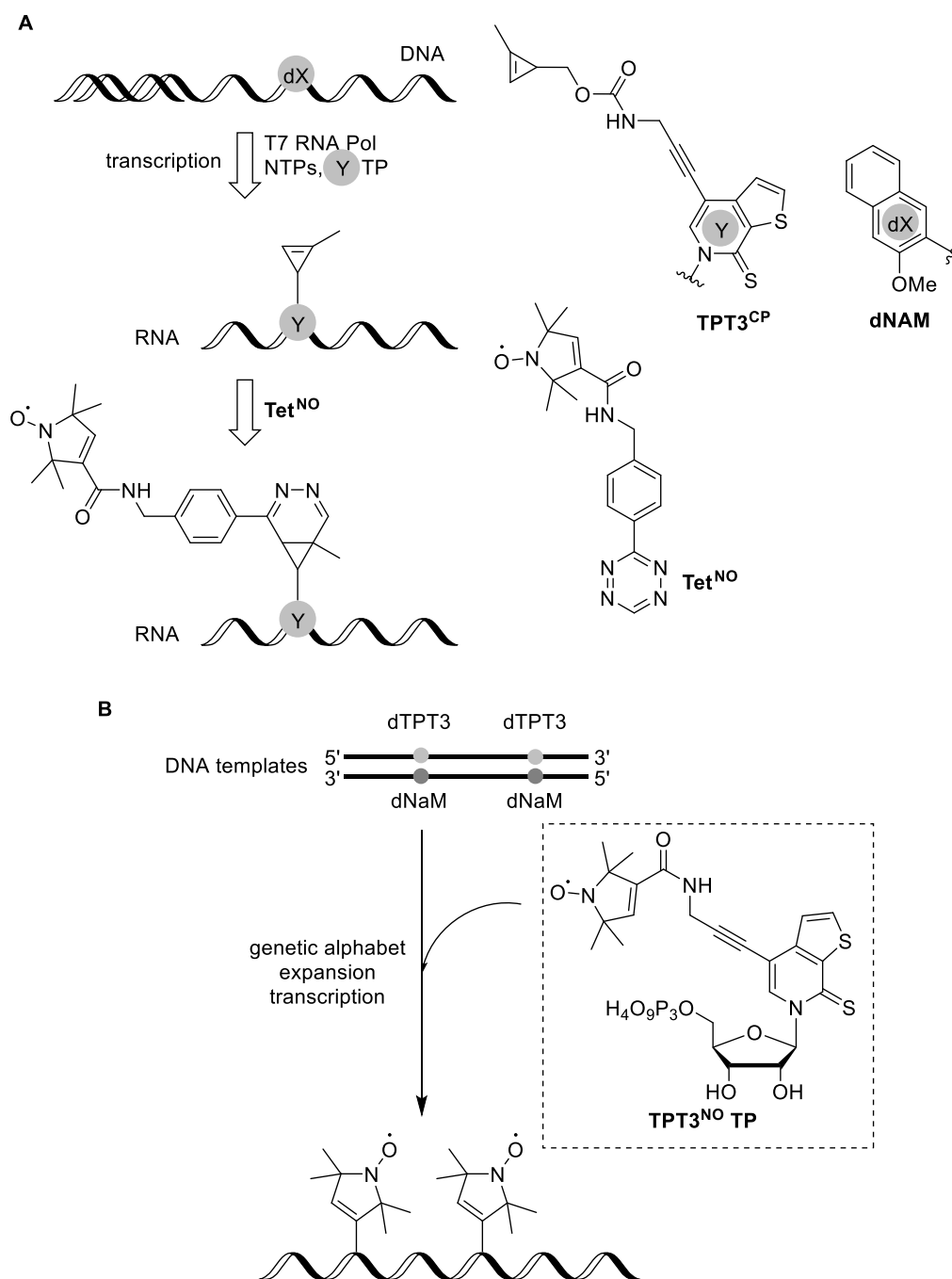

Fig. 24: Synthesis of spin-labeled RNA by in vitro transcription with an expanded genetic alphabet. (A) Incorporation of TPT3^{CP} for postsynthetic labeling with TET^{NO}. (B) Direct incorporation of spin labeled nucleoside TPT3^{NO}. The figures were reproduced based on [134] and [135].

The drawback of using a modified version of a canonical nucleoside is that it will be incorporated opposite all occurrences of its canonical base-pairing partner in the template, so site-specific labeling is challenging.

One way to address this problem is in vitro transcription with an expanded genetic alphabet. When a DNA template containing the artificial nucleotide dNAM (naphthalene methoxide) is used for in vitro transcription, the 5'-triphosphate of the nucleoside TPT3 (thienopyridinethione) can be incorporated into the resulting RNA opposite of dNAM. This has been used to generate an RNA duplex containing the TPT3[CP] modification which could be labeled post-synthetically by inverse electron demand Diels-Alder (iEDDA) reaction using the modified nitroxide compound Tet[NO] (Fig. 24 A)[134]. This process was later improved by using the spin-labeled triphosphate TPT3[NO] TP to obtain site-specifcally spin labeled version of different RNAs with a length of up to 377 nt, allowing them to be studied by EPR without any additional reaction to introduce the spin labels (Fig. 24 B)[135].

An entirely different approach to spin labeling is non-covalent labeling. Early approaches used nitroxides attached to an intercalator, which was connected to an adenine by a long linker. Binding of the adenine at an abasic site would ensure site specificity of the labeling, as the intercalator would otherwise bind to the DNA nonspecifically[136, 137]. Recently, different purine nucleobases with an isoindoline nitroxide moiety attached to one of their amino groups have been tested for their ability to bind site-specifically at an abasic site by pairing to the opposing base in double stranded DNA, RNA and DNA/RNA hybrids[138, 139].

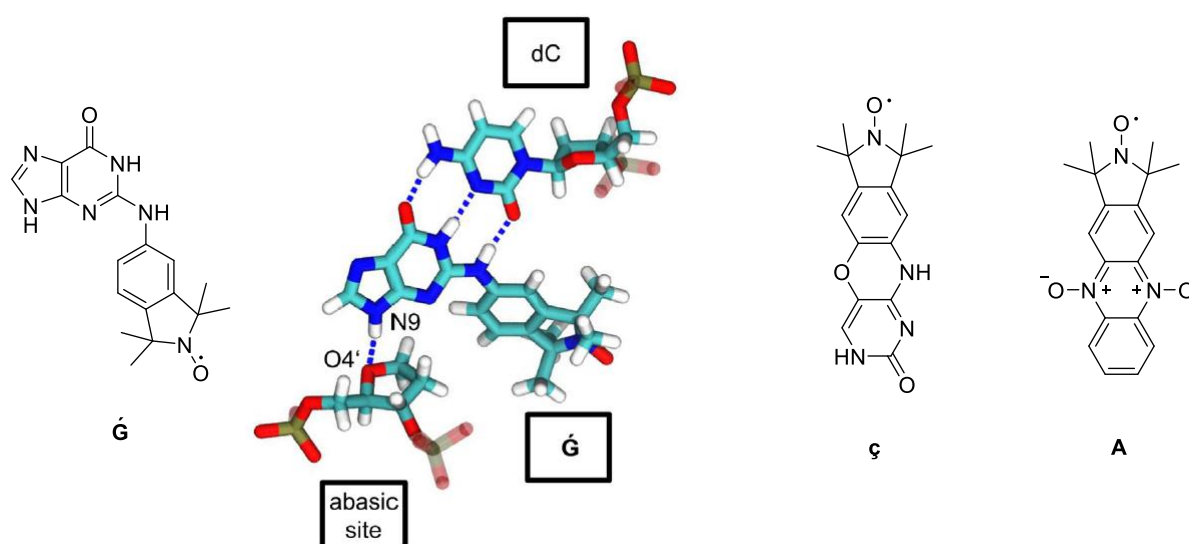**Fig. 25: Spin label Ǵ and its hydrogen bonds when incorporated into a DNA duplex opposite to cytidine (left) and rigd spin labels ç and phenazine label A (right). Hydrogen bonds are marked as dashed lines. The figure in the center was taken from [140].**

This resulted in several promising candidates, the best of which is Ǵ (G-spin). While other labels only showed significant binding at temperatures below 0 °C, Ǵ is able to bind to abasic sites in double stranded RNA opposite cytidine even at 20 °C. It has recently been studied in greater detail, including molecular dynamics simulations[140]. The study concluded that Ǵ forms hydrogen bonds to the opposing cytidine, as well as to the 4'-oxygen of the abasic site sugar and causes only minor perturbations of the duplex structure, with the isoindoline pointing into the minor groove (Fig. 25). Non-covalent labeling was also done with rigid labels. The nucleobase of Ç, called ç (Fig. 25), was used for labeling of abasic sites opposite to guanosine[141-143], while a recent study introduced a number of phenazine based spin labels[144]. Among them, one in particular showed good affinity for abasic sites opposite cytidine or adenosine (Fig. 25 **A**).

A different approach to non-covalent spin labeling has been developed recently[145]. It makes use of the malachite green aptamer to bind different derivatives of tetramethylrosamine (TMR), which are modified with different nitroxide moieties (Fig. 26).
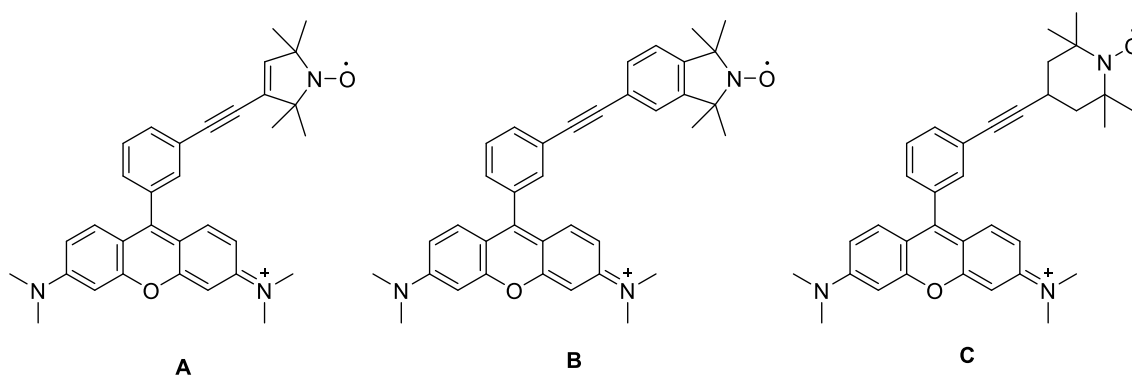
Fig. 26: Spin-labeled derivatives of tetramethylrosamine (TMR) for noncovalent spin labeling with the malachite green aptamer.

This is the first example of spin labeling of a completely unmodified RNA. The authors conclude that some helices or stem-loops of long RNAs could be replaced with the malachite green aptamer, as it is similar to a helix, to allow for the labeling of such RNAs without the need for incorporation of modifications, which would be beneficial for their synthesis.

1.4 EPR spectroscopy on nucleic acids

1.4.1 CW EPR spectroscopy

CW EPR spectroscopy on nucleic acids usually relies on the effect of spin label mobility on the EPR spectra. Hybridization of oligonucleotides leads to a significant reduction in the speed of molecular tumbling, which results in spectral broadening. This was used to investigate DNA triplex formation[146].

The EPR spectra of spin-labeled 15 nt DNAs ($^{sp}T_{15}$) as single strands and double strands with a complementary strand ($^{sp}T_{15}$:A_{15}) were measured. Then, the spin labeled single strand was added to a duplex made up of its non-labeled equivalent and the complementary strand to form triplexes ($^{sp}T_{15}$-A_{15}:T_{15}). Simulations based on the EPR spectra after annealing revealed a larger rotational correlation time compared to duplexes, which was expected. It should be noted however, that the EPR spectra at 0 °C for duplex and triplex look very similar (Fig. 27 C and E) and the difference in correlation times is the result of using a two-species fit for the triplexes, while a one-species fit resulted in a similar correlation time as for the duplexes. Afterwards, the samples were warmed to room temperature, where the triplexes are not stable, shown by melting curve measurements. The EPR spectra that were measured at 25 °C then corresponded to the spectra of the single stranded DNA (Fig. 27 B and F), showing that the spin labeled strand was the Hoogsteen base-paired strand and no strand exchange had occurred during annealing.
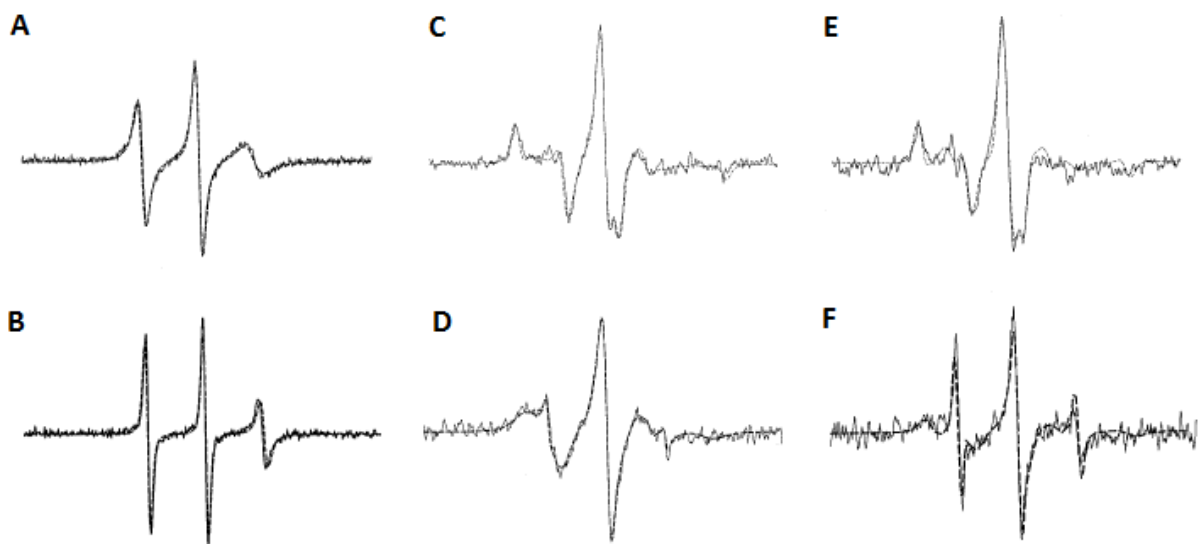

Fig. 27: CW EPR spectra of the single strand $^{5sp}T_{15}$ at 0 °C (A) and 25 °C (B), the duplex $^{5sp}T_{15}$:A_{15} at 0 °C (C) and 25 °C (D) and the triplex $^{5sp}T_{15}$-A_{15}:T_{15} at 0 °C (E) and 25 °C (F). The spectrum F closely resembles the spectrum B, which shows that $^{5sp}T_{15}$ has dissociated from the triplex. The solid lines are experimental spectra, the dashed lines are simulations. The figure was taken from [146].

In a different study, an RNA sequence called TL1, which contains a GAAA tetraloop was spin-labeled and mixed with various concentrations of an RNA called TLR, which contains a GAAA tetraloop receptor, and the binding confirmed by an increase in the correlation times determined from EPR spectra simulations[99]. Much smaller changes were observed when a mutated version of TL1 with a UUCG tetraloop was used, which confirms that the spectral changes were due to specific binding of TL1 to TLR (Fig. 28). Subtraction of the EPR spectra of free TL1 from the spectra of the TL1/TLR complex allowed for determination of the fraction of free TL1 at various concentrations of TLR, which was used to calculate the dissociation constant K_d of the complex. It was found to be significantly

smaller compared to the UUCG mutant, which further confirmed the specific binding of TL1 to TLR. Further measurements at different concentrations of MgCl₂ revealed a strong dependence of the binding on the magnesium concentration, where the fraction of unbound TL1 in the absence of magnesium was similar to that of the UUCG mutant. This study thus demonstrated the suitability of EPR for investigations of complex formation.

Fig. 28: (A) Structures of TL1 and TLR. The tetraloop and receptor are marked with dashed boxes. R is the spin label attached to the backbone of TL1 (B) CW EPR spectra of TL1 in the absence (dotted line) and presence (solid line) of 1.75 mM TLR and the difference spectrum obtained from subtracting them (dashed line). The inset shows the high-field section of the spectrum enlarged. (C) CW EPR spectra of a TL1 mutant with a UUGC tetraloop in the absence (dotted line) and presence (solid line) of 1.75 mM TLR. The figure was taken from [99].

Not only the motions of the molecule as a whole have an effect on the EPR spectra. It was also shown that the mobility of the nucleosides where the spin label is attached can be determined from EPR[103]. The well-characterized trans-activation responsive (TAR) region from HIV RNA, which plays an important role for the replication of the virus, was chosen as a test system. It was spin-labeled in four different positions. The EPR spectra of compounds where a base-paired nucleotide (U38 and U40) was labeled were significantly broader than those of compounds where an unpaired nucleotide in a loop (U23 and U25) was labeled, which show mobility similar to a single strand (Fig. 29). It was thus shown that CW EPR spectroscopy can report on local structure and dynamics.

Fig. 29: (A) Structure of the TAR RNA highlighting the four uridines which were spin-labeled. (B) CW EPR spectra of TAR RNA spin-labeled in different positions. The arrows mark the high and low field extrema of the spectra. The figure was taken from [103].

1.4.2 PELDOR spectroscopy

While CW EPR spectroscopy can provide some insight into the structure and dynamics of nucleic acids, pulsed EPR techniques have become more important. The best example for these is pulsed electron-electron double resonance (PELDOR) spectroscopy, also known as double electron-electron resonance (DEER)[147, 148]. It enables distance measurements between two spin labels which are sufficiently close together, about 1 - 10 nm[149] compared to about 2 nm which can be measured by CW EPR. If the labels are rigid enough, information about their relative orientation can also be obtained[150]. PELDOR was first performed as a three-pulse experiment but towards the end of the last century an improved four-pulse PELDOR was developed (Fig. 30)[151, 152].
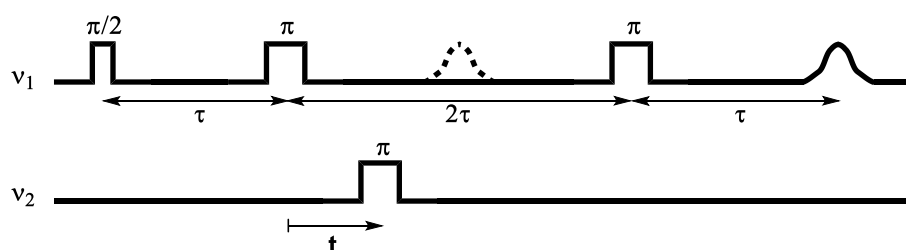
Fig. 30: Pulse sequence of a four-pulse PELDOR experiment.

This starts with a Hahn-echo sequence at frequency ν_1, called observe frequency. A $\pi/2$ pulse causes the spins to flip by 90°, causing them to rotate around the z-axis. They do this at a different speed, causing them to dephase. This is followed by a π pulse after an evolution time τ, which flips them by 180°, causing them to refocus after another time τ, resulting in an echo signal (Fig. 31), after which the spins start dephasing again. The echo is then refocused by another π pulse after the time 2τ after the first one, which leads to the PELDOR signal with amplitude V after another evolution time τ.
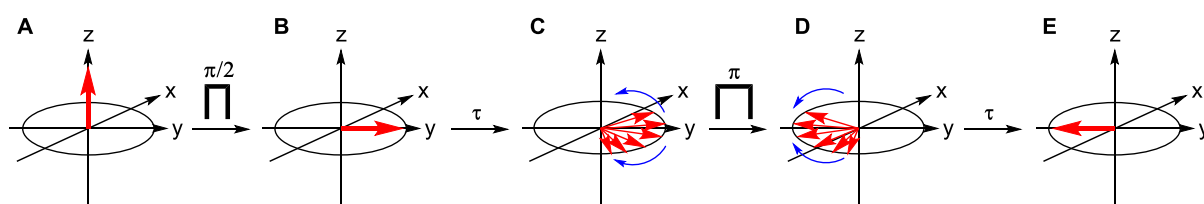

Fig. 31: Spin vector diagrams during a Hahn-echo sequence. (A) Initially the spins are aligned to the z-axis. (B) The $\pi/2$ pulse flips the spins by 90° onto the y-axis. (C) The spins start rotating in the x-y-plane (blue arrows) with different speed, causing them to dephase. (D) The π pulse flips the spins by 180° in the x-y-plane. The spins continue to rotate. (E) Because the slower spins are now ahead of the faster ones, the spins will refocus along the y-axis after the time τ, causing a detectable echo signal.

This signal is modulated by a π pulse of a second frequency ν_2, called pump frequency. If the two labels are close enough to have significant dipolar interactions, the inversion of the spins of one label will affect the spins of the other, which reduces the amplitude V of the PELDOR signal. The time t at which this pulse is applied is varied, which leads to different amplitudes of the PELDOR signal as a

function $V(t)$ of the pulse time, which oscillates with the dipolar coupling frequency v_{dd}. The distance that can be measured with PELDOR depends on the maximum value of t[87]. Since t in a four pulse PELDOR experiment ranges from the first π pulse to the second, a longer time 2τ between the pulses allows for a larger t, so τ should be as large as possible. However, the length of τ is limited by relaxation of the spins. How fast relaxation occurs depends on the phase memory time T_m, so a longer T_m enables determination of longer distances. This is the reason why PELDOR with nitroxides is mostly done with frozen samples, where T_m is longer than at room temperature. The main advantage of the four-pulse PELDOR experiment over the older three-pulse version is that the range of t starts at τ rather than 0, allowing the initial data points to be obtained, which would be lost in the three-pulse experiment due to the length of the pump π pulse. $V(t)$ contains both an intermolecular $V_{inter}(t)$ and an intramolecular part $V_{intra}(t)$. $V_{inter}(t)$ can be represented by a monoexponential decay function and subtracted from $V(t)$ to obtain $V_{intra}(t)$ (Fig. 32 A and B).
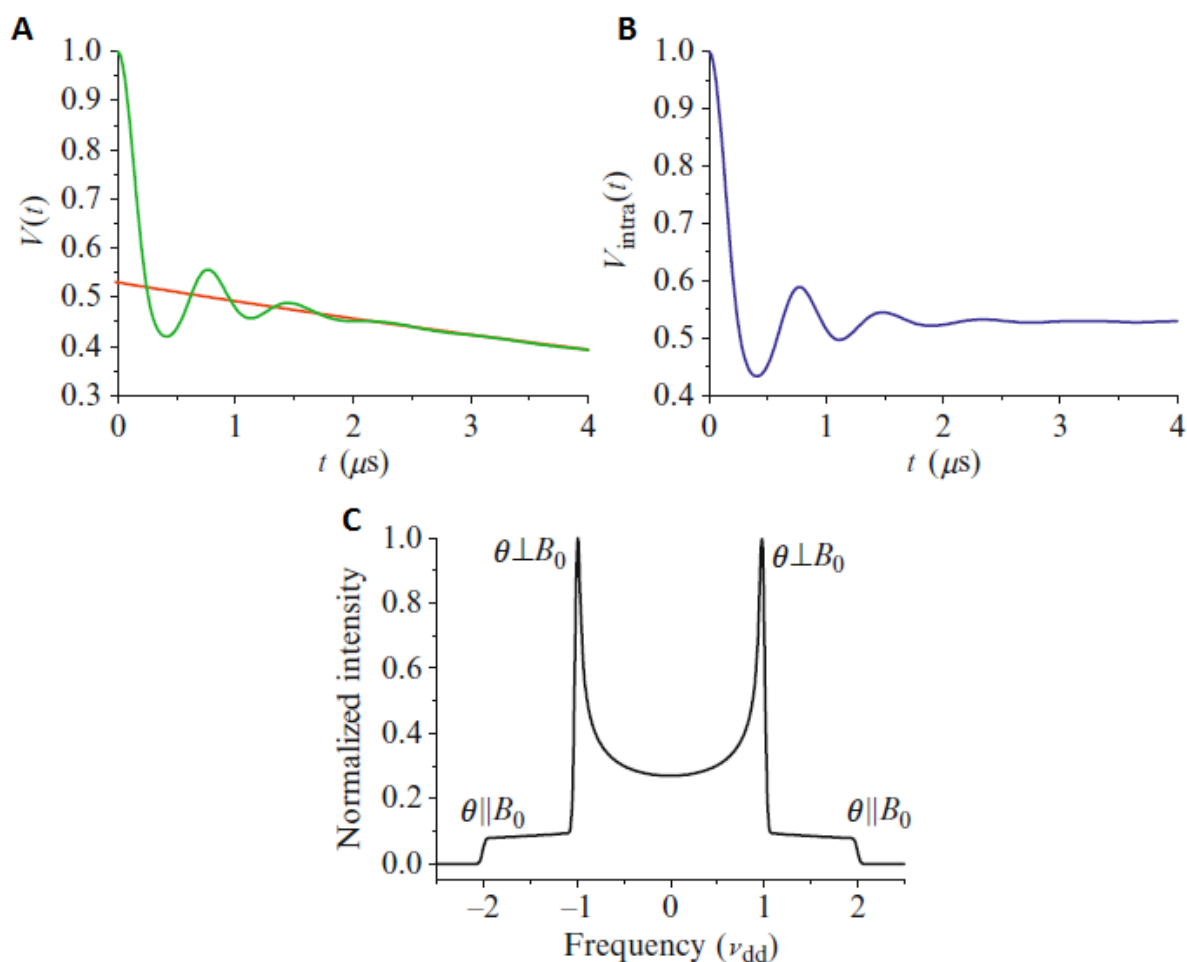

Fig. 32: (A) PELDOR signal V as a function of time t (green) and intermolecular part $V_{inter}(t)$ as a monoexponential decay (red). (B) Intramolecular PELDOR signal $V_{intra}(t)$ obtained by subtracting $V_{inter}(t)$ from $V(t)$. (C) Pake pattern obtained from Fourier transformation of $V_{intra}(t)$. Peaks represent perpendicular alignment of the interspin vector r_{AB} and the external magnetic field B_0, edges represent parallel alignment. The figure was adapted from [147].

This function is then Fourier-transformed to obtain the so-called Pake pattern, from which the dipolar frequency at perpendicular aligment of the interspin vector r_{AB} and the external magnetic field B_0 can be determined (Fig. 32 C). The relationship between ν_{dd} and r_{AB} is given by the following equation

$$\nu_{dd} = \frac{\mu_0 \hbar \gamma_A \gamma_B}{4\pi r_{AB}^3}(1 - 3\cos^2\theta)$$

where μ_0 is the vacuum permeability, $\hbar$ is the reduced Planck constant, γ_A and γ_B are the gyromagnetic ratios of the two spins and θ is the angle between r_{AB} and B_0. For perpendicular alignment of r_{AB} and B_0, the equation can be written as

$$r_{AB}(\mathrm{nm}) = \sqrt[3]{\frac{52.16}{\nu_{dd\perp}(\mathrm{MHz})}}$$

allowing for the calculation of r_{AB}. The process of PELDOR data is usually done by software lke DeerAnalysis2006, based on Tikhonov regularization[153]. Recently, an even newer version of PELDOR with a Carr-Purcell sequence, called seven-pulse-CP-PELDOR was developed, mainly for membrane proteins with a short relaxation time[154].
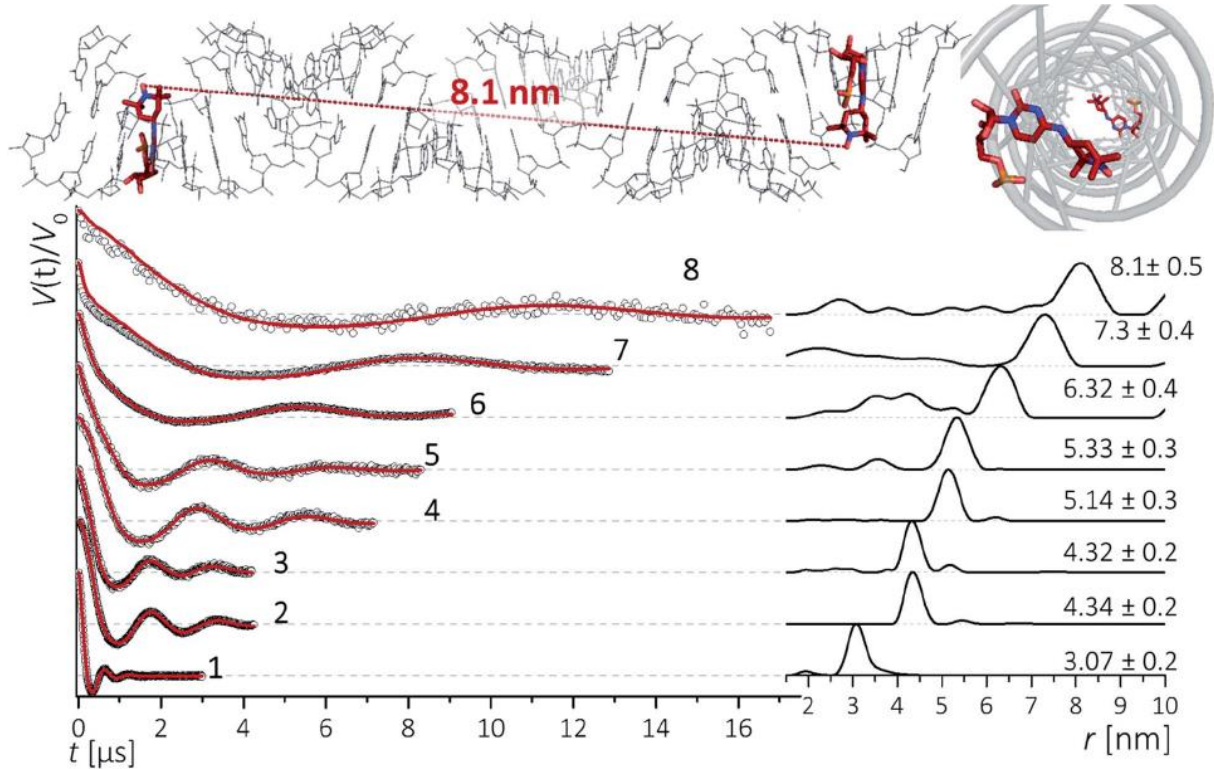

Fig. 33: Background-corrected PELDOR time traces of eight different samples with the spin labels 10 to 28 bp apart (bottom left) the distances derived from these time traces (bottom right) and visual representations of duplex 8, from side and front, with 28 bp distance between the labels (top). The figure was taken from [149].

This technique makes use of even more pulses to refocus the echo multiple times, thereby allowing for a longer detection time.

PELDOR has found many applications on nucleic acids in recent years. It was shown that PELDOR distances between two C^{TEMPO} labels in an RNA duplex or hairpin allow for easy determination of the number of base pairs (bp) between the spin labels in an A-form duplex[149]. Spin label distances in seven different duplexes und one hairpin were measured, in which the spin labels were 10 to 28 bp apart (Fig. 33). C^{TEMPO}, despite not being itself very rigid, allowed for accurate distance measurements due to nitroxide motion being restricted inside the duplex. In contrast to other flexible labels, which result in broader distance distributions that are harder to interpret, for C^{TEMPO}, a linear correlation between the distance and the number of base pairs between the labels was observed. The rigidity of C^{TEMPO} was confirmed by MD simulations, which showed only two spin label conformations in the RNA which resulted in similar distances between the nitroxides. Thus, C^{TEMPO} was shown to be well suited for PELDOR measurements in duplex RNA with high accuracy. A similar study, using the rigid spin label Ç, was also done on DNA duplexes[155].

PELDOR measurements, especially with nitroxides, have usually been done with frozen samples, as relaxation is too fast at room temperature and the dipolar interactions are averaged by molecular motions. A recent publication showed that Ç is rigid enough to enable PELDOR measurements at room temperature[156]. A 20 bp DNA duplex with two Ç labels was immobilized on Nucleosil silica beads. This immobilization enabled PELDOR measurements at room temperature. When measuring frozen samples, the authors found that the Nucleosil beads dampened the time traces compared to a non-immobilized sample. However, at room temperature this dampening was lessened (Fig. 34).
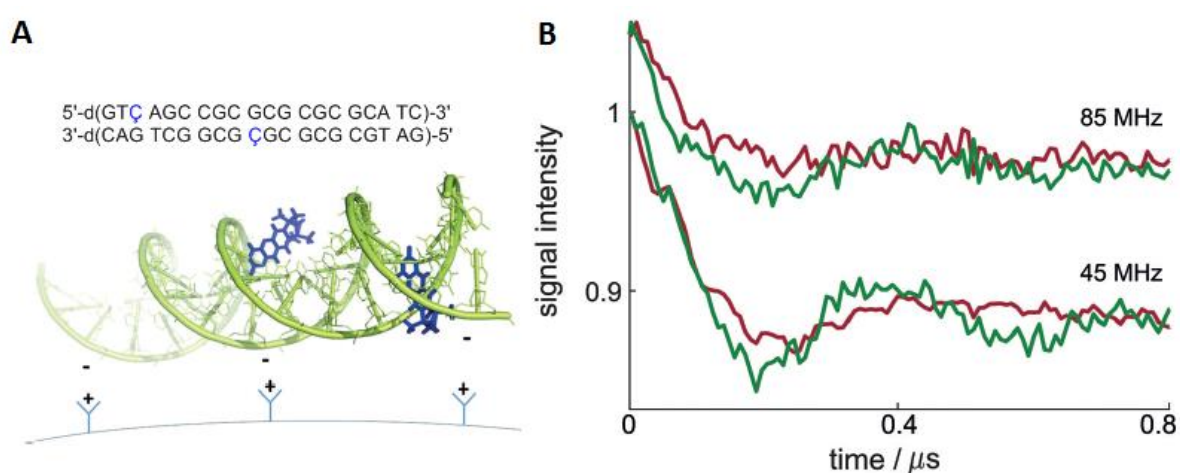

Fig. 34: (A) Sequence and structure of the DNA duplex immobilized on Nucleosil beads and (B) PELDOR time traces at different frequency offsets at 50 K (red) and 295 K (green). The figure was adapted from [156].

This suggests that the dampening was due to interactions between the DNA and the Nucleosil, which caused the DNA to adopt more conformations than it normally would. At room temperature, these conformations would be averaged due to fast motions of the DNA. The ability to perform PELDOR experiments at room temperature is a significant advantage of rigid spin labels over more flexible ones and shows that rigid spin labels are a research topic that should be pursued further.

Most PELDOR experiments are done on samples in buffered solutions. While these experiments can provide valuable results, studying biomolecules under biological conditions is a desirable goal. A recent PELDOR study investigated the structure of RNA in cells[157]. The conformationally unambiguous label E[Im]Um was used in a 20 bp RNA duplex for PELDOR measurements in a buffered solution and in *xenopus laevis* oocytes. The result was a reduction of spin label distance by about 3 Å in the cells compared to the solution. To determine the reason for this change, further PELDOR measurements were made in cytoplasmic extract and a concentrated solution of the protein lyzozyme (Fig. 35). The distance in the cell extract was the same as in the buffered solution, probably due to dilution reducing the interactions of different cell components. The distance measured in the lyzozyme solution showed a reduced distance like the in-cell measurement. When bovine serum albumin was used instead of lyzozyme, no distance reduction was observed which suggests that unspecific binding of the positively charged lyzozyme to the RNA was the reason. The implication is that such interactions are also the reason for compaction of the RNA in the cells. The results agree with MD simulations, which also predicted a small compaction in lyzozyme solution. This study could represent a major step towards establishing EPR spectroscopy as a tool for investigation of nucleic acids under in vivo conditions.
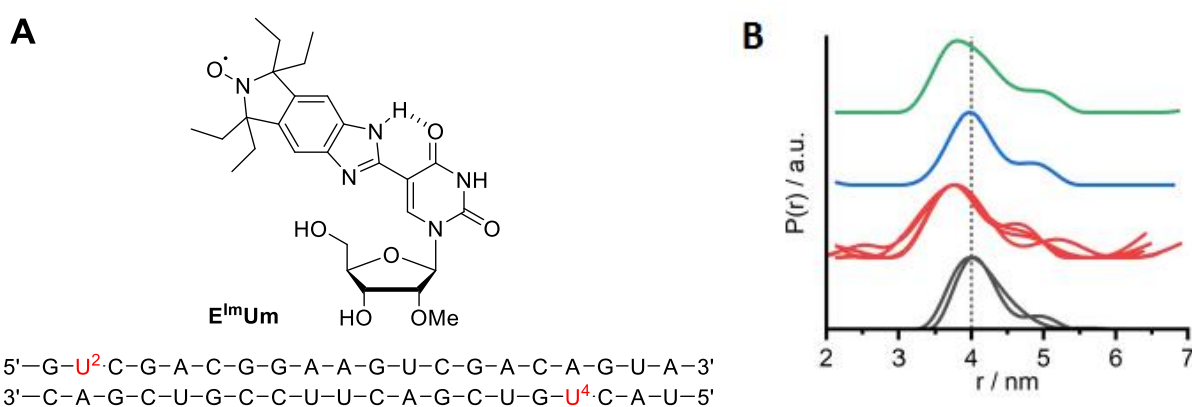

5'—G—U^2·C—G—A—C—G—G—A—A—G—U—C—G—A—C—A—G—U—A—3'
3'—C—A—G—C—U—G—C—C—U—U—C—A—G—C—U—G—G—U^4·C—A—U—5'

Fig. 35: (A) Spin label E[Im]Um and the sequence of the RNA in which it was incorporated. Red nucleotides mark the positions of the spin labels. (B) PELDOR distance distributions from the RNA in phosphate buffer solution (black), *xenopus laevis* oocytes (red), cytoplasmic extract (blue) and 200 mg/ml lyzozyme solution (green). Multiple lines represent multiple measurements. Figure B was taken from [157].

Another field where PELDOR spectroscopy has been applied was the study of interactions between nucleic acids and proteins. An extensive study on PELDOR experiments with RNA-binding domains

(RBDs) of a protein and short RNA fragments was done in 2017[158]. The authors tested different spin labels, both nitroxides and Gd(III)-labels in terms of their labeling efficiency and the agreement of PELDOR data obtained with them with predicted distances. For this, they analyzed nitroxide-nitroxide, Gd-Gd and nitroxide-Gd spin label pairs (Fig. 36). They conclude that nitroxides are generally preferable to Gd labels, because the experimentally obtained distances are more similar to the predictions when nitroxides are used. Another argument for this is that the larger Gd-complexes can have a larger influence on the structure than the smaller nitroxides. However, they also mention that Gd labels can be preferable to nitroxides if NMR data can be used in combination with the PELDOR experiments, or if orthogonal labeling is required, where both nitroxides and Gd labels are used together.
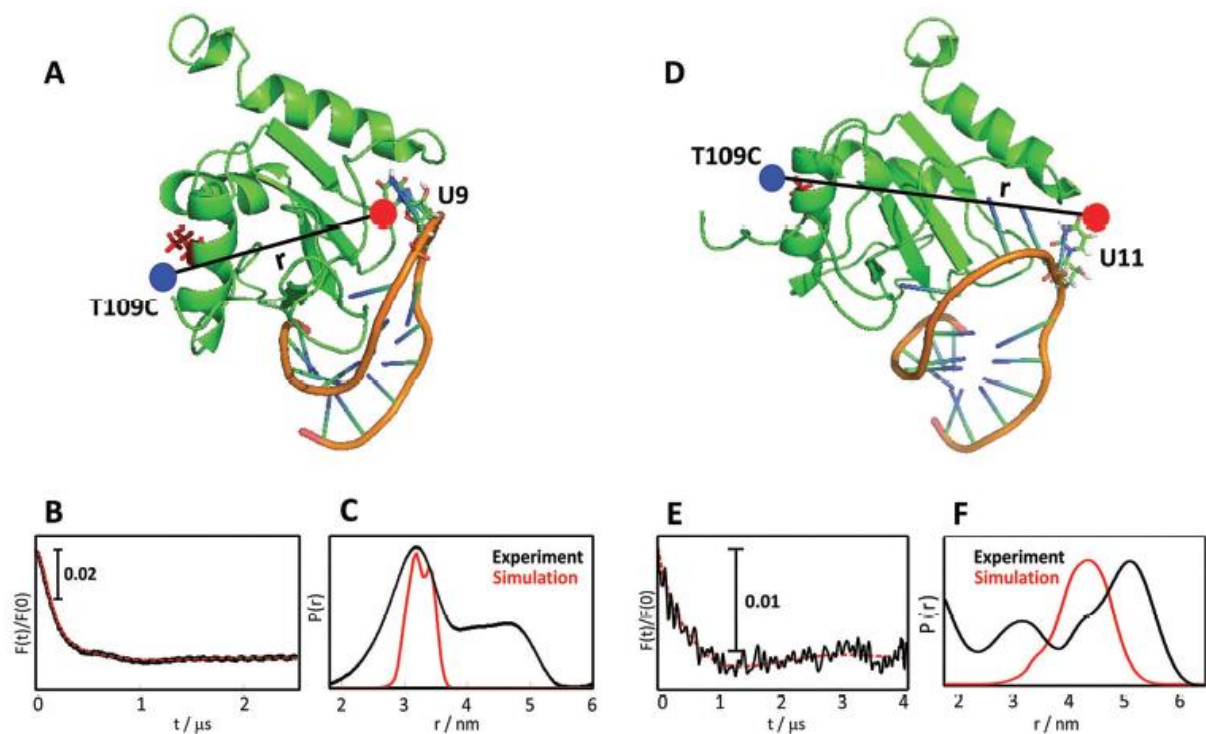
Fig. 36: (A and D) Structures of the RBD1/SL-E complexes with the protein labeled with a Gd(III) label (blue dot) and the RNA labeled with a nitroxide label (red dots) in two different positions. (B and E) PELDOR time traces of the complexes. (C and F) Distance distributions obtained from PELDOR spectroscopy of the two complexes (black) and simulations (red). The figure was taken from [158].

The approach of using orthogonal spin labels was taken further in another publication[159]. Here, the *antennapedia* homeodomain, labeled at different positions with a Gd and a Mn label, in complex with its cognate DNA binding site labeled with a nitroxide was used to show the possibility of selectively measuring one of three different distances by PELDOR spectroscopy. By selecting the PELDOR pulse frequencies depending on which labels they want to excite, the authors claim they were able to selectively obtain three distinct distances (Fig. 37). However, there is a problem with this claim. There is a minor peak which appears in the measurement of the Mn-Gd distance without the DNA in the distance distribution slightly above 4 nm (Fig. 37 B black). In the measurement where

the DNA is present, this peak is shifted to 4.5 nm (Fig. 37 B red), which is the same as the nitroxide-Mn distance (Fig. 37 B magenta). It is therefore not possible to say whether this peak is just the minor peak of the Mn-Gd distance or if the nitroxide-Mn distance is visible in this spectrum. The same peak also appears in the measurement of the nitroxide-Gd distance (Fig. 37 B blue), which further speaks for the nitroxide-Mn distance to be visible in experiments where it should not be. The spin labels thus appear as if they might not be completely orthogonal. Further experiments would be required to prove the orthogonality. This might become a useful method if it can be fully developed.
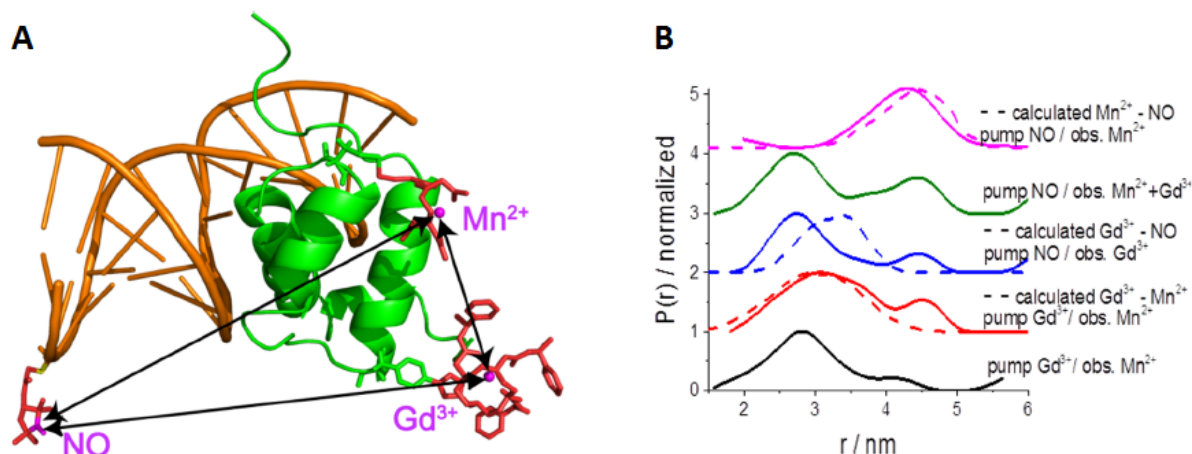
Fig. 37: (A) Structure of the *antennapedia* homeodomain, labeled at different positions with a Gd and a Mn label, in complex with its cognate DNA binding site labeled with a nitroxide and (B) distance dirstributions obtained by PELDOR spectroscopy. Only the homeodomain (black), full complex with the protein only labeld with the Mn label (magenta) and the complex with three labels present (green,blue,red). Dashed lines indicate calculated distances. The figure was taken from [159].

Recently, PELDOR was used to study human apurinic/apyrimidinic endonuclease 1 (APE1), an enzyme involved in base-excision repair, which cleaves DNA at apurinic/apyrimidinic (AP) sites[160]. A 12 bp DNA duplex was labeled with TAM spin labels at one or both ends, while a mutant of APE1, APE1N212A, which can bind DNA with the same efficiency as the wild type but has significantly lower cleavage activity, was labeled with three nitroxides. This gave the authors seven different systems to study (Fig. 38). They first determined the distance between the trityl labels at the ends of the duplexes in systems I-III. They found that an AP site causes the distance to become smaller, which may be the result of bending of the DNA, but previous studies suggest that it results from a part of the duplex around the AP site collapsing, because the AP site and the opposite nucleotide flipping outside the helix. They also studied the DNA cleavage by APE1 with PELDOR. Since cleavage of the DNA results causes the trityl labels to end up in different fragments, they can no longer interact which leads to the reduction of the modulation depth of the PELDOR signal. Measurements at different time points allowed the generation a kinetic curve. The authors then investigated the structures of the APE1N212A/DNA complex with undamaged and damaged DNA, by measuring the distances of the trityl labels on the DNA and the nitroxides on the enzyme by PELDOR spectroscopy.

The presence of the AP site did not result in any significant change to the distance when the trityl label was on the 5'-end of the damaged strand, but when it was on the 5'-end of the complementary strand, a significant change in the distance from damaged to undamaged DNA was observed. These results were shown to be in good agreement with MD simulations and the x-ray crystal structure, which show bending of damaged DNA in complex with the enzyme and flipping of the AP site outside the helix into a binding pocket of the enzyme. Therefore this study is another example for the applicability of EPR for investigations into structure and dynamics of nucleic acids.
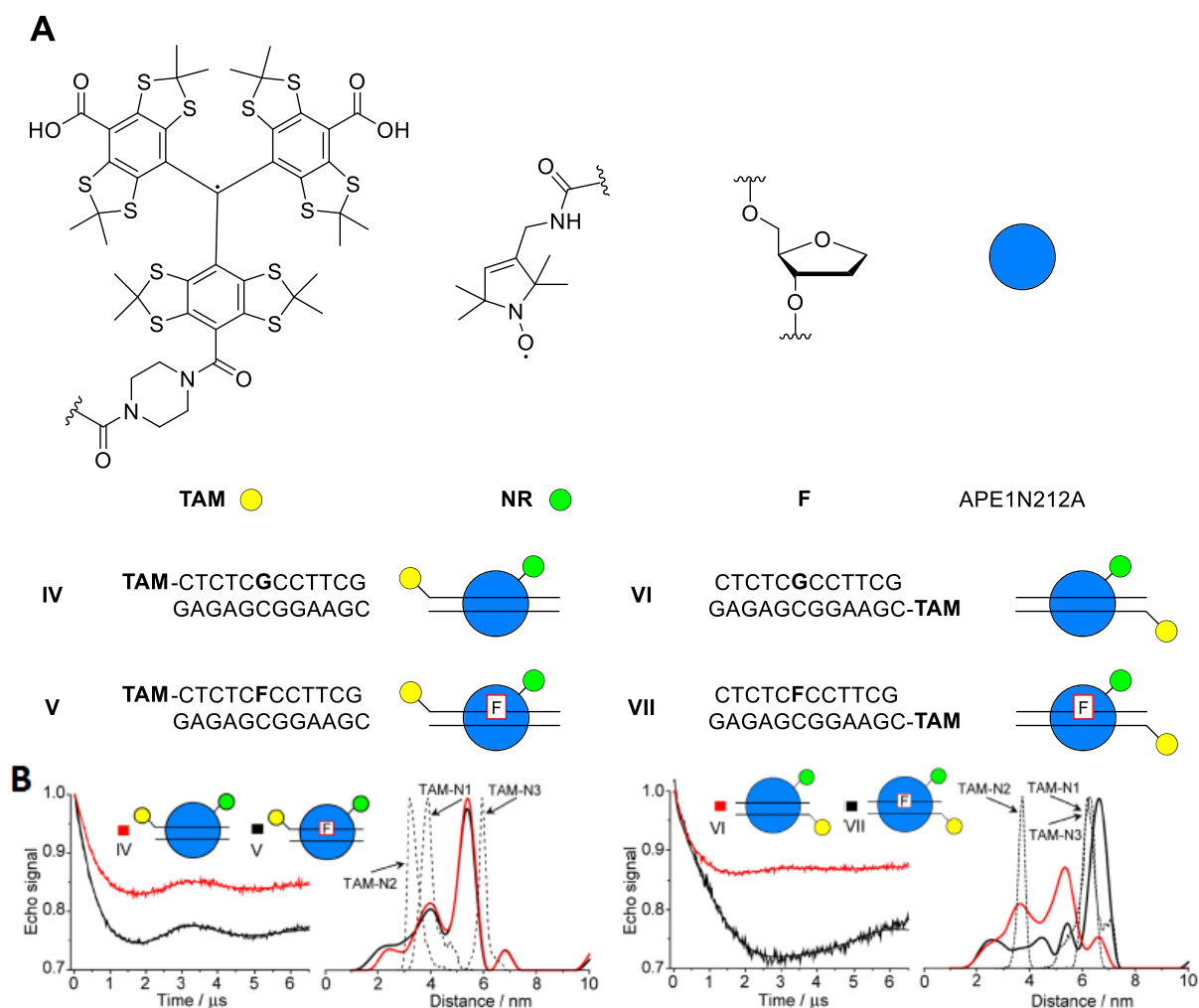
Fig. 38: (A) Structures of spin labels TAM (yellow dot) and NR (green dot), as well as 3-hydroxy-2-hydroxymethyl tetrahydrofuran (F) used as an AP site (top). Sequences of DNA duplexes IV-VII and schematic representations of their complexes with the mutant enzyme APE1N212A (blue dot) (bottom). (B) PELDOR time traces and distance distributions for TAM-nitroxide distances (IV-VII) (right). Dashed lines indicate distances determined from MD simulations. N1-N3 are the three different nitroxides in the enzyme. The figure was adapted from and reproduced based on [160].

Another recent study investigated the interaction of short RNAs with the 40S subunit of the human ribosome[161]. A short 11 nt RNA (MR11) was labeled with nitroxide labels at both ends (Fig. 39 A). PELDOR measurements of the free RNA resulted in a short distance, which fits structure predictions. When the 40S ribosomal subunit was present, a longer distance was obtained, which fits with an

extended structure of the RNA, as a result of binding to the ribosome. This result did not change when the mRNA binding channel was occupied by a 19 nt mRNA, held in place by interaction with a tRNA, showing that MR11 does not bind there (Fig. 39 B). PELDOR measurements with the analogous DNA sequence (MD11) did not result in any differences between the presence and absence of the 40S subunit, which the authors attribute to the B-type helix adopted by DNA, which might fit worse to the amino acids in the binding region compared to the A-type helix of RNA (Fig. 39 C). In order to gain information about the binding site for small RNAs, the authors fixed the 19 nt mRNA, now modified with a spin label at the 3'-end, in the mRNA binding channel and investigated the binding of a 9 nt RNA, also modified with a single spin label at the 3'-end. This did result in a distance of about 3.6 nm, but the distribution was fairly broad. Therefore, the binding of the small RNA does take place close to the mRNA channel in a variety of different positions. The importance of the peptide 55-64 of the ribosomal protein uS3 for RNA binding was investigated as well. This peptide can be cross-linked with RNA, so its involvement in RNA binding was assumed.
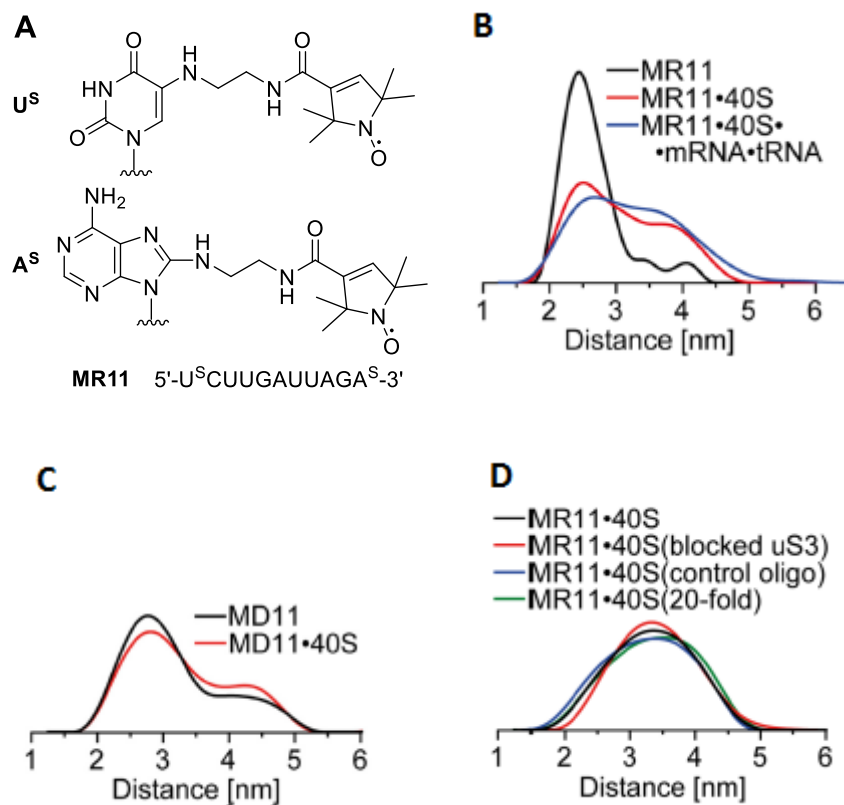

Fig. 39: (A) Structure of spin labels US and AS and sequence of MR11. (B-D) PELDOR distance distributions. (B) MR11 (black), MR11 and the 40S subunit (red), MR11 and the 40S subunit containing an mRNA strand in the mRNA channel fixed by a tRNA strand (blue). (C) MD11 (black), MD11 and the 40S subunit (red). (D) MR11 and the 40S subunit (black), with the uS3 protein locked by cross-linking with a 9 nt RNA (red), with a non-crosslinked control RNA (blue) and with the unmodified MR11 in 20-fold excess (green). The figure was adapted from [161].

However, PELDOR measurements of MR11 in the presence of the 40S subunit with a 9 nt RNA cross-linked to the 55-64 peptide revealed that binding did still take place unhindered, so the peptide 55-64 does not seem to be important for RNA binding (Fig. 39 D). It was also shown that no reduction in binding efficiency is visible when the unmodified version of MR11 was added, even in 20-fold excess over MR11. The authors attribute this to hydrophobic interactions between the spin labels and the 40S subunit which increase the binding affinity (Fig. 39 D). In conclusion, the authors speculate that the binding site might be used to queue up mRNA which is to be translated in front of the ribosome's mRNA entry site.

A few months ago, PELDOR spectroscopy was used to provide support for the proposed mechanism of the guanidine-II riboswitch[162]. This riboswitch is part of the family of riboswitches that control the expression of genes depending on the guanidine concentration in a bacterial cell. The guanidine-II riboswitch is fairly small, consisting of two stem loops (P1 and P2), which are connected by 7-40 nucleotides. A mechanism for translation initiation was proposed, by which the Shine-Dalgarno sequence, which is normally base-paired and thus inaccessible for the ribosome, becomes accessible due to a change in structure of the riboswitch where the stem loops adopt a kissing loop motif upon binding of two guanidinium cations (Fig. 40 A). This mechanism is based on in-line probing and fluorescence measurements. Also, several crystal structures of kissing loop dimers exist (e.g. Fig. 40 B), but so far, only homodimers of either the P1 or the P2 stem loop are known, the formation of the heterodimer has not been validated yet. In order to change this, the separate P1 and P2 strands were spin-labeled at one position each by attaching an azido-modified isoindoline nitroxide to 5-ethynyl-2'-deoxyuridine residues by copper-catalyzed click reaction (Fig. 40 C). Two oligonucleotides, P_1^{U18} and P_2^{U14}, were initially used for PELDOR experiments. When the strands where measured separately, formation of the respective homodimers in presence of guanidine could be confirmed by comparing the obtained distances with predictions based on the known crystal structures. However, when a mixture of P_1^{U18} and P_2^{U14} was measured, presence of the heterodimer could not be confirmed, because the predicted distances are so close together that the experimentally obtained distance could be a mixture of hetero- and homodimers. To solve this problem, the authors used a different oligonucleotide, P_1^{U20}, with the spin label in a different position further away from the loop. With a mixture of P_1^{U20} and P_2^{U14}, three distances, corresponding to both homodimers and the heterodimer, could be measured, thereby proving the formation of the heterodimer (Fig. 40 F). However, all dimers were present only in a statistical mixture, without any preference for the heterodimer. Further experiments should be done on a complete riboswitch to investigate whether intramolecular formation of the kissing loop structure can be confirmed and if there is a bias towards forming it compared to intermolecular dimers.
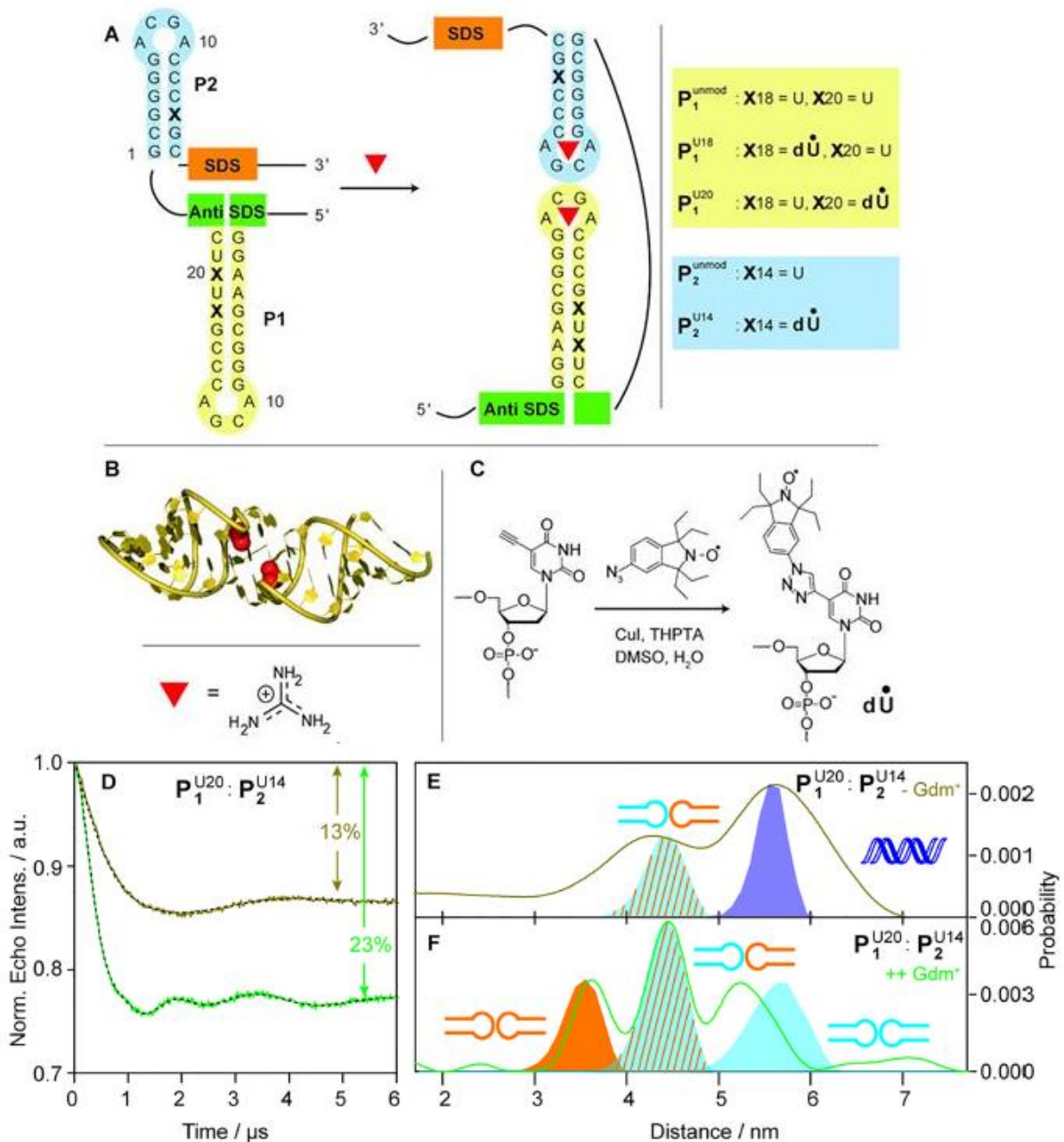
Fig. 40: (A) Proposed switching mechanism of the guanidine-II riboswitch with the base-paired Shine-Dalgarno-sequence (SDS) (left) and in the kissing loop structure with two guanidinium ions bound in the loops where the SDS is accessible by the ribosome (right). The spin-labeled positions are marked as X. **(B)** Crystal structure of the P1 homodimer and structure of the guanidinium cation. **(C)** Reaction scheme for the labeling of 5-ethynyl-2'-deoxyuridine by CuAAC. **(D)** Background corrected PELDOR time traces for a 1:1 mixture of P_1^{U20} and P_2^{U14} in the absence (olive) and presence (green) of 40 mM guanidinium and their fits (black dots). **(E and F)** Distance distributions derived from the time traces in D. Colored areas below the peaks represent predicted distance distributions (blue: P_1^{U20} duplex, cyan: P_1^{U20} homodimer, orange: P_2^{U14} homodimer, cyan with orange stripes: P_1^{U20} P_2^{U14} heterodimer). The structures assigned to the peaks are shown schematically. The figure was taken from [162].

The examples presented here demonstrate the wide range of applications for which EPR spectroscopy can be used. Its importance for investigations into nucleic acids has increased over the last decades and will certainly increase even more in the future, especially due to the ongoing development of rigid spin labels for precise determination of distances. The development of more rigid spin labels to add to their still fairly small number is therefore a desirable goal. This thesis will

contribute to this by presenting three new rigid spin labels for use in EPR spectroscopy on nucleic acids.

2 Aim of this work

Rigid spin labels still hold a lot of potential for future research. One of the factors limiting the applicability of the PELDOR technique on nucleic acids is the limited number of rigid spin labels available. While Ç[115] is already well established and isoxyl-A[119] also holds great promise, analogs for guanosine and thymidine/uridine have not been produced yet. Additionally, while Çm[117] exists as a version of Ç for RNA, unmodified ribose as a natural analog would be preferred over the artificial 2'-O-methylribose.

Therefore, this work aims to add several new compounds to the family of rigid spin-labeled nucleoside analogues (Fig. 40).

Benzi-spin (**1**) is based on the benzi-nucleoside (Fig. 41 left), which has been shown to form a base pair with O-6-methylguanosine (m[6]G)[163]. The difference between benzi-spin and other rigid spin labels, like the Ç family, is that benzi-spin is not designed to mimic the base pairing of a canonical nucleoside. Instead, it is supposed to interact with a variety of different nucleosides in a way that results in enough rigidity for PELDOR experiments. Such a universal[164] spin label should prove useful for nucleic acid structure determination.

The idea for lumi-spin (**2**), named after lumichrome, was a result of trying to find a more efficient synthetic route for a Ç-like spin label. The synthetic route of Ç contains certain steps which are problematic, like a nitration which results in a significant amount of an unwanted isomer or a ring closing step which takes multiple days to complete[115]. It was thus considered worthwhile to pursue the synthesis of a similar compound, resulting in lumi-spin. It features a similar structure to EÇ[118] which should result in similar rigidity. The main difference is the position at which the ribose is attached, which results in a different hydrogen bonding pattern due to the different orientation of the nucleobase in a duplex. Lumi-spin has the same Watson-Crick site as uridine, but it needs to be determined whether it might be usable as a uridine analogue, because steric clash between the expanded ring system and the phosphate backbone might cause the duplex to be perturbed to an extent where base pairing is no longer possible. In addition to its use as a uridine analog, there are other possible applications for it as well. G-quadruplexes for example, are a structural motif which has been studied by a fluorescent pteridine probe[165]. Since the lumi-spin nucleobase is essentially an expanded pteridine-2,4-dione, it should be possible to incorporate it into G-quadruplexes, thus enabling the possibility to gain information about them by EPR spectroscopy.

Finally, EÇr (**3**) was prepared as a new version of EÇ for RNA, which has a free 2'-OH group. EÇ was chosen rather than Ç because of the increased stability of the nitroxide radical resulting from ethyl groups adjacent compared to methyl groups. So far, rigid spin labels have mostly been incorporated

by solid phase synthesis, which comes with several limitations. Enzymatic incorporation could offer an interesting alternative, which has been used only rarely so far[132, 135]. Thus, the EÇr triphosphate was prepared and used in primer extension experiments to probe the feasibility of this approach.
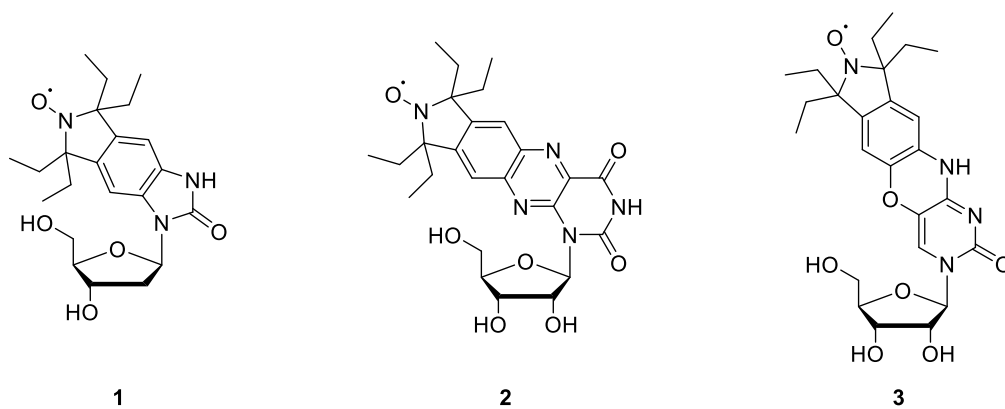

Fig. 41: Spin labels benzi-spin, lumi-spin and EÇr

3 Results and discussion

3.1 Universal rigid spin label benzi-spin

3.1.1 Initial design

Benzi-spin is based on the benzi nucleoside (Fig. 42 left), which was used to detect *O*-6-methyl-2'-deoxyguanosine (m^{6}G) in the K-Ras gene[163]. This was done by extension of a benzi-modified primer with KlenTaq polymerase, where benzi was placed opposite to either unmodified guanosine (G) or m^{6}G in the template. The authors found that extension only happens when benzi is opposite to m^{6}G, which they consider to be the result of different base pairing behavior. In m^{6}G, unlike G, the N1 is a hydrogen bond acceptor rather than a donor and can thus form a hydrogen bond with the N3 of benzi, which is not possible in case of G. In an earlier study, the authors had investigated the melting temperatures of several 15-mer DNA duplexes containing the benzi nucleoside[166]. The melting temperatures of duplexes containing a C:G, benzi:G or benzi:m^{6}G base pair were determined as 64.3 °C, 54.0 °C and 58.6 °C respectively. The benzi:m^{6}G base pair being more stable than benzi:G, but less stable than the canonical pair, would be consistent with benzi's suggested base pairing behavior. Benzi-spin is a nitroxide-modified version of the benzi nucleoside, to be used as a rigid spin label. Spin labels of different rigidity show differences in their EPR spectra when incorporated at the same position, because more rigid labels show increased sensitivity to their environment[117, 119]. Benzi-spin might be expected to behave similarly to the benzi nucleoside with respect to base pairing, where it should be more stable when paired with m^{6}G compared to G (Fig. 42). However, the additional destabilizing effect of the sterically demanding ethyl groups might lead to reduced discrimination between different partners, as local perturbation of the duplex structure, which disrupts base pairs, should have a larger effect on stable base pairs compared to those that are already weak. Benzi-spin might therefore be usable as a universal spin label, which does not depend on the identity of the opposing nucleoside for its rigidity, and could be used in different sequences without the need for a specific base pairing partner.
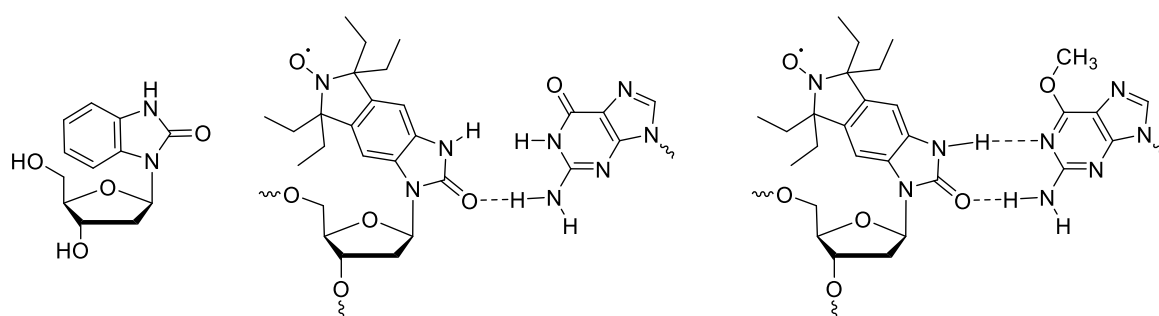

Fig. 42: Benzi nucleoside (left) and base pairing between benzi-spin and guanosine (center) or m^{6}G (right).

The benzi-spin nucleobase should be accessible by reacting diaminoisoindoline compound **8** with 1,1'-carbonyldiimidazole (CDI), followed by attachment of the sugar. At this point, the nitroxide could be introduced by oxidation, prior to sugar deprotection and subsequently turned into phosphoramidite **4** for solid phase synthesis (Fig. 43). Initially, benzi-spin was designed with methyl groups instead of the ethyl groups, because methyl groups had been used for most rigid spin labels up to that point, but this was changed because ethyl groups provide more stability to nitroxides as well as providing advantages during synthesis, which will be explained later.
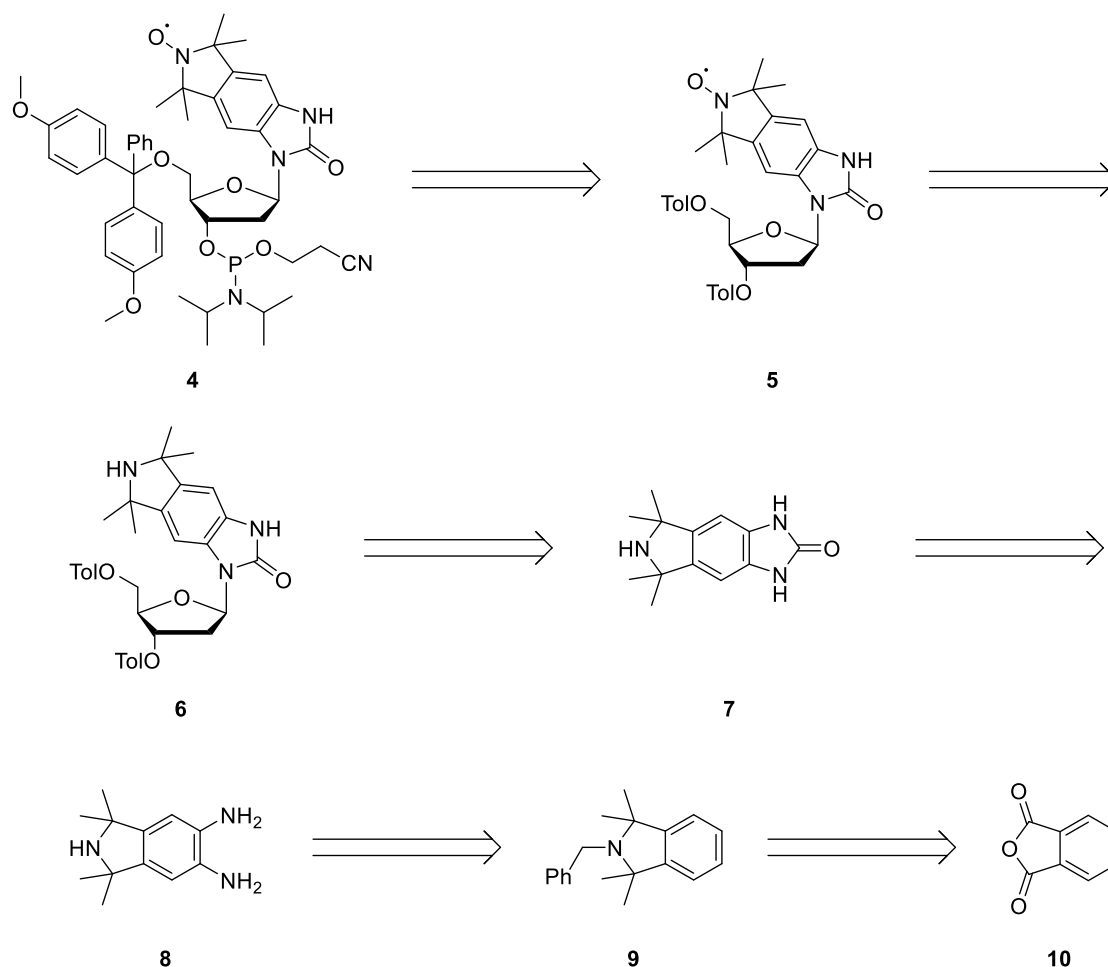
Fig. 43: Initial retrosynthetic pathway for the synthesis of the benzi-spin phosphoramidite with methyl groups.

3.1.2 Preparation of imidazoisoindolone nucleobase 7

The starting material for the synthesis was phthalic anhydride (**10**), which was converted to *N*-benzylphthalimide (**12**) by reaction with benzylamine (**11**) (Fig. 44)[167]. This reaction was usually done in a scale of around 270 mmol, because the yield of the next step was relatively low, thus necessitating a large scale.
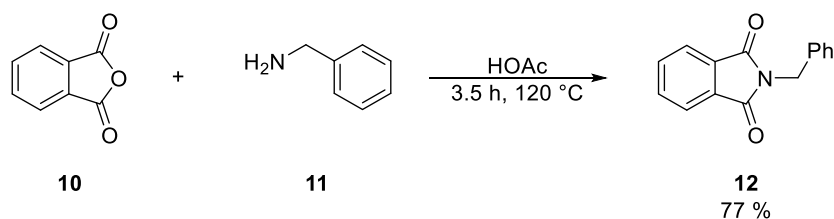
Fig. 44: Synthesis of *N*-benzylphthalimide (12).

The next step was a Grignard reaction with methyl iodide to introduce the methyl groups, which are required for stabilizing the radical once it has been introduced (Fig. 45). The conditions for this reaction have been optimized in earlier works[119], for example it has been shown that removal of the diethyl ether after addition of *N*-benzylphthalimide (**12**) by a special distillation apparatus can lead to an increased yield from around 20 % to slightly over 30 %. This is still fairly low, but since it happens at an early stage in the synthesis and the starting material can easily be produced in large scale, it is acceptable. Afterwards, the benzyl protecting group on the nitrogen was removed by palladium catalyzed hydrogenation, which resulted in quantitative deprotection (Fig. 45)[119].
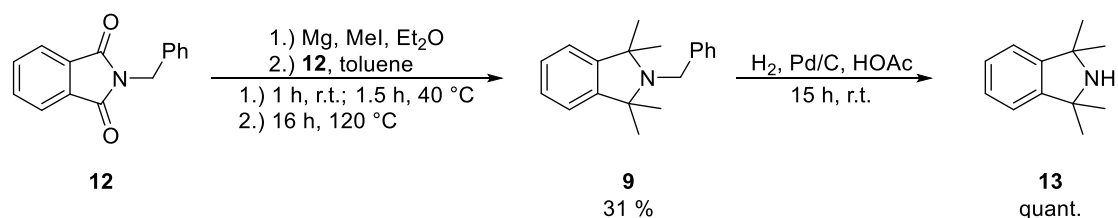
Fig. 45: Synthesis of compounds 9 and 13.

Next, the aromatic ring needed to be functionalized, starting with nitration using sulfuric acid and nitric acid, which was possible with high yield (Fig. 46)[168]. The next step was the introduction of the amino group in position 6 by vicarious nucleophilic substitution using 1,1,1-trimethylhydrazinium iodide (TMHI, **17**)[169] as the nucleophile (Fig. 46) with KO*t*Bu as a base. TMHI can easily be prepared from 1,1-dimethylhydrazine (**16**) by reaction with methyl iodide (Fig. 46).
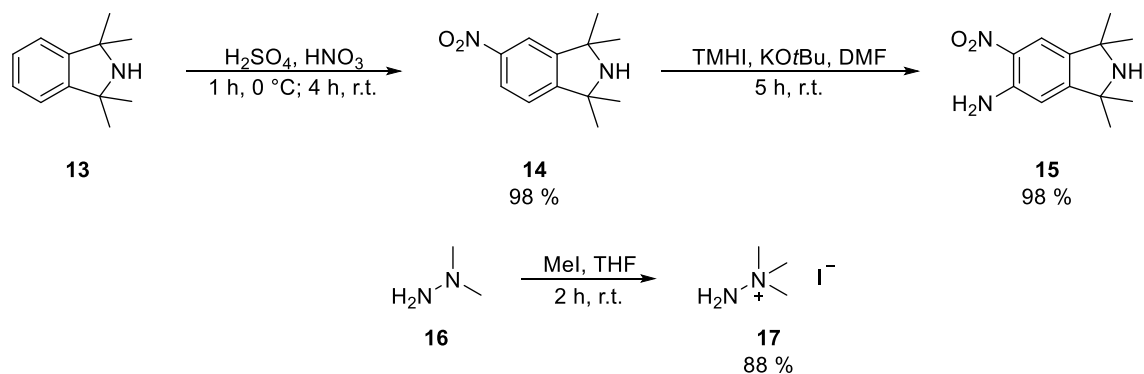
Fig. 46: Synthesis of compounds 14 and 15 as well as TMHI (17).

After the introduction of the amino group, the nitro group had to be reduced to an amino group as well, to result in diaminoisoindoline **8**. This was once again done with palladium under hydrogen atmosphere and resulted in excellent yield (Fig. 47)[168].
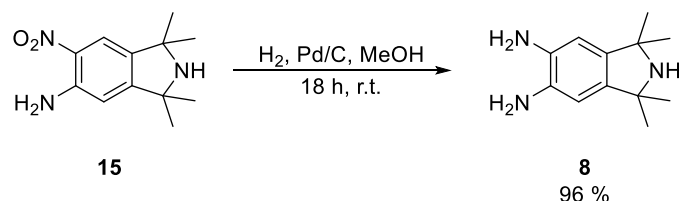

Fig. 47: Synthesis of compound 8.

At this point, the only step left to complete the synthesis of compound **7** was the cyclization, by having both amino groups react with one of a number of carbonyl compounds with various leaving groups (Fig. 48).
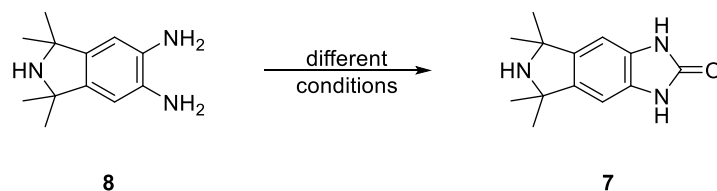
Fig. 48: Synthesis of compound 7.

The initial idea was to use CDI as the electrophile for the substitution. However, while the desired product could be isolated, the yield was only 13 %. One reason for this might be the purification by column chromatography, which was necessary to remove imidazole. Otherwise the imidazole might interfere in the next step due to its nucleophilicity, by reacting with the sugar. Therefore, two other compounds, urea and diethyl carbonate (DEC), were tested instead of CDI, under different conditions (Table 1).

Table 1: Reagents and conditions for the cyclization.

No.	reagents	solvent	conditions	result
1	2 eq. CDI	MeCN	20 h, r.t.	compound **7** (13 %)
2	4.4 eq. urea	*n*BuOH	20 h, 120 °C	compound **18**
3	1.0 eq. urea	EtOH	60 h, 80 °C	compound **18**
4	1.2 eq. DEC	MeCN	22 h, r.t.	no reaction
5	1.2 eq. DEC	MeCN	16 h, 80 °C	no reaction
6	3.0 eq. DEC, cat. HCl	MeCN	24 h, 80 °C	no reaction

None of these reactions resulted in the formation of the desired product. When DEC was used, there was no reaction even at high temperature, while the reactions with urea resulted in a compound

which was heavier than compound **7** by an *m/z* of 26, which would fit compound **18**, resulting from reaction with two molecules of urea (Fig. 49). Even when one equivalent of urea was used, a significant amount of this compound was still formed.
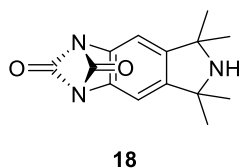

18

Fig. 49: Possible structure of the compound formed by reaction of compound 8 with urea.

Because alternative reagents did not result in the desired compound, it was decided to use CDI despite the low yield and continue the synthesis.

3.1.3 Synthesis of the nucleoside

The next step was the reaction of compound **7** with protected chlorodeoxyribose **19** to yield nucleoside **6** (Fig. 50)[119]. Sodium hydride was used as a base for deprotonation of **7**.

7   **19**   **6**
21 % (isomeric mixture)
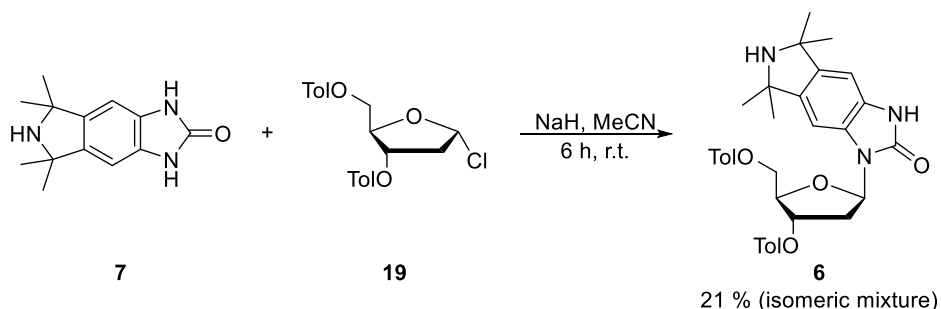
Fig. 50: Synthesis of compound 6, obtained as a mixture of isomers.

As the NMR spectra showed, a mixture of two compounds was obtained. The ^{1}H-NMR spectrum is shown in Fig. 51. Since the mass spectrum showed no other compound, it was concluded that two isomers had to have formed. The reaction was supposed to be an S_N2-type nucleophilic substitution, so with nitrogen atoms N1 and N3 being equivalent due to the symmetry of compound **7**, the most obvious possible isomer would be compound **20**, resulting from an attack by N6 after deprotonation (Fig. 52). This hypothesis would fit well with the observed ratio of the isomers, which seems to be close to 2:1. This would of course assume equal reactivity of all nitrogen atoms, which might be unlikely because the methyl groups flanking N6 should reduce its reactivity, but judging from the low overall yield, N1 and N3 seem to not be very nucleophilic either, which makes some sense considering that they are essentially amides.
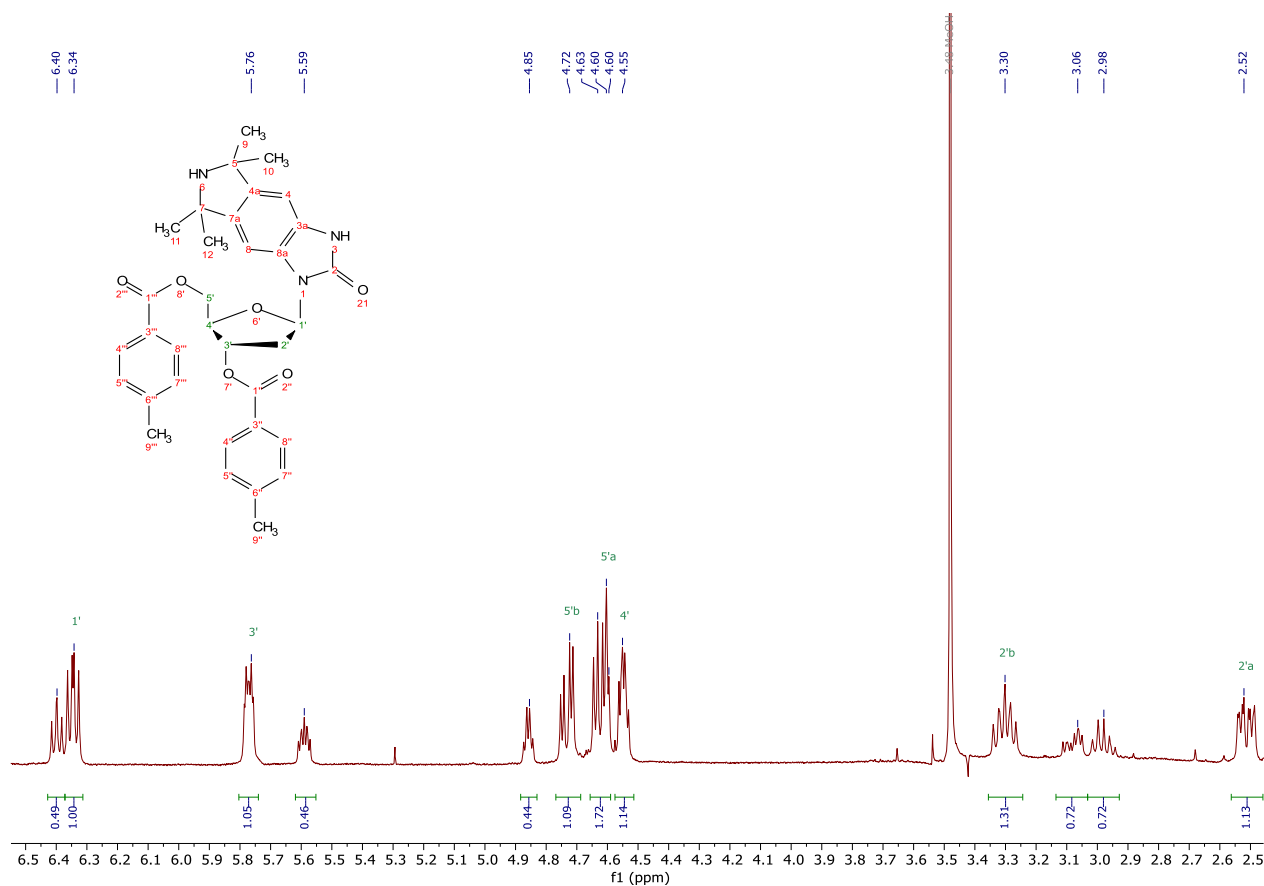
Fig. 51: Part of the ¹H-NMR spectrum of compound 6 in CDCl₃ showing the signals of the ribose protons. Two compounds with a ratio of about 2:1 can be identified. Signals of compound 6 are assigned.

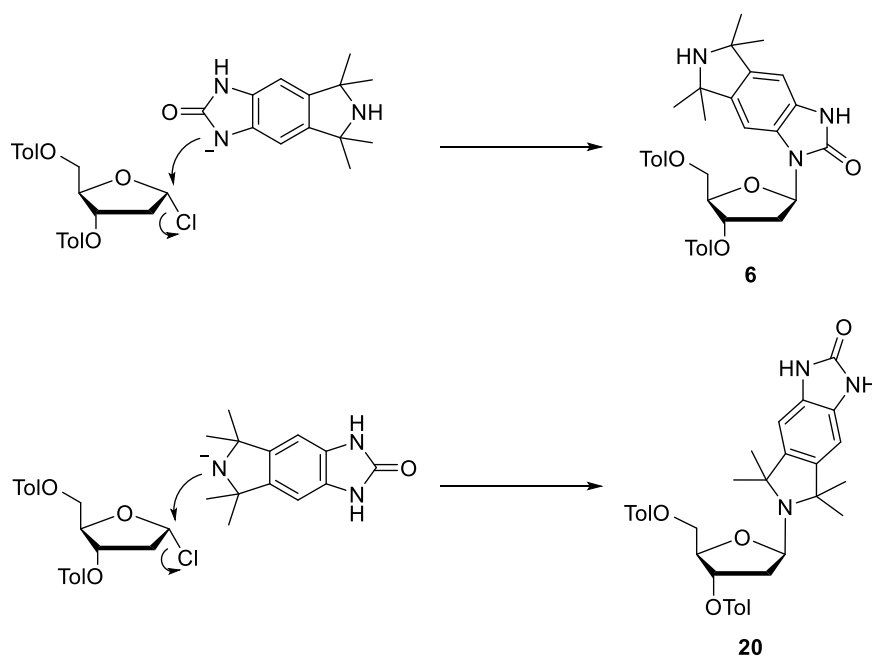**Fig. 52: Nucleosidation of deprotonated compound 7 by S$_N$2 reaction with sugar 19. Attack from N1 leads to compound 6, attack from N6 would lead to compound 20.**

To prevent the formation of compound **20**, a protecting group was to be introduced at N6. Here, *tert*-butyloxycarbonyl (Boc) was chosen, because it should be stable under the conditions of all

reactions after the nitration, so the best point in the synthesis to introduce it was at compound **14** (Fig. 53). Reaction of compound **14** with di-*tert*-butyl dicarbonate afforded the protected compound **21** in good yield[170]. Because there are known issues with removing protecting groups from this position[119], deprotection with HCl was also tested to see if Boc can be removed efficiently (Fig. 53). After it was confirmed that Boc could be easily removed when necessary, the synthesis was continued with the introduction of the amino group (Fig. 53). Unfortunately, Boc is cleaved under the conditions of this reaction, most likely due to nucleophilic attack by TMHI, which would be consistent with the major product being deprotected **14** with a small amount of compound **15** as side product.
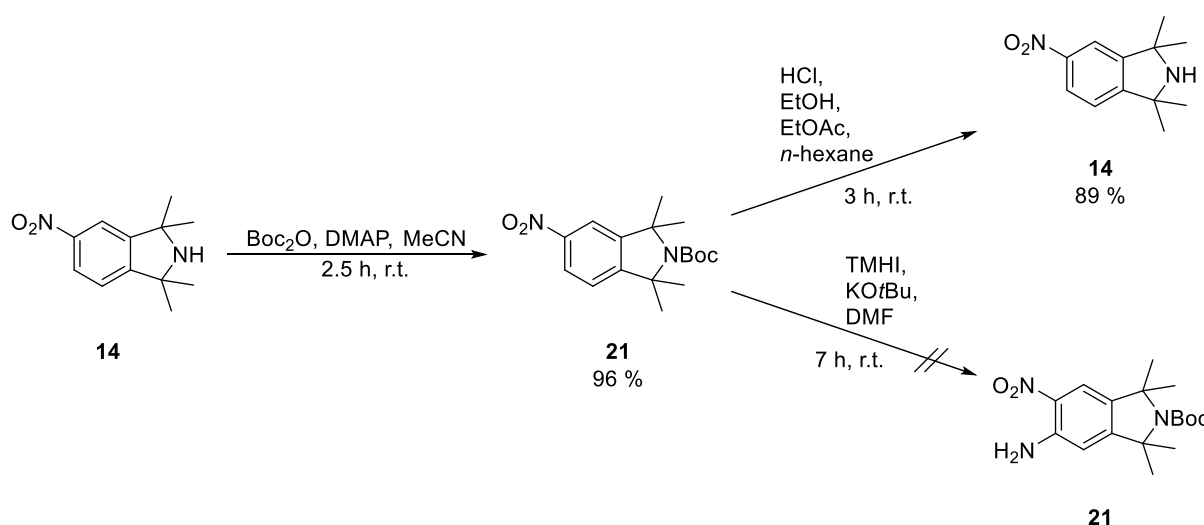
Fig. 53: Boc protection and deprotection of compound 14.

As an alternative point of introduction for the Boc group, compound **15** was tested next. This was not the first choice because the 6-amino group would also be protected, which was considered to likely be detrimental to its reactivity with CDI later. This reaction was not very efficient, with an isolated yield of only 32 % (Fig. 54). Nonetheless, compound **22** was then reduced to compound **23** in quantitative yield (Fig. 54).
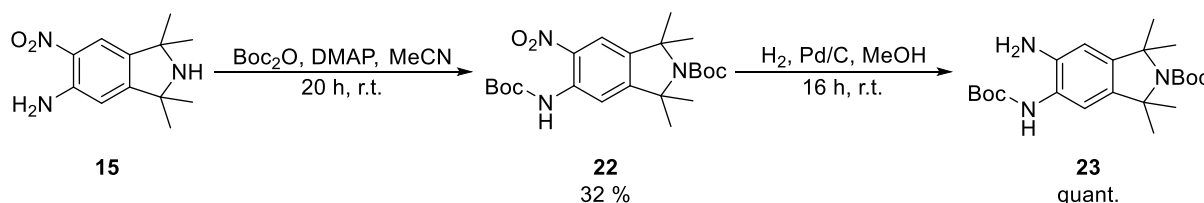

Fig. 54: Synthesis of compounds 22 and 23.

This alternative strategy did not work, because as it turned out, having a protected amino group did not just reduce its reactivity, it completely prevented the reaction from taking place (Fig. 55). This is somewhat surprising considering that these amino groups can apparently react twice with urea. Nonetheless, this strategy was discontinued.
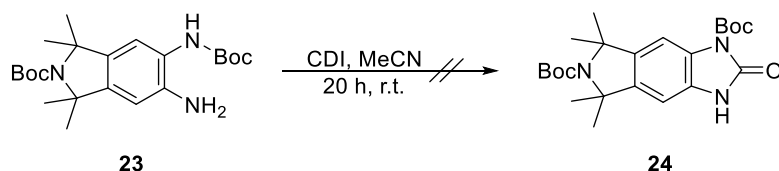
Fig. 55: Boc protection of the 5-amino group prevents reaction with CDI.

3.1.4 Synthesis of nucleoside 31 from tetraethylisoindoline

While the Boc protection was attempted, another strategy was begun in parallel. The idea was to start from the beginning of the synthesis and introduce ethyl groups rather than methyl groups next to the nitroxide. The primary motivation for this approach was the possibility of the ethyl groups preventing the formation of an unwanted isomer like **20** during nucleosidation due to their increased steric hindrance. Using ethyl groups would also have the additional effect of causing greater stability of the radical, which was another desirable result. As it turned out, using ethyl groups is also beneficial to some of the steps in the synthesis, with the first example being the Grignard reaction, now done with ethyl iodide rather than methyl iodide, which now results in higher yield (Fig. 56), increasing from barely 30 % to almost 40 %. The following steps were carried out in a similar way as before, starting with hydrogenolytic cleavage of the benzyl group (Fig. 56).
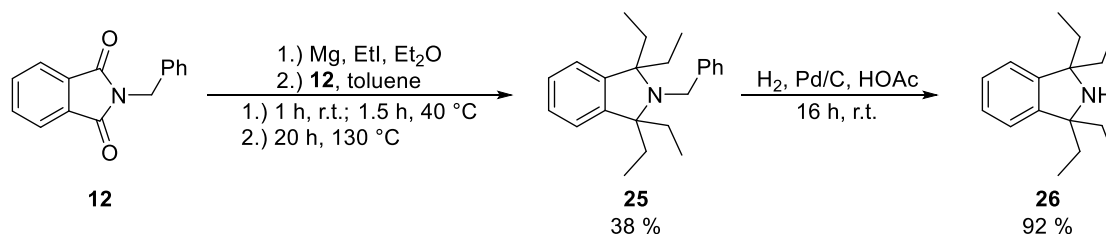

Fig. 56: Synthesis of compounds 25 and 26.

Next, nitration was performed and then the amino group introduced by vicarious nucleophilic substitution (Fig. 57).
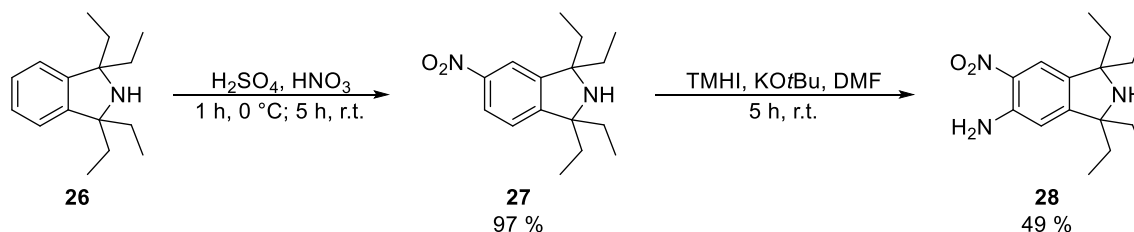

Fig. 57: Synthesis of compounds 27 and 28.

After this, compound **29** was prepared by reduction of the nitro group once again using hydrogen with palladium as catalyst (Fig. 58).
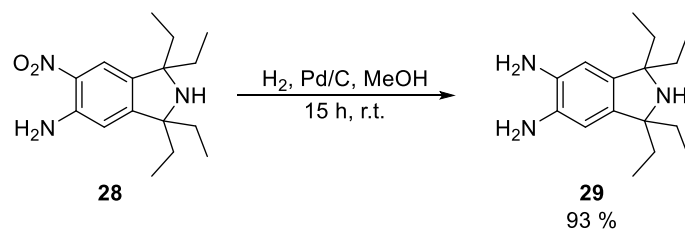
Fig. 58: Synthesis of compound 29.

The next step showed a clear advantage of using ethyl groups, a significantly improved yield of the cyclization with CDI. Before, the yield had been below 20 %, one reason for this probably being the purification by column chromatography, as the compounds is fairly polar. As it turned out, when the same reaction was done with compound **29**, the product precipitated from the reaction mixture, allowing it to be collected by filtration, after which it was pure enough to be used without further purification, resulting in a higher yield (Fig. 59). The ^{1}H-NMR spectrum is shown in Fig. 61.
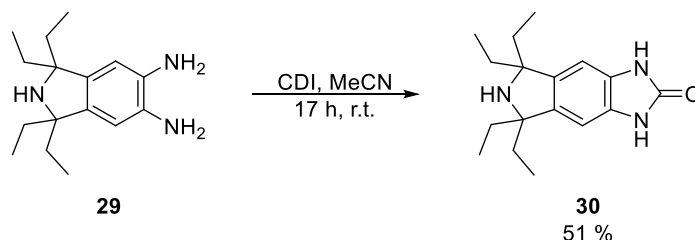

Fig. 59: Synthesis of compound 30.

After compound **30** was obtained, nucleosidation was performed. The conditions were similar to those used in the earlier attempt (Fig. 60). The result was similar as well, with the reaction once again resulting in an isomeric mixture.
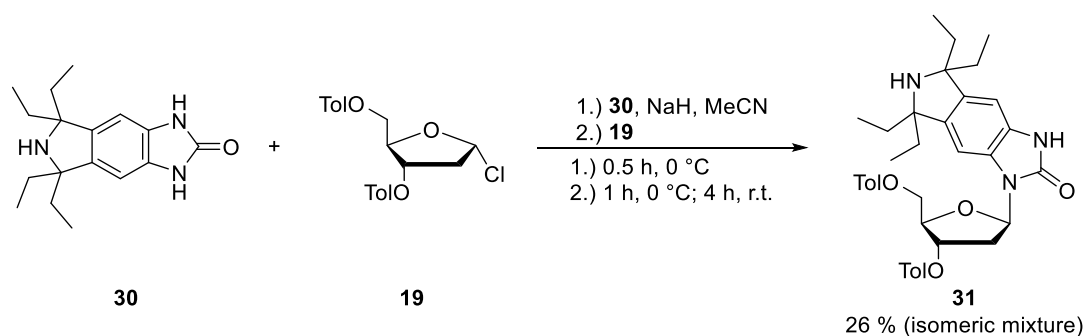

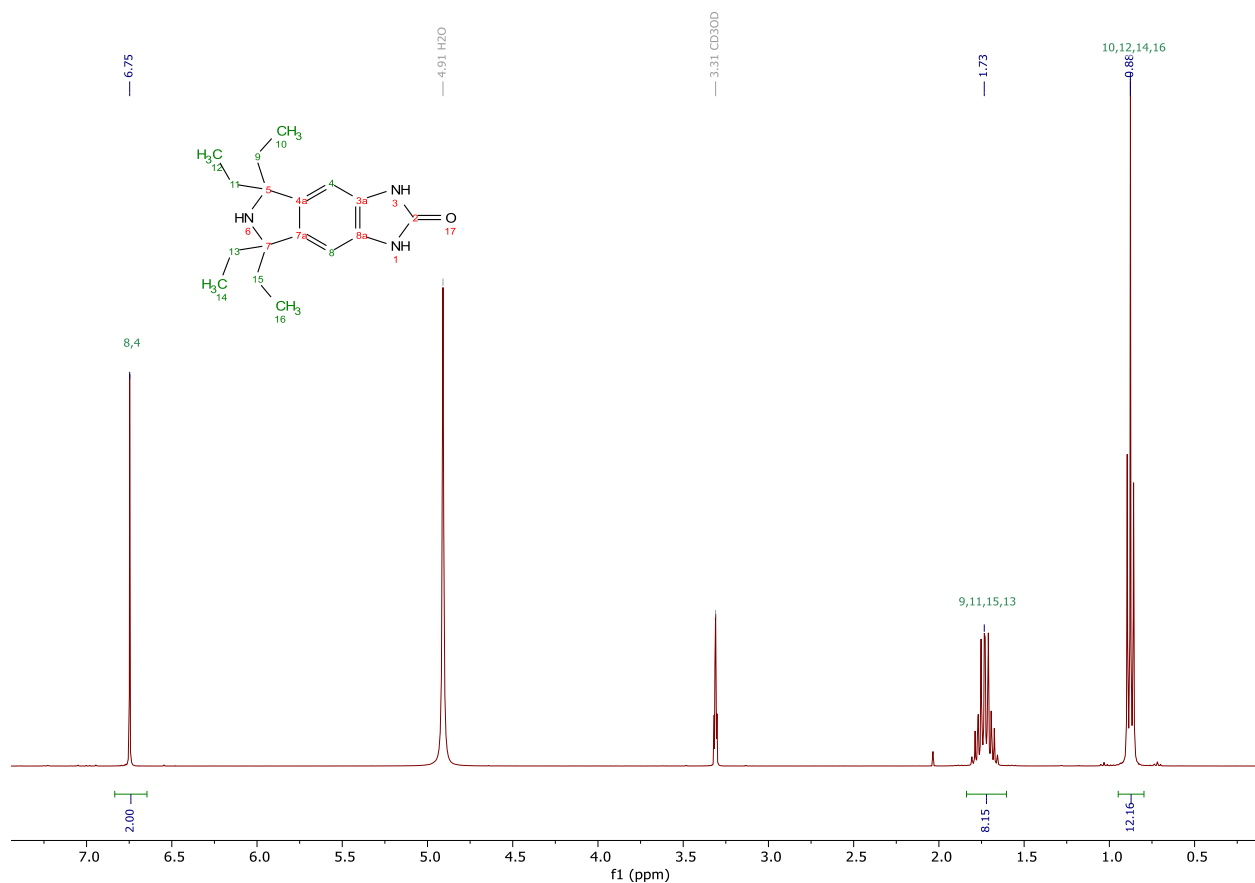**Fig. 60: Attempted synthesis of compound 31 resulting in an isomeric mixture.**

Fig. 61: ¹H-NMR spectrum of compound 30 in CD₃OD.

It was not expected that N1 would react with the sugar, considering the steric demand of the neighboring ethyl groups. It was thus tested if N1 would react with Boc₂O (Fig. 62).
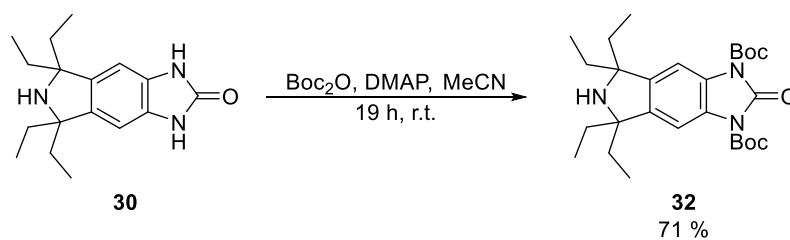

Fig. 62: Protection of compound 30 with Boc.

The reaction resulted in a compound which according to ESI-MS and ¹H-NMR contained two Boc groups. Because the NMR spectrum shows only one singlet for the aromatic protons and one for the Boc protons, it was concluded that compound **32** was formed, due to its symmetry (Fig. 62). This would mean that N1 did not react with Boc₂O. Because of this, it was considered unlikely that N1 would attack the sugar during nucleosidation. Thus, the identity of the product isomers was reconsidered, with the conclusion being that the unwanted isomer could be the α-isomer **33** (Fig. 63).
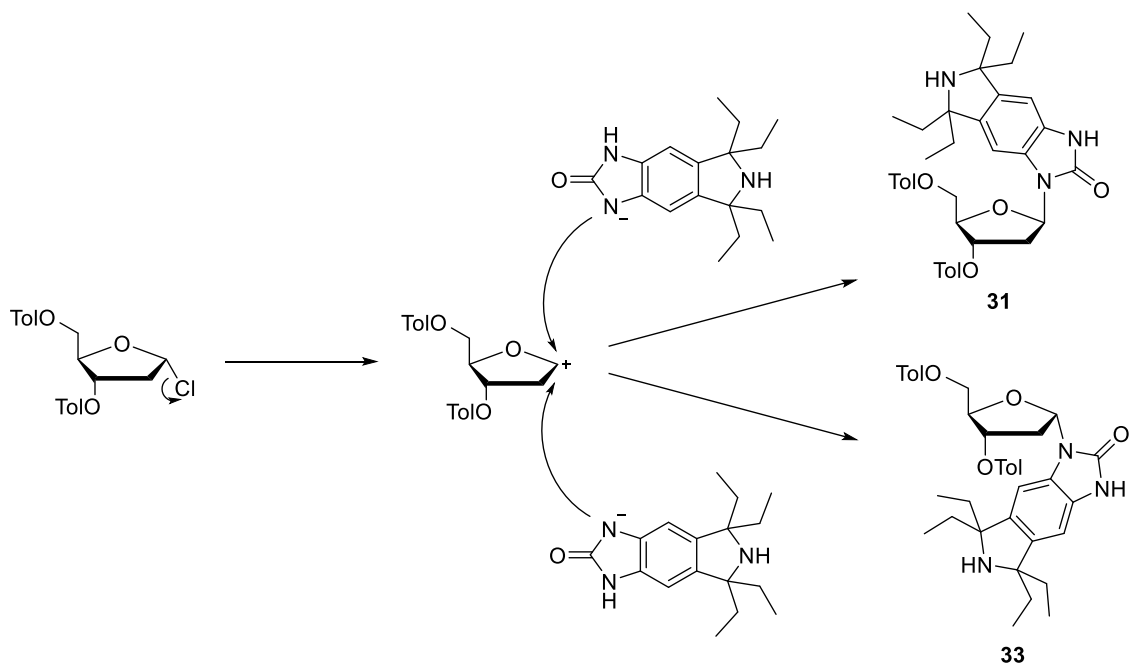
Fig. 63: Proposed nucleosidation of deprotonated compound 7 by S$_N$1 reaction with sugar 19. Because the nucleophilic attack can happen from both sides, anomers 31 and 33 could both be formed.

The nucleosidation is supposed to be an S$_N$2 reaction, so the α-isomer should not be formed. The formation of compound **33** might be the result of low nucleophilicity of compound **30**, which causes the reaction to take place according to an S$_N$1 mechanism (Fig. 63). Because of this, the conditions for the reaction were changed in the next attempt (Fig. 64)[166]. The reaction was done at 0 °C instead of room temperature to prevent the chloride from leaving prematurely. Also, the solvent was changed to THF.
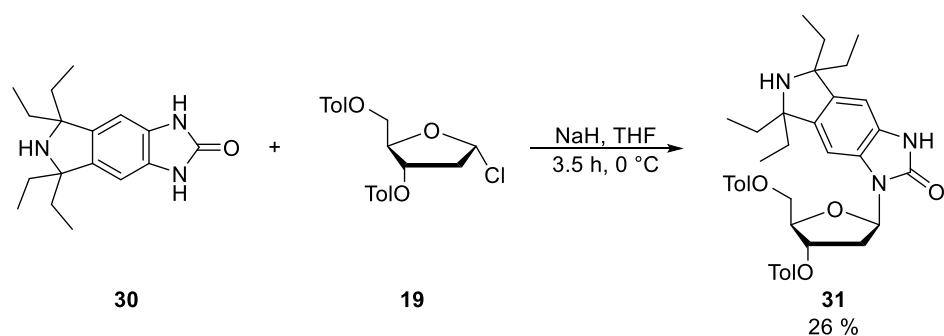

Fig. 64: Synthesis of compound 31 showing the final reaction conditions.

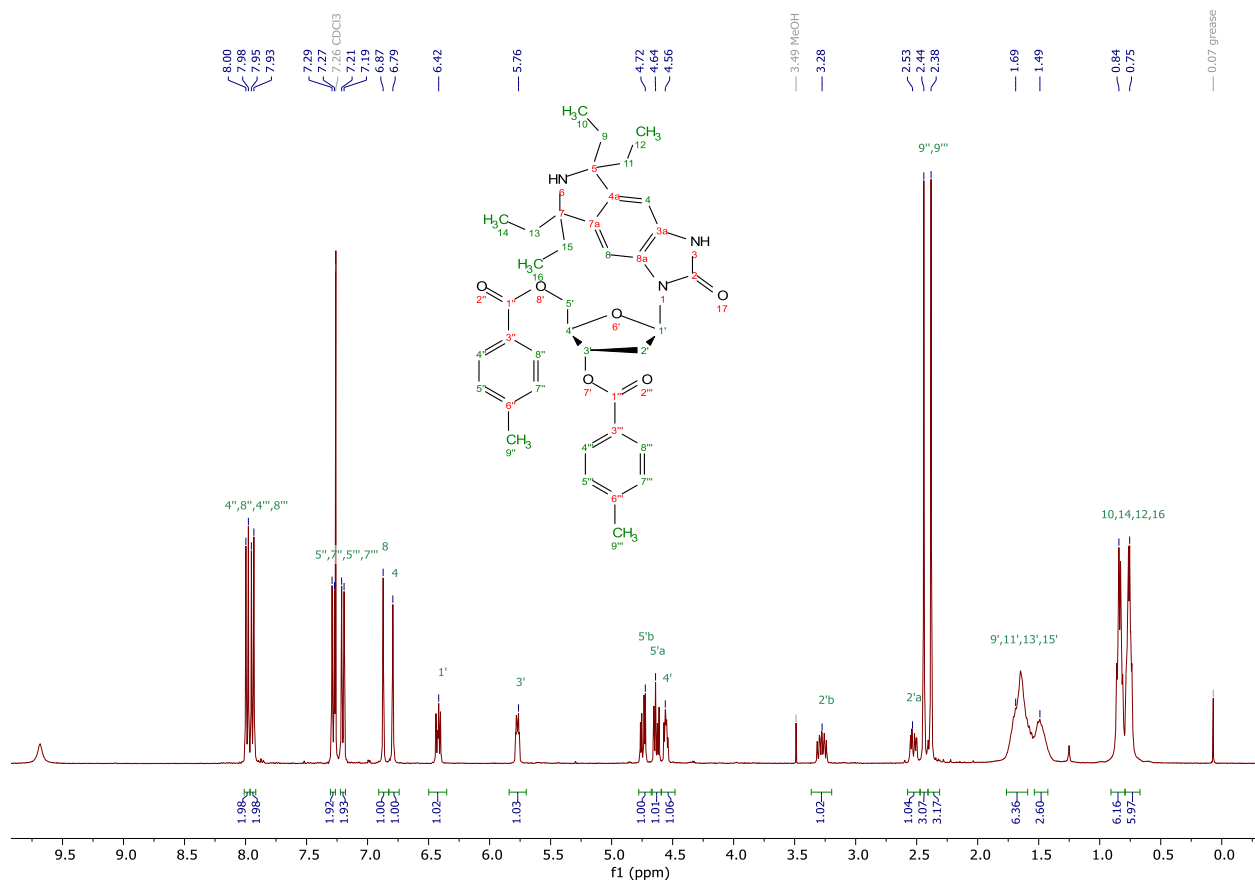Under these new conditions, only one isomer was formed as can be seen from the ^{1}H-NMR spectrum (Fig. 65).

Fig. 65: ¹H-NMR spectrum of compound 31 in CDCl₃.

The yield of the reaction was low, which is due to low conversion, probably resulting from low nucleophilicity, as well as formation of 39 % of double-nucleosidated product **34** (Fig. 66). While 39 % is more than the 26 % of the desired product, it should be noted that these yields were calculated based on the ribose, of which two equivalents are needed to form compound **34**. When compound **30** is used as the reference instead, 19 % of desired product **31** and 14 % of **34** are obtained.
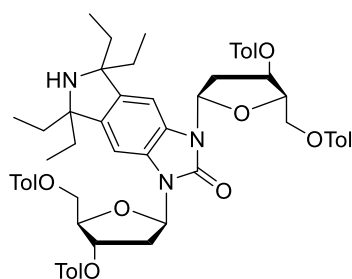
34

Fig. 66: Side product 34.
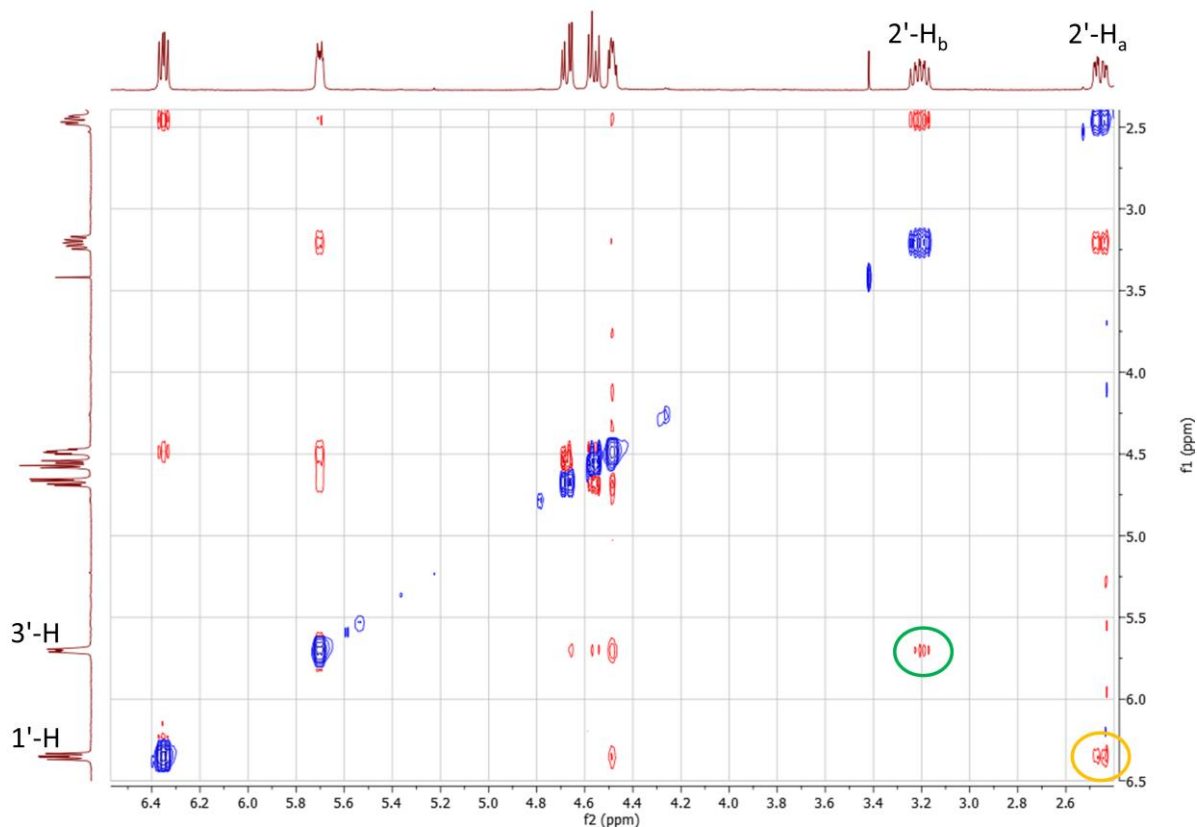
Fig. 67: Part of the NOESY spectrum of compound 31 in CDCl₃. Circles mark crosspeaks between 2'-H_b and 3'-H (green) and 2'-H_a and 1'-H (orange).

The product formed in the reaction was identified as β-isomer **31** from the NOESY spectrum (Fig. 67). One of the 2'-protons shows a correlation with the 1'-proton, while the other 2'-proton shows a correlation to the 3'-proton. In an α-isomer one of the 2'-protons would show correlations to both the 1'- and 3'-protons, while the other would show none.

The connection of the sugar to N1 rather than N6 was verified by using an HMBC spectrum (Fig. 68). Correlations between the 1'-proton and C2 and C8a are visible.
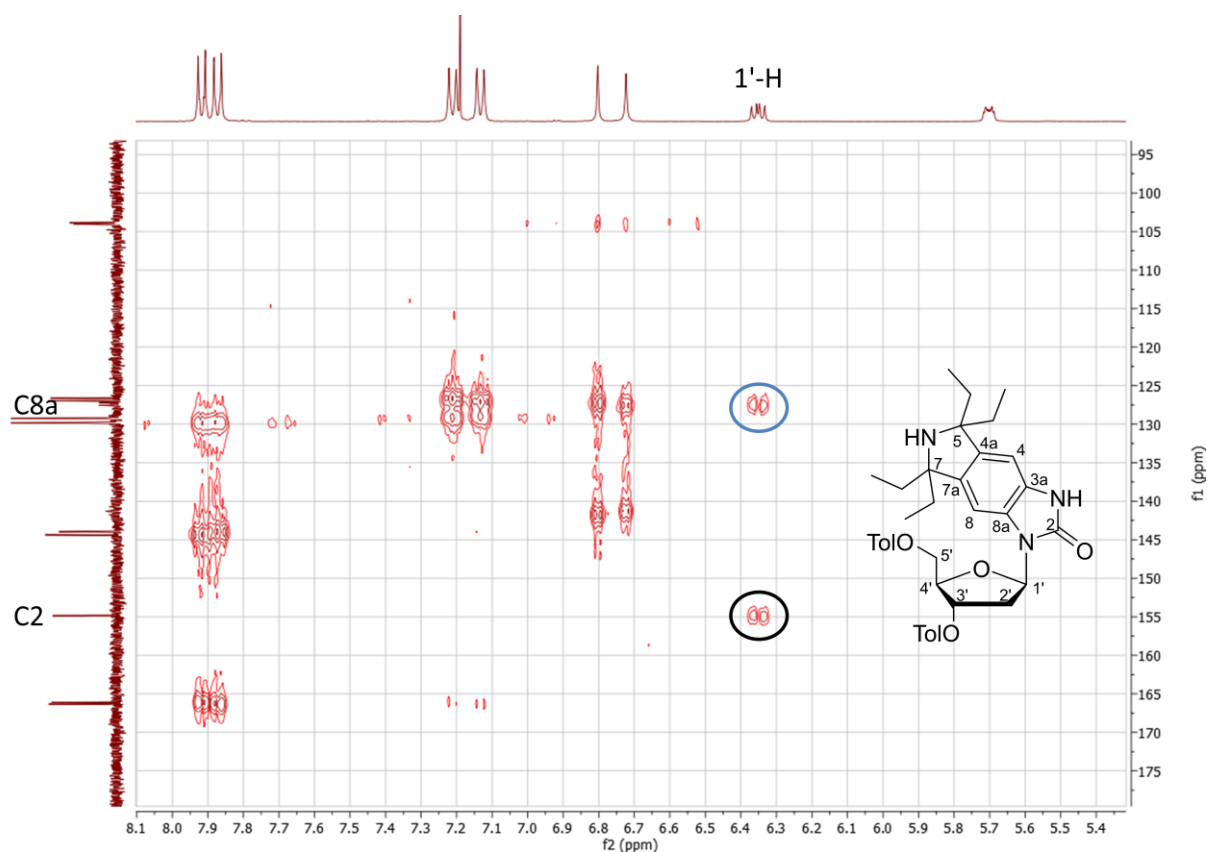
Fig. 68: Part of the HMBC spectrum of compound 31 in CDCl₃. Circles mark crosspeaks between 1'-H and C8a (blue) and C2 (black).

3.1.5 Preparation of the benzi-spin phosphoramidite

After the synthesis of nucleoside **31** was successful, the final steps towards preparation of the phosphoramidite **37** were taken. First, the nitroxide was introduced by oxidation with *meta*-chloroperoxybenzoic acid (*m*CPBA) (Fig. 69)[119]. After this had been achieved, the free nucleoside benzi-spin (**1**) was obtained by cleaving the toluoyl protecting groups with NaOMe (Fig. 69)[166].
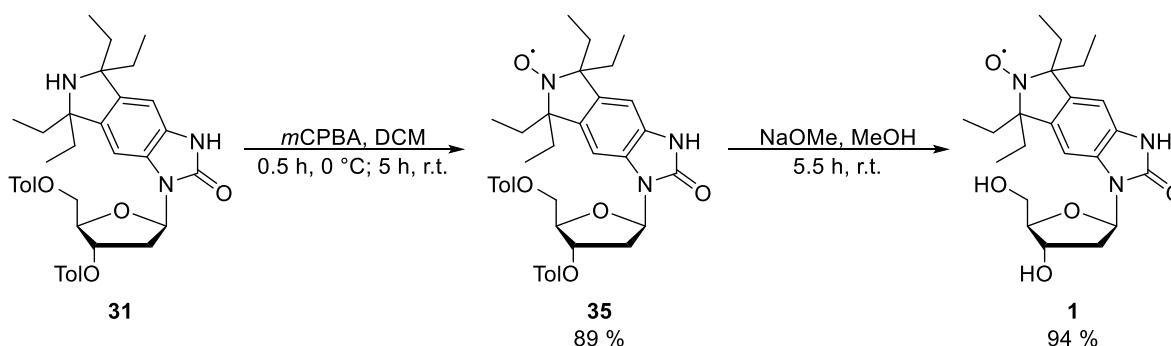

Fig. 69: Oxidation of compound 31 to compound 35 and deprotection of the sugar leading to free nucleoside benzi-spin (1).

At this point, benzi-spin was essentially complete, it just had to be converted to phosphoramidite **37** in order to be used in solid phase synthesis. The first step towards this was to introduce a

54

4,4'-dimethoxytrityl (DMT) group at the 5'-hydroxy group (Fig. 70)[166]. This was possible in acceptable yield.
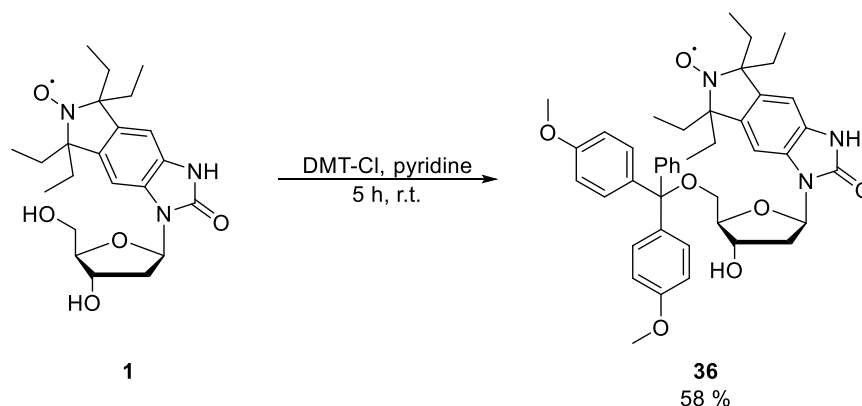
Fig. 70: DMT protection of benzi-spin (1).

Finally, compound **36** was converted to phosphoramidite **37** using *O*-β-cyanoethyl-*N,N*-diisopropylchlorophosphoramidite (CEP-Cl)[166].
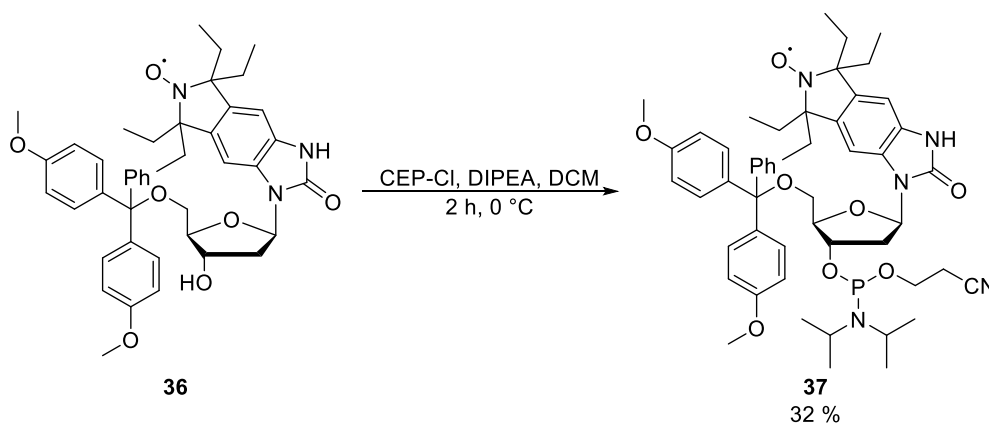
Fig. 71: Synthesis of phosphoramidite 37.

The first attempt was done at room temperature, with 1.6 eq of CEP-Cl, but it resulted in the formation of a compound which, according to ESI-MS, carried two CEP groups, with the second one probably attached to N3 or O2. To prevent this, only 1.2 eq of CEP-Cl were used in subsequent attempts and the temperature lowered to 0 °C. With these changes, phosphoramidite **37** could be synthesized successfully (Fig. 71). The product contained an impurity, the amount of which could not be determined because of the paramagnetic nature of compound **37**, which makes integrals unreliable. It could not be removed by column chromatography, but the impure phosphoramidite was used for solid phase synthesis regardless. The ESI mass spectrum is shown in Fig. 72.

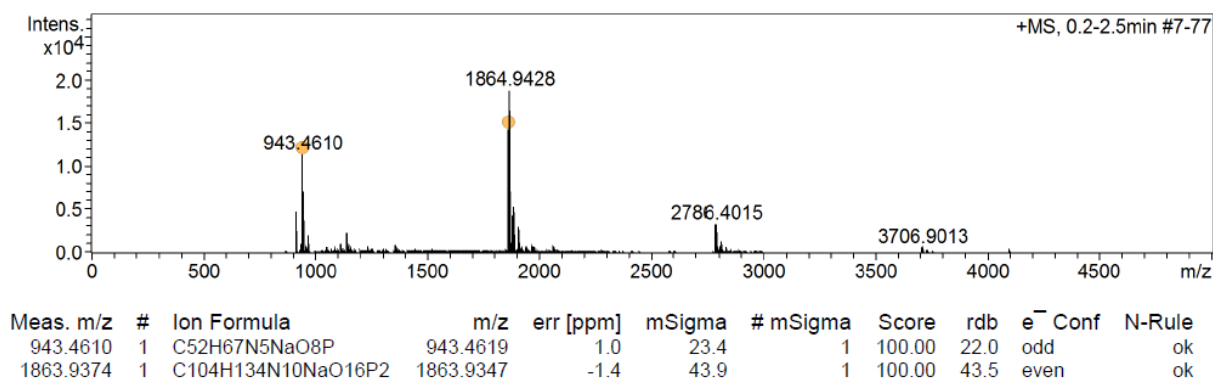| Meas. m/z	#	Ion Formula	m/z	err [ppm]	mSigma	# mSigma	Score	rdb	e⁻ Conf	N-Rule
943.4610	1	C52H67N5NaO8P	943.4619	1.0	23.4	1	100.00	22.0	odd	ok
1863.9374	1	C104H134N10NaO16P2	1863.9347	-1.4	43.9	1	100.00	43.5	even	ok

Fig. 72: ESI mass spectrum of benzi-spin phosphoramidite 37. [M+Na]⁺ and [2M+Na]⁺ peaks are marked.

3.1.6 Synthesis of oligonucleotides

Phosphoramidite **37** was then incorporated into an oligonucleotide by solid phase synthesis. Further experiments also required several other oligonucleotides (Table 2), which were synthesized or provided by co-workers.

Table 2: Oligonucleotides used for melting curve measurements and EPR experiments. C^T is C^{TEMPO}, B^S is benzi-spin, m⁶G is O-6-methyl-2'-deoxyguanosine and m^{6DA}P is N-6-methyldiaminopurine deoxyribonucleotide.

No.	Sequence
I	5'-GACGTCGGAAGACGTCAGTA-3'
II	5'-GACGTC^{T}GGAAGACGTCAGTA-3'
III	5'-GACGTB^{S}GGAAGACGTCAGTA-3'
IV	5'-TACTGACGTCTTCCGACGTC-3'
V	5'-TACTGACGTCTTCCm⁶GACGTC-3'
VI	5'-TACTGACGTCTTCCm^{6DA}PACGTC-3'
VII	5'-TACTGACGTCTTCCAACGTC-3'
VIII	5'-TACTGACGTCTTCCTACGTC-3'
IX	5'-TACTGACGTCTTCCIACGTC-3'
X	5'-TACTGACGTCTTCCCACGTC-3'

These sequences were chosen because they had already been used to study C^T and Çm[106, 117], albeit as RNA rather than DNA, thus allowing for direct comparisons between the labels. The sequences are partially self-complementary and can form a hairpin structure when no complementary strand is present (Fig. 73).
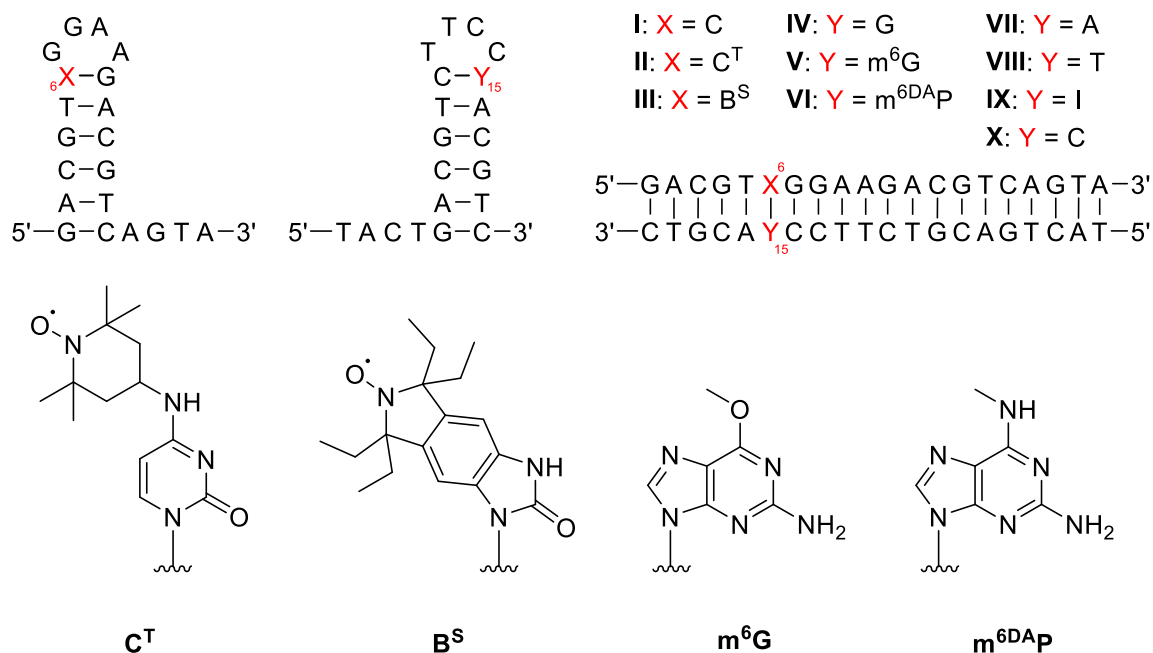
Fig. 73: Top: Structures formed by the oligonucleotides as single strands (left) and double strand (right). **Bottom:** Structures of modified nucleobases present in the mentioned sequences.

Oligonucleotides **IV** and **II** were provided by Jan Seikowski, **I**, **III**, **V**, **VI** and **VII** were synthesized, **VIII**, **IX** and **X** were purchased. For the synthesis of **III**, phosphoramidite **37** was used. For the synthesis of **V** and **VI**, phosphoramidite **38** (Fig. 74), provided by Dr. Surjendu Dey, was used.
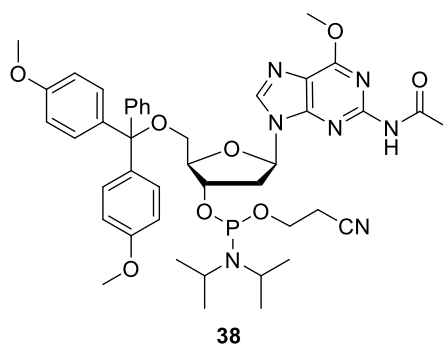
Fig. 74: Phosphoramidite 38, which was used for the synthesis of D2681 and D2681NHMe.

To obtain **VI**, the oligonucleotide was deprotected with methylamine for 10 h at 37 °C after synthesis, which caused substitution of the 6-methoxy group with a methylamino group. **V** was deprotected with aqueous ammonia to prevent the substitution from taking place. This was also done at 37 °C but required 48 h for complete deprotection. Shorter deprotection times caused incomplete removal of acetyl protecting groups.

Fig. 75: HPLC chromatogram of oligonucleotide III on a Dionex DNAPac PA200 2 x 250 mm column (Buffer A: 25 mM Tris HCl, 6 M urea, pH 8.0; Buffer B: 25 mM Tris HCl, 6 M urea, 0.5 M NaClO₄, pH 8.0; 60 °C), 0 % to 48 % B in A in 12 CV.

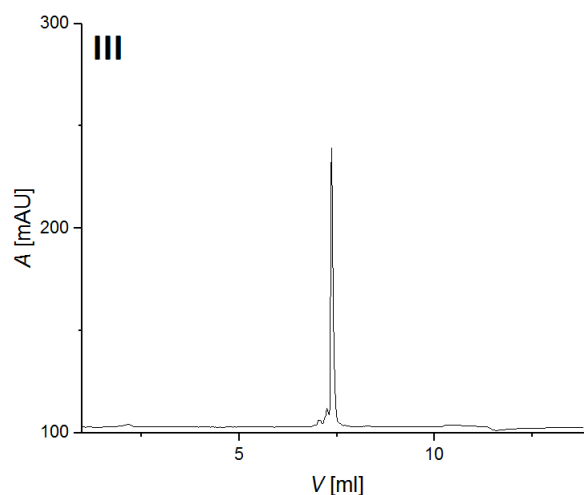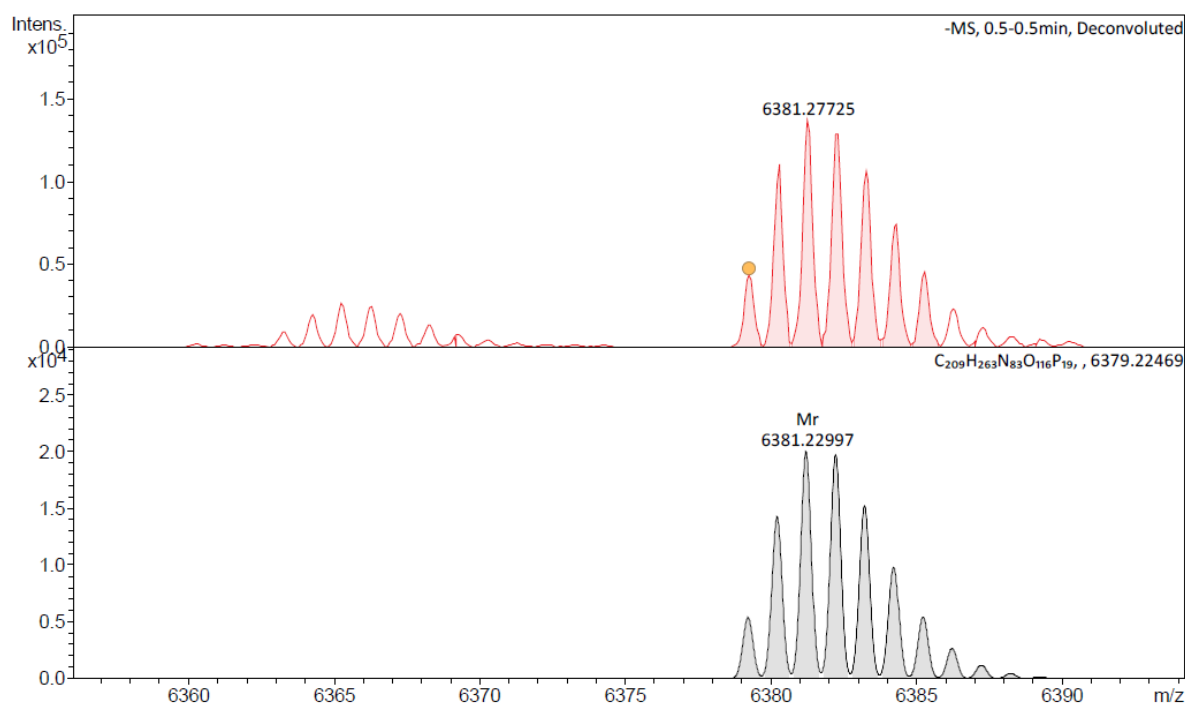| Meas. m/z	#	Ion Formula	m/z	err [ppm]	mSigma	# mSigma	Score	rdb	e⁻ Conf	N-Rule
6379.25611	1	C209H263N83O116P19	6379.22469	-4.93	65.2	1	100.00	129.5	even	ok

Fig. 76: Deconvoluted ESI mass spectrum of III (top) and calculated peak pattern (bottom). The peaks to the left result from reduction of benzi-spin to the amine.

Benzi-spin was successfully incorporated into oligonucleotide **III**, as evidenced by the HPLC chromatogram (Fig. 75) and ESI-MS spectrum (Fig. 76), but the coupling efficiency was low. This could be due to lower reactivity compared to canonical phosphoramidites, or more likely because of the impurity which phosphoramidite **37** still contained. Standard conditions, including iodine as oxidant were used, but the nitroxide remained mostly intact during the synthesis. The radical content was 99 % as determined by spin-counting using a TEMPOL calibration curve (see chapter 3.1.9).

3.1.7 Melting curve analysis of oligonucleotide duplexes

The effect of benzi-spin (**1**) on the stability of DNA duplexes was then studied by UV thermal denaturation experiments. Heating of a DNA duplex causes an increase in absorbance, known as hyperchromicity, because absorbance of the nucleobases is partially quenched in a duplex, and will thus increase when the duplex is denatured. The melting temperature of the duplex, derived from the hyperchromicity, can provide information about the stability of a given duplex, because less stable duplexes will denature at lower temperatures compared to more stable ones. Modified nucleotides which cannot form stable base pairs should destabilize the duplex, leading to denaturation at lower temperatures. The UV absorbance of single strand **III** and seventeen different combinations of oligonucleotides was measured while repeatedly heating and cooling the samples (Fig. 77).
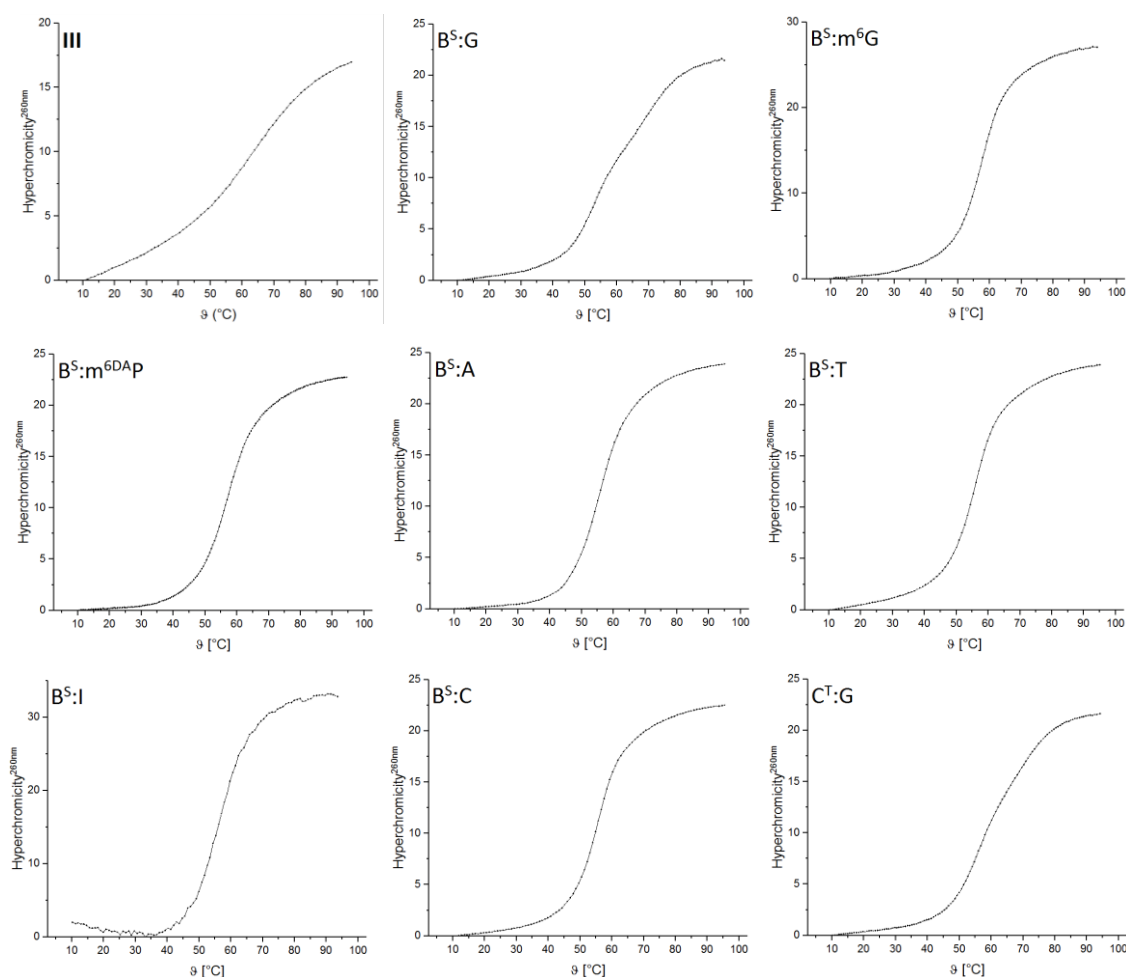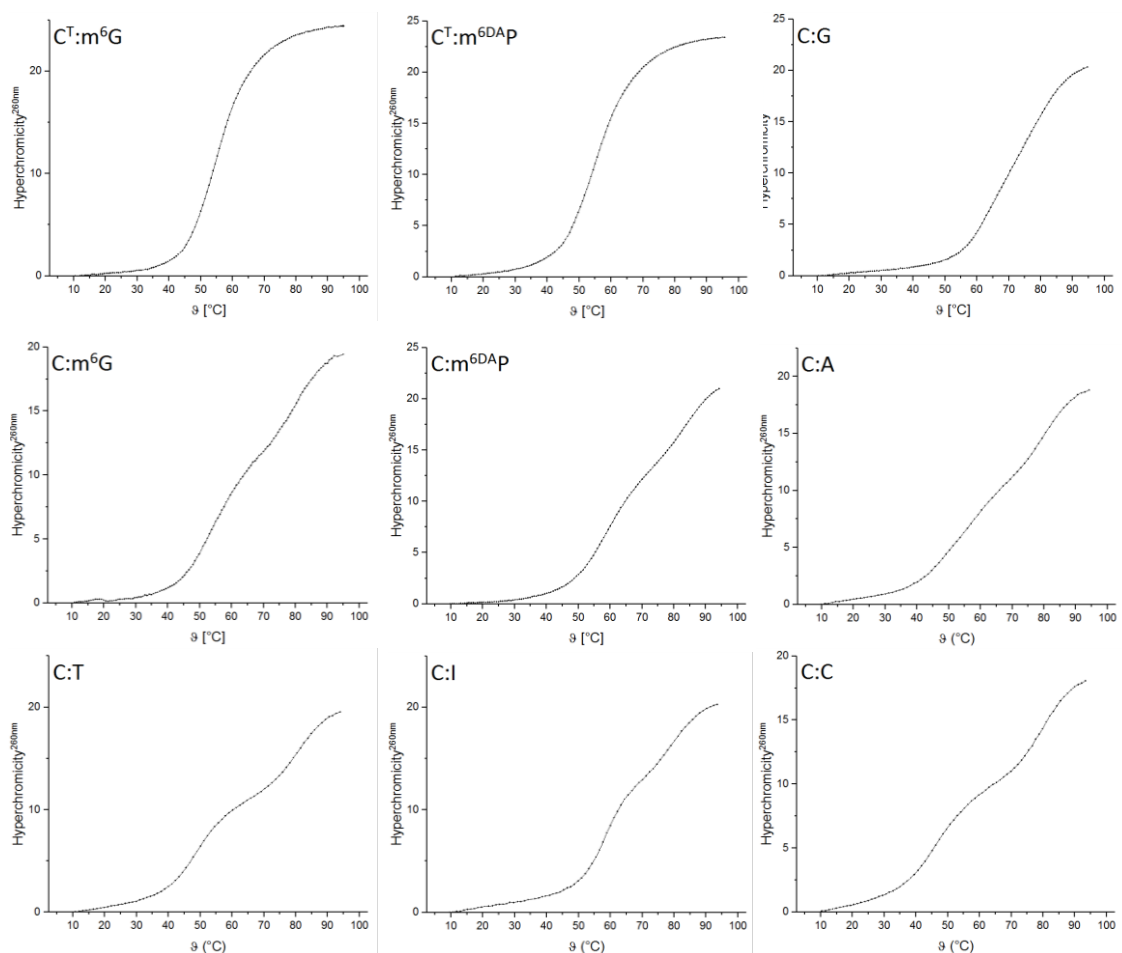
Fig. 77: Melting curves of single strand III and the seventeen different combinations of oligonucleotides made up of I, II, III and the complementary strands IV, V, VI, VII, VIII, IX and X.

Some of the curves, especially those for the unmodified strand **I**, show an unusual shape with a second melting temperature, which could be due to the hairpin structure, which can be formed by the single strands, having a different melting temperature. Nonetheless, fitting of the data to a ninth order polynomial was possible, and the melting temperatures of the nine duplexes were determined as the maximum of the first derivative (Table 3). In cases with two maxima, the lower temperature, attributed to melting of the duplex, was used.

Table 3: Melting temperatures of the duplexes made up of I, II and III and the complementary strands IV-X.

T_m [°C]	G	m^{6}G	m6^{DA}P	A	T	I	C
C	69.9	54.3	59.6	53.4	50.1	59.5	47.3
C^T	58.4	55.0	54.7				
B^S	55.4	57.3	56.9	55.5	55.3	55.6	55.2

As expected, the completely unmodified **I:IV** duplex with the G:C base-pair is by far the most stable. Melting temperatures of the other duplexes are mostly between 50 °C and 60 °C. However, there is a

noticeable difference between **II** and **III**. While both C^{TEMPO} and benzi-spin (**1**) cause a significant drop in melting temperature compared to cytidine, C^{TEMPO} seems to be slightly more stable when paired to guanosine compared to m^6G and $m^{6DA}P$, while the opposite seems true for benzi-spin. These results agree with the expected base pairing behavior of the two nucleotides. In both cases, there is little difference, less than 0.5 °C, between **V** and **VI** as the complementary strand, thus indicating that the methoxy or methylamino group in position 6 is not involved in base pairing. While benzi-spin causes a significant decrease in melting temperature compared to the unmodified duplex, all melting temperatures with B^S are within a range of about 2 °C. The melting temperatures for most base-pairs even fall within 0.5 °C, only the methylated nucleotides are slightly more stable. By comparison, the melting temperatures for the duplexes involving strand **I** are further apart, from almost 70 °C for the canonical G:C pair to less than 50 °C for the C:C pair. This speaks for the universal applicability of benzi-spin, as it shows little discrimination between all opposing nucleotides tested in this study.

3.1.8 EPR spectroscopic investigation of benzi-spin

To check if the different base pairs have an effect on the EPR spectra, CW EPR spectra of benzi spin (**1**) as well as oligonucleotide III containing benzi-spin as a single strand and double strand paired with oligonucleotides **IV**-**X** were recorded in cooperation with Dr. Ivo Krummenacher (Fig. 78).
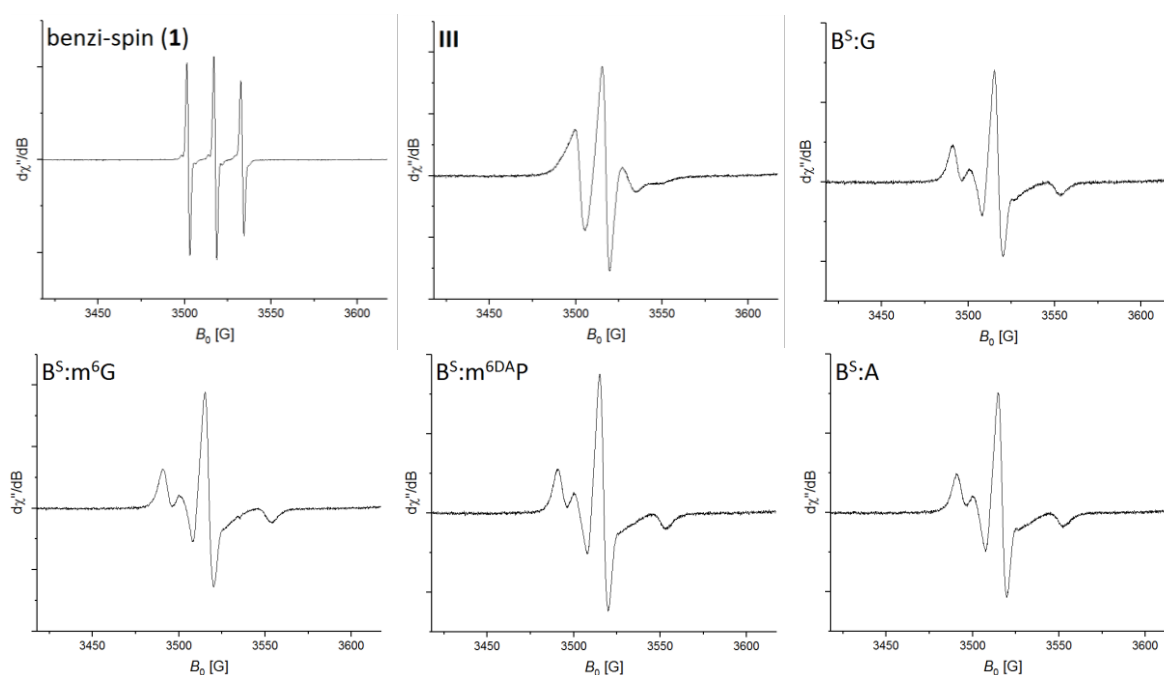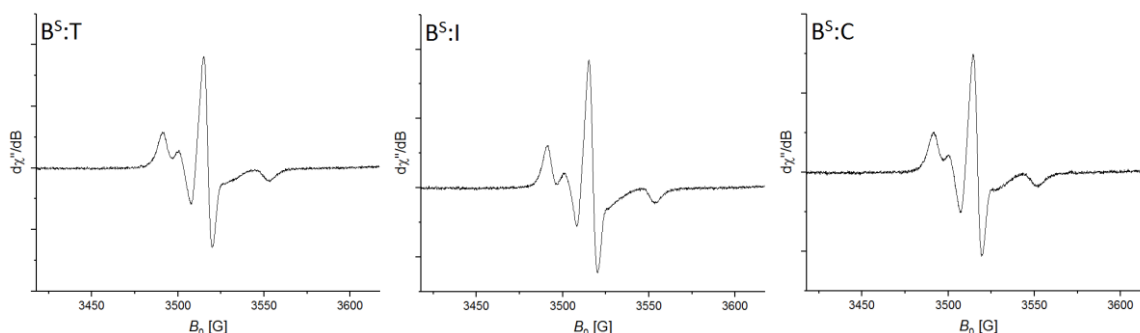
Fig. 78: CW EPR spectra of benzi-spin (1) and benzi-spin containing oligonucleotide III as a single strand and as double strands paired with IV-XI.

From the EPR spectra, the central line width ΔH_0 and the spectral width $2A_{zz}$ were determined. The spectra were simulated to obtain information about the rotational correlation time τ_r (Table 4).

Table 4: Central line widths (ΔH_0), spectral widths ($2A_{zz}$) and rotational correlation times (τ_r) for benzi-spin labeled oligonucleotide III as a single strand and double strands paired with oligonucleotides IV-X.

Name	base pair	ΔH_0 [mT]	$2A_{zz}$ [mT]	τ_r [ns]
III	B^S:G	0.43	7.49	3.1
III:IV	B^S:G	0.50	6.97	11.8
III:V	B^S:m^{6}G	0.49	7.13	10.0
III:VI	B^S:m^{6DA}P	0.49	7.14	9.3
III:VII	B^S:A	0.50	7.02	9.7
III:VIII	B^S:T	0.50	7.09	8.5
III:IX	B^S:I	0.49	7.04	10.7
III:X	B^S:C	0.53	6.94	8.5

The spectrum of benzi-spin (**1**) features three narrow lines, as expected from a nitroxide, because of hyperfine coupling of the unpaired electron to the nitrogen, which has a nuclear spin $I(^{14}N) = 1$. The intensity of the third line is smaller compared to the other two, which could be indicative of slower tumbling of the nucleoside compared to a smaller molecule like TEMPOL, which usually shows three lines of equal intensity. When incorporated into oligonucleotide **III**, all lines show significant broadening, as the rotational correlation time is now in the order of nanoseconds (Table 4), compared to the nucleoside, where it is in the order of picoseconds. Compared to Çm in the same sequence context[117], the spectra look very similar (Fig. 78). One notable difference is in the splitting of the third line, which is less pronounced for benzi-spin as it is for Çm. This seems to suggest that Çm is more rigid in this case. The reason for this could be that in the hairpin, there is a guanosine opposite to the spin label, with which Çm should be able to form a stable base pair, while the benzi-spin:G pair should be less stable. When it comes to the double strands, the first line is also split in two, for a total of five lines. All of the duplex spectra look fairly similar and the simulations show

significantly higher rotational correlation times than the single strand. This suggests that benzi-spin does not discriminate much between different base pairing partners, which is the desired property for a universal nucleoside. In order to answer the question of whether benzi-spin is rigid enough for applications like PELDOR, the spectra were compared to those of Çm in the same duplex context[117] (Fig. 79). This comparison shows little difference between the two spin labels, which means that benzi-spin should be similarly rigid, which means it should show similar performance as the successful Ç family of spin labels.
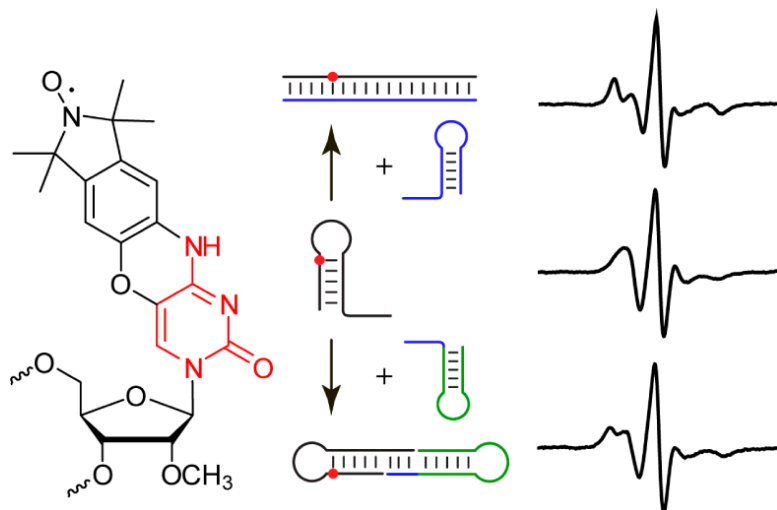
Fig. 79: Structure of rigid spin label Çm and its CW EPR spectra in different secondary structures. The figure was taken from [117].

3.1.9 Characterization and photoreactivity of nucleoside 1a

Nucleoside **31** was deprotected with NaOMe to obtain free nucleoside **1a**, the non-oxidized derivative of benzi-spin (**1**), for characterization (Fig. 80).
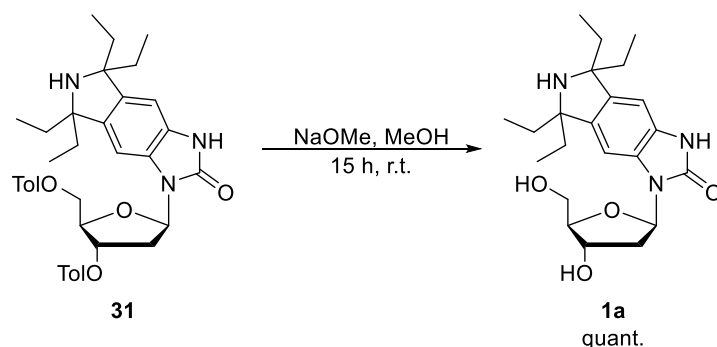
Fig. 80: Deprotection of compound 31 to obtain free nucleoside 1a.

Even though rigid spin labels are generally not fluorescent, as the radical quenches the fluorescence, their non-oxidized precursors often are, as is the case with Ç[115] and lumi-spin (see chapter 3.2.4). This makes them potentially applicable as fluorescence labels. To investigate the possibility of nucleoside **1a** being usable as a fluorescence label as well, UV/VIS and fluorescence spectra were recorded

(Fig. 81). The UV absorption maximum is at 290 nm; therefore, the first fluorescence emission spectrum was recorded with an excitation wavelength of 290 nm. It contained two peaks, at 319 nm and 420 nm respectively. While the excitation spectrum at 319 nm did show a maximum at 290 nm as expected, the spectrum at 420 nm showed three different signals instead, at 250 nm, 305 nm and 316 nm. Emission spectra recorded with excitation at those wavelengths did result in the emission maximum at 420 nm.

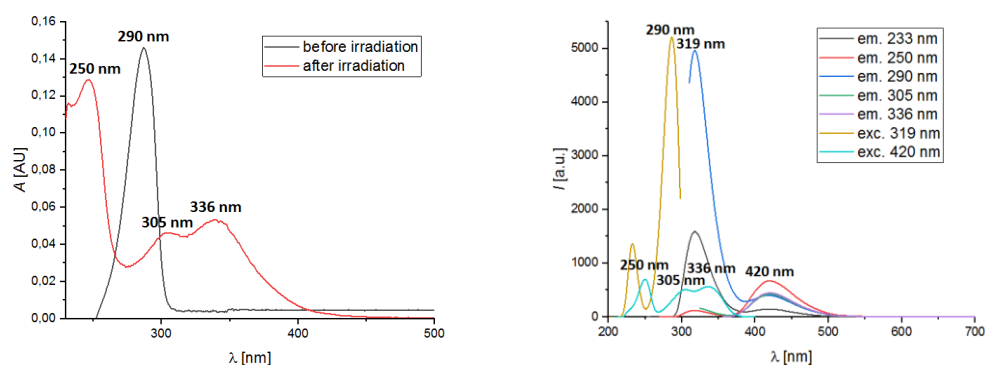**Fig. 81: Left: UV/VIS absorption spectra of nucleoside 1a at 20 μM in water with 2 % DMSO before (black) and after (red) irradiation for 16 h at 290 nm. Right: Fluorescence emission (exc. at 233 nm (black), exc. at 250 nm (red), exc. at 290 nm (blue), exc. at 305 nm (green), exc. at 336 nm (purple)) and excitation (em. at 319 nm (yellow), em. at 420 nm (cyan)) spectra of nucleoside 1a at 20 μM in water with 2 % DMSO.**

The existence of the additional excitation maxima was surprising, considering that only one absorption peak was visible in the UV/VIS spectrum. Upon further investigation, it was found that each emission spectrum recorded with an excitation wavelength of 290 nm did result in an increase in the intensity of the fluorescence emission at 420 nm. A series of 240 spectra was recorded in a 30 s interval, the results of which are shown in Fig. 82 (top left). Both emission peaks show significant changes with the number of spectra recorded (Fig. 82 top right). The initially larger maximum at 319 nm decreases in intensity with subsequent measurements, while the maximum at 420 nm, which is barely visible in the beginning, shows an increase in intensity. The difference between beginning and end of this experiment are shown in more detail in Fig. 82 (bottom), where 3D fluorescence emission graphs for a fresh, not previously irradiated sample of nucleoside **1a** (left), and the sample subjected to the previously mentioned measurement of the series of 240 spectra (right) are shown. The results further visualize the results obtained with the normal spectra in Fig. 81. Without prior irradiation, the excitation maximum is at 290 nm with emission mostly at 319 nm, after irradiation the behavior of the compound changes significantly, with three different excitation maxima, 250 nm, 305 nm and 336 nm, causing emission at 420 nm. A sample of **1a** was irradiated for 16 h at 290 nm and another UV/VIS spectrum was recorded, showing absorption maxima at 250 nm, 305 nm and 336 nm instead of the original maximum at 290 nm (Fig. 81 left, red graph).
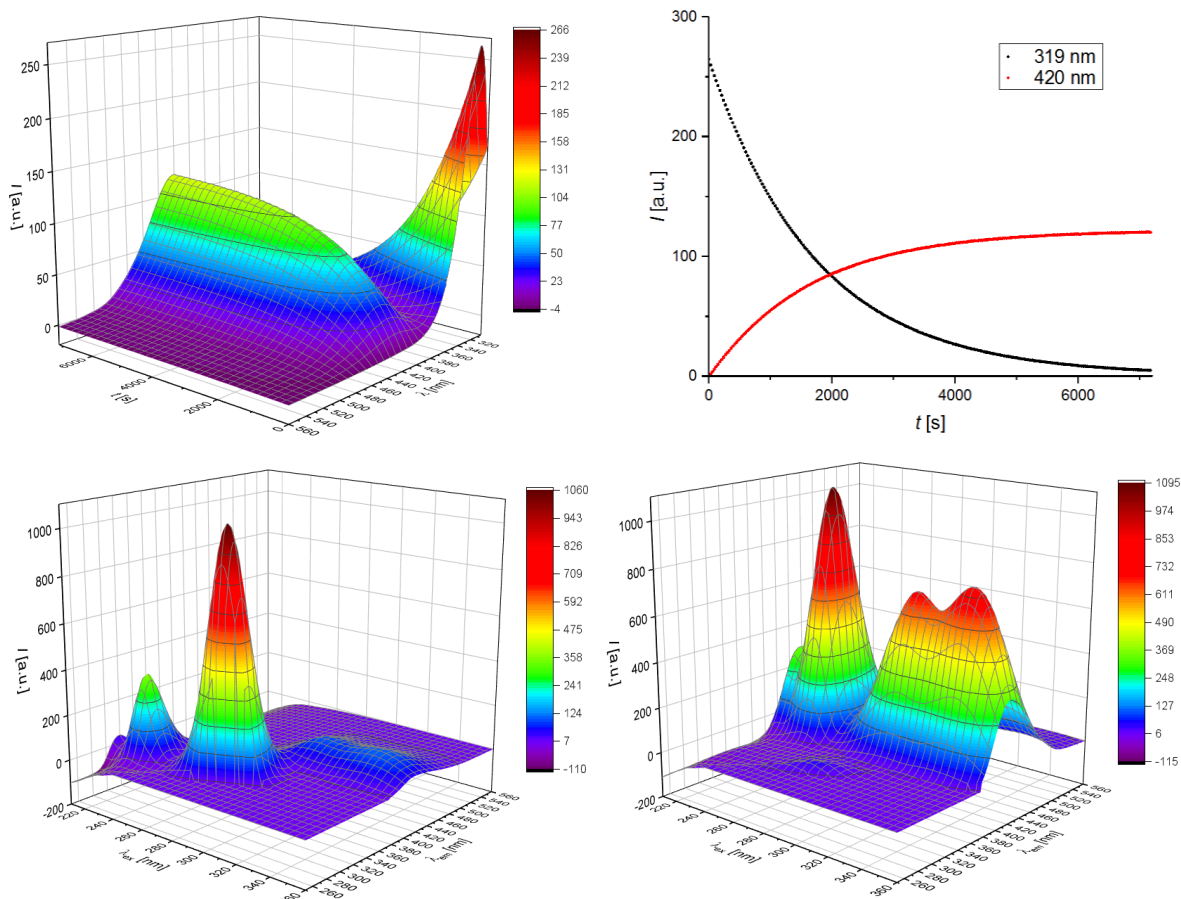
Fig. 82: Top left: Fluorescence emission spectra of nucleoside 1a (20 µM in water with 2 % DMSO) recorded at an excitation wavelength of 290 nm. 240 spectra were recorded in total, with a 30 s interval between measurements. Top right: Fluorescence emission curves at 319 nm and 420 nm extracted from the spectra in top left. Bottom: 3D fluorescence spectra with excitation wavelengths from 210 nm to 360 nm and emission wavelengths from 250 nm to 560 nm, of a fresh sample of nucleoside 1a (bottom left) and a sample of 1a previously subjected to the interval measurements shown in the top graph (bottom right).

The spectroscopic data suggest that irradiation of **1a** triggers a photochemical reaction, which forms a fluorescent product. For confirmation, an irradiated (290 nm, 16 h) sample of **1a** was analyzed by HPLC-MS, to check for the formation of a new compound (Fig. 83). As the chromatograms show, **1a** ($C_{22}H_{33}N_3O_4$, upper EIC) is not present in the sample anymore. Instead, there are two peaks with the sum formula $C_{20}H_{27}N_3O_4$ (lower EIC), which are also visible in the UV chromatograms for both 290 nm and 340 nm. A number of compounds which would fit the new sum formula are shown in Fig. 84. It should be noted that for compounds **1d** and **1e** only the *Z*-isomers of the new double bond are shown, though formation of the corresponding *E*-isomers would also be possible, resulting in six possible compounds.
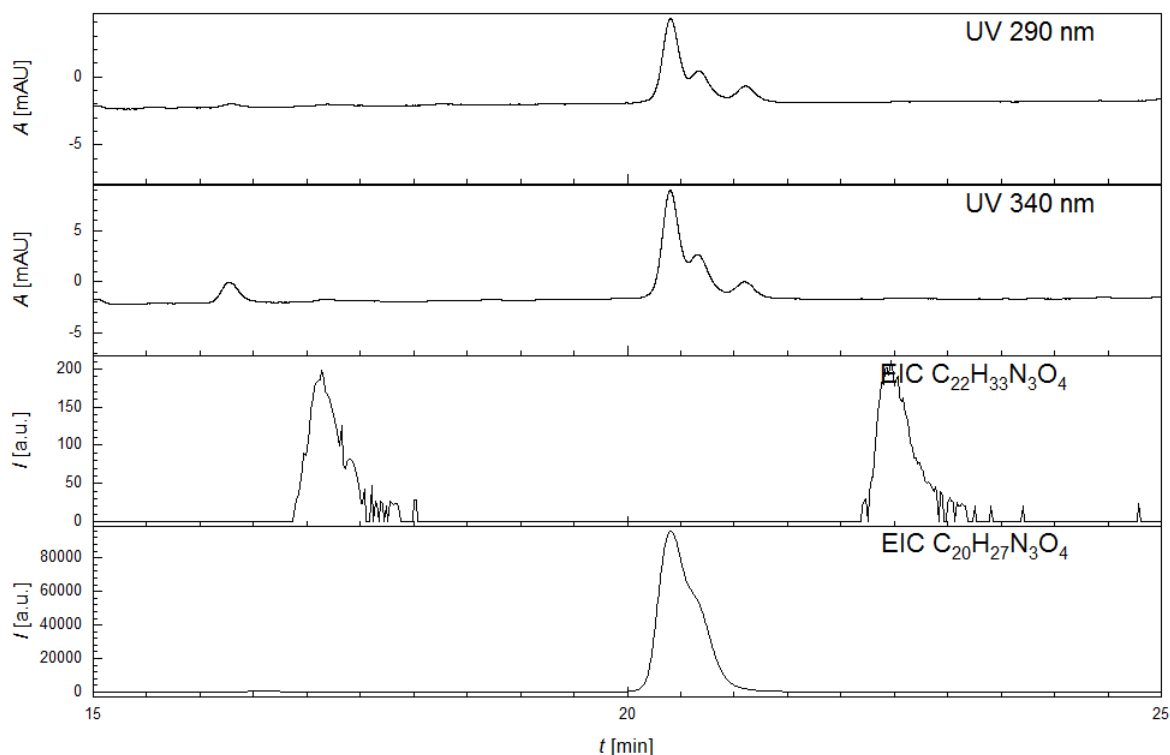
Fig. 83: HPLC-MS chromatograms of an irradiated sample (16 h, 290 nm) of nucleoside 1a. UV chromatograms with absorption at 290 nm and 340 nm and extracted ion chromatograms for the sum formulas of 1a and 1b-e are shown.
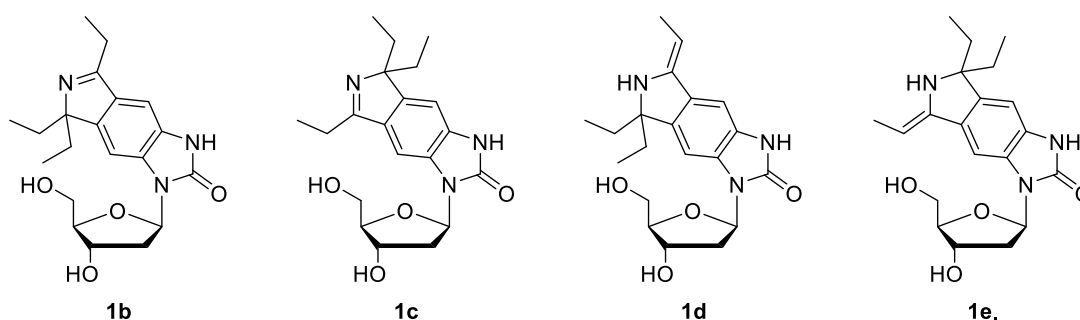
Fig. 84: Possible products resulting from the photochemical reaction of nucleoside 1a.

A common feature of all these compounds is that they have lost one of the four ethyl groups, and in its place, contain a new double bond, which is conjugated to the aromatic ring. The expansion of the aromatic system could explain the different spectroscopic behavior of the product compared to **1a**. An attack of the nitrogen to form a double bond to the neighboring carbon atom, like in compounds **1b** and **1c**, is part of the accepted mechanism of the tetraalkylation by Grignard reaction, while it has also been shown that elimination to an ethylidene group, as in structures **1d** and **1e**, is also possible under certain conditions, but with the nitrogen being protected[171]. However, the dealkylation of **1a** is a photochemical reaction, which likely proceeds by an entirely different mechanism, so a decision about the product cannot be made based on this information. A more thorough investigation would be required to determine which products are formed exactly. If they could be isolated and turned into a phosphoramidite, they might be incorporated into oligonucleotides as fluorescent probes.

3.2 Synthesis of rigid spin label lumi-spin

3.2.1 Original plan

The usefulness of a spin label for distance measurements depends on its rigidity. It has been shown that Ç is well suited for this, due to its rigid scaffold where the isoindoline and pyrimidine parts are linked by an oxazine ring[116-118]. Therefore, using Ç as a starting point for the development of further spin labels was considered a logical choice. The idea was to replace the oxazine ring with a diazine ring, which can be formed in one step from diaminoisoindoline compound **8** and alloxane monohydrate (**43**). This would have the advantage of being a shorter and thus more efficient synthesis. Also, by attaching the sugar after preparation of the nucleobase rather than coupling the isoindoline part to a nucleoside it should be possible to achieve a different orientation of the spin label compared to Ç, because the sugar would be attached at another position on the nucleobase, resulting in lumi spin (**2**) (Fig. 86). The lumi-spin nucleobase could be considered an expanded pteridine. It is related to alloxazine (Fig. 85 A). The name lumi-spin was derived from lumichrome, a derivative of alloxazine (Fig. 85 B). Substitution in position 10 causes the compounds to exist as isoalloxazine (Fig. 85 C), a tautomer of alloxazine. Isoalloxazines are especially biologically relevant, because flavins, like riboflavin (Fig. 85 D), are part of this class of molecules.

A   **B**   **C**   **D**

Fig. 85: Structures of alloxazine (A), lumichrome (B), isoalloxazine (C) and riboflavin (D).

Nucleosidation of the lumi-spin nucleobase could result in a number of different structures, depending on which nitrogen is the most reactive (Fig. 86). Nucleosidation in position 1 leads to lumi-spin (**2**), position 11 of would result in flavi-spin, which resembles riboflavin. Those isomers are similar in their structure, as the orientation of the nucleobase with respect to the ribose is similar and their Watson-Crick face resembles uridine in both cases, although in case of flavi-spin, it protrudes further into the duplex, which would probably destabilize a base-pair with adenosine. Substitution in position 3 can also be considered, which would result in a Ç-like structure. In this compound, the nucleobase could exist as both the alloxazine (allo) and isoalloxazine (iso) tautomers.

Which tautomer is preferably adopted should determine the base-pairing capabilities of the nucleoside. While the iso form should behave like cytidine, the allo form might be expected to behave more like uridine. It could also be possible that tautomerization would allow the spin label to pair with both adenosine and guanosine by adopting the required form depending on the opposing nucleotide, if the less favored tautomer is sufficiently stabilized by the hydrogen bonds.
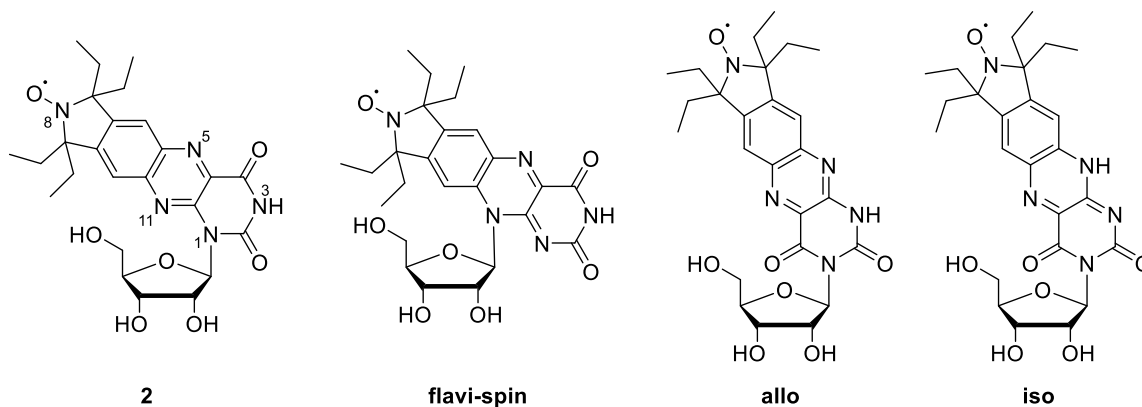

Fig. 86: Comparison of lumi-spin (2) and its hypothetical isomers.

Like benzi-spin, lumi-spin was initially designed with methyl groups for radical stabilization, but at a later point this choice was reevaluated and ethyl groups were introduced instead due to their larger stabilizing effect. The synthesis would begin from phthalic anhydride (**10**), like all syntheses for isoindoline labels. In fact, the first part of this synthesis is exactly the same as for benzi-spin (**1**), because diaminoisoindoline compound **8** is required here as well. But instead of reacting with CDI, it would need to react with alloxane monohydrate (**43**) to form compound **42**. The most critical step of the synthesis would be the nucleosidation by Vorbrüggen reaction, which could result in several possible products. After determining which compound was obtained, oxidation to nitroxide **40** and further steps to obtain phosphoramidite **39** could follow (Fig. 87).
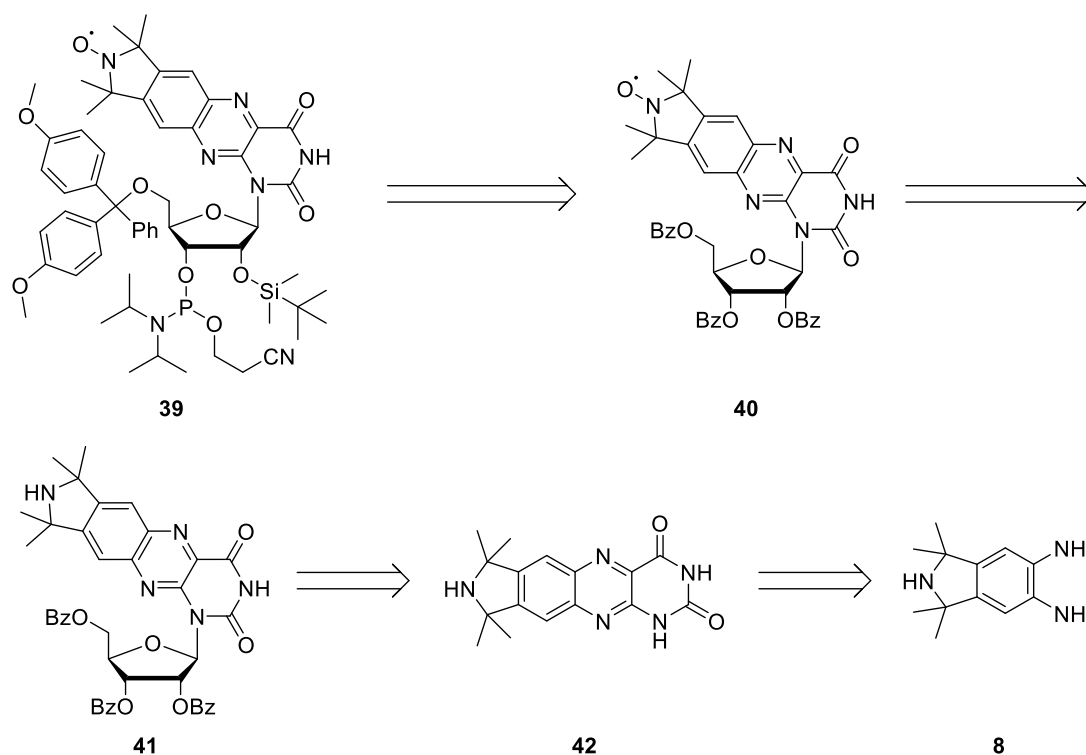
Fig. 87: Retrosynthetic overview of the synthesis of lumi-spin phosphoramidite 39.

3.2.2 Initial synthesis of the tetramethyl analog of lumi-spin

Diaminoisoindoline **8** was prepared as described in detail in chapter 3.1.2. Once it was finished, a condensation with alloxane monohydrate (**43**) under acidic condition was performed to get lumi-spin nucleobase **42** (Fig. 88)[172].
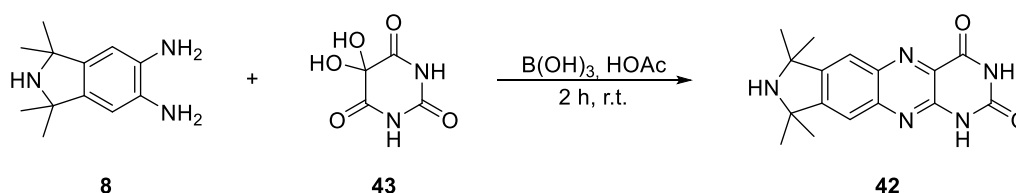

Fig. 88: Synthesis of compound 42.

Removal of acetic acid from compound **42** was challenging, and therefore the crude product was used for the next step without purification. This was the nucleosidation by Vorbrüggen reaction, also known as silyl-Hilbert-Johnson reaction[173]. In this reaction, trimethylsilyl (TMS) groups are first attached to the carbonyl groups of the nucleobase. Then, a Lewis acid and the protected ribose, where position 1 is protected with an acetyl group and positions 2, 3 and 5 with benzoyl groups, are added. In the presence of the Lewis acid, a cyclic cation will be formed by the ribose, where one benzoyl group is attached to positions 1 and 2. This cation will be attacked by the silylated nucleobase in position 1 to form the nucleoside. This reaction results in stereoselective formation of the β-anomer, because the nucleophilic attack can only happen from one side (Fig. 89).

N,O-bis(trimethylsilyl)acetamide (BSA) was used to transfer TMS groups to compound **42**, trimethylsilyl trifluoromethanesulfonate (TMSOTf) was used as the Lewis acid[119].
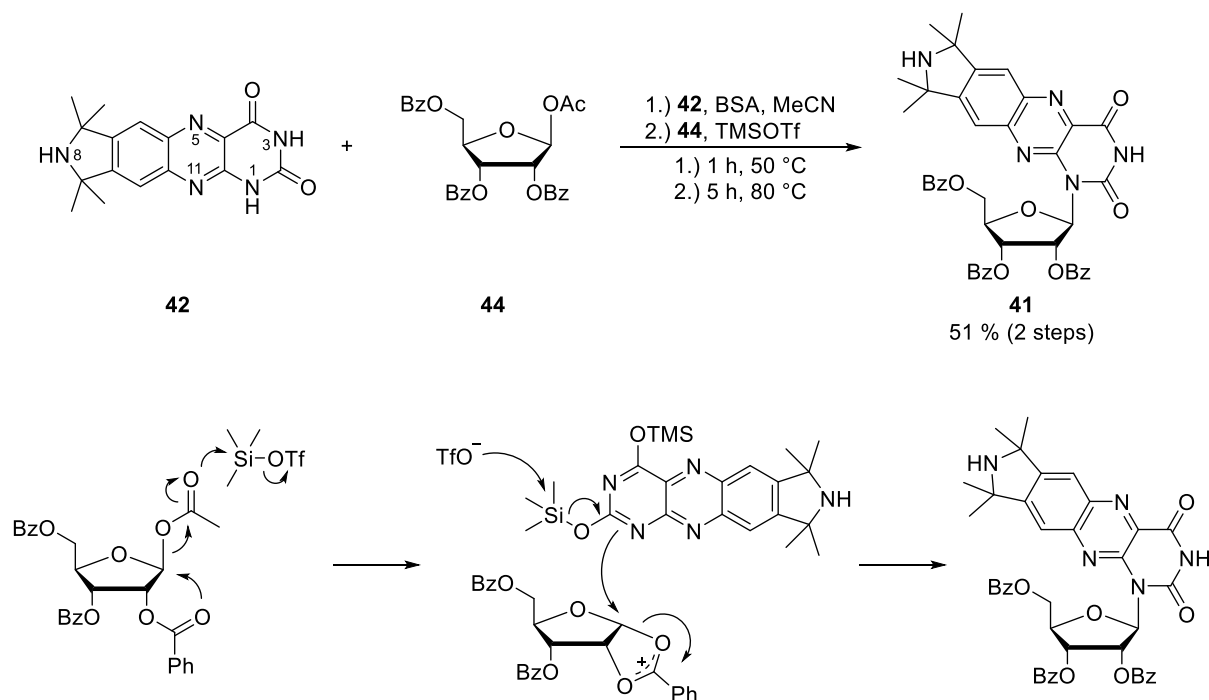

Fig. 89: Synthesis of protected nucleoside 41 by Vorbrüggen reaction. Top: Reaction scheme. Bottom: Illustration of the reaction mechanism including the cyclic cation formed as an intermediate, which causes stereoselectivity.

This reaction could potentially result in a number of different products, as there are multiple non-equivalent nitrogen atoms in compound **42**. Nitrogen 1 is the one which reacts when pteridine-2,4-dione is subjected to Vorbrüggen conditions[174], but of course confirmation from 2D-NMR spectra would be required. In order to obtain NMR spectra with fewer signals in the aromatic region, allowing for easier identification of the aromatic isoindoline protons, the benzoyl groups were cleaved off with sodium methoxide (Fig. 90)[166].
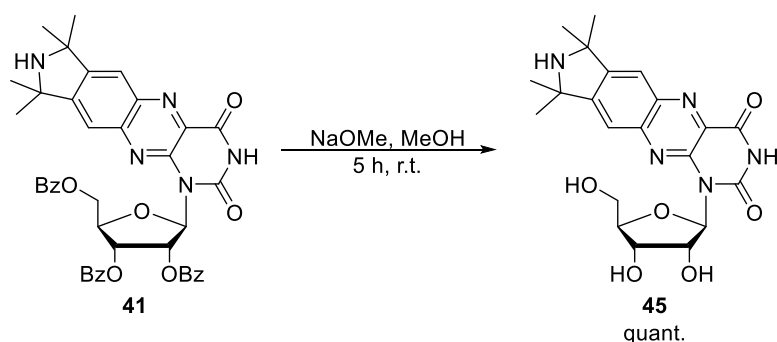

Fig. 90: Deprotection of compound 41 to obtain free nucleoside 45.

While NMR spectra of compound **45** could be obtained, the identification was hampered by some of the proton signals from the sugar being too broad to show correlation signals in the HMBC spectrum.

Among them was the 1'-proton, which would have been the most important for determination of the structure. It was tried to record a ^{15}N-HMBC spectrum, but no correlation between nucleobase and sugar was observed.

It was then decided to continue the synthesis regardless. A more detailed structural analysis was necessary at a later point anyway, for identification of 2'-and 3'-protected isomers. The next step was the introduction of a DMT group at the 5'-hydroxy function (Fig. 91)[166].
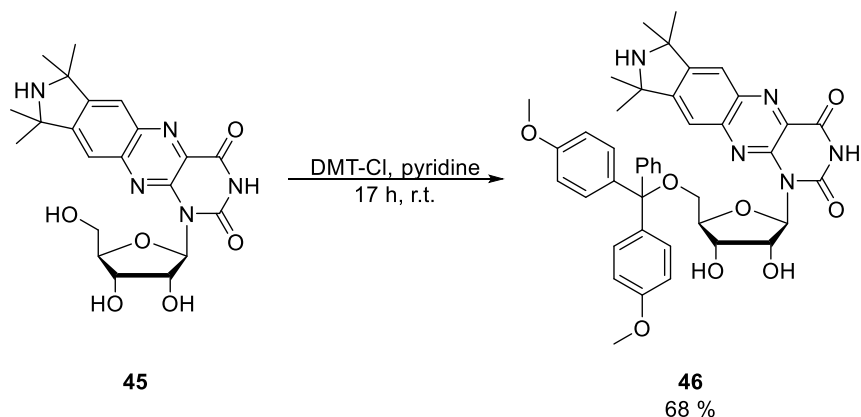

Fig. 91: Synthesis of DMT-protected nucleoside 46.

Next, the 2'-hydroxy group was protected with a *tert*-butyldimethylsilyl (TBDMS) group (Fig. 92). Silver nitrate was added because it has been reported to improve the selectivity towards the desired 2'-TBDMS isomer in some cases[175].
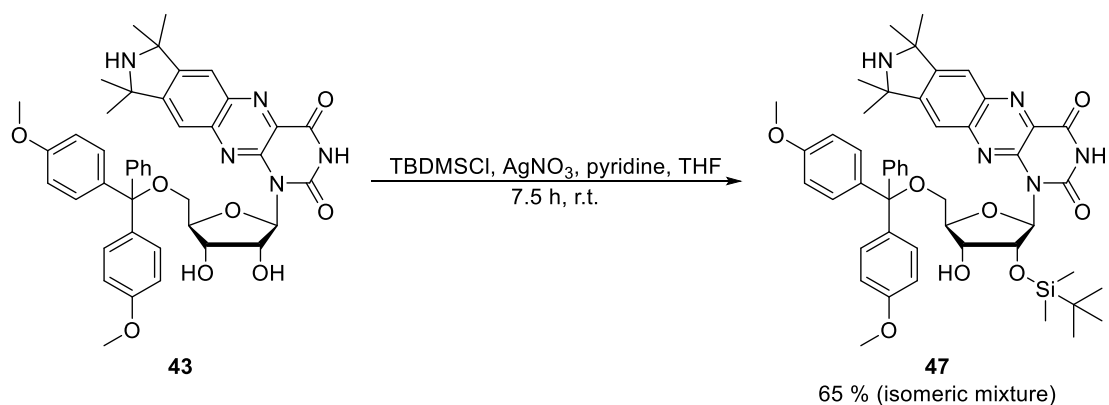

Fig. 92: Synthesis of compound 47, obtained in a mixture with the 3'-TBDMS isomer 48.

This reaction is not selective for the 2'-position and thus results in a mixture of 2'- and 3'-TBDMS isomers. Separation of those isomers can be challenging for some compounds and it was in this case as well. It was found that DCM/acetone (2:3 + 1 % NEt₃) at least caused partial separation. Still, only small amounts of pure isomers could be obtained after each column. Sets of spectra for both isomers were recorded, but identification proved to be impossible. Many peaks are broad, so in an attempt

to decrease their line width a set of NMR spectra of a sample containing both isomers in DMSO was measured at 80 °C, including a COSY spectrum (Fig. 93).
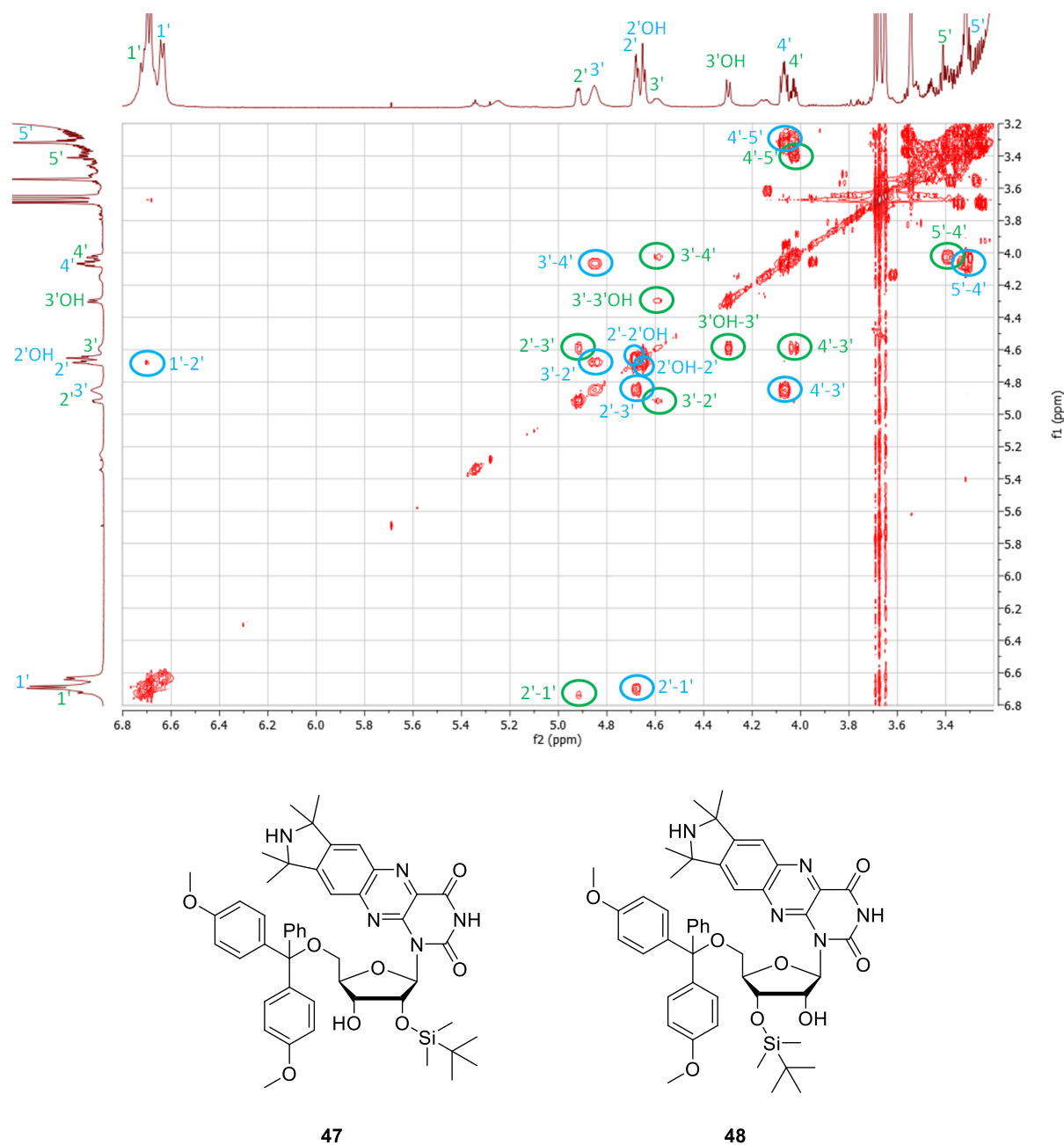

Fig. 93: Top: Part of the COSY spectrum of the mixture of compounds 47 and 48 in DMSO at 80 °C. Signals marked in green belong to the 2'-isomer 47, signals marked in blue belong to the 3'-isomer 48. Bottom: TBDMS regioisomers 47 and 48.

With this spectrum it was possible to assign all peaks, including the hydroxy groups, which then allowed identification of the isomers. Comparison to spectra of the pure compounds showed that 2'-TBDMS isomer **47** is the one which is eluting faster in column chromatography. Unfortunately, it could still not be determined at which position the sugar is attached to the nucleobase. It was clear at this point that the strategy had to be reworked, and because the benzi-spin project had by this

point shown the advantage of ethyl groups over methyl groups for nitroxide stability in solid phase synthesis, the methyl groups were changed to ethyl groups.

3.2.3 Synthesis of lumi-spin from a tetraethylisoindoline precursor

The synthesis branched off the synthesis of benzi-spin after diaminoisoindoline **29**. The synthesis of compound **29** is described in chapter 3.1.5. With it, the double condensation with alloxane monohydrate (**43**) was done to get compound **49**, which was again used for the next reaction without further purification (Fig. 94)[172]. The ^{1}H-NMR spectrum is shown in Fig. 95.
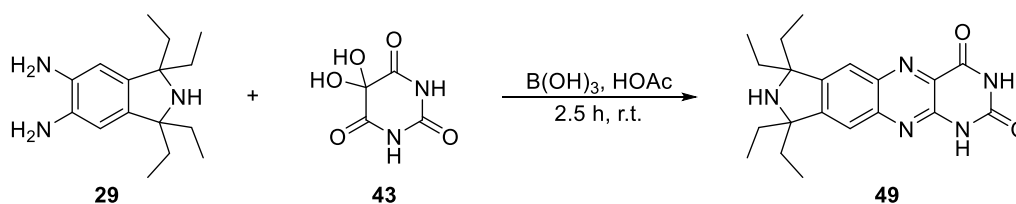

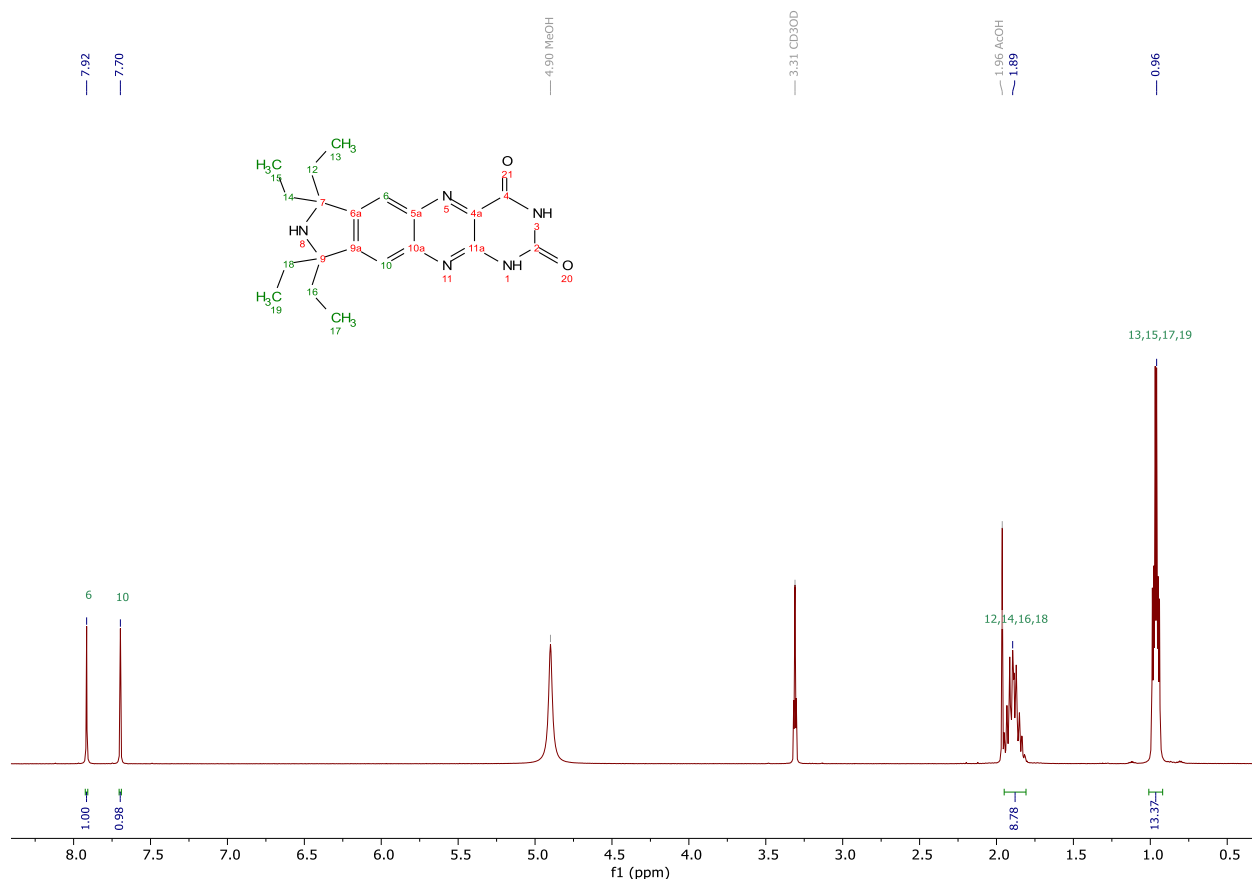**Fig. 94: Synthesis of compound 49.**

Fig. 95: ^{1}H-NMR spectrum of compound 49 in CD$_3$OD.

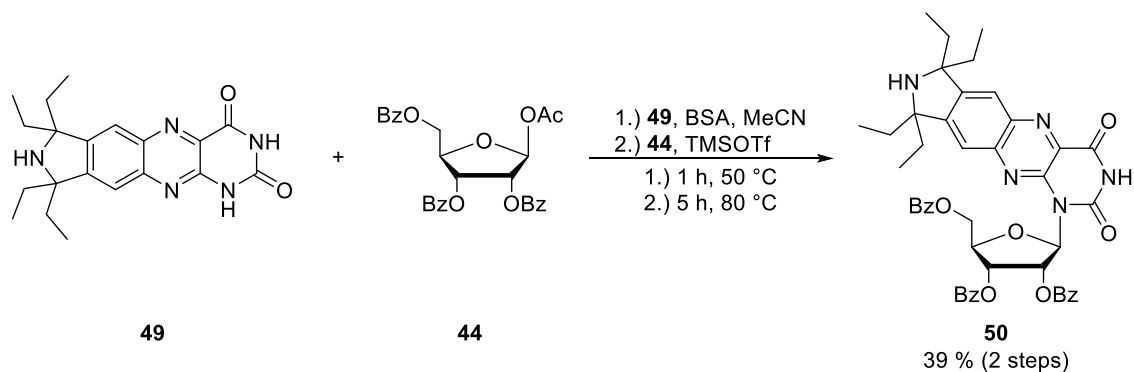Compound **49** was then used for nucleosidation, again using the Vorbrüggen method (Fig. 96)[119].

Fig. 96: Synthesis of protected nucleoside 50.

Next, the benzoyl groups were removed from a portion of compound **50** to obtain free nucleoside **51** for structure determination (Fig. 97)[166].
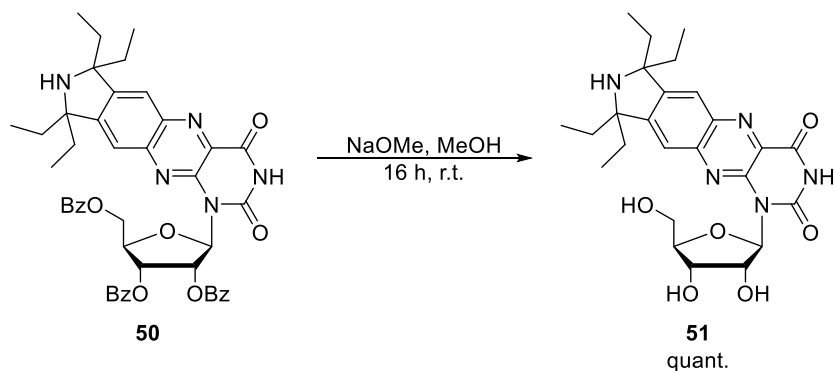

Fig. 97: Synthesis of nucleoside 51 by deprotection of compound 50.

Nucleoside **51** was then used to identify which of the possible regioisomers had been formed during nucleosidation. A set of NMR spectra was recorded, like the ^{1}H-NMR spectrum (Fig. 98). The spectra looked similar to those of compound **45**, with the 1'-proton signal not showing any HMBC correlations, even on a 600 MHz spectrometer with the pulse sequence being optimized for small coupling constants. However, the 2'-proton shows HMBC correlations and while no correlations to carbon atoms on the nucleobase can be seen, there is a visible correlation between the 2'-proton and a nitrogen atom in the ^{15}N-HMBC spectrum (Fig. 99).
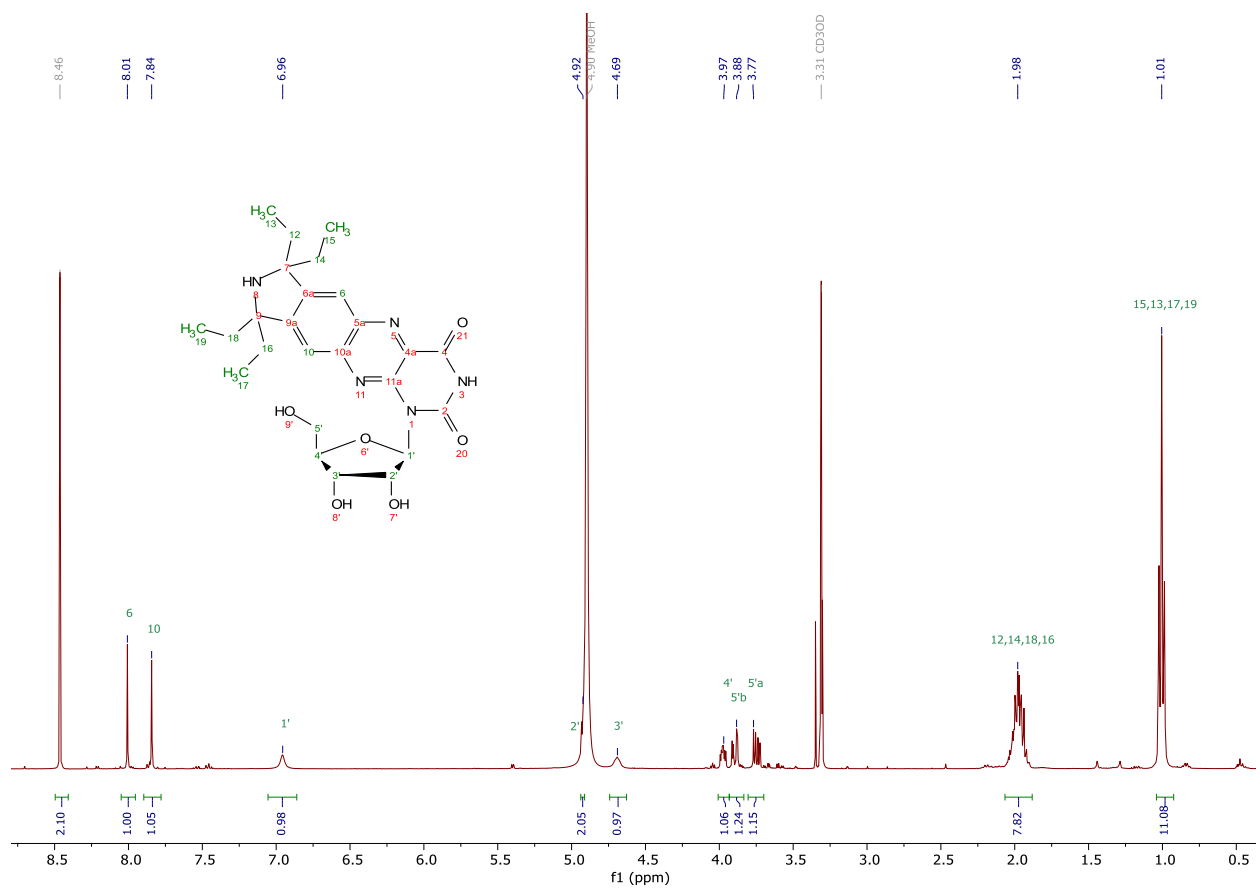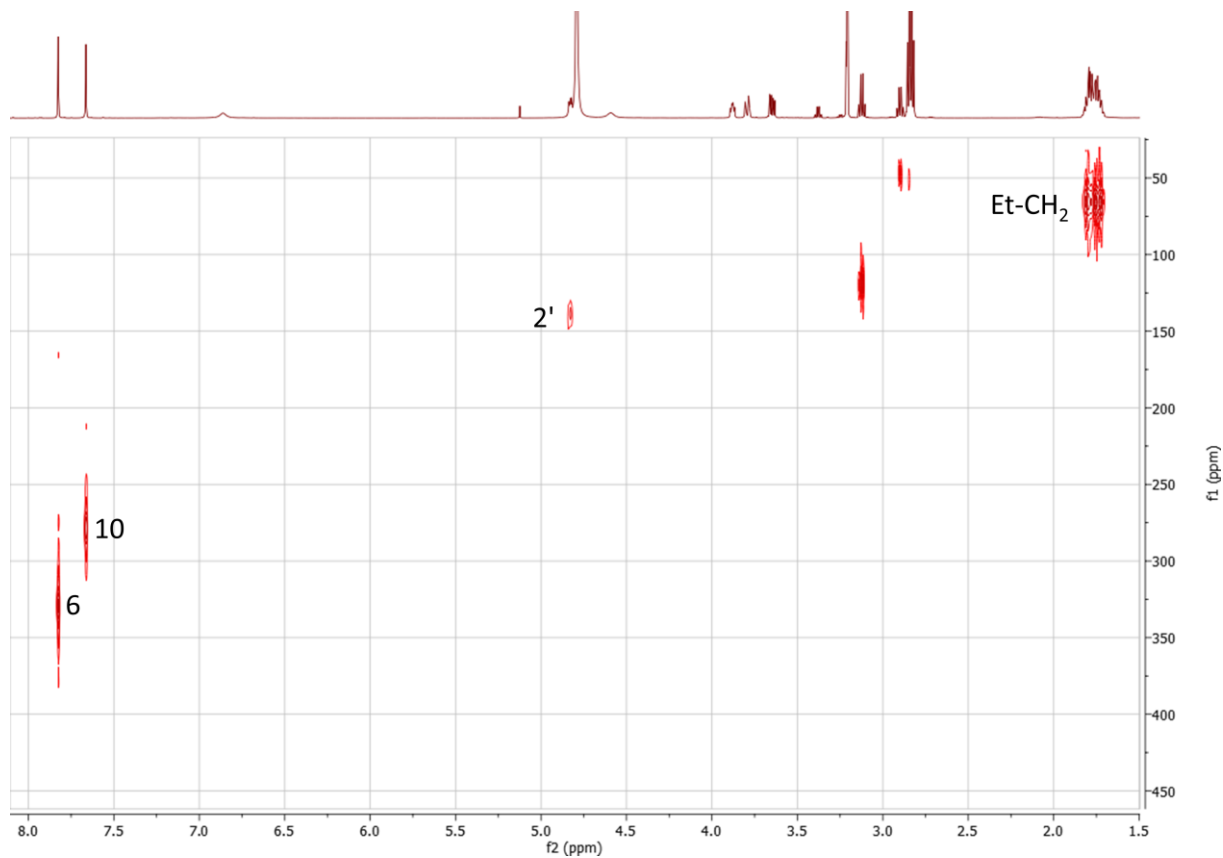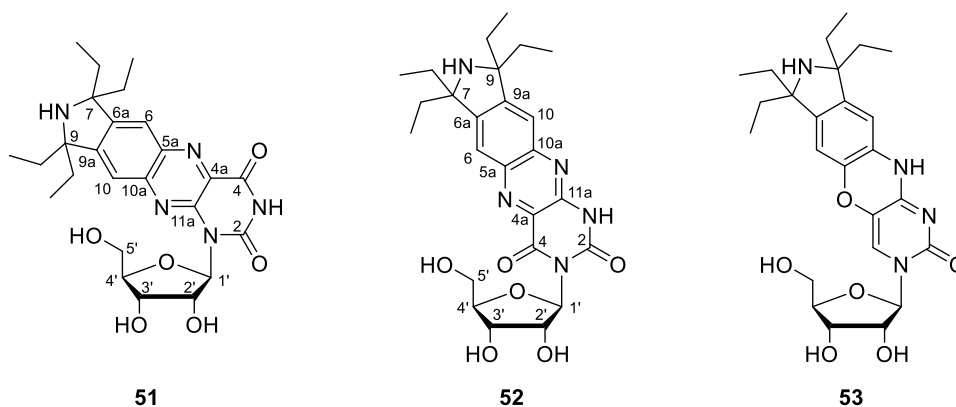
Fig. 98: ^{1}H-NMR spectrum of nucleoside 51 in CD$_3$OD.

51   **52**   **53**

The ethyl groups in positions 7 and 9 as well as the aromatic protons 6 and 10 show correlations to different nitrogen atoms than the 2'-proton. Therefore, nitrogen atoms 5, 8 and 11 cannot be the positions where the sugar is attached, so flavi-spin (Fig. 86) is out of consideration. This leaves two possible structures, **51** and the more Ç-like structure **52** (Fig. 99).

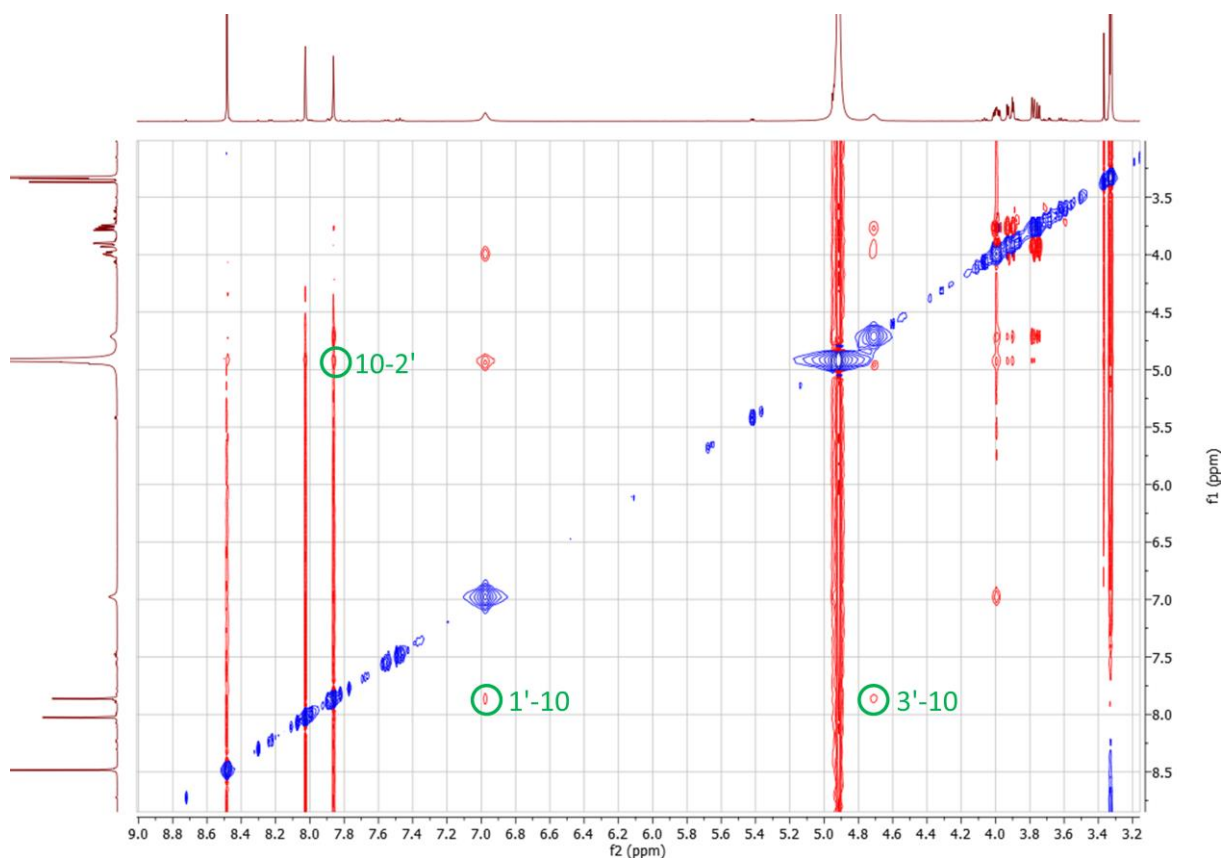**Fig. 100: Part of the NOESY spectrum of compound 51 in CD₃OD. Relevant signals are marked with green circles and annotations showing which protons are responsible for the signals.**

Reaction of pteridine-2,4-dione under Vorbrüggen conditions leads to a product analogous to compound **51**[174], so it was considered to be the more likely product. To confirm this, the NOESY

spectrum of compound **51** was compared to the NOESY spectrum of EÇr precursor **53**. While the spectrum of compound **51** shows correlations between proton 10 and multiple sugar protons (Fig. 100), no such correlations are visible for compound **53**. Based on these results it was concluded that structure **51** is correct. This means that lumi-spin should behave differently compared to Ç when it comes to base pairing and therefore applications. Structure **52** by contrast would have had similar characteristics as Ç. Once the structure was determined, the synthesis was continued. Protected nucleoside **50** needed to be oxidized to compound **54** with *m*CPBA. This was possible in good yield (Fig. 101)[119].
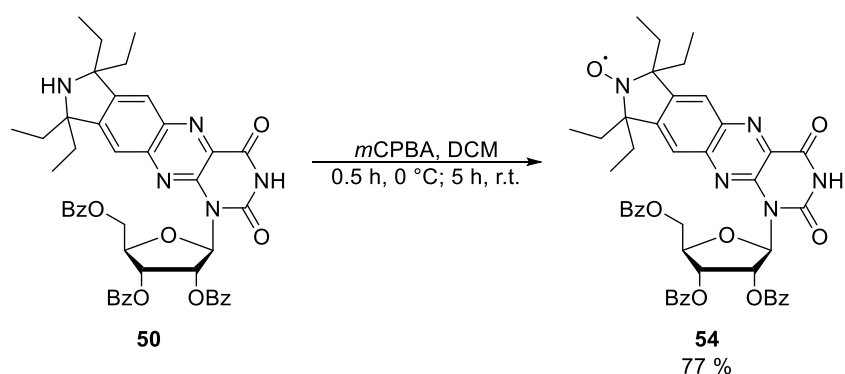

Fig. 101: Synthesis of protected spin label 54.

Compound **54** was then deprotected to yield the new spin label lumi-spin (**2**) in quantitative yield (Fig. 102)[166]. The ESI mass spectrum is shown in Fig. 103.
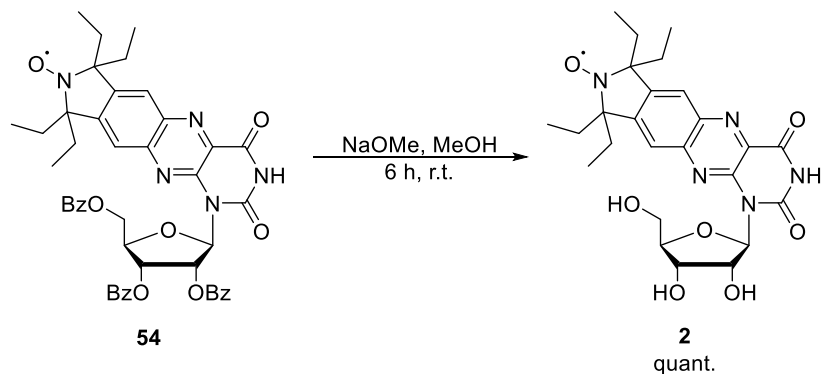

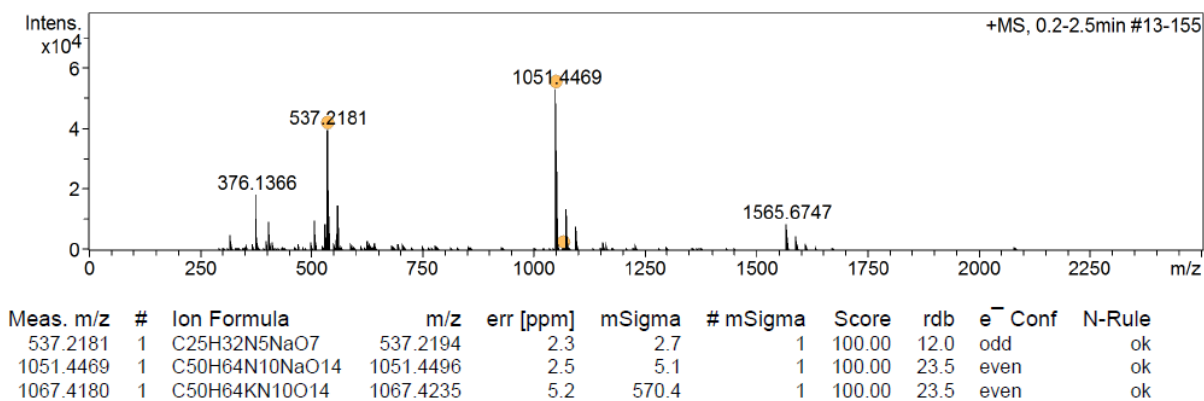**Fig. 102: Deprotection of compound 54 resulting in lumi-spin (2).**

Fig. 103: ESI mass spectrum of lumi-spin (2). The [M+Na]⁺ and [2M+Na]⁺ peaks are marked.

Meas. m/z	#	Ion Formula	m/z	err [ppm]	mSigma	# mSigma	Score	rdb	e⁻ Conf	N-Rule
537.2181	1	C25H32N5NaO7	537.2194	2.3	2.7	1	100.00	12.0	odd	ok
1051.4469	1	C50H64N10NaO14	1051.4496	2.5	5.1	1	100.00	23.5	even	ok
1067.4180	1	C50H64KN10O14	1067.4235	5.2	570.4	1	100.00	23.5	even	ok

With this, synthesis of lumi-spin (**2**) was complete. From here, the next steps which would need to be taken are to prepare a phosphoramidite for solid phase synthesis, and incorporating it into oligonucleotides.

3.2.4 Characterization by UV/VIS and fluorescence spectroscopy

Both alloxazines and isoalloxazines are fluorescent. The two classes show different spectroscopic characteristics, where in isoalloxazines, the absorption and emission maxima are shifted to higher wavelengths compared to alloxazines, while the fluorescence lifetime and quantum yield is increased[176]. An example of the differences in fluorescence characteristics between alloxazines and isoalloxazines is shown in Fig. 104. The UV absorption spectra of both compounds show two large maxima at short wavelengths and two smaller ones at higher wavelengths. The distance between the smaller maxima is larger for 3-methyllumiflavin (left), with the peaks at 342 nm and 444 nm, while they are at 335 nm and 375 nm for 1,3-dimethyllumichrome (right). The fluorescence spectrum of 3-methyllumiflavin shows the emission maximum at 531 nm, emission of 1,3-dimethyllumichrome appears at 437 nm, a significantly lower wavelength.
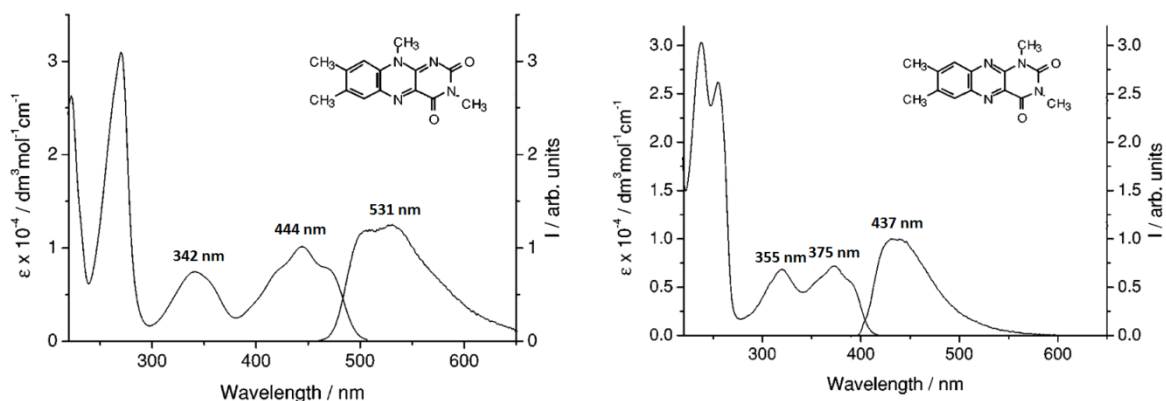

Fig. 104: Absorption and fluorescence spectra of 3-methyllumiflavin (left) and 1,3-dimethyllumichrome (right). The figure was adapted from [176].

78

While lumi-spin (**2**) is not expected to be fluorescent because the nitroxide should quench the fluorescence[115], nucleoside **51** before oxidation should be. Therefore, UV/VIS absorption as well as fluorescence emission and excitation spectra were recorded (Fig. 105).
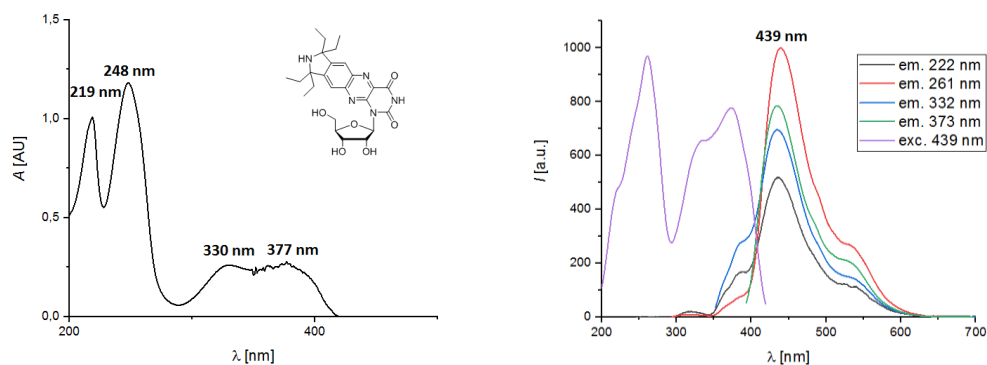

Fig. 105: Left: UV/VIS absorption spectrum of nucleoside 51 at 50 μM in water. Right: Fluorescence emission (exc. at 222 nm (black), exc. at 261 nm (red), exc. at 332 nm (blue), exc. at 373 nm (green)) and excitation (em. at 439 nm (purple)) spectra of nucleoside 51 at 50 μM in water.

Compound **51** exhibits a typical fluorescence behavior for alloxazine compounds, as can be seen from a comparison of the spectra with those shown in Fig. 104. The UV absorption maxima are at 219 nm, 248 nm, 330 nm and 377 nm. Most of them are close to those of 1,3-dimethyllumichrome (Fig. 104, right), especially the two low energy maxima. The signal at the longest wavelength at 377 nm is the best indicator of similarity to the lumichrome (375 nm) rather than the flavin (444 nm). The same trend is also observed for the fluorescence emission, where the maximum is at 439 nm, which is significantly closer to the maximum of 1,3-dimethyllumichrome compared to 3-methyllumiflavin. This can be seen as more evidence that the ribose is not attached in position 11, because in that case the compound should show fluorescence similar to other isoalloxazines (compare Fig. 104, left), which it clearly does not.

3.2.5 CW EPR spectrum of lumi-spin

A CW EPR spectrum of lumi-spin (**2**) was recorded for comparison to other isoindoline-based nitroxide spin labels for nucleic acids (Fig. 106).
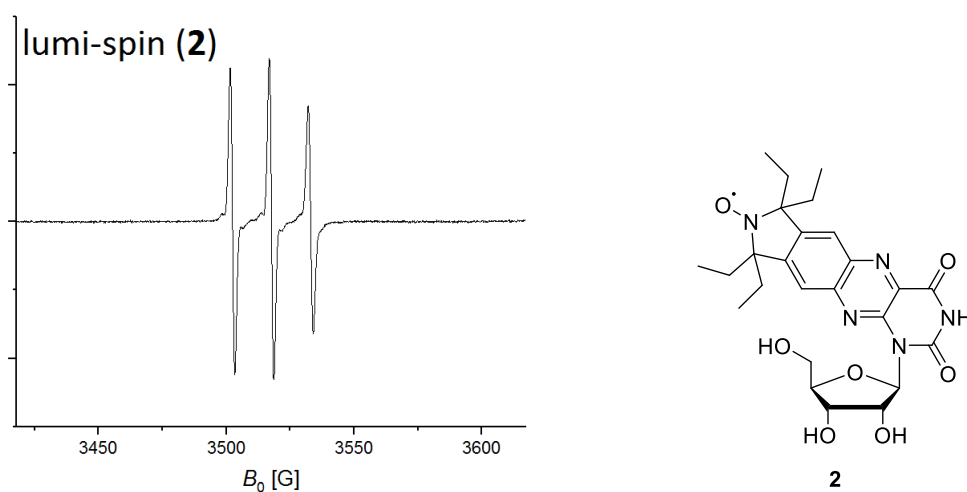

Fig. 106: Left: CW EPR spectrum of lumi-spin (2). Right: Structure of lumi-spin (2).

The spectrum shows three narrow lines, as expected from coupling to the nitrogen, where the third one is smaller than the other two. This weakening is the result of tumbling of the nucleoside in solution being slower compared to a small molecule[119], and is also observed for other nucleoside labels like Ç[115] or isoxyl-A[119]. The isotropic *g*-factor is the same as for benzi-spin (**1**) and EÇr (**3**), the hyperfine coupling constants are similar, which is not surprising as all compounds are nitroxides on nucleosides of similar size.

3.3 EÇr, a new rigid spin label in the Ç family

3.3.1 Objectives

Ç and Çm have been prime examples of rigid spin labels for nucleic acids in recent years[115-117], but there is still room for improvement. For example, the new versions EÇ and EÇm have been published recently, which use ethyl instead of methyl groups, resulting in improved stability of the nitroxide[118]. One point which was addressed in this work is the ribose. EÇ contains deoxyribose, making it suitable for use in DNA, but EÇm, which is supposed to be used in RNA, contains 2'-*O*-methylribose. This is useful for making the synthesis easier, because a 2'-silylation step, which would result in isomers that may be hard to separate, is not necessary. However, it does have the drawback that the methyl group is never removed, so there is no free 2'-hydroxy group, which can affect the structure of the final RNA, as the ability to function as a hydrogen donor has been lost. It was therefore considered desirable to create EÇr (**3**), a version of EÇ with an unmodified ribose (Fig. 107).

Additionally, a different method of incorporation into nucleic acids was to be tested. Until now, most rigid spin labels were incorporated by solid phase synthesis, which has some drawbacks. The problem of nitroxide stability during the synthesis can at least to some extent be overcome by using ethyl groups to stabilize the radical[118]. A problem which remains is the limited length of oligonucleotides that can be achieved in solid phase synthesis. Longer sequences have to be synthesized in pieces which are then ligated. Thus, EÇr (**3**) was converted to triphosphate EÇrTP (**55**) for enzymatic incorporation by primer extension (Fig. 107).
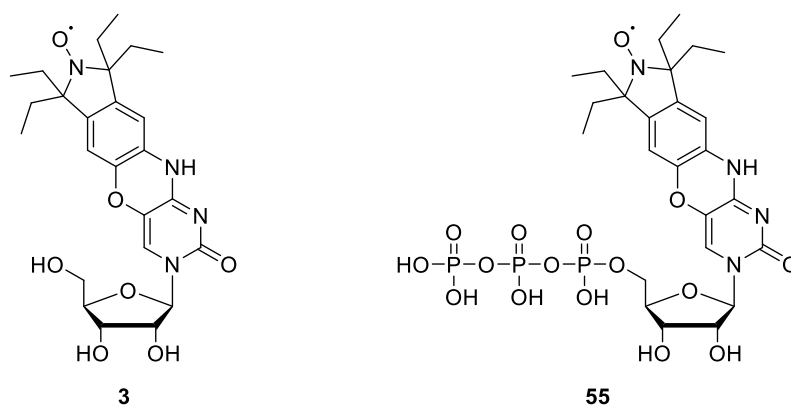
Fig. 107: Rigid spin label EÇr (3) and the corresponding triphosphate EÇrTP (55).

The synthesis was mostly based on the reported procedures for the synthesis of Ç and Çm[115, 117], with some changes, like using uridine (**59**) as the starting nucleoside, or using ethyl iodide instead of methyl iodide for the Grignard reaction. Two parts, modified isoindoline **58** and modified nucleoside **57** were prepared separately and then combined to form nucleoside **56**, which is then oxidized and converted to triphosphate **55** (Fig. 108).
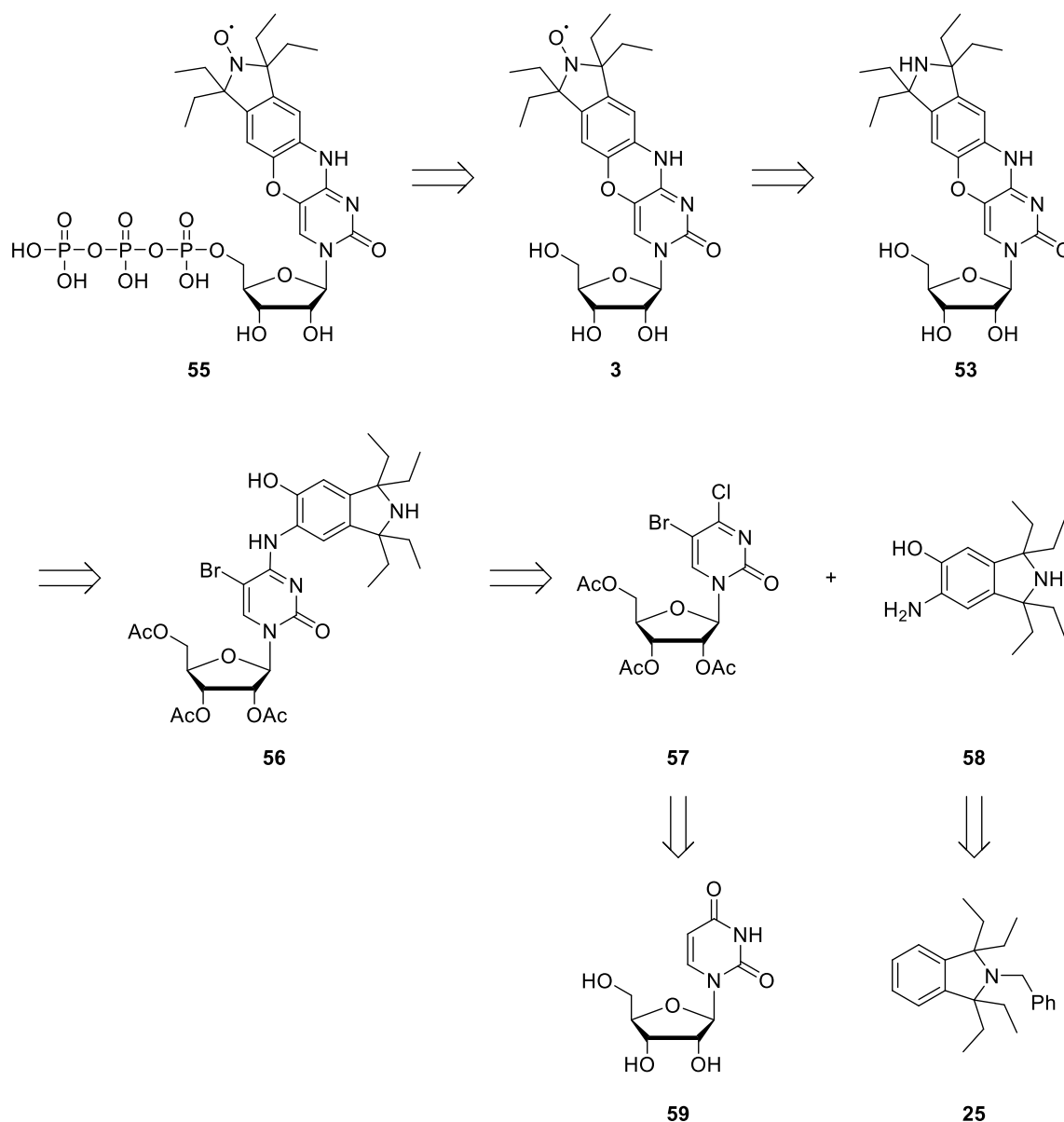
Fig. 108: Retrosynthetic scheme for the synthesis of EÇr (3) and EÇrTP (55).

3.3.2 Preparation of isoindoline 57 and modified nucleoside 58.

The initial steps of the synthesis are identical to those of benzi-spin and lumi-spin. The synthesis of compound **27** is described in chapters 3.1.2 and 3.1.5. The nitro group was then reduced to an amino group with hydrogen and palladium (Fig. 109)[168]. This amino group was then substituted by a hydroxy group, after being converted to a diazonium species with NaNO$_2$ (Fig. 109)[115]. Both compounds were obtained in good yield.

Fig. 109: Synthesis of compounds 60 and 61.

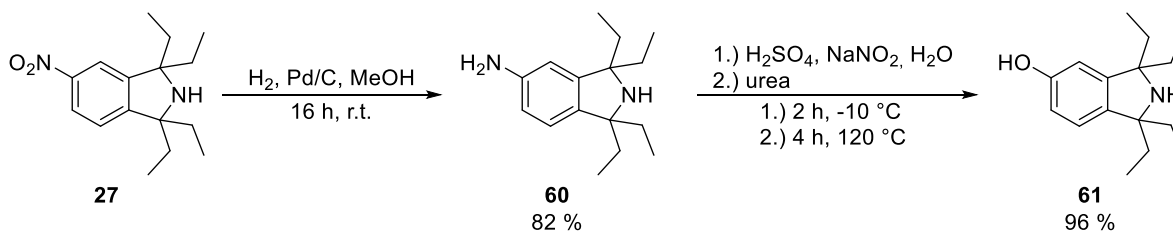Next, a nitro group had to be introduced by use of nitric acid. The yield of this reaction was fairly low, due to the 4-nitro isomer being formed in addition to the desired 6-nitro isomer (Fig. 110)[115]. This step is thus an important factor in limiting the overall yield of the synthesis of Ç analogues. Afterwards, the newly introduced nitro group also had to be reduced to an amino group, with hydrogen catalyzed by palladium (Fig. 110)[115].
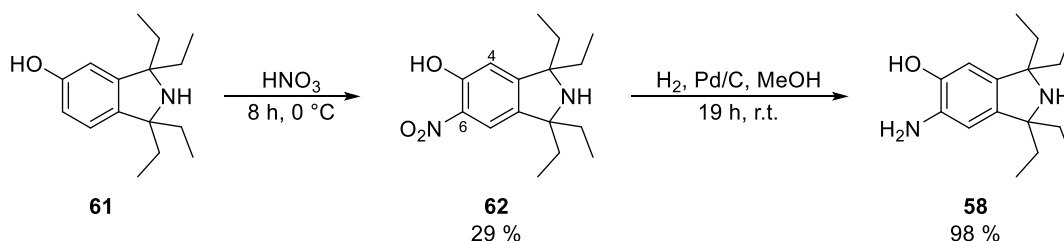
Fig. 110: Synthesis of compounds 62 and 58.

In addition to isoindoline **58**, nucleoside **57** had to be prepared by protection and halogenation of uridine (**59**). To achieve this, all hydroxyl groups of uridine were first protected with acetyl groups by using Ac$_2$O (Fig. 111)[117]. Then, 1,3-dibromo-5,5-dimethylhydantoin (DBH) was used to introduce bromine at position 5 (Fig. 111)[177].

Fig. 111: Synthesis of compounds 63 and 64.

The next step was chlorination by Appel reaction (Fig. 112)[117]. The purpose of this reaction is to introduce chlorine as a leaving group for the next step. Because of the sensitivity of compound **57** to nucleophilic attack, it is advised to set up the next reaction shortly after purification.

Fig. 112: Synthesis of halogenated nucleoside 57.

3.3.2 Synthesis of EÇr and its triphosphate

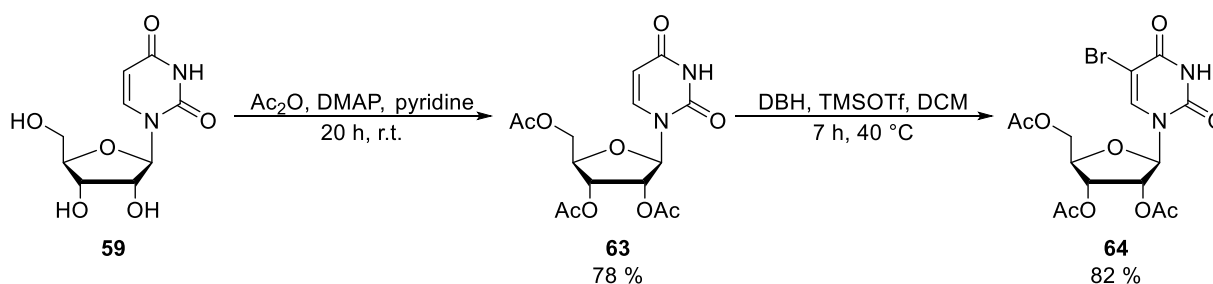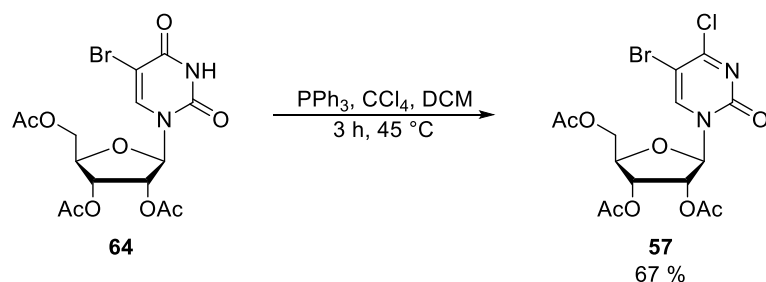With the synthesis of isoindoline **58** and nucleoside **57** complete, the two building blocks had to be combined to build up the core of the later spin label. This was done in two steps. The first was a nucleophilic substitution, where the 6-amino group of compound **58** performed an attack on position 4 of the nucleoside (Fig. 113)[117].
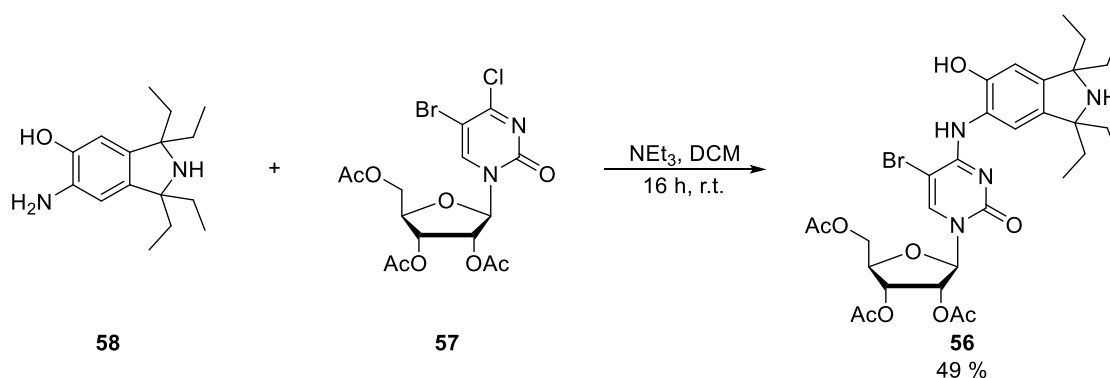
Fig. 113: Synthesis of compound 56.

This position is more reactive than position 5, so the reaction is selective for substitution of the chloride. If compound **57** was purified, purification at this step could be skipped and the crude product used for the next step, as no major impurities are formed during the reaction. If compound **57** was used directly without purification, purification needs to be done at this point[115]. In the second step, an oxazine ring was closed by an attack of the hydroxyl group of the isoindoline on the pyrimidine in the presence of potassium fluoride. The acetyl groups on the sugar were also cleaved under these conditions (Fig. 114)[115]. One problem of this reaction is the long reaction time. A more serious problem was the formation of a side product, which could not be separated from compound **53** by column chromatography. This side product was not identified conclusively.
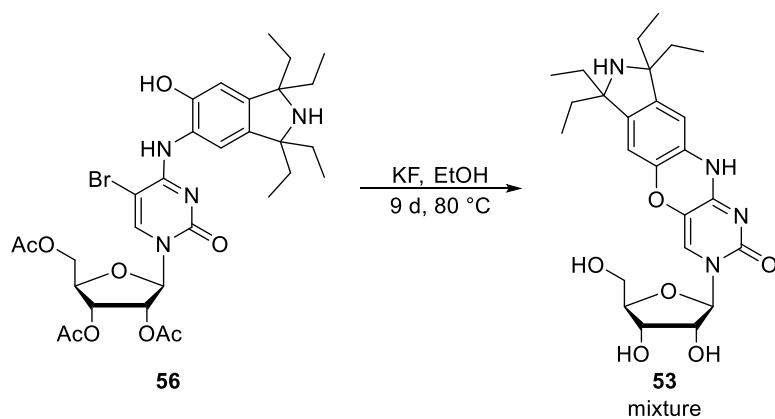
Fig. 114: Synthesis of compound 53, resulting in a mixture with an unidentified side product.

Because separation of compound **53** and the side product could not be achieved, the decision was made to acetylate the sugar again to make the compounds less polar, with the intention of achieving separation then (Fig. 115). By this strategy, compound **65** could be obtained in pure form as can be seen from the ^{1}H-NMR spectrum in Fig. 116.
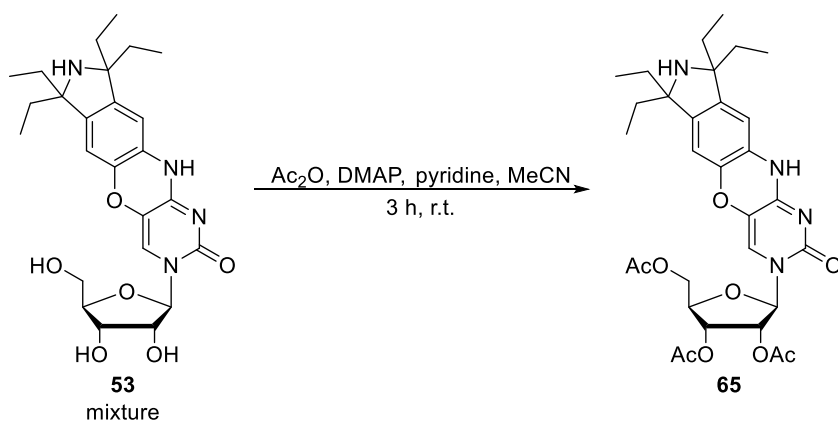
Fig. 115: Acetylation of compound 65 and the side product.
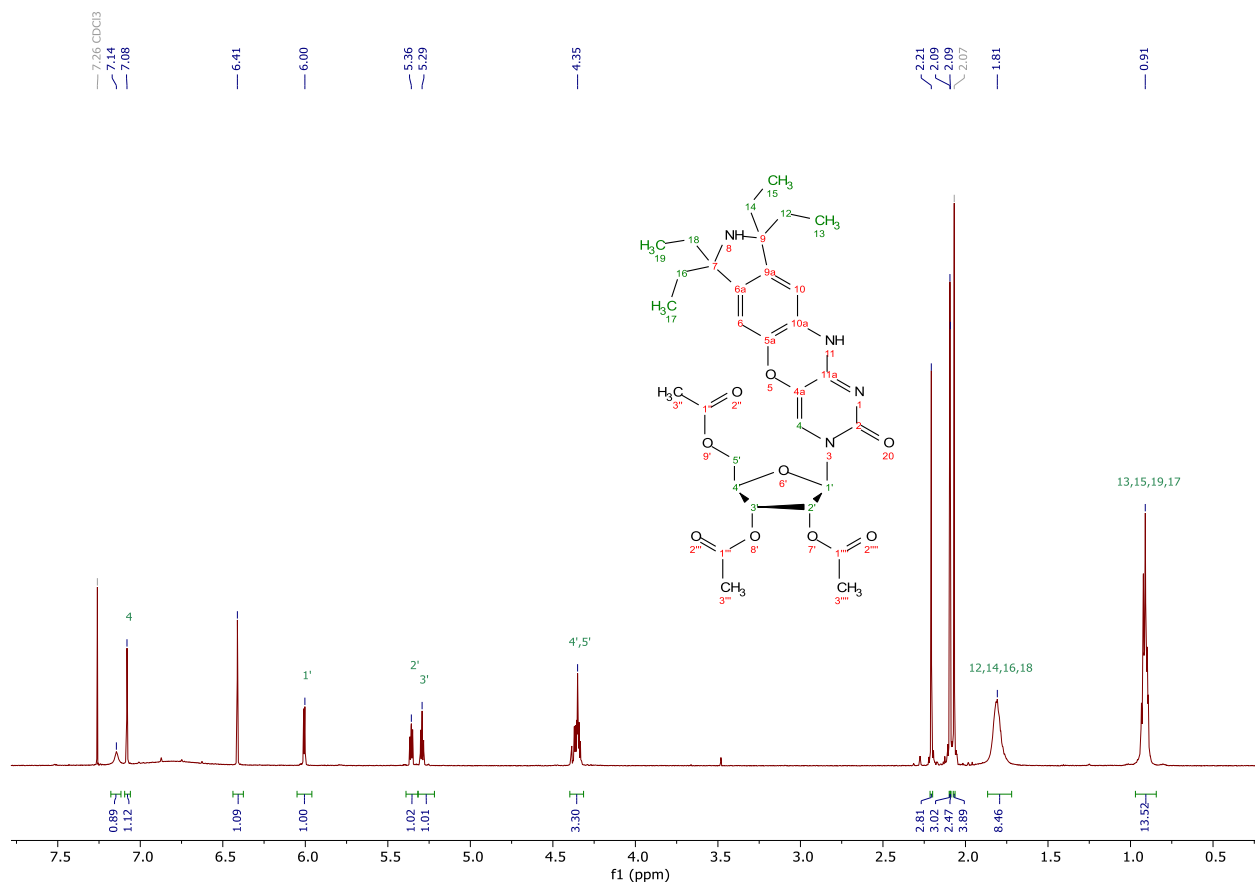
Fig. 116: ¹H-NMR spectrum of compound 65 in CDCl₃.

After successful purification of compound **65** it was oxidized with *m*CPBA (Fig. 117)[119]. It would also have been possible to use hydrogen peroxide and sodium tungstate after deprotection of the sugar, as was the case with Ç and Çm[115, 117]. After the oxidation, the acetyl groups were removed from compound **65** again, to yield spin label EÇr (**3**) as a free nucleoside (Fig. 117)[166].
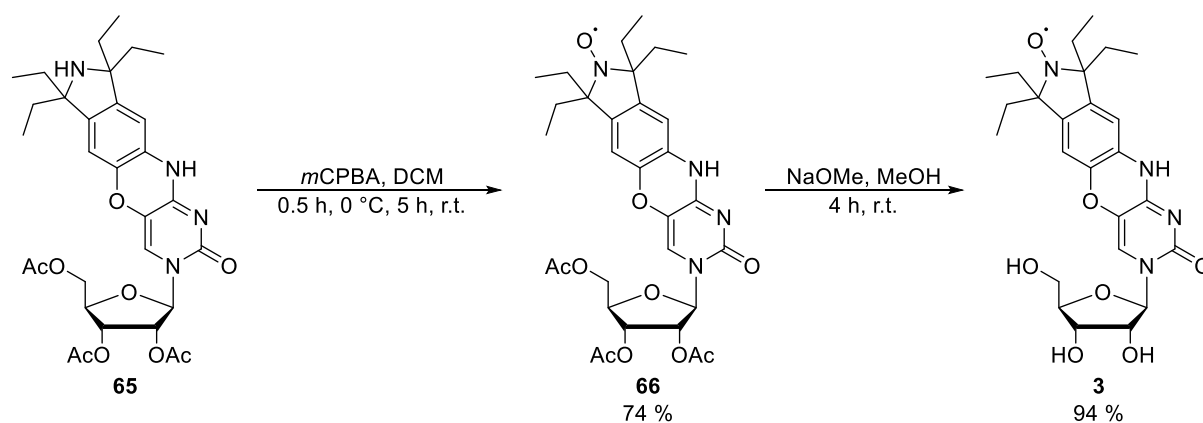
Fig. 117: Synthesis of compound 66 and EÇr (3).

At this point, it would have been possible to carry the synthesis forward towards the phosphoramidite. But it was decided to convert EÇr (**3**) to triphosphate EÇrTP (**55**)[178] for enzymatic incorporation. In preparation for this, tetrasodium pyrophosphate was converted to

86

bis(tetrabutylammonium) pyrophosphate by protonation with Dowex-H⁺ ion exchange resin followed by titration with tetrabutylammonium hydroxide solution. This reagent could then be used in the synthesis of the triphosphate (Fig. 118). In this procedure, the 5'-hydroxy group of the nucleoside reacts with phosphoryl chloride. The phosphorus is then attacked twice by the pyrophosphate to form a cyclic triphosphate which is opened during workup.
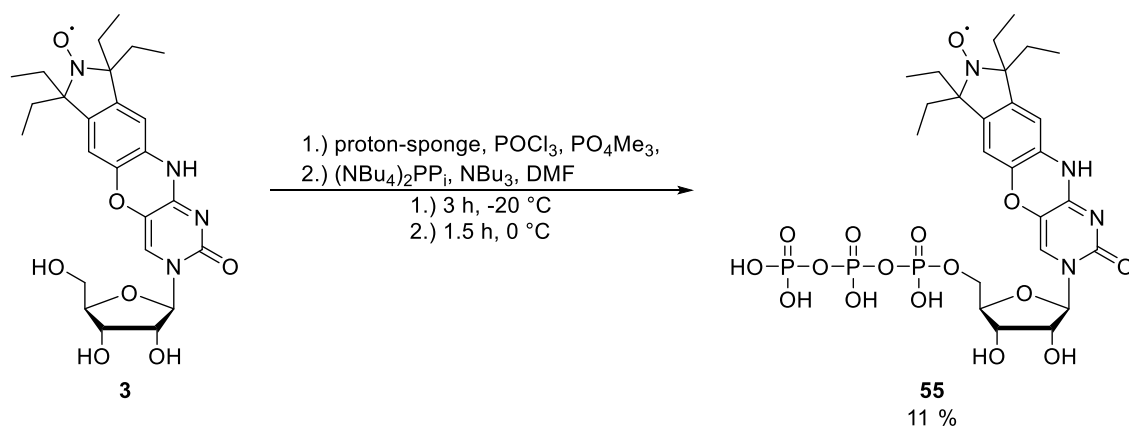
Fig. 118: Synthesis of EÇrTP (55).
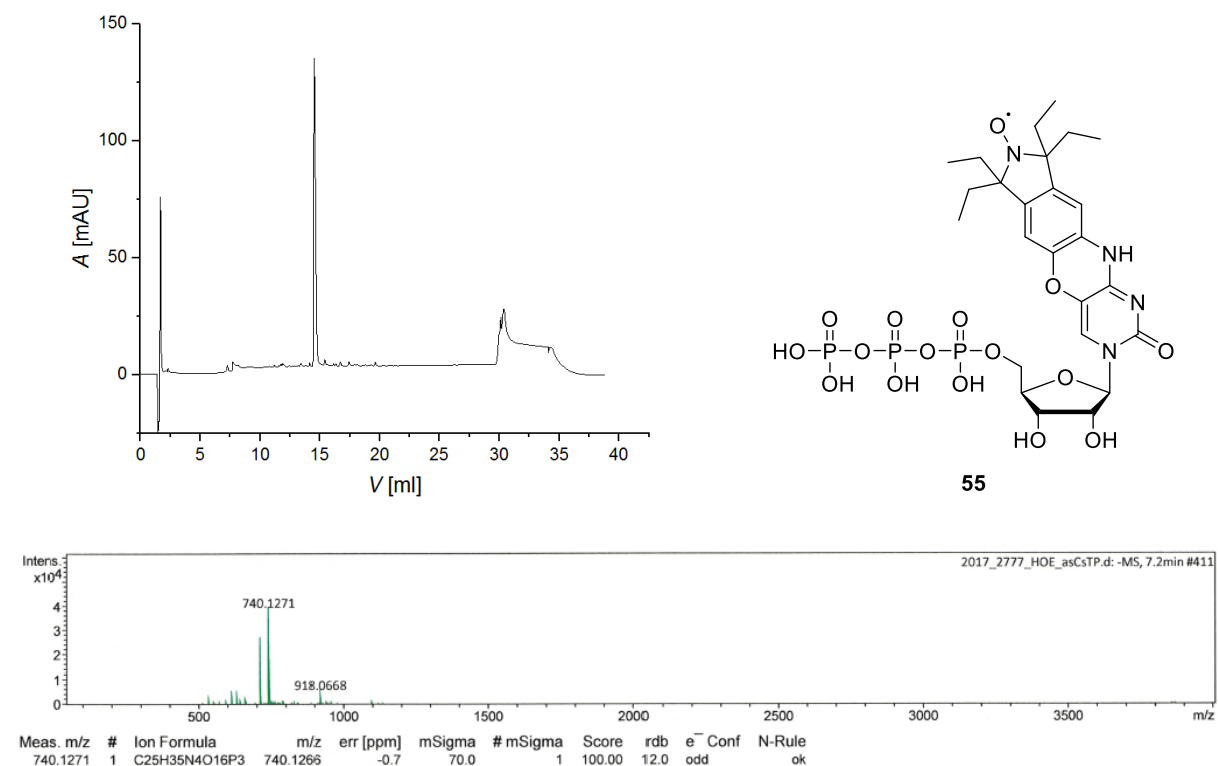
Fig. 119: Characterization of EÇrTP (55). Top: HPLC chromatogram (Dionex DNAPac PA200 4 x 250 mm column (Buffer A: 25 mM Tris HCl, 6 M urea, pH 8.0; Buffer B: 25 mM Tris HCl, 6 M urea, 0.5 M NaClO₄, pH 8.0; 60 °C), 0 % to 20 % B in A in 8 CV). Bottom: ESI-MS spectrum (bottom).

The triphosphate could be separated from monophosphate which was formed as a side product by ion exchange HPLC, as can be seen in the HPLC chromatogram and ESI-MS spectrum (Fig. 119).

3.3.3 CW EPR spectrum of EÇr

To see if EÇr (**3**) shows similar behavior to other spin labels of the Ç family, a CW EPR spectrum was recorded (Fig. 120).
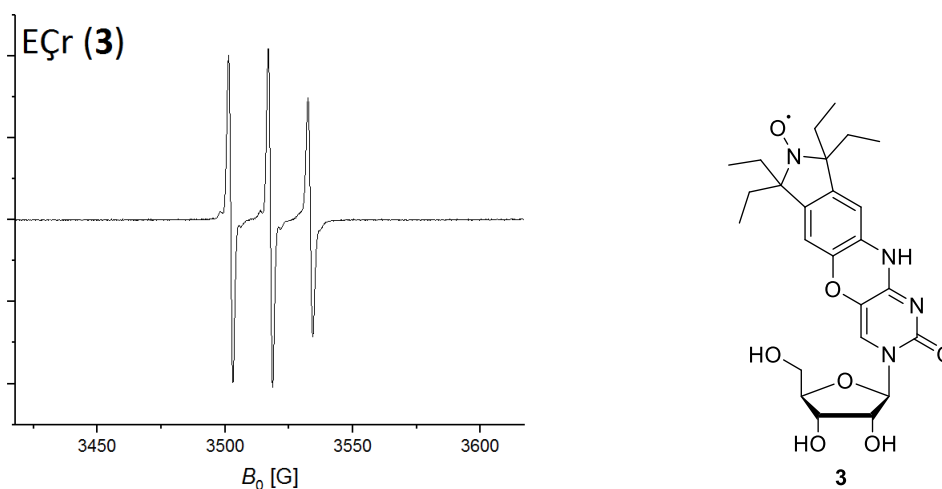
Fig. 120: Left: CW EPR spectrum of EÇr (3). Right: Structure of EÇr (3).

As expected, the spectrum shows great similarity to the spectrum of Ç[115]. Furthermore, it is also very similar to the other spin labels presented in this work, benzi-spin (**1**) and lumi-spin (**2**), with the same g-factor and almost the same isotropic coupling constant.

3.3.4 Synthesis and labeling of oligonucleotides

For the primer extension experiments several oligonucleotides were needed as primers and templates (Table 5).

Table 5: Oligonucleotides used for primer extension experiments. FAM-Alk is 6-carboxyfluorescein linked to the oligonucleotide by an alkyl linker. Incorporation sites of EÇR are marked in red in the templates.

Name	Sequence
XI	5'-FAM-Alk-CTGTAATACGACTCACTATA-3'
XII	5'-CTCACTGCTTCCTATAGTGAGTCGTATTACAG-3'
XIII	5'-CACGACCTCCGTATAGTGAGTCGTATTACAG-3'
XIV	5'-FAM-Alk-UAAUACGACUCACUAUA-3'

Templates **XII** and **XIII** were purchased and subsequently purified by gel electrophoresis. Primer **XI** was synthesized by solid phase synthesis. To enable the later labeling with 6-carboxyfluorescein (FAM), a hexynyl linker had to be introduced at the 5'-end. This was done by using phosphoramidite **68**, which had previously been prepared from 5-hexyn-1-ol (**67**) by use of CEP-Cl (Fig. 121)[179].

Fig. 121: Synthesis of phosphoramidite 68.

After synthesis and purification by gel electrophoresis, **XI** was labeled with 6-carboxyfluorescein polyethylene glycol azide (6-FAM-PEG$_3$-azide) by copper(I)-catalyzed azide-alkyne cycloaddition (CuAAC) and purified again by gel electrophoresis.

XIV was provided as a crude product by Sebastian Mayer and was purified by gel electrophoresis, labeled with 6-FAM-PEG$_3$-azide by CuAAC and purified again, but a major impurity remained.

3.3.5 Primer extension experiments

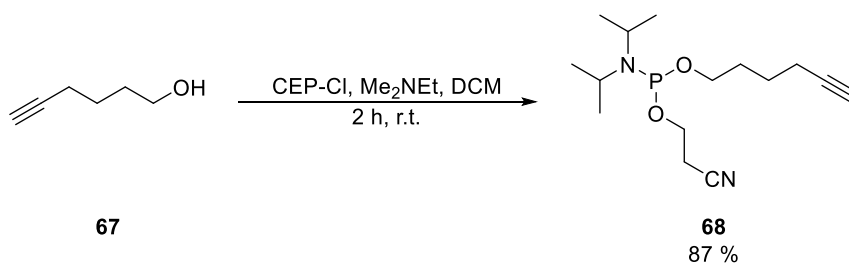With all necessary oligonucleotides prepared, the first tests for incorporation of EÇrTP (**55**) into DNA could be conducted. It was decided to use DNA instead of RNA, despite EÇr (**3**) being intended as a version of EÇ for RNA, because a DNA polymerase was used. EÇr is heavily modified compared to cytidine, so it was unclear if polymerases would accept it. The choice fell on Therminator III DNA polymerase, which is known for being capable of incorporating modified nucleotides, including spin labels[132, 178]. All experiments were performed at 72 °C. As the initial tests, single-nucleotide primer extensions were done to check if EÇrTP can be incorporated at all and under which conditions. For these tests, **XIII** was used as the template, because the first nucleotide not paired to the primer is a guanosine, which should lead to a cytidine being incorporated. Reactions with dCTP and CTP were also done. These would act as a positive control showing if the enzyme is active under the reaction conditions and provide references to which the incorporation of EÇrTP can be compared. For each of the NTPs, concentrations of 1 µM, 10 µM and 100 µM were used and the experiment run for 5 min (Fig. 122 left). For dCTP and CTP, there was virtually complete incorporation even at 10 µM. Incorporation was significantly less efficient for EÇrTP, as there was unextended primer left in all reactions. But still, there was visible elongation, so EÇrTP is accepted as a substrate by the Therminator polymerase. There was also a difference in gel shift compared to the canonical nucleotides, which could be the result of EÇr being significantly larger, the same was also reported for a different spin label[132]. What could also be seen is that apparently the incorporation was more efficient with 10 µM EÇrTP than with 100 µM. To rule out an experimental error, another single-nucleotide extension was performed with six different concentrations of EÇrTP, this time for 15 min (Fig. 122 right). The incorporation of EÇrTP seemed to be less efficient at 100 µM than at lower

concentrations. This might point towards substrate inhibition, although the reason why EÇrTP would inhibit the polymerase is unknown. This result was kept in mind for later experiments. Another unexpected result was the appearance of an additional band between unextended and extended primer. This band can also be seen in the previous experiment with 10 µM EÇrTP. There are also faint bands above the primer band, so it might be an artifact, but it seems too intense for that.
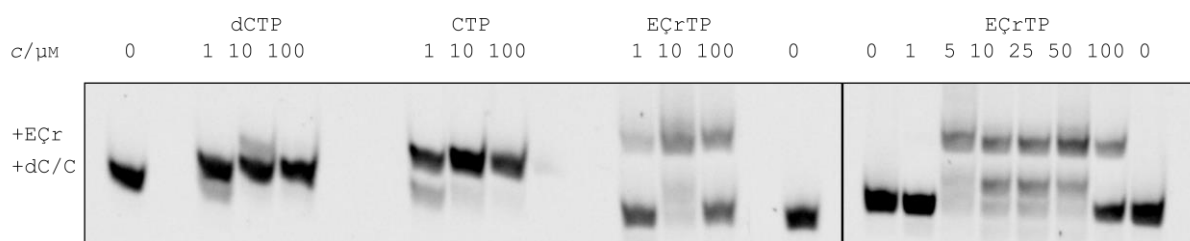

Fig. 122: PAGE analysis of single-nucleotide primer extension experiments with XIII as template. Left: dCTP, CTP and EÇrTP at three different concentrations. Right: EÇrTP at six different concentrations. Lanes marked with 0 correspond to reference reactions without any NTPs. Product bands are labeled.

After the initial tests had shown that incorporation of EÇrTP (**55**) is possible, full-length primer extensions were performed. Here, **XII** was used as the template, so EÇr (**3**) should be the sixth nucleotide to be incorporated. In addition to the negative control without dNTPs there were three reactions. One with dATP, dGTP, dTTP and dCTP which should result in full-length extension, one without CTP which should cause extension by only five nucleotides as there is no CTP analogue to be incorporated in that case, and one with EÇrTP instead of CTP to see if there is full-length extension with EÇr. The first test was done with 10 µM concentration for all dNTPs and EÇrTP for 15 min (Fig. 123 left). The result showed an oddity that kept appearing in later experiments as well. In the reaction with all four canonical dNTPs, there is a band above the band for the full-length product, which would belong to an oligonucleotide which is significantly longer than the expected full-length product. Considering there is only one such band, random addition of more nucleotides seems unlikely. Another explanation might be that the extended primer can bind to the template again and be extended further. Hybridisation of two extended primers might also be possible, which would also result in further extension. When it comes to the incorporation of EÇrTP, there is a band on the same height as the one from the negative control without CTP analogue, so the incorporation was not complete. However, there are also additional bands for longer products, including a faint one which corresponds to the full-length product from the positive control, again slightly shifted because of EÇr. This means that EÇr does not prevent the further extension of the primer after its incorporation, but it does seem to hinder it, as there are additional bands below the full-length product. There is also a faint band corresponding to the overextended product. It looks as if that band might be shifted further compared to the reference than the one from the full-length product, which might indicate the presence of two EÇr nucleotides in the overextended product. This would support the theory of

90

wrong binding of the primer, but the bands are too faint to make conclusive statements. The same experiment was then repeated with different concentrations of NTPs. First, all dNTPs were used in a concentration of 200 µM (Fig. 123 center). This was well above the concentration where EÇrTP showed inhibition in earlier tests, but nonetheless in this case there are bands including one corresponding to the full-length product, again slightly shifted because of EÇr. However, 200 µM does not seem to be a good concentration to use for the canonical NTPs, as there is full-length extension and overextension in the negative control without any CTP analogue. At high concentrations, Therminator polymerase seems to incorporate random dNTPs when the correct one is unavailable. The experiment was then repeated with a concentration of 10 µM for canonical dNTPs and 200 µM for EÇr (Fig. 123 right). In this case no incorporation of EÇr was observed, the extension stopped at the same length as the negative control. This seems consistent with the earlier tests showing inhibition at high concentrations. These results suggest that high concentrations of dNTPs can overcome the inhibition.
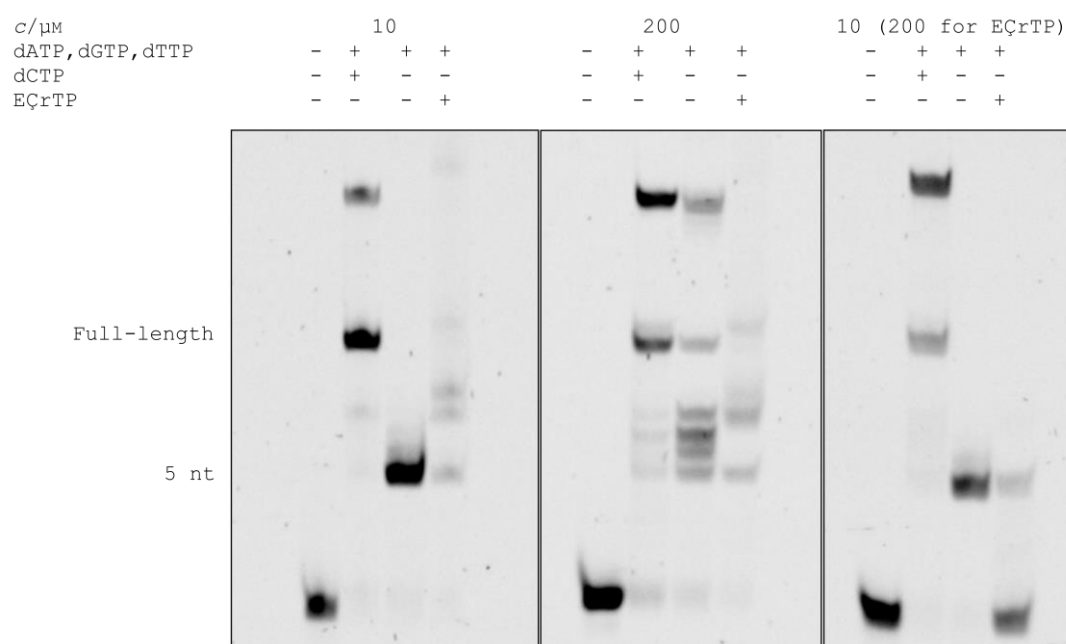
Fig. 123: PAGE analysis of primer extension experiments with XII as template at different concentrations. Left: all triphosphates at 10 µM. Center: all triphosphates at 200 µM. Right. EÇrTP at 200 µM, dNTPs at 10 µM.

For the next set of experiments, **XIII** was used as the template again. This time, full extension was the goal, which means incorporation of two EÇr (**3**) labels. Because EÇr would be the first nucleotide to be incorporated, a two-step procedure was tested in addition to the one-step procedure. The control sample was incubated with dCTP as the only triphosphate and the first proper sample with only EÇrTP (**55**), each for 15 min. Afterwards they were cooled down to 0 °C to stop the reaction, dATP, dGTP and dTTP were added and another incubation performed for 15 min. In the second sample, all triphosphates were added together and the mixture incubated once for 15 min. Concentration of

dNTPs and EÇrTP was 10 µM in all cases (Fig. 124 left). There does not seem to be any difference between the one-step and two-step procedures, full extension was observed in both cases. The control reaction also showed overextension in this case as well. For some reason, the top bands in each lane are seen as double bands in this experiment. It is unclear what caused this, as this effect is not observed in the next experiment under similar conditions. In this experiment, the one-step procedure was used as there was no difference as compared to the procedures in the previous experiment. This time, incubation time was 3 h, to see if a longer time has any effect on product formation (Fig. 124 right).

procedure			ts	ts	os					
dATP,dGTP,dTTP			–	+	+	+		–	+	+	+
dCTP			–	+	–	–		–	+	–	–
EÇrTP			–	–	+	+		–	–	+	+

Full-length
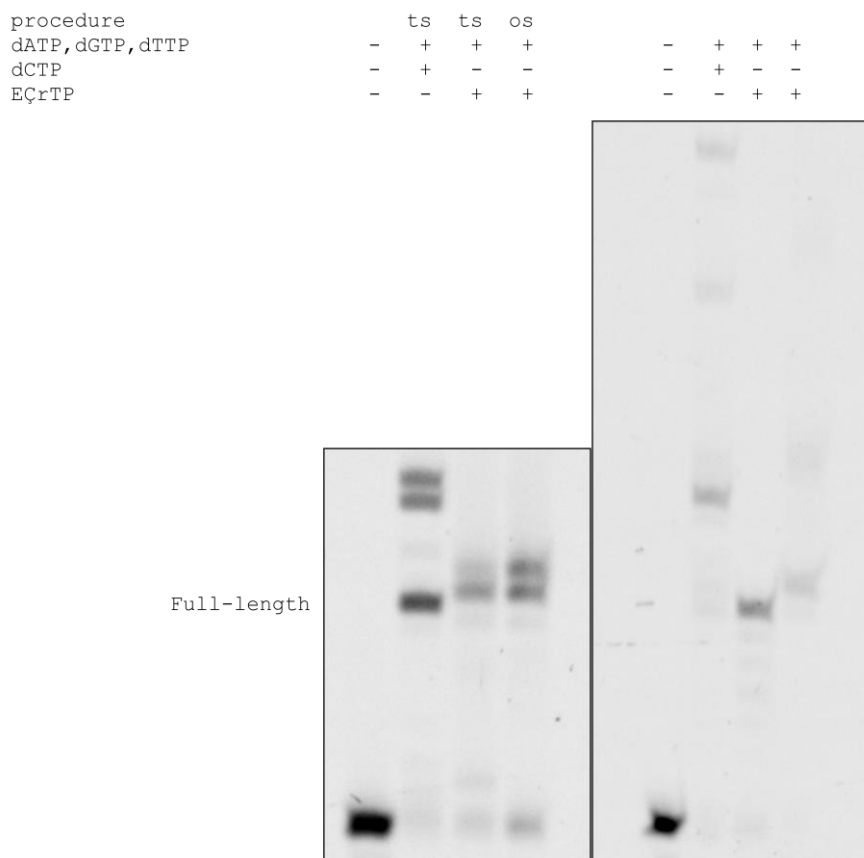
Fig. 124: PAGE analysis of primer extension experiments with XIII as template. Left: Two step procedure (ts) or one step procedure (os), 15 min incubation. See text for details. Right: One step procedure, 3 h incubation.

The longer reaction time caused more overextension than shorter experiments. The full-length product is almost unobservable in the positive control, but additional overextension products, even longer than previously, were formed. Interestingly, even the negative control without any CTP analogue resulted in full-length product, so it seems like Therminator polymerase is able to incorporate random dNTPs even at low concentrations, when given enough time. There is also some overextension in the real sample with EÇrTP, but to a much lesser extent than in the positive control. The shift compared to the control bands proves the incorporation of EÇr, so there seems to be no reaction with random dNTPs when EÇrTP is available, despite the low efficiency of incorporation.

Because EÇr (**3**) is a spin label intended for use in RNA, it was tested whether Therminator polymerase can also use an RNA primer. Single-nucleotide extensions of **XIV** with **XIII** as the template were tried. First, the incorporation of CTP and EÇrTP (**55**) was tested in concentrations of 1 μM, 10 μM and 100 μM. The reaction was run for 5 min (Fig. 125 left). This resulted in no incorporation of EÇrTP, only partial incorporation of CTP at 100 μM and no reaction at lower concentrations. The experiment was repeated with dCTP and CTP (Fig. 125 right). For dCTP, there was no incorporation at 1 μM, partial incorporation at 10 μM and still incomplete reaction at 100 μM. It was therefore concluded that Therminator polymerase is not well suited for RNA primers.
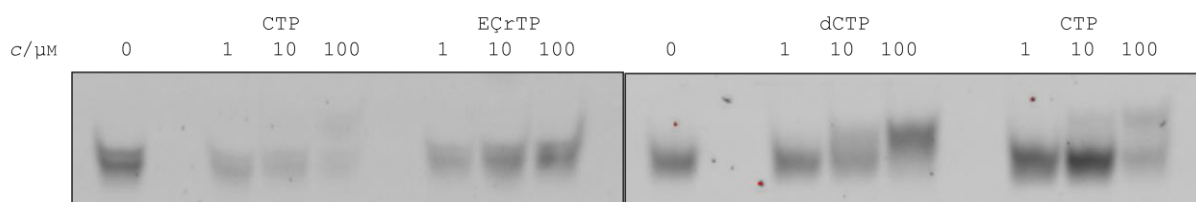
Fig. 125: PAGE analysis of single-nucleotide RNA primer extension experiments with XIII as template. Left: CTP and EÇrTP at three different concentrations. Right: dCTP and CTP at three different concentrations. Lanes marked with 0 correspond to reference reactions without any NTPs.

3.3.6 Towards the synthesis of EÇTP

After the attempts at primer extension with EÇr (**3**) had shown that Therminator III polymerase can incorporate EÇr into DNA, but not RNA, it was decided that using a DNA spin label In DNA oligonucleotides would be more desirable, as the 2'-hydroxy group of a ribonucleotide might unnecessarily disrupt the structure. The next plan was therefore to synthesize the recently published EÇ[118] and convert it into the triphosphate EÇTP (**69**) (Fig. 126).
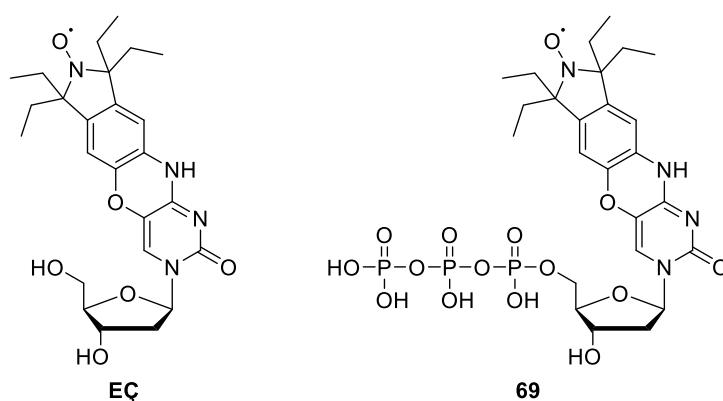
Fig. 126: Rigid spin label EÇ and its triphosphate EÇTP (69).

The synthesis of EÇTP follows the same general strategy as EÇrTP, as the compounds only differ in terms of the 2'-OH group. The synthesis was begun with deoxyuridine (**70**), which was first acetylated at the 3'- and 5'-hydroxy groups by using Ac_2O[117] and then brominated, again using 1,3-dibromo-5,5-dimethylhydantoin as the bromination reagent (Fig. 127)[177].
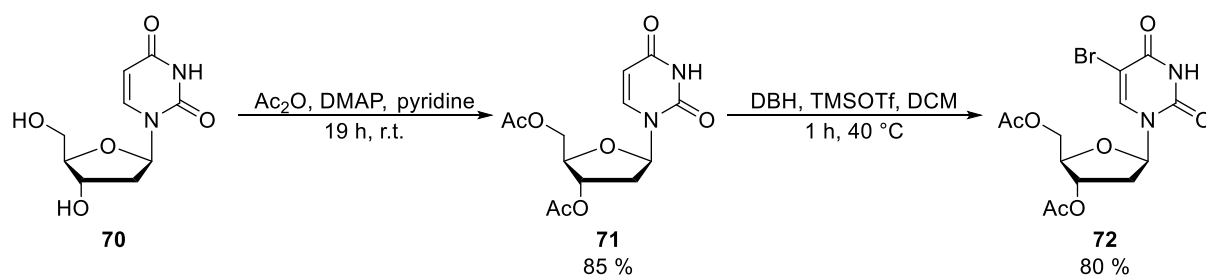
Fig. 127: Synthesis of compounds 71 and 72.

The brominated nucleoside **72** was then chlorinated in position 4 and reacted with isoindoline compound **58** to obtain compound **73**. Here, a different approach was used compared to the synthesis of EÇrTP, based on the original procedures for the synthesis of Ç[115]. Rather than isolating the chlorinated intermediate, compound **58** was added to the reaction mixture after chlorination was complete (Fig 128). The advantage of this one pot strategy is that the risk of degradation of the highly reactive chlorinated nucleoside by unwanted substitution is reduced. However, it also comes with a disadvantage, namely the purification of compound **73**. Even after several attempts at purification by column chromatography the product could not be completely separated from the triphenylphosphine oxide generated by the Appel reaction.
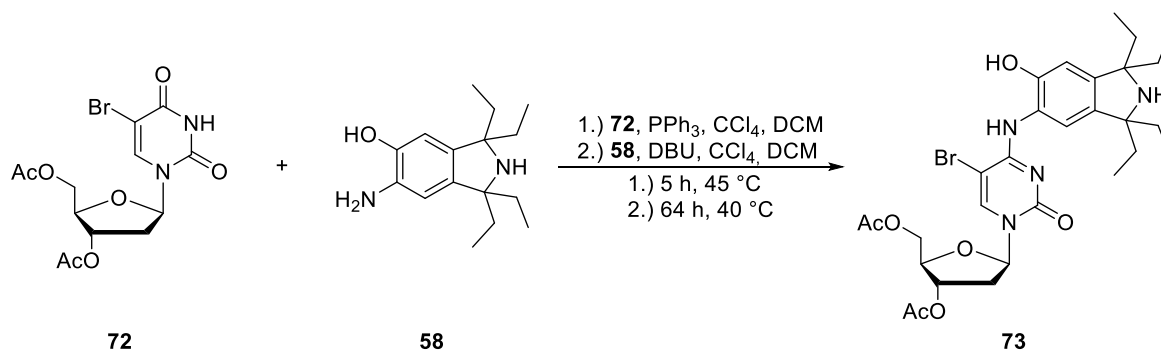
Fig. 128: Synthesis of compound 73.

After multiple purification attempts did not result in complete purification of compound 73, it was decided to use the impure compound for the next reaction, expecting purification to be easier due to the different polarity of the deprotected nucleoside **74**. The procedure for the cyclization was the same as had been used previously for the synthesis of EÇrTP, heating for multiple days in presence of potassium fluoride (Fig. 129)[115].

Fig. 129: Synthesis of compound 74.

While the EÇ precursor **74** could be obtained, purification proved just as difficult as it had been with compound **73**. Multiple attempts by column chromatography could not separate the product from t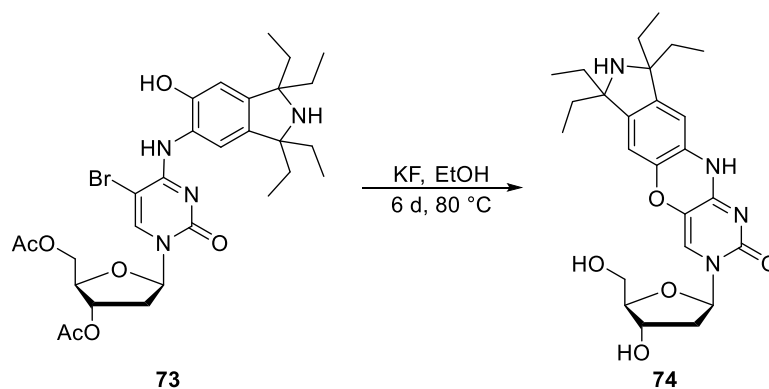he triphenylphosphine oxide. It is therefore highly recommended to isolate the chlorinated nucleoside after the Appel reaction and use it for the reaction with compound **58** only after it has been thoroughly purified. Some degradation might occur, for example due to water in the solvents used for column chromatography which are usually not completely dry. But the loss of material at later stages on several purification attempts, which may then not even yield the pure product is likely more detrimental.

3.4 Future directions of spin-labeled nucleosides

This thesis presents the synthesis of three new spin-labeled nucleosides. This chapter will provide an outline of further steps which can be taken in the projects, as well as possible fields of application for the new spin labels.

Rigid spin labels have already been proven to be useful for the study of nucleic acids by EPR spectroscopy, first among them being distance determination by PELDOR measurements. With benzi-spin (**1**) showing similar characteristics to established labels like Çm, it is to be expected that it has the potential to become equally successful. What sets benzi-spin apart from these other labels is its universal base-pairing character, which allows it to be used as a replacement for any other nucleoside rather than just a specific one. This means that the scope of applications in which benzi-spin can be used is larger, as any desired position can be labeled without the need for different spin labels. In order to fully evaluate its usefulness, benzi-spin needs to be tested in different sequence contexts, different positions inside a duplex or in other secondary structure motifs. These tests could reveal limitations for the applicability of benzi-spin. Another point which can be addressed in the future is the application of benzi-spin in RNA. While incorporation of deoxynucleotides into RNA is

possible in principle, the lack of a 2'-hydroxy group can disturb the structure, which may lead to a reduction of the rigidity of the spin label. Preparation of a dedicated RNA version of benzi-spin would therefore be useful, if benzi-spin is to be used in RNA.

As far as lumi-spin (**2**) is concerned, the synthesis is not quite at its end. The next steps in the project seem obvious. For incorporation by solid-phase synthesis, lumi-spin needs to be protected with DMT in 5'-position, a silyl group in 2'-position and then turned into a phosphoramidite with CEP-Cl. However, this might not be as straightforward as it seems. Silylation will lead to a mixture of 2'-and 3'-silyl isomers, which then need to be separated. Attempts with the earlier design using methyl groups, showed that separation of compound **47** and its isomer required multiple columns with a specific solvent mixture, DCM/acetone (2:3 + 1 % NEt$_3$), to achieve separation of a significant extent. Separation of paramagnetic compounds is made even more complicated by the broadening of the NMR signals, which makes determination of the ratio of isomers in a sample nearly impossible. Thus, other methods for purity control, like HPLC, might be preferable. For small amounts of product mixture, the separation itself could also be done with HPLC. Alternatively, the nitroxide could be protected which would enable determination of purity from the NMR spectra. A suitable candidate that was used for Ç was published recently[118, 129]. This would have the positive side-effect of preventing degradation of the nitroxide during solid-phase synthesis, although with ethyl groups next to the nitroxide this is not as necessary as it would be with ethyl groups. Another possible approach would be to prevent formation of the 3'-silyl isomer altogether[180]. It would need to be tested, if the nitroxide remains intact when treated with hydrogen fluoride. A catalyst which causes high selectivity for the 2'-isomer could also be used[181]. If lumi-spin could be successfully incorporated into oligonucleotides, a new rigid spin label would be ready for use. It has the same Watson-Crick side as uridine, which means it might be able to form base-pairs with adenosine and be used in a similar way as Ç or isoxyl-A. However, those labels are designed in such a way that the nitroxide points into the major groove, resulting in only small perturbation of the duplex structure. Lumi-spin on the other hand is oriented in a different direction, where more steric clash with the backbone is to be expected, thus causing more significant structural changes which might limit its usefulness. An alternative use might be in G quadruplexes. As G quadruplexes are a topic of interest for many research groups, a spin label which might be able to provide further structural insight could be useful. It is questionable if a single G quartet would be formed with lumi-spin as one of its constituents, as compared to guanosine it has a hydrogen acceptor in position 2 rather than a donor. But if lumi-spin is employed in one of the inner layers of a G quadruplex it might be able to form. An alternative approach would be introduce a second modification, 8-oxoguanine, to form the equivalent of a G-G-X-O tetrad[182], where lumi-spin would replace xanthine (Fig. 130 left). This should allow for the formation of a stable quartet.
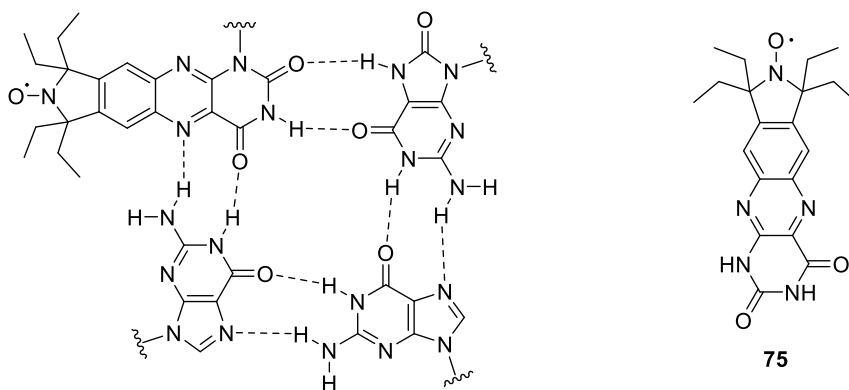
Fig. 130: Structure of lumi-spin incorporated in a tetrad with two guanines and an 8-oxoguanine (left) and non-covalent spin label 75 (right).

Lumi-spin is still a few steps away from completion, so it is hard to judge its usefulness at this point, but if it can be incorporated into oligonucleotides, it could become a useful tool for PELDOR spectroscopy, similar to Ç. A different application, which would not require as much synthetic effort, is non-covalent labeling. While it would not be advisable to use lumi-spin itself for this, as the ribose is not required in this case, if nucleobase **49** would be oxidized to acquire compound **75** (Fig. 130 right), it could be used for non-covalent labeling of duplex structures like similar labels which have been tested previously[143, 144]. This might even come with the advantage of different ways of base-pairing being available. In chapter 3.2.1, different possible spin labels resulting from nucleosidation at different nitrogen atoms were discussed. With compound **75** not being covalently attached to an oligonuclotide, its base-pairing behavior is not predetermined. It may bind in the same way lumi-spin is expected to bind, or it might bind in a more Ç-like way, which might be more likely due to reduced steric clash with the backbone, in which case the question regarding the preferred tautomer would come up again. In order to make the lumi-spin like binding mode more favorable, replacing the ribose at the abasic site where **75** is supposed to bind with a flexible and less sterically demanding C_3 or C_4 linker may help to reduce steric clash. This was reported to not result in a significant difference in case of ç[141], where the label points into the major groove, but might have a positive effect on the lumi-spin like orientation, as the steric clash there is more severe.

Enzymatic incorporation is a spin-labeling approach which has not been extensively investigated so far, especially when it comes to direct introduction of the spin label[132, 135]. Conversion of EÇr (**3**) to EÇrTP (**55**) and the primer extension experiments done with it represent another successful step towards establishing it as a viable alternative to solid-phase synthesis. Some work however, remains to be done. The extension products were not characterized beyond their gel shift, because of the small scale of the experiments. The experiments should be repeated in larger scale to enable ESI-MS characterization, which could also help to identify all the side-products which were produced. The possible degradation of the nitroxide during should also be investigated, but since there are no

strong reducing agents in the reaction mixture, it is not expected to be a problem. The conditions might also be further improved for greater efficiency of incorporation. Also, after the synthesis of EÇr was complete, new procedures for the synthesis of Ç and its derivatives were published[118]. Future attempts at the synthesis of EÇr should follow the revised procedures for a better overall yield. Another change which can lead to better results is to use EÇTP (**69**) instead of EÇrTP, as Therminator polymerase should work more efficiently with a deoxynucleotide. Also, having a ribonucleotide in DNA might lead to structural perturbations. Alternatively, RNA polymerases could be tested regarding their ability to incorporate EÇrTP into RNA. EÇr could also be turned into a phosphoramidite rather than a triphosphate to use it in solid-phase synthesis. To circumvent the problem of having to separate 2'- and 3'-silyl isomers, using a protecting group on the nitroxide to turn the compound diamagnetic is recommended, as has been done for EÇ previously[118]. So far, Çm and EÇm have been used in RNA, but EÇr with its free 2'-hydroxy group should be more useful for this, as the 2'-hydroxy group is important for RNA structure, so EÇr should not perturb the structure as much.

Another method of spin labeling which might be worth investigating is labeling by ribozyme. Recently, ribozymes that can transfer a functional group from an *O*-6-modified guanine to a specific adenine in a target RNA strand were developed by in vitro selection[183]. Among them are the CA13 and CA21 ribozymes, which can transfer benzyl and 4-(aminomethyl)benzyl groups. While TEMPO is bulkier than these aromatic groups, some (re)selection might produce a ribozyme which can successfully transfer it (Fig. 131).

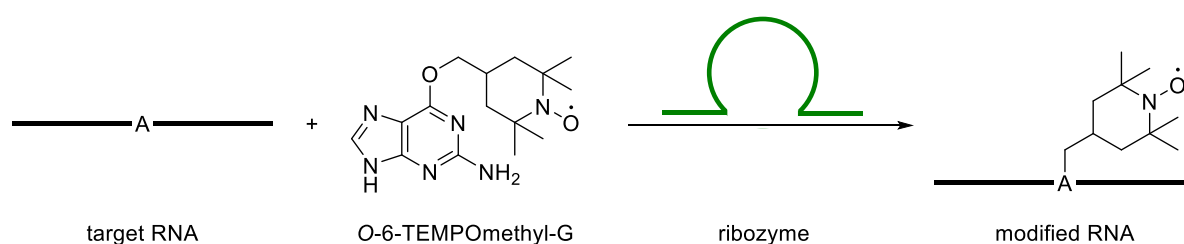Fig. 131: Spin labeling of RNA by ribozyme.

The advantage of this approach would be that site-specificity can be achieved purely by the ribozyme, which can be designed with binding arms that selectively bind at the desired position. Unlike in other methods, the target RNA does not need to be modified in any way prior to the TEMPO labeling, which would make site-specific labeling, especially of long RNA, easier.

3.5 Other modified nucleosides

3.5.1 Synthesis and incorporation of a benzimidazole phosphoramidite

The results of this chapter were published in: T. P. Hoernes, K. Faserl, M. A. Juen, J. Kremser, C. Gasser, E. Fuchs, X. Shi, A. Siewert, H. Lindner, C. Kreutz, R. Micura, S. Joseph, C. Höbartner, E. Westhof, A. Hüttenhofer, M. D. Erlacher, *Nat. Commun.* **2018**, *9*, 4865-4877.

Watson-Crick base-pairing between nucleobases plays an important role for interactions between nucleic acids. One process which depends on base-pairing is the translation of mRNA at the ribosome. The interaction between the codon on the mRNA and a fitting anticodon on the tRNA determines which amino acid will be incorporated into the peptide that is being synthesized. To gain further insight into the effect of Watson-Crick interactions on mRNA translation, nine modified nucleotides, with different patterns of hydrogen donors and acceptors compared to canonical nucleotides, were incorporated into mRNA sequences.
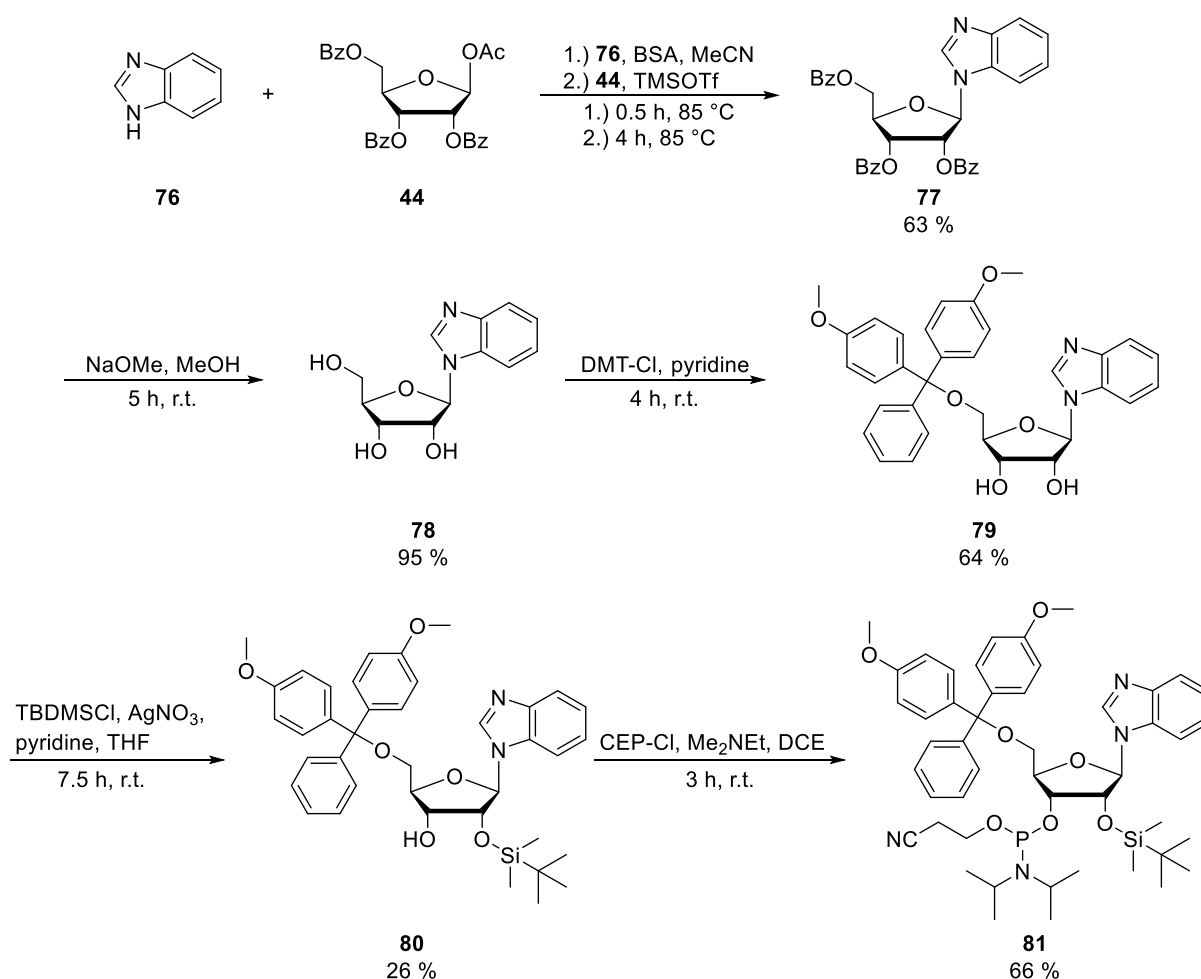

Fig. 132: Synthesis of benzimidazole nucleoside phosphoramidite 74.

Multiple RNAs were synthesized per modification, to have the modifications in each of the three positions of a codon. It was then tested if the modified RNAs could be translated and which amino acids the modified codons would code for. One of the modifications that were tested was benzimidazole nucleoside **78**[184]. It was synthesized by Vorbrüggen nucleosidation of benzimidazole (**69**), followed by deprotection of the sugar. To enable its incorporation by solid-phase synthesis, it was converted to phosphoramidite **81** in three steps, starting with 5'-DMT protection, followed by 2'-TBDMS protection and phosphitylation with CEP-Cl (Fig. 132). Because the complete mRNA would be too long to be efficiently synthesized by SPS, shorter pieces were synthesized, which could be attached to another piece by ligation.
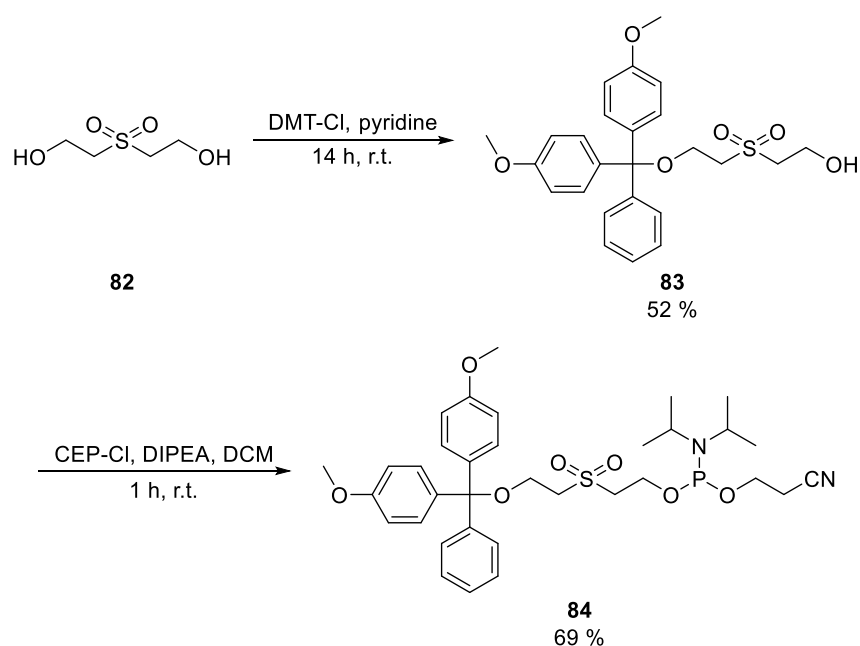
Fig. 133: Synthesis of phosphoramidite X for introduction of a 5'-phosphate group.

For this ligation, it was necessary to have a 5'-phosphate in the modified RNA strands. For incorporation of a 5'-phosphate in SPS, phosphoramidite **84** was synthesized. 2,2'-Sulfonyldiethanol (**82**)[185] was protected with one DMT group and then the other OH-group phosphitylated with CEP-Cl (Fig. 133). Compounds **81** and **84** were then used to synthesize oligonucleotides **XV**-**XVII** by solid-phase synthesis.

Table 6: RNA sequences synthesized with benzimidazole phosphoramidite 81. X = benzimidazole nucleoside, P = 5'-phosphate

Name	Sequence
XV	5'-P-AUUAU**X**GGCCAAACAAAAAUAA-3'
XVI	5'-P-AUUAUG**X**GCCAAACAAAAAUAA-3'
XVII	5'-P-AUUAUGG**X**CCAAACAAAAAUAA-3'

These were then used to obtain full-length mRNAs by ligation, which were then used in translation experiments in bacterial and human cells. Since benzimidazole does not have any hydrogen donors or acceptors on its Watson-Crick edge, it is unable to form hydrogen bonds. Translation was not possible when benzimidazole was in the first or second codon position, but when it was placed in the third position, a full-length protein could be obtained. This is in contrast to an abasic site, which did not allow for translation in any position. The results were similar for the other modifications that were tested. Those that can form a base-pair to one of the canonical nucleosides allowed for translation at any codon position, while those that are unable to form base-pairs prevented translation except, in most cases, when placed in the third position. Overall, it was concluded that, for the first and second codon position, at least a hydrogen bond between pyrimidine-N3 and purine-N1 is necessary for efficient translation, while the third position is less restrictive. For those nucleosides which did allow for translation, the resulting peptides were analyzed by mass spectrometry to determine which nucleoside they are identified as by the ribosome. The result was that especially in the first two positions, the major product always resulted from the nucleoside being identified based on its pyrimidine-N3 and purine-N1. The results were similar in the third position, except that 2-aminopurine was read as G rather than A in the bacterial cells. One of the modifications, inosine, was studied in greater detail. It was demonstrated that the presence of inosine in place of guanosine in a codon significantly weakens the codon-anticodon interactions. Despite this, mRNA containing a single inosine was efficiently translated. The presence of multiple inosines had a noticeable effect on translation, as two inosines in the same codon completely prevented translation, while two inosines in different codons reduced the translation rate.

3.5.2 Synthesis of remdesivir triphosphate

The results of this chapter were published in: G. Kokic, H. S. Hillen, D. Tegunov, C. Dienemann, F. Seitz, J. Schmitzova, L. Farnung, A. Siewert, C. Höbartner, P. Cramer, *Nat. Commun.* **2021**, *12*, 279-286.

Remdesivir is a drug used against COVID-19. When it is introduced into cells, it is metabolized to remdesivir triphosphate (**87**), which can stall replication of viral RNA by the RdRp enzyme. In order to investigate the mechanism by which the stalling occurs, **87** was prepared by a two step procedure starting from nucleoside **85**, which was first converted to remdesivir monophosphate (RMP, **86**) with $POCl_3$ and then after isolation converted to triphosphate **87** by activating the monophosphate with CDI, followed by reaction with bis(tributylammonium) pyrophosphate[43]. The original intention was to obtain **87** by the first reaction[178], but only **86** was obtained, likely because the pyrophosphate was not dry enough, so the second reaction had to be done (Fig. 134).
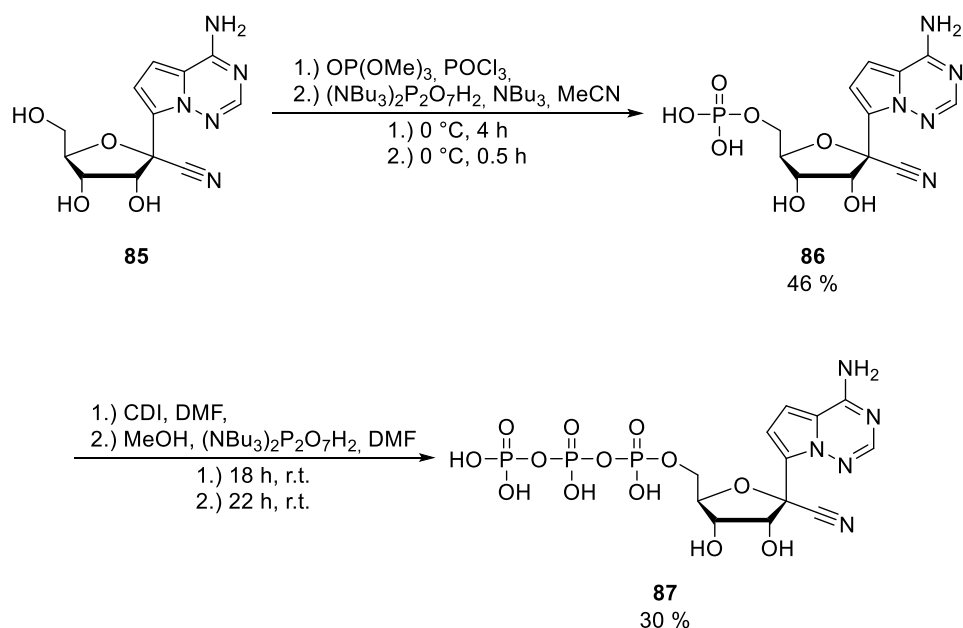
Fig. 134: Synthesis of remdesivir triphosphate 80.

Triphosphate **87** was then used in elongation experiments. In coronaviruses, the polymerase will stop after incorporating three additional nucleotides, which was confirmed by the experiments. It was also observed that higher concentrations of NTPs caused the full-length product to be formed, showing that remdesivir only stalls the elongation, but does not terminate it. In a parallel experiment, three complexes of RdRp and different RNA sequences, two of which contained RMP, were studied by cryogenic electron microscopy. In the first complex, RMP was located three nucleotides away from the triphosphate binding site, with two additional nucleotides after it. The binding site was free for the next triphosphate. In the second complex, three nucleotides were placed after RMP, yet RMP was again located at the same position, with the triphosphate binding site now being occupied by the nucleotide at the 3'-end. Therefore, binding of the next triphosphate was prevented. In a control complex, where adenosine was present in place of RMP, the adenosine was located four nucleotides away from the binding site, as expected, and the binding site free. It was concluded that the stalling of RdRp by remdesivir is caused by steric clash between the 1'-cyano group of remdesivir and a serine residue of the polymerase, which hinders passage of the RNA past the serine.

4 Summary

EPR spectroscopy has become a useful method for detailed analyses of nucleic acid structures and dynamics. In order to measure EPR spectra, paramagnetic spin labels need to be incorporated into these nucleic acids. There is a particular need for rigid spin labels, because rigid labels enable more accurate distance determination by PELDOR spectroscopy. This thesis adds three new examples to the small number of rigid spin labels available thus far.

Benzi-spin phosphoramidite **4** was successfully incorporated into oligonucleotide **III** by solid-phase synthesis. The ethyl groups proved useful here, as the synthesis could be done under standard conditions while leaving the nitroxide mostly intact. The same conditions are known to lead to reduction of nitroxides flanked by methyl groups[146]. The melting temperatures of duplexes containing benzi-spin are very similar when benzi-spin is paired with G, A, T, I or C. They are slightly higher when benzi-spin is opposite m^6G or $m^{6DA}P$ compared to guanosine. The opposite effect was observed when C^{TEMPO} was used instead of benzi-spin. This suggests that benzi-spin forms slightly more stable base-pairs with the methylated nucleosides, which was expected based on the behavior of the benzi nucleoside in primer extension[163]. Nevertheless, the differences are fairly small which speaks for benzi-spin being usable as a universal spin label. The EPR spectra support further this conclusion, as there is no significant difference in appearance depending on the opposing nucleoside for seven different nucleosides which were tested. The spectra resembled those recorded with $Çm^{117}$, thus demonstrating benzi-spin's rigidity and versatility. Therefore, benzi-spin is a promising tool for EPR spectroscopy on nucleic acids. Furthermore, upon irradiation of benzi-spin precursor **1a** at a wavelength of 290 nm, photochemical dealkylation was observed.

A synthetic route for the alloxazine-based spin label lumi-spin (**2**) was developed and the new paramagnetic nucleoside analog was fully characterized. Lumi-spin holds great promise to become a useful spin label especially for distance measurements due to its rigid scaffold, which is similar to the spin labels of the Ç family, which have been shown to be well suited for accurate distance and orientation determination by PELDOR spectroscopy.

The ribonucleoside EÇr (**3**), a new spin label in the Ç family, was synthesized and confirmed by CW EPR spectroscopy. It was converted to triphosphate EÇrTP (**55**), which was then used for primer extension experiments with Therminator III DNA polymerase. First, the concentration dependence of the incorporation efficiency was determined by single-nucleotide primer extensions. These tests showed that a concentration of 1 μM is too low for efficient incorporation, while a high concentration like 100 μM leads to inhibition. At intermediate concentrations, incorporation was still less efficient compared to cytidine, but that was to be expected as EÇr is highly modified compared to C, so the

fact that it can be incorporated at all is a good result. After it had been shown that EÇrTP is accepted by Therminator polymerase, various primer extensions were performed with different templates and concentrations to achieve enzymatic incorporation of EÇrTP into short oligonucleotides. These results showed that in spite of the low efficiency of incorporation, full-length products can be obtained. EÇr can become an important member of the Ç family, which has already been successfully used in different experiments. The synthesis of EÇ[118] was also begun, with the intention of generating its triphosphate EÇTP (**69**), to test its suitability for enzymatic incorporation.

All of these three spin labels have the potential to become useful additions to the pool of rigid spin labels currently available and might contribute to making EPR spectroscopy a more widely used technique in the study of nucleic acids.

In addition to the new spin labels, bezimidazole nucleoside **78** was prepared and converted into phosphoramidite **81**, which was then incorporated into oligonucleotides. These oligonucleotides were modified with a 5'-phosphate to allow for ligation to a larger piece of RNA, to generate modified mRNA sequences with the benzimidazole nucleotide in different positions of a codon. These could then be used in translation experiments to investigate the effect of hydrogen bonding on the codon-anticodon interactions, where benzimidazole, with its inability to form hydrogen bonds to an opposing nucleobase, represented a valuable addition to the other modifications that were tested.

Remdesivir triphosphate (RTP, **87**) was prepared from nucleoside **85** with isolation of the intermediate, remdesivir monophosphate (**86**). RTP was then used to study the mechanism by which the antiviral drug remdesivir inhibits the RNA polymerase. Experiments with RTP were able to show that remdesivir likely only causes stalling of the RNA elongation, but not termination, because high concentrations of NTPs enabled the synthesis of full-length RNA product even in presence of RTP.

5 Experimental section

5.1 Reagents and solvents

Reagents were bought from various suppliers and used without further purification.

Dry solvents were taken from a solvent purification system PS-MD-5/7-EN from Inert or bought in pure quality and stored over molecular sieves.

Solvents for chromatography were bought in technical quality and distilled before use.

Reactions were done under nitrogen atmosphere when necessary.

5.2 Chromatography and analytics

Thin layer chromatography was done on plates from Macherey-Nagel with silica gel 60 F_{254}. Substances were detected under UV light (λ = 254 nm).

Column chromatography was done using silica gel 60 (40-63 µm) from Macherey-Nagel. For samples containing a DMT group, NEt_3 was added to the solvent mixture for packing the column and then washed out before loading the crude product mixture on the column.

Benzi-spin triphosphate (**55**) was purified by ion exchange HPLC (0.1 M to 1 M TEAB buffer pH 7.5) on an ÄKTAprime plus HPLC system using a Sephadex column.

NMR spectra were recorded on one of the following spectrometers:

Bruker Avance 300, Bruker Avance III 300, Varian Mercury 300, Varian Mercury VX 300, Varian VNMRS 300, Bruker Avance III 400, Bruker Avance III HD 400, Bruker Avance III HD 500, Varian Inova 500, Bruker Avance III HD 600 or Varian Inova 600.

Samples for high temperature NMR measurements were measured in a high pressure NMR tube from Wilmad.

As NMR solvents, deuterated chloroform, methanol, dimethyl sulfoxide or deuterium oxide were used. The solvent signals were used as references ($CDCl_3$: 7.260/77.160 ppm, CD_3OD: 3.310/49.000 ppm, DMSO-d_6: 2.500/39.520 ppm, D_2O: 4.790 ppm). For samples containing a DMT group, $CDCl_3$ was filtered over aluminium oxide 90 basic before dissolving the sample. In case of a solvent mixture, the underlined solvent is used as the reference. Chemical shifts (δ) are given in ppm, coupling constants (J) are given in hertz (Hz). For easier assignment, COSY, HSQC, HMBC and, when necessary, NOESY spectra were recorded.

Mass spectra were recorded on a Bruker Daltonics micrOTOF spectrometer, using electrospray ionization (ESI) and a time of flight detector. Signals are given in *m/z*. For HPLC-MS measurements, it was used together with an Agilent 1100 HPLC equipped with a Phenomenex Synergi 4 µm Fusion-RP 80 Å 2 x 25 mm column (Buffer A: 10 mM NH₄OAc pH 5.4; Buffer B: MeCN, 25 °C), 0 % to 70 % B in A in 35 min.

UV/VIS absorption spectra were recorded on a Cary 100 Bio UV-visible spectrophotometer from Varian at 25 °C in quartz cuvettes with a path length of 10 mm. Blank solvent spectra were recorded separately and manually subtracted from the sample spectra.

Fluorescence spectra, including interval and 3D measurements, were recorded on an FP-8300 Spectrofluorometer from Jasco at 25 °C. Photomultiplier tube voltage, response time as well as excitation and emission bandwidths were varied depending on the sample, to obtain acceptable peak intensities. Measurements with lumi-spin were done in quartz cuvettes with a light path of 10 x 2 mm, measurements with benzi-spin precursor **1a** were done in a 5 x 5 mm cuvette containing a stirring bar to ensure even distribution of the photoreaction product in the solution. Blank solvent spectra were recorded separately and manually subtracted from the sample spectra.

5.3 Oligonucleotide synthesis and purification

Phosphoramidites of canonical nucleosides (DMT-dA(bz) phosphoramidite, DMT-dC(bz) phosphoramidite, DMT-dC(ac) phosphoramidite, DMT-dG(dmf) phosphoramidite, DMT-dT phosphoramidite) were purchased from Sigma-Aldrich or SAFC. Controlled pore glass (CPG) beads (pore size 1000 Å, 25-35 µmol/g) were purchased from Sigma-Aldrich. MeCN was purchased in DNA synthesis quality (≥99.9 %) from Roth, DCE was purchased in synthesis quality (≥99 %) from Roth, DCM was purchased in gas chromatography quality from Merck. Freshly activated molecular sieves were added to all solutions of phosphoramidites and 5-ethylthio-(1*H*)-tetrazole (ETT) and the solutions stored at 4 °C.

Unmodified oligonucleotides or oligonucleotides with a 5'-hexynyl modification were synthesized with an Applied Biosystems 392 DNA/RNA Synthesizer on a CPG support (20-30 mg). 70 mM solutions of phosphoramidites (100 mM for 2-Cyanoethyl-hex-5-yn-1-yl-*N*,*N*-diisopropylphosphoramidite (**68**)) in MeCN were used. Activation was done with 0.25 M ETT in MeCN. For detritylation, oxidation and capping, commercially available solutions for ABI synthesizers from J.T. Baker were used. Coupling time was 4 min.

Modified oligonucleotides were synthesized with a Pharmacia LKB Gene Assembler Plus on a CPG support (20-30 mg). Phosphoramidites were used as 100 mM solutions in MeCN (for

m⁶G-phosphoramidite **38** DCE was used instead). Activation was done with 0.25 M ETT in MeCN, detritylation was done with 3 % dichloroacetic acid (DCA) in DCE. For oxidation 10 mM iodine in MeCN/2,4,6-trimethylpyridine/water (10/1/5) was used, for capping 0.5 M DMAP in MeCN and Ac₂O/2,4,6-trimethylpyridine/MeCN (20/30/50) were used. Coupling time was 4 min for canonical phosphoramidites, 12 min for modified phosphoramidites.

After completion of the synthesis the solid support was dried under reduced pressure. Then, the oligonucleotides were cleaved from the solid support and deprotected under different conditions. For most oligonucleotides, 1 ml 25 % aq. ammonia for 10-18 h at 55 °C or 1 ml of a mixture of 25 % aq. ammonia and EtOH (3:1) for 18 h at 55 °C was used. For D2681NHMe, 1 ml of a solution of MeNH₂ in H₂O/EtOH (1:1) for 10 h at 37 °C was used to achieve substitution of the methoxy group. For D2681, 1 ml 25 % aq. ammonia for 48 h at 37 °C was used to prevent substitution.

After deprotection the solvent was removed under reduced pressure, the residue taken up in H₂O (500 µl), the concentration determined with an IMPLEN Nanophotometer and the synthesis quality checked by ion-exchange HPLC on an ÄKTA Purifier equipped with a Dionex DNAPac PA200 2 x 250 mm or 4 x 250 mm column (Buffer A: 25 mM Tris HCl, 6 M urea, pH 8.0; Buffer B: 25 mM Tris HCl, 6 M urea, 0.5 M NaClO₄, pH 8.0; 60 °C), 0 % to 48 % B in A in 12 CV.

20 % polyacrylamide gels for electrophoresis were prepared from a stock solution containing TBE buffer (89 mM Tris, 89 mM boric acid, 2 mM ethylenediaminetetraacetic acid (EDTA), pH 8.0), urea (7 M) and acrylamide/bisacrylamide 19:1 (20 %). 45 ml of the stock solution were mixed with a solution of ammonium peroxodisulfate (APS, 25 %, 125 µl) and *N,N,N',N'*-tetramethylene diamine (TEMED, 30 µl) and poured between two glass plates of a length of 30 cm separated by spacers to achieve a gel thickness of 0.7 mm. After 45 min, the gel was prerun for 30 min with constant power of 35 W (60 W for two gels) with TBE buffer. Samples were prepared by mixing solutions of crude oligonucleotides with an equal volume of loading buffer (TBE buffer with 50 mM EDTA, 80 % formamide, 0.025 % bromophenol blue, 0.025 % xylene cyanol).

Portions of crude oligonucleotides mixed with loading buffer were loaded on a 20 % polyacrylamide gel. It was run with constant power of 35 W (60 W for two gels) with TBE buffer for 2.5 h. Bands were visualized by UV light on TLC plates with fluorescence indicator, cut, crushed by centrifugation (16400 rpm) and extracted twice with 300 µl TEN buffer (10 mM Tris HCl, 1 mM EDTA, 300 mM NaCl, pH 8.0), first for 1.5 h at 37 °C, then for 12 h at room temperature. 900 µl EtOH were added and the oligonucleotides precipitated by addition of 900 µl EtOH, freezing in liquid nitrogen and centrifugation (25 min, 4 °C, 16400 rpm). After removal of the supernatant, 75 µl 75 % EtOH were added to the precipitates and the samples subjected to centrifugation (10 min, 4 °C, 16400 rpm)

again. The supernatant was removed, the dry residue dissolved in 30 µl H_2O, samples of the same oligonucleotide pooled, the concentration determined with an IMPLEN Nanophotometer and the purity checked by ion-exchange HPLC on an ÄKTA Purifier equipped with a Dionex DNAPac PA200 2 x 250 mm or 4 x 250 mm column (Buffer A: 25 mM Tris HCl, 6 M urea, pH 8.0; Buffer B: 25 mM Tris HCl, 6 M urea, 0.5 M $NaClO_4$, pH 8.0; 60 °C), 0 % to 48 % B in A in 12 CV. The identity of the oligonucleotides was confirmed by ESI-MS.

5.4 Melting curves

Melting curves were measured on a Cary 100 Bio UV-visible spectrophotometer from Varian equipped with a temperature controller. Samples were prepared in 500 µl phosphate buffer (10 mM phosphate, 150 mM NaCl, pH 7.4) to obtain a 1 µM oligonucleotide solution, filled in a quartz cuvette with a path length of 10 mm, and a layer of silicone oil placed on top to prevent evaporation. Samples were heated to 95 °C, then cooled to 10 °C and heated to 95 °C twice at a rate of 0.7 °C/min. Every 0.5 °C, the absorbance at 250 nm, 260 nm and 280 nm was measured. The measured data were analyzed with the software OriginPro. For each sample, the absorbance at 260 nm of four ramps was converted to the hyperchromicity (Hyp) according to the formula

$$Hyp = 100 \cdot \frac{(A - A_{\min})}{A_{\min}}$$

where A is the absorbance and $A_{\min}$ is the lowest absorbance value. A ninth order polynomial was fitted to the data and the melting point determined as the maximum of the first derivative. The overall melting point for each sample was determined as the mean value of the melting temperatures of the four ramps.

5.5 EPR spectroscopy

EPR measurements at X-band (9.87 GHz) were carried out using a Bruker ELEXSYS E580 CW EPR spectrometer. CW EPR spectra were measured using 10 mW microwave power and 1 G field modulation at 100 kHz, with a conversion time of 20 ms at a temperature of 295 K. The spectral simulations were performed using MATLAB 8.6.0 and the EasySpin 5.2.25 toolbox[186]. Samples were dissolved in EPR buffer (10 mM Na_2HPO_4, 100 mM NaCl, 0.1 mM Na_2EDTA, pH 7.0) and samples containing oligonucleotides heated to 95 °C for 2 min followed by cooling to 4 °C for annealing. 10 µl sample solution were taken up in a 10 µl glass capillary and the ends sealed with silicone grease. For the calibration curve different concentrations of TEMPOL (0.1 mM, 0.2 mM, 0.3 mM, 0.4 mM, 0.5 mM) were used. Samples were measured at a concentration of 0.2 mM.

5.6 Primer extension experiments

A solution containing ThermoPol buffer, Therminator III polymerase and the template and primer strands was prepared and distributed into PCR tubes. Solutions of appropriate NTPs were added to give final concentrations of 1x ThermoPol buffer, 1 U/µl polymerase, 1.0 µM template strand and 0.5 µM primer strand. The samples were placed in a T100 Thermal Cycler from Bio-Rad, annealed by heating to 90 °C for 3.5 min followed by 1 min at 45 °C. Then they were heated to 72 °C for different durations. Afterwards, the samples were put on ice and mixed with 10 µl loading buffer (TBE buffer with 50 mM EDTA and 80 % formamide).

For analysis, a polyacrylamide gel was prepared from a stock solution containing TBE buffer (89 mM Tris, 89 mM boric acid, 2 mM ethylenediaminetetraacetic acid (EDTA), pH 8.0), urea (7 M) and 15 % acrylamide (20 % for single nucleotide extensions). 18 ml of the stock solution were mixed with a solution of APS (25 %, 40 µl) and TEMED (10 µl) and poured between two glass plates of a length of 20 cm separated by spacers to achieve a gel thickness of 0.4 mm. After 45 min, the gel was prerun for 30 min with constant power of 35 W with TBE buffer. 4 µl of the samples were then loaded on the gel and run for 45 min (1 h for 20 % gels) with constant power of 35 W with TBE buffer.

Bands were visualized by fluorescence of the attached FAM label in a ChemiDoc MP Imager from Bio-Rad.

5.7 Synthesis procedures

5.4.1 Synthesis of benzi-spin

N-Benzylisoindoline (12)

$C_8H_4O_3$
[148.12]

C_7H_9N
[107.16]

$C_{15}H_{11}NO_2$
[237.26]
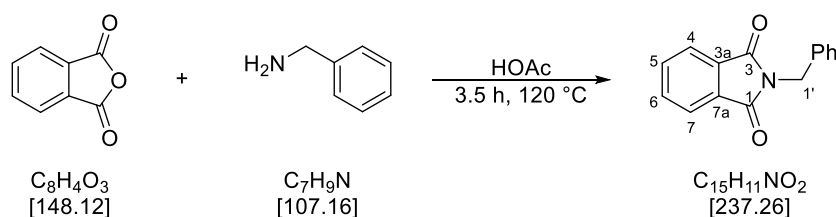
Phthalic anhydride (40.3 g, 272 mmol, 1.0 eq) was suspended in acetic acid (140 ml). Benzylamine (32 ml, 272 mmol, 1.0 eq) was added dropwise and the reaction mixture stirred for 3.5 h at 120 °C. The reaction mixture was then poured on ice, filtered and the residue washed with cold water. The crude product was recrystallized from ethanol. The product was obtained as colorless crystals (49.47 g, 210 mmol, 77 %). The NMR data agree with literature data[167].
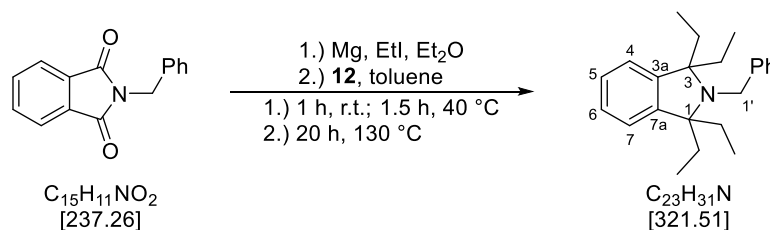
TLC (*n*-hexane/EtOAc 4:1): R_f = 0.45

¹H-NMR (300 MHz, CDCl₃): δ (ppm) = 4.85 (s, 2 H, 1'-H), 7.24-7.35 (m, 3 H, 4'-H, 5'-H, 6'-H), 7.42-7.45 (m, 2 H, 3'-H, 7'-H), 7.69-7.72 (m, 2 H, 5-H, 6-H), 7.83-7.86 (m, 2 H, 4-H, 7-H).

¹³C-NMR (75 MHz, CDCl₃): δ (ppm) = 41.75 (C-1'), 123.48 (C-4, C-7), 127.95 (C-5'), 128.75, 128.81 (C-3', C-4', C-6', C-7'), 132.26 (C-3a, C-7a), 134.11 (C-5, C-6), 136.49 (C-2'), 168.17 (C-1, C-3).

HR-MS (ESI): calc. $C_{15}H_{11}NNaO_2$ ([M+Na]⁺): 260.0682, found: 260.0678.

N-Benzyl-1,1,3,3-tetraethylisoindoline (25)

To a suspension of magnesium turnings (18.5 g, 760 mmol, 9.0 eq) in dry diethyl ether (80 ml) under inert atmosphere ethyl iodide (52 ml, 647 mmol, 7.7 eq) was added slowly and the mixture stirred for 1 h at room temperature and 1.5 h at 40 °C. After cooling to room temperature, it was diluted with dry toluene (100 ml) and *N*-benzylphthalimide (20.0 g, 84.3 mmol, 1.0 eq) was added portionwise, part of the solvent distilled off, and the mixture stirred for 15 h at 130 °C. After cooling to room temperature, *n*-hexane was added and the resulting mixture stirred for 2 h under air. The mixture was filtered over aluminium oxide 90 basic and the solvent removed under reduced pressure. The crude product was purified by column chromatography (*n*-hexane to *n*-hexane/EtOAc 3:1). The product was obtained as a colorless solid (10.2 g, 31.9 mmol, 38 %). The NMR data agree with literature data[168].

TLC (*n*-hexane): R_f = 0.64.

¹H-NMR (600 MHz, CDCl₃): δ (ppm) = 0.76 (t, *J* = 8 Hz, 12 H, CH₂-C*H₃*), 1.53 (dq, *J* = 8.0 Hz, *J* = 8.0 Hz, 4 H, C*H₂*-CH₃), 1.92 (dq, *J* = 8.0 Hz, *J* = 8.0 Hz, 4 H, C*H₂*-CH₃), 4.00 (s, 2 H, 1'-H), 7.03-7.06 (m, 2 H, 4-H, 7-H), 7.18-7.21 (m, 2 H, 5-H, 6-H), 7.23-7.25 (m, 1 H, 5'-H), 7.27-7.31 (m, 2 H, 3'-H, 7'-H), 7.44-7.46 (m, 2 H, 4'-H, 6'-H).

¹³C-NMR (125 MHz, CDCl₃): δ (ppm) = 9.74 (CH₂-*C*H₃), 30.48 (*C*H₂-CH₃), 46.87 (C-1'), 71.42 (C-1, C-3), 123.56 (C-4, C-7), 125.72 (C-5, C-6), 126.66 (C-5'), 127.90 (C-3', C-7'), 129.40 (C-4', C-6'), 142.54 (C-2'), 144.70 (C-3a, C-7a).

HR-MS (ESI): calc. $C_{23}H_{32}N$ ([M+H]⁺): 322.2457, found: 322.2518.

1,1,3,3-Tetraethylisoindoline (26)

C$_{23}$H$_{31}$N
[321.51]

H$_2$, Pd/C, HOAc
16 h, r.t.

C$_{16}$H$_{25}$N
[231.38]
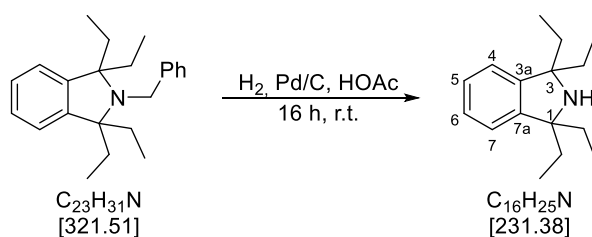
To a solution of *N*-benzyl-1,1,3,3-tetraethylisoindoline (4.33 g, 13.4 mmol, 1.0 eq) in acetic acid (25 ml) was added palladium (10 % on charcoal, 0.69 g, 0.67 mmol, 5 mol-%) and the mixture was stirred for 17 h at room temperature under hydrogen atmosphere. Afterwards, the mixture was filtered over Celite, the solvent was removed under reduced pressure, the residue neutralized with aq. NaOH and the aqueous phase extracted with EtOAc. The combined organic phases were dried over Na$_2$SO$_4$, filtered, and the solvent removed under reduced pressure. The product was obtained as a colorless solid (2.87 g, 12.4 mmol, 92 %) and used in the next step without further purification. The NMR data agree with literature data[168].
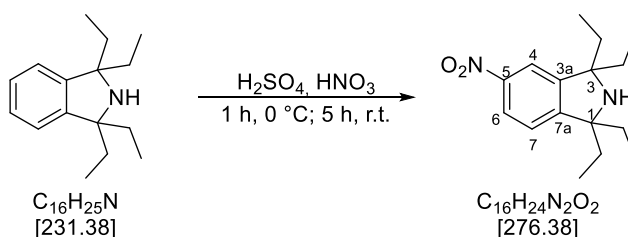
TLC (DCM/MeOH 98:2): *R*$_f$ = 0.18.

^{1}H-NMR (400 MHz, CDCl$_3$): δ (ppm) = 0.87 (t, *J* = 8.0 Hz, 12 H, CH$_2$-C*H*$_3$), 1.68 (dq, *J* = 8.0 Hz, *J* = 8.0 Hz, 4 H, C*H*$_2$-CH$_3$), 1.72 (dq, *J* = 8.0 Hz, *J* = 8.0 Hz, 4 H, C*H*$_2$-CH$_3$), 7.06 (dd, *J* = 5.6 Hz, *J* = 3.1 Hz, 2 H, 4-H, 7-H), 7.21 (dd, *J* = 5.6 Hz, *J* = 3.1 Hz, 2 H, 5-H, 6-H).
^{13}C-NMR (100 MHz, CDCl$_3$): δ (ppm) = 9.06 (CH$_2$-*C*H$_3$), 33.91 (*C*H$_2$-CH$_3$), 68.41 (C-1, C-3), 122.59 (C-4, C-7), 126.64 (C-5, C-6), 147.61 (C-3a, C-7a).

HR-MS (ESI): calc. C$_{16}$H$_{26}$N ([M+H]$^+$): 232.2060, found: 232.2076.

1,1,3,3-Tetraethyl-5-nitroisoindoline (27)

C$_{16}$H$_{25}$N
[231.38]

H$_2$SO$_4$, HNO$_3$
1 h, 0 °C; 5 h, r.t.

C$_{16}$H$_{24}$N$_2$O$_2$
[276.38]

1,1,3,3-Tetraethylisoidoline (2.87 g, 12.4 mmol, 1.0 eq) was dissolved in conc. H$_2$SO$_4$ (22 ml). Conc. HNO$_3$ (6 ml) was added dropwise at 0 °C and the resulting mixture stirred for 1 h at 0 °C and 5 h at room temperature. It was then neutralized with aq. NaOH and extracted with EtOAc. The combined organic phases were dried over Na$_2$SO$_4$, filtered and the solvent removed under reduced pressure.

The crude product was purified by column chromatography (2 % MeOH in DCM). The product was obtained as a yellow oil (3.33 g, 12.1 mmol, 97 %). The NMR data agree with literature data[168].

TLC (DCM/MeOH 98:2): R_f = 0.66.

^{1}H-NMR (400 MHz, CDCl$_3$): δ (ppm) = 0.87 (t, J = 7.6 Hz, 6 H, CH$_2$-CH_3), 0.89 (t, J = 7.6 Hz, 6 H, CH$_2$-CH_3), 1.62-1.82 (m, 8 H, CH_2-CH$_3$), 7.18 (dd, J = 8.4 Hz, J = 0.4 Hz, 1 H, 7-H), 7.90 (dd, J = 2.1 Hz, J = 0.4 Hz, 1 H, 4-H) 8.11 (dd, J = 8.4 Hz, J = 2.1 Hz, 1 H, 6-H).
^{13}C-NMR (100 MHz, CDCl$_3$): δ (ppm) = 8.91, 8.92 (CH$_2$-CH$_3$), 33.76, 33.79 (CH$_2$-CH$_3$), 68.44 (C-3), 68.76 (C-1), 117.99 (C-4), 122.81 (C-6), 123.12 (C-7), 147.77 (C-5), 149.65 (C-7a), 155.37 (C-3a).

HR-MS (ESI): calc. C$_{16}$H$_{25}$N$_2$O$_2$ ([M+H]$^+$): 277.1911, found: 277.1922.

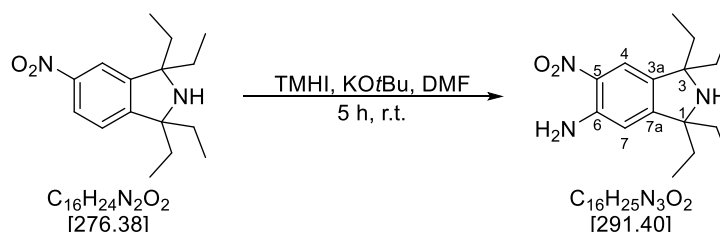**1,1,1-Trimethylhydrazinium iodide (TMHI, 17)**
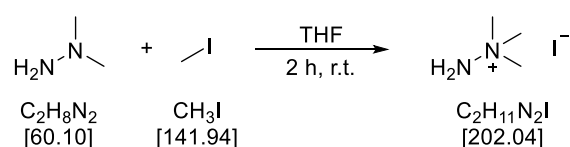
To a solution of 1,1-dimethylhydrazine (8.0 ml, 104 mmol, 1.0 Äq.) in THF (170 ml) methyl iodide (6.5 ml, 102 mmol, 1.0 Äq.) was added dropwise and the mixture stirred for 2 h at room temperature, filtered and the crude product recristallized from ethanol. The product was obtained as a colorless solid (18.4 g, 91.07 mmol, 88 %).

TLC (DCM/MeOH 9:1): R_f = 0.34.

^{1}H-NMR (300 MHz, CD$_3$OD): δ (ppm) = 3.39 (s, 9 H, Me).
^{13}C-NMR (125 MHz, CD$_3$OD): δ (ppm) = 58.83 (Me).

6-Amino-1,1,3,3-tetraethyl-5-nitroisoindoline (28)

To a solution of 1,1,3,3-tetraeethyl-5-nitroisoindoline (2.01 g, 7.26 mmol, 1.0 eq) in dry DMF (32 ml) under inert atmosphere was added 1,1,1-trimethylhydrazinium iodide (1.79 g, 7.99 mmol, 1.1 eq). After a clear solution was obtained, KOtBu (2.04 g, 17.4 mmol, 2.4 eq) was added and the mixture stirred for 5 h at room temperature. It was then poured on ice, neutralized with conc. HCl, and extracted with EtOAc. The combined organic phases were dried over Na$_2$SO$_4$, filtered and the solvent

removed under reduced pressure. The crude product was purified by column chromatography (2 % MeOH in DCM). The product was obtained as an orange oil (1.04 g, 3.57 mmol, 49 %).

TLC (DCM/MeOH 98:2): R_f = 0.11.

^{1}H-NMR (400 MHz, CDCl$_3$): δ (ppm) = 0.87 (t, J = 7.4 Hz, 12 H, CH$_2$-CH_3), 1.58-1.75 (m, 8 H, CH_2-CH$_3$), 6.04 (s$_{br}$, 2 H, NH$_2$), 6.45 (s, 1 H, 7-H), 7.79 (s, 1 H, 4-H).
^{13}C-NMR (100 MHz, CDCl$_3$): δ (ppm) = 8.92, 8.97 (CH$_2$-CH$_3$), 33.69, 33.84 (CH$_2$-CH$_3$), 67.64, (C-3), 68.42 (C-1), 111.61 (C-7), 119.73 (C-4), 132.15 (C-6), 138.25 (C-7a), 144.63 (C-5), 157.72 (C-3a).

HR-MS (ESI): calc. C$_{16}$H$_{26}$N$_3$O$_2$ ([M+H]$^+$): 292.2020, found: 292.2012.

5,6-Diamino-1,1,3,3-tetraethylisoindoline (29)

C$_{16}$H$_{25}$N$_3$O$_2$ [291.40]   H$_2$, Pd/C, MeOH, 15 h, r.t.   C$_{16}$H$_{27}$N$_3$ [261.41]
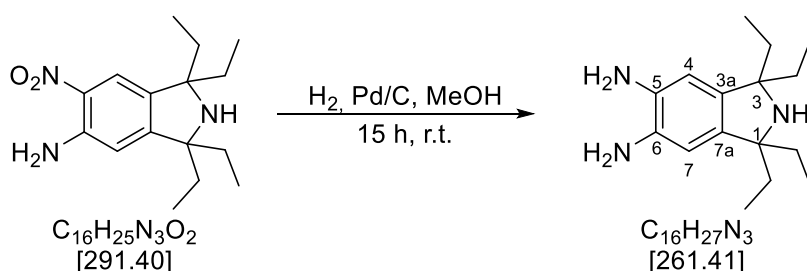
To a solution of 6-amino-1,1,3,3-tetraethyl-5-nitroisoindoline (1.03 g, 3.53 mmol, 1.0 eq) in MeOH (50 ml) palladium (10 % on charcoal, 0.38 g, 0.36 mmol, 10 mol-%) was added and the mixture stirred for 15 h under hydrogen atmosphere. Then the mixture was filtered over Celite and the solvent removed under reduced pressure. The product was obtained as an light brown solid (0.86 g, 3.27 mmol, 93 %) and used in the next step without further purification.
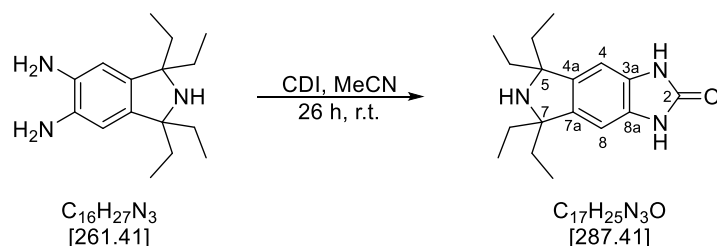
TLC (DCM/MeOH 95:5): R_f = 0.31.

^{1}H-NMR (400 MHz, CDCl$_3$): δ (ppm) = 0.86 (t, J = 7.6 Hz, 12 H, CH$_2$-CH_3), 1.57-1.75 (m, 8 H, CH_2-CH$_3$), 6.40 (s, 2 H, 4-H, 7-H).
^{13}C-NMR (100 MHz, CDCl$_3$): δ (ppm) = 9.12 (CH$_2$-CH$_3$), 33.87 (CH$_2$-CH$_3$), 68.04 (C-1, C-3), 110.84 (C-4, C-7), 133.87 (C-5, C-6), 139.33 (C-3a, C-7a).

HR-MS (ESI): calc. C$_{16}$H$_{28}$N$_3$ ([M+H]$^+$): 262.2278, found: 262.2287.

5,5,7,7-tetraethyl-3,5,6,7-tetrahydroimidazo[4,5-*f*]isoindol-2-one (30)

C$_{16}$H$_{27}$N$_3$ [261.41]   CDI, MeCN, 26 h, r.t.   C$_{17}$H$_{25}$N$_3$O [287.41]

113

5,6-Diamino-1,1,3,3-tetraethylisoindoline (501 mg, 1.92 mmol, 1.0 eq) and 1,1'-carbonyldiimidazole (582 mg, 3.44 mmol, 1.8 eq) were dissolved in dry MeCN (20 ml) under inert atmosphere and stirred for 17 h at room temperature. The precipitated product was collected by filtration and obtained as a light brown solid (352 mg, 1.35 mmol, 70 %).

TLC (DCM/MeOH 9:1): R_f = 0.35.

^{1}H-NMR (400 MHz, CD$_3$OD): δ (ppm) = 0.88 (t, J = 7.4 Hz, 12 H, CH$_2$-CH_3), 1.66-1.81 (m, 8 H, CH_2-CH$_3$), 6.75 (s, 2 H, 4-H, 8-H).
^{13}C-NMR (100 MHz, CD$_3$OD): δ (ppm) = 9.25 (CH$_2$-CH$_3$), 34.83 (CH$_2$-CH$_3$), 69.68 (C-5, C-7), 104.52 (C-4, C-8), 130.23 (C-3a, C-8a), 141.74 (C-4a, C-7a), 158.33 (C-2).

HR-MS (ESI): calc. C$_{17}$H$_{26}$N$_3$O ([M+H]$^+$): 288.2070, found: 288.2065.

1-*N*-(3',5'-Di-*O*-toluoyl-2'-deoxy-β-D-ribofuranosyl)-5,5,7,7-tetraethyl-3,5,6,7-tetrahydro-imidazo[4,5-*f*]isoindol-2-one (31)

C$_{17}$H$_{25}$N$_3$O
[287.41]

C$_{21}$H$_{21}$O$_5$Cl
[388.84]

C$_{38}$H$_{45}$N$_3$O$_6$
[639.79]
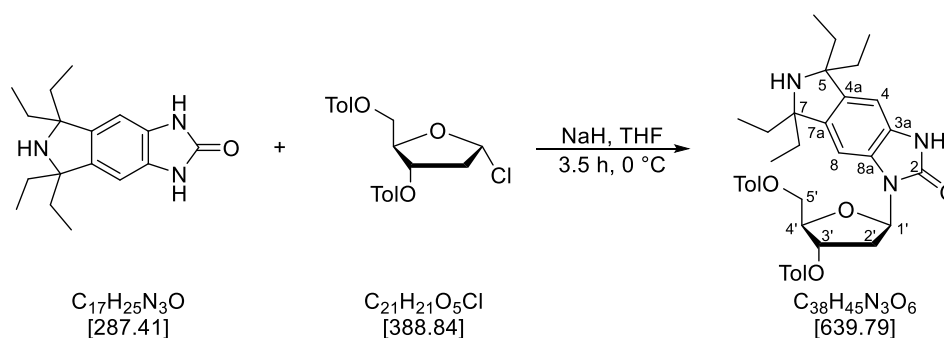
5,5,7,7-tetraethyl-3,5,6,7-tetrahydroimidazo[4,5-*f*]isoindol-2-one (636 mg, 2.21 mmol, 1.1 eq.) was dissolved in dry THF (30 ml) under inert atmosphere. NaH (119 mg, 4.97 mmol, 2.5 eq.) was added at 0 °C and the mixture stirred for 15 min. Afterwards, 1-chloro-3,5-di-*O*-toluoyl-2-deoxy-α-D-ribofuranose (765 mg, 1.97 mmol, 1.0 eq.) was added and the mixture stirred for 3.5 h at 0 °C. Water was added, the mixture was extracted with EtOAc and the combined organic phases washed with brine, dried over Na$_2$SO$_4$, filtered and the solvent removed under reduced pressure. The crude product was purified by column chromatography (2 % to 5 % MeOH in DCM). The product was obtained as an off-white foam (333 mg, 0.52 mmol, 26 %).

TLC (DCM/MeOH 95:5): R_f = 0.19.

^{1}H-NMR (400 MHz, CDCl$_3$): δ (ppm) = 0.73-0.79 (m, 6 H, CH$_2$-CH_3), 0.81-0.87 (m, 6 H, CH$_2$-CH_3), 1.40-1.54 (m, 6 H, CH_2-CH$_3$), 1.55-1.75 (m, 2 H, CH_2-CH$_3$), 2.38, 2.44 (2 x s, 6 H, Tol-Me), 2.52 (ddd, J = 14.2 Hz, J = 6.0 Hz, J = 2.0 Hz, 1 H, 2'-H$_a$), 3.28 (ddd, J = 14.1 Hz, J = 9.0 Hz, J = 7.0 Hz, 1 H, 2'-H$_b$), 4.54-4.57 (m, 1 H, 4'-H), 4.63 (dd, J = 11.8 Hz, J = 5.6 Hz, 1 H, 5'-H$_a$), 4.74 (dd, J = 12.0 Hz, J = 4.4 Hz, 1 H, 5'-H$_b$), 5.77 (ddd, J = 6.7 Hz, J = 2.2 Hz, J = 2.2 Hz, 1 H, 3'-H), 6.42 (dd, J = 9.0 Hz, J = 5.8 Hz, 1 H, 1'-H), 6.79 (s, 1 H, 4-H), 6.87 (s, 1 H, 8-H), 7.20 (d, J = 8.0 Hz, 2 H, Tol-CH), 7.28 (d, J = 7.9 Hz, 2 H, Tol-CH), 7.94 (d, J = 8.2 Hz, 2 H, Tol-CH), 7.99 (d, J = 8.2 Hz, 2 H, Tol-CH).

13C-NMR (100 MHz, CDCl$_3$): δ (ppm) = 9.06 (CH$_2$-CH$_3$), 21.82 (Tol-Me), 33.89 (CH$_2$-CH$_3$), 34.47 (C-2'), 64.79 (C-5'), 68.35 (C-5, C-7), 75.00 (C-3'), 81.51 (C-4'), 83.25 (C-1'), 103.97 (C-8), 104.16 (C-4), 126.74, 127.07 (*i*-Tol), 127.32 (C-8a), 127.65 (C-3a), 129.35, 129.38, 129.90, 129.98 (Tol-CH), 141.39 (C-4a), 141.87 (C-7a), 144.08, 144.49 (*p*-Tol), 154.98 (C-2), 166.23, 166.44 (Tol-CO).

HR-MS (ESI): calc. C$_{38}$H$_{46}$N$_3$O$_6$ ([M+H]$^+$): 640.3381, found: 640.3329.

1-*N*-(2'-Deoxy-β-D-ribofuranosyl)-5,5,7,7-tetraethyl-3,5,6,7-tetrahydroimidazo[4,5-*f*] isoindol-2-one (1a)
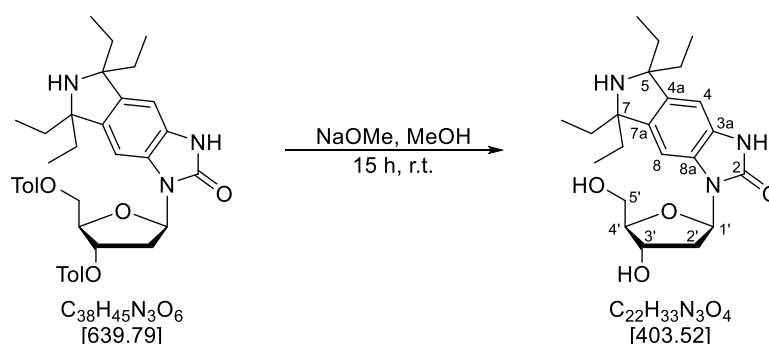
C$_{38}$H$_{45}$N$_3$O$_6$
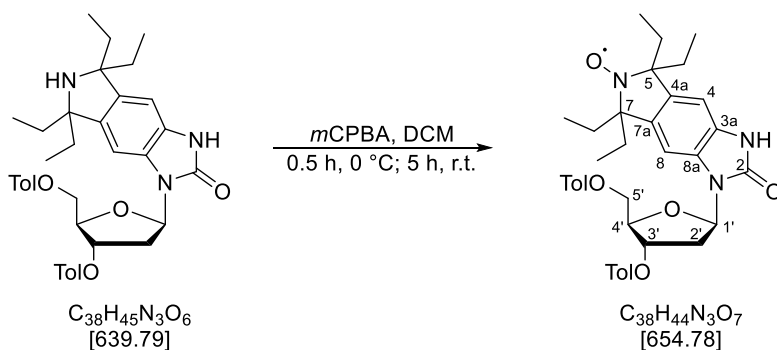[639.79]

C$_{22}$H$_{33}$N$_3$O$_4$
[403.52]

1-*N*-(3',5'-Di-*O*-toluoyl-2'-deoxy-β-D-ribofuranosyl)-5,5,7,7-tetraethyl-3,5,6,7-tetrahydroimidazo [4,5-*f*]isoindol-2-one (50 mg, 0.08 mmol, 1.0 eq.) was dissolved in dry MeOH (2 ml). NaOMe (28 mg, 0.52 mmol, 6.7 eq.) was added and the mixture stirred for 15 h at room temperature. Dowex-H$^+$ (142 mg) was washed with MeOH and MeOH/H$_2$O (1:1) and added to the reaction mixture. After 1 h the mixture was filtered, the Dowex washed with MeOH and MeOH/H$_2$O (1:1) and the solvent removed under reduced pressure. The product was obtained as an off-white foam (40 mg, quant.).

1H-NMR (400 MHz, CD$_3$OD): δ (ppm) = 0.99-1.06 (m, 12 H, CH$_2$-CH_3), 2.01-2.18 (m, 9 H, CH_2-CH$_3$, 2'-H$_a$), 2.73 (dq, *J* = 8.9 Hz, *J* = 6.6 Hz, 1 H, 2'-H$_b$), 3.81 (d, *J* = 3.0 Hz, 2 H, 5'-H), 3.96 (q, *J* = 3.2 Hz, 1 H, 4'-H), 4.55-4.95 (m, 1 H, 3'-H), 6.33 (dd, *J* = 8.8 Hz, *J* = 6.0 Hz, 1 H, 1'-H), 6.95 (s, 1 H, 4-H), 7.65 (s, 1 H, 8-H).

13C-NMR (100 MHz, CD$_3$OD): δ (ppm) = 8.67 (CH$_2$-CH$_3$), 31.55, 31.66, 31.87, 31.99 (CH$_2$-CH$_3$), 38.37, (C-2'), 62.94 (C-5'), 72.45 (C-3'), 76.18 (C-5), 76.29 (C-7), 84.27 (C-1'), 88.47 (C-4'), 105.19 (C-4), 107.38 (C-8), 130.31 (C-3a), 130.50 (C-8a), 135.08 (C-4a), 135.41 (C-7a), 155.99 (C-2).

HR-MS (ESI): calc. C$_{22}$H$_{34}$N$_3$O$_4$ ([M+H]$^+$): 404.2544, found: 404.2533.

1-*N*-(3',5'-Di-*O*-toluoyl-2'-deoxy-β-D-ribofuranosyl)-5,5,7,7-tetraethyl-6-oxyl-3,5,6,7-tetra-hydroimidazo[4,5-*f*]isoindol-2-one (35)

C₃₈H₄₅N₃O₆
[639.79]

C₃₈H₄₄N₃O₇
[654.78]

1-*N*-(3',5'-Di-*O*-toluoyl-2'-deoxy-β-D-ribofuranosyl)-5,5,7,7-tetraethyl-3,5,6,7-tetrahydroimidazo[4,5-*f*]isoindol-2-one (100 mg, 0.16 mmol, 1.0 eq.) was dissolved in dry DCM (8 ml) under inert atmosphere. *m*CPBA (53 mg, 0.23 mmol, 1.4 eq.) was added at 0 °C and the mixture stirred for 0.5 h at 0 °C and 5 h at room temperature. The mixture was then washed with sat. aq. $NaHCO_3$ and brine, the combined aqueous phases extracted with DCM and the combined organic phases dried over Na_2SO_4, filtered and the solvent removed under reduced pressure. The crude product was purified by column chromatography (2 % MeOH in DCM). The product was obtained as a yellow foam (91 mg, 0.14 mmol, 89 %).

TLC (DCM/MeOH 98:2): R_f = 0.21.

¹H-NMR (400 MHz, CDCl₃): δ (ppm) = 0.88 (s_br), 1.27 (s_br), 2.43 (s), 2.47 (s), 2.59 (s_br), 3.33 (s_br), 4.61 (s_br), 4.59-4.81 (m), 5.83 (s_br), 6.46 (s_br), 7.32 (s_br), 8.02 (s_br).
¹³C-NMR (100 MHz, CDCl₃): δ (ppm) = 21.85, 34.61, 64.63, 74.90, 81.66, 83.35, 126.58, 129.37, 129.66, 129.94, 130.22, 144.52, 166.15.

HR-MS (ESI): calc. C₃₈H₄₄N₃NaO₇ ([M+Na]⁺): 677.3071, found: 677.3065.

1-*N*-(2'-Deoxy-β-D-ribofuranosyl)-5,5,7,7-tetraethyl-6-oxyl-3,5,6,7-tetrahydroimidazo [4,5-*f*]isoindol-2-one (1)


C₃₈H₄₄N₃O₇
[654.78]

C₂₂H₃₂N₃O₅
[418.51]
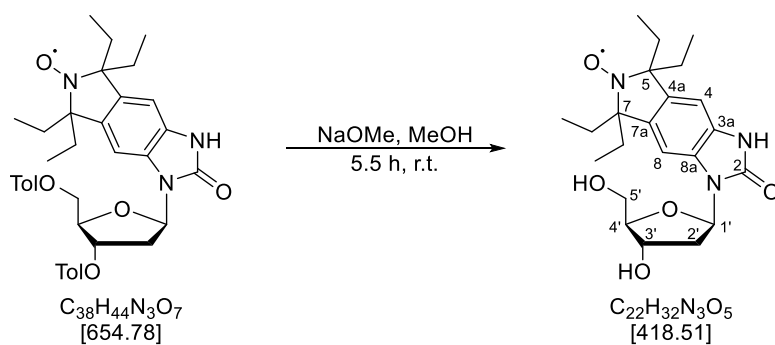
1-*N*-(3',5'-Di-*O*-toluoyl-2'-deoxy-β-D-ribofuranosyl)-5,5,7,7-tetraethyl-6-oxyl-3,5,6,7-tetrahydro-imidazo[4,5-*f*]isoindol-2-one (91 mg, 0.14 mmol, 1.0 eq.) was dissolved in dry MeOH (3 ml). NaOMe (39 mg, 0.72 mmol, 5.2 eq.) was added and the mixture stirred for 5 h at room temperature. Additional NaOMe (7.6 mg, 0.14 mmol, 1.0 eq.) was added and the mixture stirred for 0.5 h. Dowex-H^+ (255 mg) was washed with MeOH and MeOH/H_2O (1:1) and added to the reaction mixture. After 1 h the mixture was filtered, the Dowex washed with MeOH and MeOH/H_2O (1:1) and the solvent removed under reduced pressure. The product was obtained as a yellow foam (55 mg, 0.13 mmol, 94 %).

^{1}H-NMR (400 MHz, CD$_3$OD): δ (ppm) = 0.89 (s$_{br}$), 1.28 (s$_{br}$), 2.40 (s$_{br}$), 2.81 (s$_{br}$), 3.81 (s$_{br}$), 3.95 (s$_{br}$), 4.22 (s$_{br}$), 4.57 (s$_{br}$), 6.33 (s$_{br}$), 7.55 (s$_{br}$), 7.88 (s$_{br}$).
^{13}C-NMR (100 MHz, CD$_3$OD): δ (ppm) = 38.22, 63.19, 72.48, 84.18, 88.34, 130.55, 130.93, 153.21, 155.92.

HR-MS (ESI): calc. $C_{22}H_{32}N_3NaO_5$ ([M+Na]$^+$): 441.2234, found: 441.2222.

1-*N*-(5'-*O*-(4,4'-Dimethoxytrityl)-2'-deoxy-β-D-ribofuranosyl)-5,5,7,7-tetraethyl-6-oxyl-3,5,6,7-tetrahydroimidazo[4,5-*f*]isoindol-2-one (36)
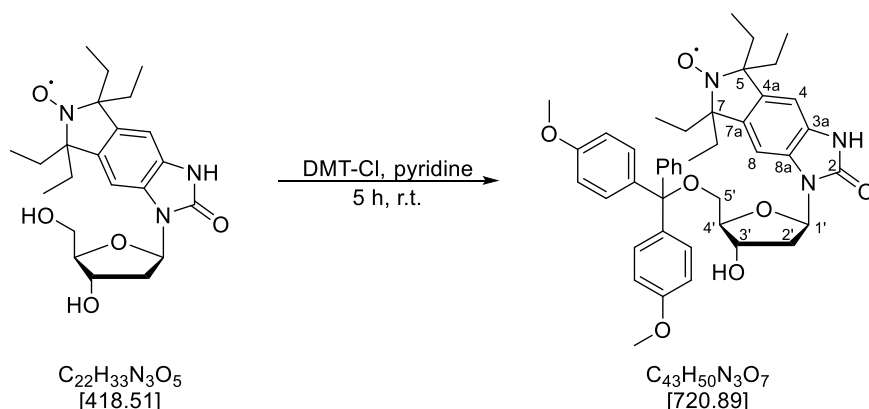
C$_{22}$H$_{33}$N$_3$O$_5$
[418.51]

DMT-Cl, pyridine
5 h, r.t.

C$_{43}$H$_{50}$N$_3$O$_7$
[720.89]

1-*N*-(2'-Deoxy-β-D-ribofuranosyl)-5,5,7,7-tetraethyl-6-oxyl-3,5,6,7-tetrahydroimidazo[4,5-*f*]isoindol-2-one (145 mg, 0.35 mmol, 1.0 eq.) was dissolved in dry pyridine (6.5 ml) under inert atmosphere. DMT-Cl (166 mg, 0.50 mmol, 1.4 eq.) was added portionwise over 1 h and the mixture stirred for 5 h at room temperature, after which the solvent was removed under reduced pressure. The crude product was purified by column chromatography (2 % to 5% to 10% MeOH in DCM). The product was obtained as a yellow foam (145 mg, 0.20 mmol, 58 %).

TLC (DCM/MeOH 95:5): R_f = 0.26.

^{1}H-NMR (400 MHz, CDCl$_3$): δ (ppm) = 1.28 (s$_{br}$), 2.41 (s$_{br}$), 2.98 (s$_{br}$), 3.33 (s$_{br}$), 3.56 (s$_{br}$), 3.79 (s$_{br}$), 4.06 (s$_{br}$), 4.70 (s$_{br}$), 6.36 (s$_{br}$), 6.82 (s$_{br}$), 7.33 (s$_{br}$), 7.45 (s$_{br}$), 7.97 (s$_{br}$).
^{13}C-NMR (100 MHz, CDCl$_3$): δ (ppm) = 36.30, 55.03, 64.05, 72.48, 81.77, 84.00, 86.12, 113.03, 126.74, 127.74, 127.88, 129.80, 135.35, 144.10, 158.24.

HR-MS (ESI): calc. C$_{43}$H$_{50}$N$_3$NaO$_7$ ([M+Na]$^+$): 743.3541, found: 743.3529.

1-*N*-(5'-*O*-(4,4'-Dimethoxytrityl)-3'-*O*-(*O*-β-cyanoethyl-*N,N*-diisopropylphosphoramidite)-2'-deoxy-β-D-ribofuranosyl)-5,5,7,7-tetraethyl-6-oxyl-3,5,6,7-tetrahydroimidazo[4,5-*f*] isoindol-2-one (37)
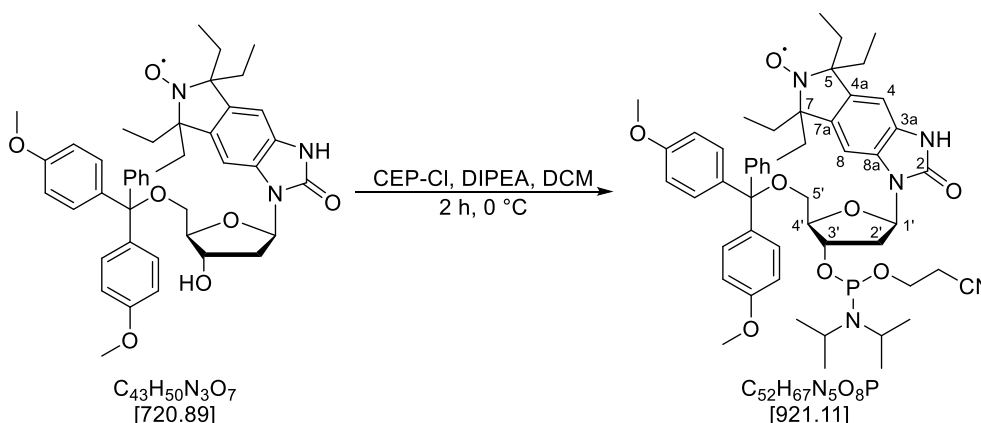
C$_{43}$H$_{50}$N$_3$O$_7$
[720.89]

CEP-Cl, DIPEA, DCM
2 h, 0 °C

C$_{52}$H$_{67}$N$_5$O$_8$P
[921.11]

1-*N*-(5'-*O*-(4,4'-Dimethoxytrityl)-2'-deoxy-β-D-ribofuranosyl)-5,5,7,7-tetraethyl-6-oxyl-3,5,6,7-tetra-hydroimidazo[4,5-*f*]isoindol-2-one (179 mg, 0.25 mmol, 1.0 eq.) was dissolved in dry DCM (8 ml) under inert atmosphere and cooled to 0 °C. DIPEA (141 mg, 1.11 mmol, 4.5 eq.) and CEP-Cl (70 mg, 0.30 mmol, 1.2 eq.) were added and the mixture stirred for 2 h at 0 °C, after which the solvent was removed under reduced pressure. The crude product was purified by column chromatography (0 % to 10 % EtOAc in DCM + 1 % NEt$_3$). The product was obtained as a yellow oil (73 mg, 0.08 mmol, 32 %).

TLC (DCM/EtOAc 9:1 + 1 % NEt$_3$): R_f = 0.22.

^{1}H-NMR (400 MHz, CDCl$_3$): δ (ppm) = 0.88 (s$_{br}$), 1.12 (s$_{br}$), 1.20 (s$_{br}$), 1.46 (s$_{br}$), 1.87 (s$_{br}$), 2.45 (s$_{br}$), 2.62 (s$_{br}$), 3.09 (s$_{br}$), 3.37 (s$_{br}$), 3.66 (s$_{br}$), 3.95 (s$_{br}$), 4.77 (s$_{br}$), 5.61 (s$_{br}$), 6.33 (s$_{br}$), 6.80 (s$_{br}$), 7.21 (s$_{br}$), 7.34 (s$_{br}$), 7.44 (s$_{br}$).
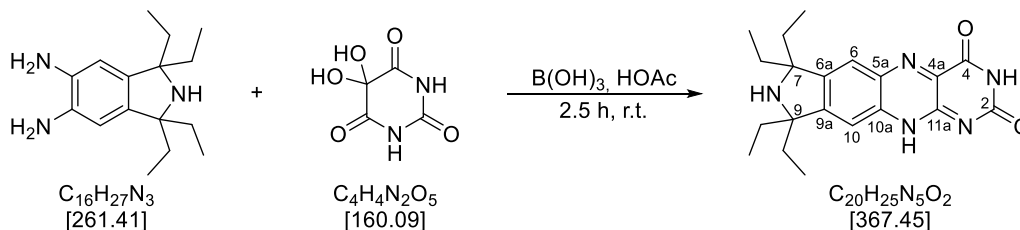**^{31}P-NMR** (162 MHz, CDCl$_3$): δ (ppm) = 148.73, 149.01.

HR-MS (ESI): calc. C$_{52}$H$_{67}$N$_5$NaO$_8$P ([M+Na]$^+$): 943.4619, found: 943.4610.

5.4.2 Synthesis of lumi-spin

(Initial steps see 5.4.1)

7,7,9,9-Tetraethyl-7,8,9,11-tetrahydroisoindolo[5,6-*g*]pteridin-2,4-dione (49)

$C_{16}H_{27}N_3$
[261.41]

$C_4H_4N_2O_5$
[160.09]

B(OH)$_3$, HOAc
2.5 h, r.t.

$C_{20}H_{25}N_5O_2$
[367.45]

5,6-Diamino-1,1,3,3-tetraethylisoindoline (501 mg, 1.92 mmol, 1.0 eq) was dissolved in HOAc (26 ml) under inert atmosphere and boric acid (187 mg, 3.07 mmol, 1.6 eq) and alloxane hydrate (307 mg, 1.92 mmol, 1.0 eq) were added. After the mixture had been stirred for 2.5 h at room temperature the solvent was removed under reduced pressure. The crude product was purified by column chromatography (2% to 10% MeOH in DCM). The product still contained a significant amount of acetic acid but was used in the next step without further purification.

TLC (DCM/MeOH 9:1): R_f = 0.12.

¹H-NMR (400 MHz, CD$_3$OD): δ (ppm) = 0.94-0.99 (m, 12 H, CH$_2$-C*H*$_3$), 1.81-1.95 (m, 8 H, C*H*$_2$-CH$_3$), 7.70, 7.92 (2 x s, 2 H, 6-H, 10-H).
¹³C-NMR (100 MHz, CD$_3$OD): δ (ppm) = 9.09 (CH$_2$-*C*H$_3$), 34.42 (*C*H$_2$-CH$_3$), 69.97, 70.34 (C-7, C-9), 121.65, 124.20 (C-6, C-10), 141.03, 144.94 (C-5a, C-10a), 151.52, 156.81 (C-6a, C-9a), 130.88, 147.64, 151.92, 162.91 (C-2, C-4, C-4a, C-11a).

HR-MS (ESI): calc. C$_{20}$H$_{26}$N$_5$O$_2$ ([M+H]$^+$): 368.2081, found: 368.2071.

1-*N*-(2',3',5'-Tri-*O*-benzoyl-β-D-ribofuranosyl)-7,7,9,9-tetraethyl-7,8,9,11-tetrahydroisoindolo[5,6-*g*]pteridin-2,4-dione (50)

$C_{20}H_{25}N_5O_2$
[367.45]

$C_{28}H_{24}O_9$
[504.49]

1.) **49**, BSA, MeCN
2.) **44**, TMSOTf

1.) 1 h, 50 °C
2.) 5 h, 80 °C

$C_{46}H_{45}N_5O_9$
[811.89]
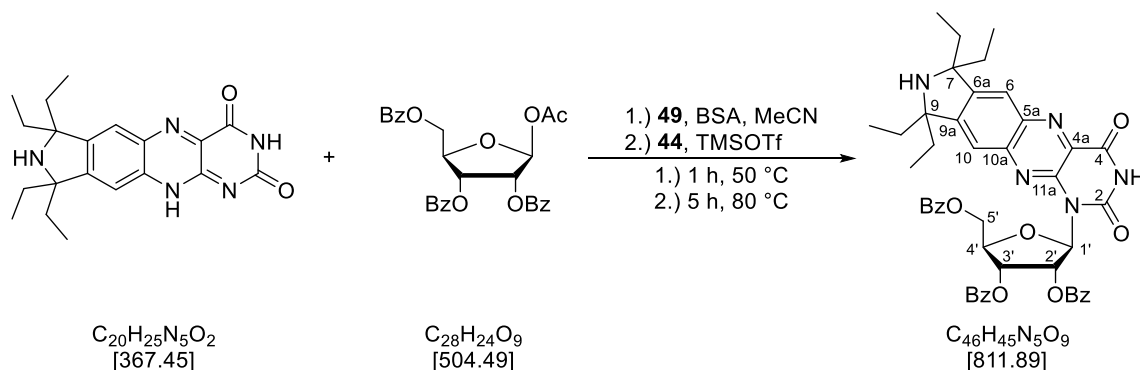
Under inert atmosphere 7,7,9,9-tetraethyl-7,8,9,11-tetrahydroisoindolo[5,6-*g*]pteridin-2,4-dione (506 mg, 1.62 mmol, 1.0 eq) was dissolved in dry MeCN (64 ml). *N,O*-Bis(trimethylsilyl)acetamide (1.7 ml, 6.9 mmol, 4.3 eq) was added and the mixture stirred for 1 h at 50 °C. After cooling to room temperature, 1-*O*-acetyl-2,3,5-tri-*O*-benzoyl-β-D-ribofuranose (973 mg, 1.93 mmol, 1.2 eq) and trimethylsilyl trifluoromethanesulfonate (0.6 ml, 3.7 mmol, 2.3 eq) were added and the mixture stirred for 5 h at 80 °C. After cooling to room temperature, the mixture was poured into sat. aq. NaHCO$_3$, the organic phase washed with brine and the aqueous phases extracted with EtOAc. The combined organic phases were dried over Na$_2$SO$_4$, filtered and the solvent removed under reduced pressure. The crude product was purified by column chromatography (2% to 5% MeOH in DCM). Mixed fractions were purified again (DCM/MeOH 98:2) to obtain the product as a yellow foam (599 mg, 0.74 mmol, 39 % over 2 steps).

TLC (DCM/MeOH 95:5): R_f = 0.36.

¹H-NMR (400 MHz, CDCl$_3$): δ (ppm) = 0.87-0.99 (m, 12 H, CH$_2$-C*H*$_3$), 1.72-1.93 (m, 8 H, C*H*$_2$-CH$_3$), 4.58-4.68 (m, 1 H, 5'-H$_a$), 4.79-4.86 (m, 2 H, 4'-H, 5'-H$_b$), 7.84, 8.09 (2 x s, 2 H, 6-H, 10-H).
¹³C-NMR (100 MHz, CDCl$_3$): δ (ppm) = 9.88 (CH$_2$-*C*H$_3$), 33.77, 34.16 (*C*H$_2$-CH$_3$), 63.70 (C-5'), 128.29, 128.55, 128.61, 129.74, 129.94 (Bz-CH), 133.19, 133.61, 133.74 (*i*-Bz), 140.24, 142.38 (C-6a, C-9a), 158.94 (C-5a, C-10a), 165.43, 165.73, 166.37 (Bz-CO).

HR-MS (ESI): calc. C$_{46}$H$_{45}$N$_5$NaO$_9$ ([M+Na]$^+$): 834.3115, found: 834.3099.

1-*N*-β-D-Ribofuranosyl-7,7,9,9-tetraethyl-7,8,9,11-tetrahydroisoindolo[5,6-*g*]pteridin-2,4-dione (51)
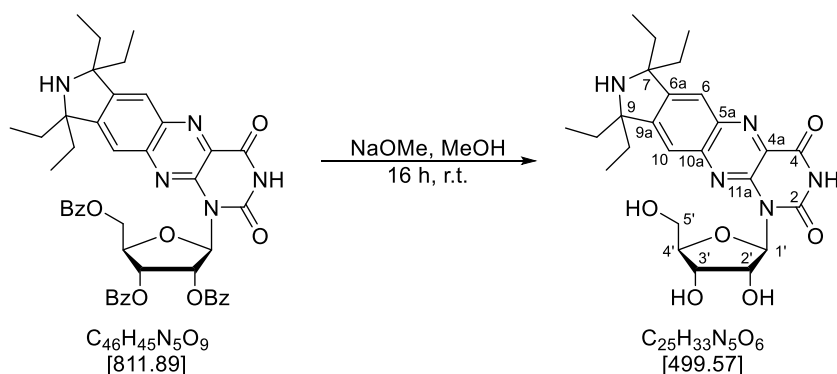
1-*N*-(2',3',5'-Tri-*O*-benzoyl-β-D-ribofuranosyl)-7,7,9,9-tetraethyl-7,8,9,11-tetrahydroisoindolo[5,6-*g*]pteridin-2,4-dione (200 mg, 0.25 mmol, 1.0 eq) and NaOMe (83 mg, 1.53 mmol, 6.2 eq) were dissolved in MeOH (20 ml) and stirred for 16 h at room temperature. Dowex-H$^+$ (508 mg) was washed with MeOH and MeOH/water (1:1) and added to the reaction mixture. After 1 h the Dowex was filtered off, washed with MeOH and MeOH/water (1:1) and the solvent removed under reduced

pressure. The product was obtained as a yellow solid (153 mg, quant.) and used for the next step without further purification.

TLC (DCM/MeOH 9:1): R_f = 0.21.

^{1}H-NMR (400 MHz, CD$_3$OD): δ (ppm) = 1.01 (t, J = 7.4 Hz, 12 H, CH$_2$-CH_3), 1.91-2.04 (m, 8 H, CH_2-CH$_3$), 3.75 (dd, J = 12.0 Hz, J = 5.5 Hz, 1 H, 5'-H$_a$), 3.89 (dd, J = 12 Hz, J = 2.9 Hz, 1 H, 5'-H$_b$), 3.98 (ddd, J = 6.8 Hz, J = 5.5 Hz, J = 2.9 Hz, 1 H, 4'-H), 4.69 (s$_{br}$, 1 H, 3'-H), 4.91-4.93 (m, 1 H, 2'-H), 6.96 (s$_{br}$, 1 H, 1'-H), 7.84 (s, 1 H, 10-H), 8.01 (s, 1 H, 6-H).

^{13}C-NMR (100 MHz, CD$_3$OD): δ (ppm) = 8.99 (CH$_2$-CH$_3$), 33.88 (CH$_2$-CH$_3$), 63.51 (C-5'), 71.13 (C-7), 71.48 (C-9), 71.23 (C-3'), 73.22 (C-2'), 85.60 (C-4'), 90.86 (C-1'), 122.14 (C-10), 124.40 (C-6), 140.15 (C-10a), 143.64 (C-5a), 150.84 (C-9a), 155.60 (C-6a), 131.59, 147.16, 151.15, 161.79 (C-2, C-4, C-4a, C-11a).

HR-MS (ESI): calc. C$_{25}$H$_{34}$N$_5$O$_6$ ([M+H]$^+$): 500.2504, found: 500.2495.

1-N-(2',3',5'-Tri-O-benzoyl-β-D-ribofuranosyl)-7,7,9,9-tetraethyl-8-oxyl-7,8,9,11-tetrahydroisoindolo[5,6-g]pteridin-2,4-dione (54)
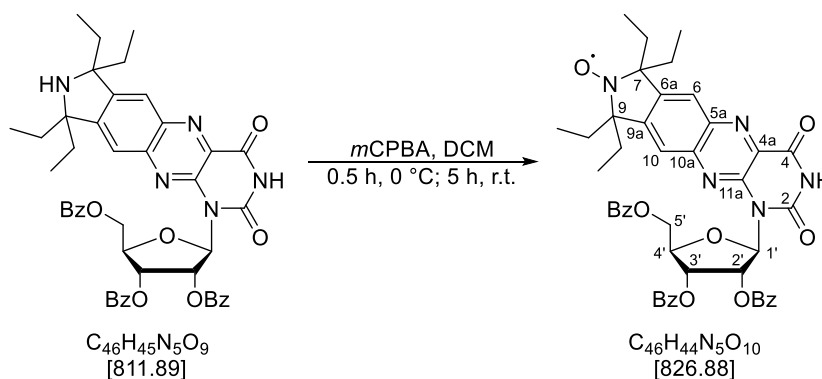
$C_{46}H_{45}N_5O_9$
[811.89]

$C_{46}H_{44}N_5O_{10}$
[826.88]

1-N-(2',3',5'-Tri-O-benzoyl-β-D-ribofuranosyl)-7,7,9,9-tetraethyl-7,8,9,11-tetrahydroisoindolo[5,6-g]pteridin-2,4-dione (399 mg, 0.49 mmol, 1.0 eq) was dissolved in dry DCM (26 ml) under inert atmosphere. mCPBA (169 mg, 0.74 mmol, 1.5 eq.) was added at 0 °C and the mixture stirred for 0.5 h at 0 °C and 5 h at room temperature. The mixture was then washed with sat. aq. NaHCO$_3$ and brine, the combined aqueous phases extracted with DCM and the combined organic phases dried over Na$_2$SO$_4$, filtered and the solvent removed under reduced pressure. The crude product was purified by column chromatography (DCM/MeOH 98:2). The product was obtained as an orange solid (313 mg, 0.38 mmol, 77 %).

TLC (DCM/MeOH 98:2): R_f = 0.18.

^{1}H-NMR (400 MHz, CDCl$_3$): δ (ppm) = 0.84 (s$_{br}$), 4.56-4.75 (m), 6.52 (s$_{br}$), 7.19 (s$_{br}$), 7.39 (s$_{br}$), 7.58 (s$_{br}$), 7.96 (s$_{br}$), 8.01 (s$_{br}$).

^{13}C-NMR (100 MHz, CDCl$_3$): δ (ppm) = 63.34, 121.38, 127.98, 128.25, 128.35, 128.44, 128.60, 128.68, 129.50, 129.60, 129.63, 132.91, 33.37, 133.521 165.16, 165.45, 166.02.

HR-MS (ESI): calc. $C_{46}H_{44}N_5NaO_{10}$ ([M+Na]$^+$): 849.2980, found: 849.2978.

1-*N*-β-D-Ribofuranosyl-7,7,9,9-tetraethyl-8-oxyl-7,8,9,11-tetrahydroisoindolo[5,6-*g*]pteridin-2,4-dione (2)

C$_{46}$H$_{44}$N$_5$O$_{10}$
[826.88]

C$_{25}$H$_{32}$N$_5$O$_7$
[514.56]
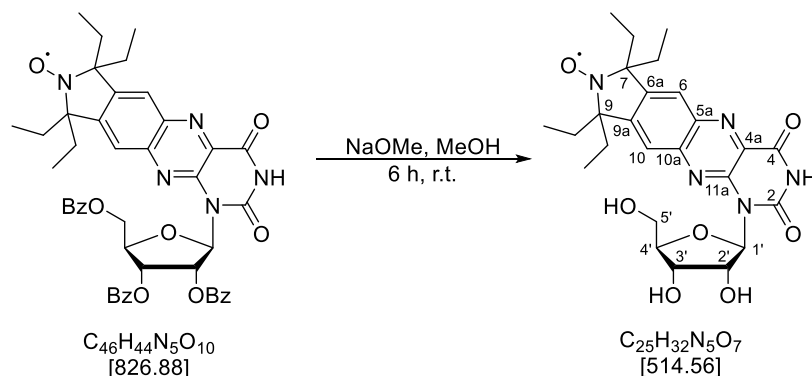
1-*N*-(2',3',5'-Tri-*O*-benzoyl-β-D-ribofuranosyl)-7,7,9,9-tetraethyl-8-oxyl-7,8,9,11-tetrahydro-isoindolo[5,6-*g*]pteridin-2,4-dione (293 mg, 0.36 mmol, 1.0 eq) and NaOMe (200 mg, 3.69 mmol, 10 eq) were dissolved in MeOH (50 ml) and stirred for 6 h at room temperature. Dowex-H$^+$ (761 mg) was washed with MeOH and MeOH/water (1:1) and added to the reaction mixture. After 1 h the Dowex was filtered off, washed with MeOH and MeOH/water (1:1) and the solvent removed under reduced pressure. The product was obtained as an orange-brown solid (277 mg, quant.).

TLC (DCM/MeOH 9:1): R_f = 0.11.

^{1}H-NMR (400 MHz, CD$_3$OD): δ (ppm) = 0.88 (s$_{br}$), 3.76 (s$_{br}$), 3.90 (s$_{br}$), 3.98 (s$_{br}$), 4.72 (s$_{br}$), 6.97 (s$_{br}$).
^{13}C-NMR (100 MHz, CD$_3$OD): δ (ppm) = 63.42, 71.13, 73.24, 85.55.

HR-MS (ESI): calc. $C_{25}H_{32}N_5NaO_7$ ([M+Na]$^+$): 537.2194, found: 537.2181.

5.4.3 Synthesis of EÇr

(Initial steps see 5.4.1)

5-Amino-1,1,3,3-tetraethylisoindoline (60)

C$_{16}$H$_{24}$N$_2$O$_2$
[276.38]

C$_{16}$H$_{26}$N$_2$
[246.40]
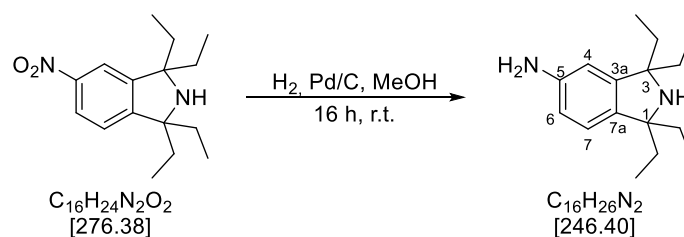
To a solution of 1,1,3,3-tetraethyl-5-nitroisoindoline (3.33 g, 12.0 mmol, 1.0 eq) in MeOH (150 ml) palladium (10 % on charcoal, 1.27 g, 1.20 mmol, 10 mol-%) was added and the mixture stirred for 16 h under hydrogen atmosphere. Then the mixture was filtered over Celite and the solvent removed under reduced pressure. The product was used in the next step without further purification. The product was obtained as a yellow oil (2.43 g, 9.87 mmol, 82 %). The NMR data agree with literature data[168].

TLC (DCM/MeOH 95:5 + 1% NEt₃): R_f = 0.42.

¹H-NMR (400 MHz, CDCl₃): δ (ppm) = 0.85, 0.86 (2 x t, J = 7.4 Hz, 12 H, CH₂-CH_3), 1.57-1.75 (m, 8 H, CH_2-CH₃), 6.39 (dd, J = 2.2 Hz, J = 0.4 Hz, 1 H, 4-H), 6.56 (dd, J = 8.0 Hz, J = 2.3 Hz, 1 H, 6-H), 6.84 (dd, J = 8.0 Hz, J = 0.4 Hz, 1 H, 7-H).
¹³C-NMR (100 MHz, CDCl₃): δ (ppm) = 9.06, 9.09 (CH₂-CH₃), 33.79, 33.92 (CH₂-CH₃), 68.02 (C-1), 68.08 (C-3), 109.33 (C-4), 114.28 (C-6), 123.18 (C-7), 138.11 (C-3a), 145.27 (C-5), 148.92 (C-7a).

HR-MS (ESI): calc. C₁₆H₂₇N₂ ([M+H]⁺): 247.2196, found: 247.2193.

1,1,3,3-Tetraethyl-5-hydroxyisoindoline (61)
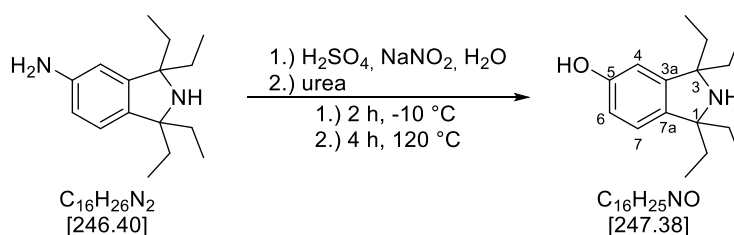
5-Amino-1,1,3,3-tetraethyl-isoindoline (312 mg, 1.27 mmol, 1.0 eq) was dissolved in H₂SO₄ (35 %, 10 ml) and cooled to -10 °C. A solution of NaNO₂ (134 mg, 1.95 mmol, 1.5 eq.) in H₂O (10 ml) was added slowly and the mixture stirred for 2 h at -10 °C. Urea (21.3 mg, 0.35 mmol, 0.3 eq) was added and the mixture stirred for 10 min at -10 °C and 4 h at 120 °C. Then the mixture was cooled to 0 °C and neutralized with aq. NaOH. The mixture was filtered and the filtrate extracted with DCM/MeOH (3:2 and 4:1). The combined organic phases were dried over Na₂SO₄, filtered and the solvent removed under reduced pressure. The crude product was purified by column chromatography (DCM/MeOH 95:5 + 1% NEt₃). The product was obtained as a red solid (317 mg, 1.22 mmol, 96 %).

TLC (DCM/MeOH 95:5 + 1% NEt₃): R_f = 0.43.

¹H-NMR (400 MHz, CDCl₃): δ (ppm) = 0.86, 0.86 (2 x t, J = 7.4 Hz, 12 H, CH₂-CH_3), 1.60-1.77 (m, 8 H, CH_2-CH₃), 6.53 (d, J = 2.3 Hz, 1 H, 4-H), 6.69 (dd, J = 8.2 Hz, J = 2.4 Hz, 1 H, 6-H), 6.90 (dd, J = 8.1 Hz, 1 H, 7-H).
¹³C-NMR (100 MHz, CDCl₃): δ (ppm) = 9.02, 9.06 (CH₂-CH₃), 33.73, 33.84 (CH₂-CH₃), 68.19 (C-1), 68.49 (C-3), 109.53 (C-4), 114.13 (C-6), 123.37 (C-7), 139.60 (C-3a), 149.29 (C-7a), 155.00 (C-5).

HR-MS (ESI): calc. C₁₆H₂₆NO ([M+H]⁺): 248.2009, found: 248.2041.

1,1,3,3-Tetraethyl-5-hydroxy-6-nitroisoindoline (62)
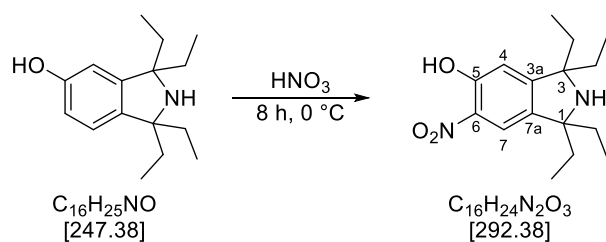
1,1,3,3-Tetraethyl-5-hydroxyisoindoline (2.33 g, 9.43 mmol, 1.0 eq) was cooled to 0 °C when cold aq. HNO_3 (54 ml) was added and the mixture stirred for 8 h at 0 °C. It was neutralized with aq. NaOH and filtered. The filtrate was concentrated under reduced pressure, while the precipitate was filtered multiple times and washed with MeOH. The crude product was purified by column chromatography (DCM). The mixture of isomers was purified again by column chromatography (*n*-hexane/EtOAc 10:1 to 2:1). The product was obtained as a yellow solid (805 mg, 2.75 mmol, 29 %). The NMR data agree with literature data[118].

TLC (DCM): R_f = 0.52.

^{1}H-NMR (400 MHz, CDCl$_3$): δ (ppm) = 0.89 (t, *J* = 7.4 Hz, 12 H, CH$_2$-C*H*$_3$), 1.60-1.79 (m, 8 H, C*H*$_2$-CH$_3$), 6.82 (s, 1 H, 7-H) 7.77 (s, 1 H, 4-H).
^{13}C-NMR (100 MHz, CDCl$_3$): δ (ppm) = 8.88, 8.93 (CH$_2$-*C*H$_3$), 33.64, 33.82 (*C*H$_2$-CH$_3$), 67.84 (C-3), 68.86 (C-1), 113.15 (C-7), 118.62 (C-4), 133.05 (C-6), 140.82 (C-7a), 155.19 (C-5), 159.78 (C-3a).

HR-MS (ESI): calc. C$_{16}$H$_{25}$N$_2$O$_3$ ([M+H]$^+$): 293.1860, found: 293.1853.

6-Amino-1,1,3,3-tetraethyl-5-hydroxyisoindoline (58)
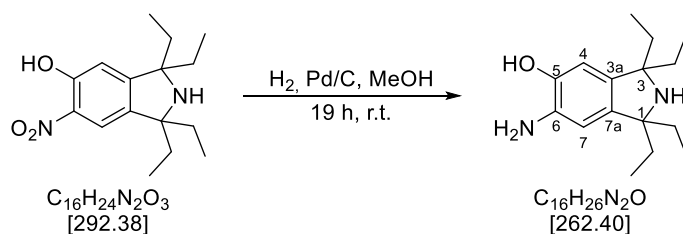
To a solution of 1,1,3,3-tetraethyl-5-hydroxy-6-nitroisoindoline (2.90 g, 9.92 mmol, 1.0 eq) in MeOH (60 ml) palladium (10 % on charcoal, 527 mg, 0.50 mmol, 5 mol-%) was added and the mixture stirred for 19 h under hydrogen atmosphere. Then the mixture was filtered over Celite and the solvent removed under reduced pressure. The product was obtained as a greenish gray solid (2.54 g, 9.68 mmol, 98 %) and used in the next step without further purification.
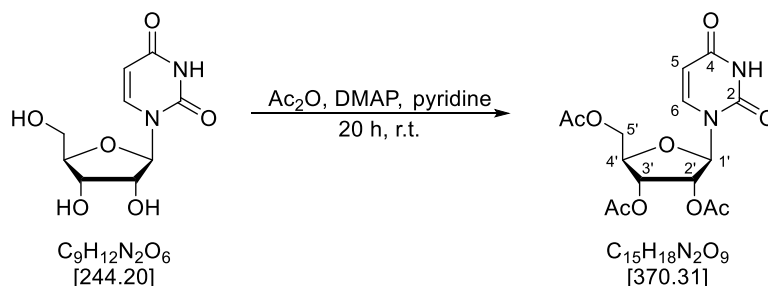
TLC (EtOAc): R_f = 0.20.

¹H-NMR (400 MHz, <u>CD₃OD</u> + CDCl₃): δ (ppm) = 0.99 (t, *J* = 7.3 Hz, 12 H, CH₂-C*H₃*), 1.93-2.13 (m, 8 H, C*H₂*-CH₃), 6.76 (s, 1 H, 7-H) 7.14 (s, 1 H, 4-H).
¹³C-NMR (125 MHz, <u>CD₃OD</u> + CDCl₃): δ (ppm) = 8.20 (CH₂-*C*H₃), 30.47, 30.59 (*C*H₂-CH₃), 75.51 (C-3), 75.69 (C-1), 110.68 (C-7), 117.86 (C-4), 122.16 (C-6), 131.53 (C-7a), 140.44 (C-3a), 151.14 (C-5).

HR-MS (ESI): calc. $C_{16}H_{27}N_2O$ ([M+H]$^+$): 263.2118, found: 263.2123.

2',3',5'-Tri-*O*-acetyluridine (63)

$C_9H_{12}N_2O_6$
[244.20]

$C_{15}H_{18}N_2O_9$
[370.31]

Uridine (1.02 g, 4.18 mmol, 1.0 eq) was dissolved in pyridine (16 ml). DMAP (128 mg, 1.07 mmol, 0.25 eq) and Ac₂O (3.4 ml, 37 mmol, 9.0 eq) were added and the mixture stirred for 20 h at room temperature. Sat. aq. NaHCO₃ was added and the solvent removed under reduced pressure, the residue taken up in DCM and washed with sat. aq. NaHCO₃. The aqueous phase was extracted with DCM and the combined organic phases dried over Na₂SO₄, filtered and the solvent removed under reduced pressure. The crude product was purified by column chromatography (*n*-hexane/EtOAc 8:2) to yield the product (1.20 g, 3.25 mmol, 78 %) as a slightly orange foam. The NMR data agree with literature data[187].

TLC (DCM/MeOH 98:2): *R*f = 0.21.

¹H-NMR (400 MHz, CDCl₃): δ (ppm) = 2.10, 2.13, 2.14 (3 x s, 9 H, Ac), 4.31-4.38 (m, 3 H, 4'-H, 5'-H), 5.32-5.34 (m, 2 H, 2'-H, 3'-H), 5.79 (dd, *J* = 8.2 Hz, *J* = 2.2 Hz, 1 H, 5-H), 6.04 (d, *J* = 5.0 Hz, 1 H, 1'-H), 7.39 (d, *J* = 8.2 Hz, 1 H, 6-H), 9.05 (s, 1 H, NH).
¹³C-NMR (100 MHz, CDCl₃): δ (ppm) = 20.57, 20.66, 20.94 (Ac-CH₃), 63.28 (C-5'), 70.31 (C-3'), 72.84 (C-2'), 80.07 (C-4'), 87.56 (C-1'), 103.57 (C-5), 139.40 (C-6), 150.27 (C-2), 162.76 (C-4), 169.78, 169.80, 170.27 (Ac-CO).

HR-MS (ESI): calc. $C_{15}H_{18}N_2NaO_9$ ([M+Na]$^+$): 393.0905, found: 393.0903.

2',3',5'-Tri-*O*-acetyl-5-bromouridine (64)
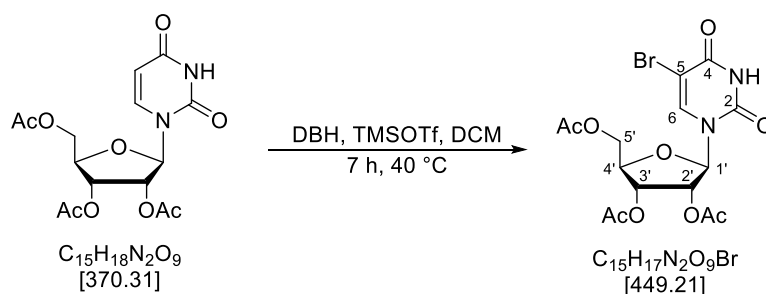
2',3',5'-Tri-*O*-acetyluridine (10.0 g, 27.0 mmol, 1.0 eq) was dissolved in DCM (100 ml) under inert atmosphere. TMSOTf (2.7 ml, 14.9 mmol, 0.55 eq) was added dropwise and 1,3-dibromo-5,5-dimethylhydantoin (4.25 g, 14.9 mmol, 0.55 eq) was added in small portions over 5 min and the mixture stirred for 7 h at 40 °C. After cooling to room temperature, sat. aq. $NaHCO_3$ was added and the mixture stirred overnight. The phases were separated and the organic phase washed with sat. aq. $NaHCO_3$ and H_2O. The combined aqueous phases were extracted with EtOAc and $CHCl_3$. The organic phases were combined and the solvent removed under reduced pressure. The residue was taken up in $CHCl_3$ and washed with H_2O. The combined aqueous phases were extracted with EtOAc, the organic phases combined and the solvent removed under reduced pressure. The product was obtained as an off-white foam (9.93 g, 22.1 mmol, 82 %). The NMR data agree with literature data[188].

TLC (DCM/MeOH 98:2): R_f = 0.49.

1H-NMR (400 MHz, $CDCl_3$): δ (ppm) = 2.11, 2.13, 2.22 (3 x s, 9 H, Ac), 4.32-4.42 (m, 3 H, 4'-H, 5'-H), 5.31-5.34 (m, 2 H, 2'-H, 3'-H), 6.09 (dd, *J* = 3.4 Hz, *J* = 1.5 Hz, 1 H, 1'-H), 7.84 (s, 1 H, 6-H), 9.00 (s, 1 H, NH).
13C-NMR (100 MHz, $CDCl_3$): δ (ppm) = 20.55, 20.66, 21.08 (Ac-CH_3), 63.08 (C-5'), 70.21 (C-3'), 73.24 (C-2'), 80.41 (C-4'), 87.37 (C-1'), 98.07 (C-5), 138.65 (C-6), 149.56 (C-2), 158.53 (C-4), 169.74, 169.80, 170.21 (Ac-CO).

HR-MS (ESI): calc. $C_{15}H_{17}BrN_2NaO_9$ ([M+Na]+): 471.0010, found: 471.0009.

1-*N*-(2',3',5'-Tri-*O*-acetyl-β-D-ribofuranosyl)-5-bromo-4-chloropyrimidin-2-one (57)
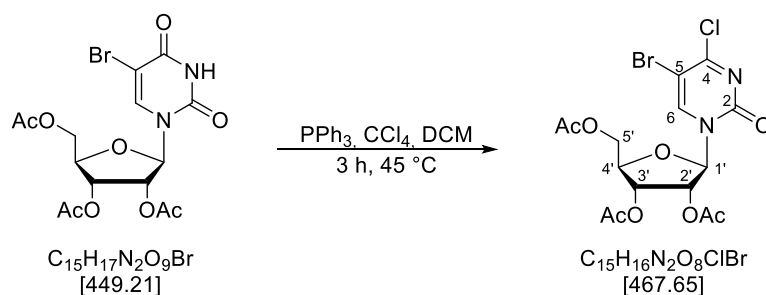
Under inert atmosphere 2',3',5'-tri-O-acetyl-5-bromouridine (2.28 g, 5.07 mmol, 1.0 eq) and triphenylphosphine (3.06 g, 11.7 mmol, 2.3 eq) were dissolved in DCM (30 ml) and CCl$_4$ (26 ml) and the mixture stirred for 3 h at 45 °C. After cooling to room temperature, the solvent was removed under reduced pressure. The crude product was purified by column chromatography (5 % to 15 % EtOAc in DCM). The product was obtained as a white foam (1.58 g, 3.39 mmol, 67 %).

TLC (DCM/EtOAc 9:1): R_f = 0.14.

^{1}H-NMR (400 MHz, CD$_3$OD): δ (ppm) = 2.08, 2.10, 2.15 (3 x s, 9 H, Ac), 4.34-4.40 (m, 3 H, 4'-H, 5'-H), 5.38-5.43 (m, 1 H, 3'-H), 5.49 (dd, *J* = 5.9 Hz, *J* = 4.8 Hz, 1 H, 2'-H), 5.94 (d, *J* = 4.8 Hz, 1 H, 1'-H), 8.05 (s, 1 H, 6-H).
^{13}C-NMR (100 MHz, CD$_3$OD): δ (ppm) = 20.34, 20.43, 20.90 (Ac-CH$_3$), 64.01 (C-5'), 71.37 (C-3'), 74.43 (C-2'), 81.43 (C-4'), 90.13 (C-1'), 97.92 (C-5), 141.62 (C-6), 151.32 (C-2), 161.19 (C-4), 171.28, 171.29, 171.97 (Ac-CO).

HR-MS (ESI): calc. C$_{15}$H$_{16}$BrClN$_2$NaO$_8$ ([M+Na]$^+$): 488.9671, found: 488.6940.

1-*N*-(2',3',5'-Tri-*O*-acetyl-β-ᴅ-ribofuranosyl)-5-bromo-4-((1,1,3,3-tetraethyl-6-hydroxyisoindolin-5-yl)amino)pyrimidin-2-one (56)
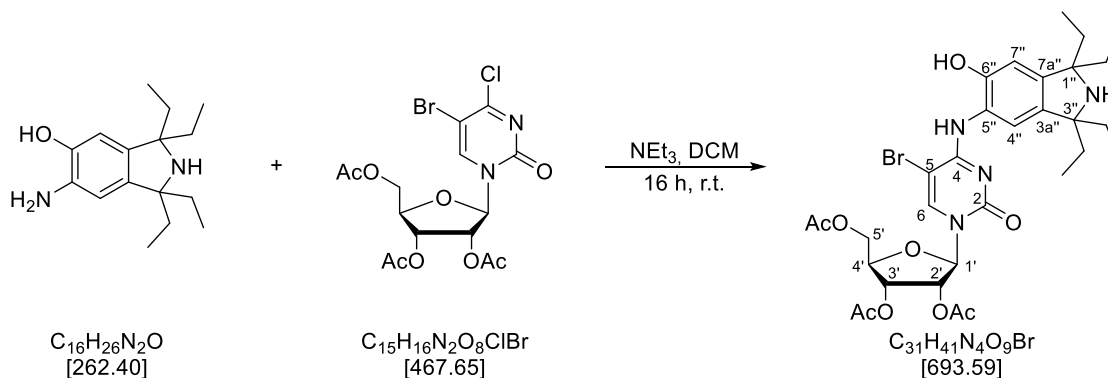
A solution of 6-amino-1,1,3,3-tetraethyl-5-hydroxyisoindoline (862 mg, 3.28 mmol, 1.0 eq), 2',3',5'-tri-*O*-acetyl-5-bromo-4-chloropyrimidin-2-one (1.92 g, 4.10 mmol, 1.3 eq) and triethylamine (432 mg, 4.26 mmol, 1.3 eq) in DCM (40 ml) under inert atmosphere was stirred for 16 h at room temperature. After cooling to room temperature, the solvent was removed under reduced pressure. The crude product was purified by column chromatography (0 % to 5 % MeOH in DCM). The product was obtained as a yellow foam (1.11 g, 1.60 mmol, 49 %).

TLC (DCM/MeOH 10:1): R_f = 0.45.

^{1}H-NMR (400 MHz, CD$_3$OD): δ (ppm) = 0.87-0.94 (m, 12 H, CH$_2$-C*H*$_3$), 1.71-1.89 (m, 8 H, C*H*$_2$-CH$_3$), 2.08, 2.10, 2.15 (3 x s, 9 H, Ac), 4.37-4.42 (m, 3 H, 4'-H, 5'-H), 5.38-5.43 (m, 1 H, 3'-H), 5.52 (dd, *J* = 5.8 Hz, *J* = 4.0 Hz, 1 H, 2'-H), 5.97 (d, *J* = 4.0 Hz, 1 H, 1'-H), 6.62 (s, 1 H, 7''-H), 8.11 (s, 1 H, 4''-H), 8.27 (s, 1 H, 6-H).

13C-NMR (100 MHz, CD3OD): δ (ppm) = 8.64, 8.76, 9.22 (CH2-*C*H3), 21.11 (Ac-CH3), 31.55, 31.73 (*C*H2-CH3), 63.83 (C-5'), 70.26 (C-3'), 76.02 (C-2'), 76.41, 77.01 (C-1'', C-3''), 82.63 (C-4'), 90.49 (C-1'), 93.39 (C-5), 109.79 (C-7''), 117.00 (C-4''), 128.61 (C-6''), 137.08 (C-7a''), 137.11, 142.66 (C-6, C-3a''), 149.79 (C-5''), 156.84, 159.01 (C-2, C-4), 172.21 (Ac-CO).

HR-MS (ESI): calc. $C_{31}H_{42}BrN_4O_9$ ([M+H]$^+$): 693.2130, found: 693.2108.

3-*N*-(β-D-Ribofuranosyl)-7,7,9,9-tetraethyl-7,8,9,11-tetrahydropyrimido[4',5':5,6][1,4]oxazino[2,3-*f*]isoindol-2-one (53)

C31H41N4O9Br
[693.59]

C25H34N4O6
[486.57]
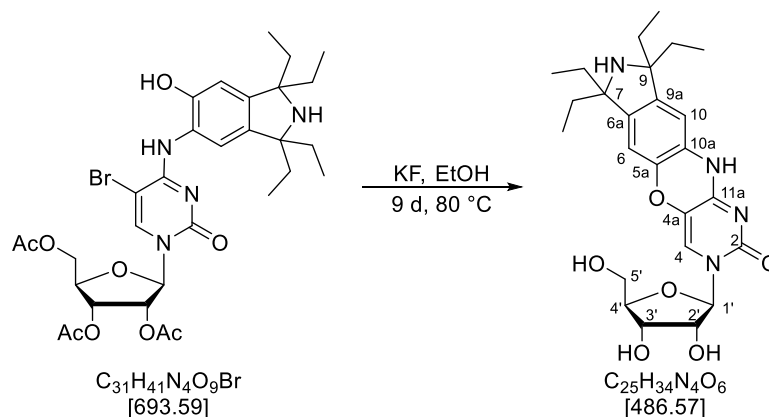
To a solution of 1-*N*-(2',3',5'-tri-*O*-acetyl-β-D-ribofuranosyl)-5-bromo-4-((1,1,3,3-tetraethyl-6-hydroxyisoindolin-5-yl)amino)pyrimidin-2-one (2.07 g, 2.99 mmol, 1.0 eq) in EtOH (200 ml), KF (1.74 g, 29.4 mmol, 9.8 eq) was added and the mixture stirred for 9 d at 80 °C. After cooling to room temperature, the mixture was filtered and the solvent removed under reduced pressure. The crude product was purified by column chromatography (0 % to 100 % MeOH in DCM). A mixture of the product and an unidentified side-product was obtained (941 mg).

TLC (DCM/MeOH 9:1): R_f = 0.06.

1H-NMR (500 MHz, CD3OD): δ (ppm) = 0.85-0.91 (m, 12 H, CH2-C*H3*), 1.60-1.79 (m, 8 H, C*H2*-CH3), 3.76 (dd, *J* = 9.9 Hz, *J* = 2.4 Hz, 1 H, 5'-Ha), 3.89 (dd, *J* = 9.8 Hz, *J* = 2.0 Hz, 1 H, 5'-Hb), 4.00-4.03 (m, 1 H, 4'-H), 4.12-4.19 (m, 2 H, 2'-H, 3'-H), 5.86 (d, *J* = 3.0 Hz, 1 H, 1'-H), 6.52, 6.54 (2 x s, 2 H, 6-H, 10-H), 7.77 (s, 1 H, 4-H).

13C-NMR (125 MHz, CD3OD): δ (ppm) = 9.16, 9.18, 9.25 (CH2-*C*H3), 34.40, 34.41, 34.43, 34.46 (*C*H2-CH3), 61.84 (C-5'), 70.81 (C-3'), 76.22 (C-2'), 69.59, 69.66 (C-7, C-9), 85.96 (C-4'), 91.69 (C-1'), 110.74, 111.46 (C-6, C-10), 123.46 (C-4), 126.83 (C-5a, C-10a), 129.91 (C-4a), 143.66, 144.70 (C-6a, C-9a), 155.77, 156.85 (C-2, C-11a).

HR-MS (ESI): calc. $C_{25}H_{35}N_4O_6$ ([M+H]$^+$): 487.2551, found: 487.2553.

3-*N*-(2',3',5'-Tri-*O*-acetyl-β-D-ribofuranosyl)-7,7,9,9-tetraethyl-7,8,9,11-tetrahydropyrimido[4',5':5,6][1,4]oxazino[2,3-*f*]isoindol-2-one (65)

C$_{25}$H$_{34}$N$_4$O$_6$
[486.57]

Ac$_2$O, DMAP, pyridine, MeCN
3 h, r.t.

C$_{31}$H$_{40}$N$_4$O$_9$
[612.68]
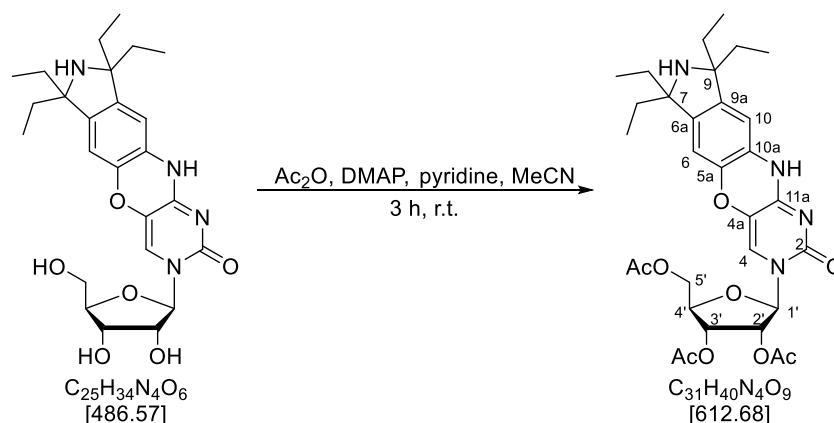
A solution of Ac$_2$O (34.3 mg, 0.34 mmol, 3.4 eq), DMAP (1.4 mg, 0.01 mmol, 0.1 eq), NEt$_3$ (38.4 mg, 0.38 mmol, 3.8 eq) and the product mixture from the previous step containing 3-*N*-(β-D-Ribofuranosyl)-7,7,9,9-tetraethyl-7,8,9,11-tetrahydropyrimido[4',5':5,6][1,4]oxazino[2,3-*f*]isoindol-2(3*H*)-one (50 mg) in MeCN (10 ml) under inert atmosphere was stirred for 3 h at room temperature. The solvent was removed under reduced pressure and the crude product purified by column chromatography (DCM/MeOH 92.5:7.5). The product was obtained as a brown solid (23.3 mg, 0.04 mmol).

**TLC** (DCM/MeOH 92.5:7.5): *R*$_f$ = 0.33.

^{1}H-NMR (600 MHz, CDCl$_3$): δ (ppm) = 0.89-0.94 (m, 12 H, CH$_2$-C*H*$_3$), 1.75-1.86 (m, 8 H, C*H*$_2$-CH$_3$), 2.09, 2.09, 2.21 (3 x s, 9 H, Ac), 4.33-4.49 (m, 3 H, 4'-H, 5'-H), 5.29 (dd, *J* = 3.6 Hz, *J* = 3.6 Hz, 1 H, 3'-H), 5.36 (dd, *J* = 3.5 Hz, *J* = 3.1 Hz, 1 H, 2'-H), 6.01 (d, *J* = 3.0 Hz, 1 H, 1$_Z$-H), 6.41, 7.14 (2 x s, 2 H, 6-H, 10-H), 7.08 (s, 1 H, 4-H).
^{13}C-NMR (125 MHz, CDCl$_3$): δ (ppm) = 8.91, 8.94, 8.95 (CH$_2$-*C*H$_3$), 20.64, 20.69, 21.06 (Ac-CH$_3$), 32.79 (*C*H$_2$-CH$_3$), 63.08 (C-5'), 69.97 (C-3'), 73.27 (C-2'), 70.63 (C-7, C-9), 79.51 (C-4'), 88.22 (C-1'), 109.48, 112.93 (C-6, C-10), 119.63 (C-4), 125.95 (C-5a, C-10a), 128.55 (C-4a), 141.17, 142.22 (C-6a, C-9a), 152.80, 154.10 (C-2, C-11a), 169.39, 169.57, 170.18 (Ac-CO).

HR-MS (ESI): calc. C$_{31}$H$_{41}$N$_4$O$_9$ ([M+H]$^+$): 613.2868, found: 613.2870.

3-*N*-(2',3',5'-Tri-*O*-acetyl-β-D-ribofuranosyl)-7,7,9,9-tetraethyl-8-oxyl-7,8,9,11-tetrahydropyrimido[4',5':5,6][1,4]oxazino[2,3-*f*]isoindol-2-one (66)
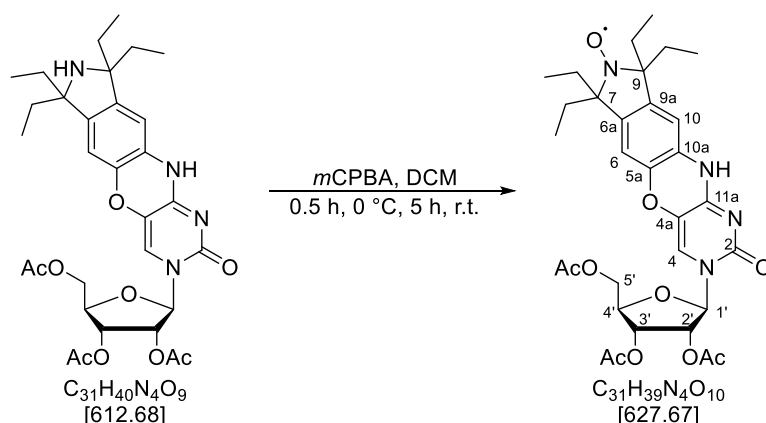
$C_{31}H_{40}N_4O_9$
[612.68]

$C_{31}H_{39}N_4O_{10}$
[627.67]

3-*N*-(2',3',5'-Tri-O-acetyl-β-D-ribofuranosyl)-7,7,9,9-tetraethyl-7,8,9,11-tetrahydropyrimido[4',5':5,6][1,4]oxazino[2,3-*f*]isoindol-2(3*H*)-one (186 mg, 0.30 mmol, 1.0 eq) was dissolved in dry DCM (16 ml) under inert atmosphere. *m*CPBA (104 mg, 0.46 mmol, 1.5 eq.) was added at 0 °C and the mixture stirred for 0.5 h at 0 °C and 5 h at room temperature. The mixture was then washed with sat. aq. $NaHCO_3$ and brine, the combined aqueous phases extracted with DCM and the combined organic phases dried over Na_2SO_4, filtered and the solvent removed under reduced pressure. The crude product was purified by column chromatography (DCM/MeOH 92.5:7.5). The product was obtained as a yellow solid (141 mg, 0.22 mmol, 74 %).

TLC (DCM/MeOH 92.5:7.5): R_f = 0.46.

^{1}H-NMR (300 MHz, $CDCl_3$): δ (ppm) = 0.85-0.95 (m), 1.92 (s_{br}), 2.15, (s_{br}), 2.27 (s_{br}), 4.40 (s_{br}), 5.35 (s_{br}), 6.10 (s_{br}), 7.02 (s_{br}), 7.38 (s_{br}), 7.57 (s_{br}), 7.91 (s_{br}).

^{13}C-NMR (125 MHz, $CDCl_3$): δ (ppm) = 20.12, 20.39, 20.69, 29.13, 62.42, 63.10, 69.11, 69.88, 72.87, 78.61, 87.80, 119.57, 126.93, 127.58, 129.06, 129.31, 129.56, 133.34, 134.01, 151.92, 152.79, 168.61, 168.80, 168.95, 169.43.

MS (ESI): calc. $C_{31}H_{40}N_4O_{10}$ ([M+H]$^+$): 628.2744, found: 628.3.

3-*N*-(β-D-ribofuranosyl)-7,7,9,9-tetraethyl-8-oxyl-7,8,9,11-tetrahydropyrimido [4',5':5,6][1,4]oxazino[2,3-*f*]isoindol-2-one (3)
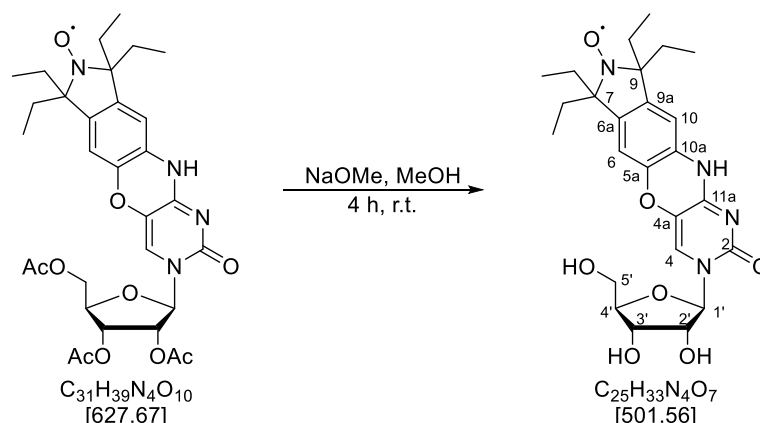
3-*N*-(2',3',5'-Tri-O-acetyl-β-D-ribofuranosyl)-7,7,9,9-8-oxyl-tetraethyl-7,8,9,11-tetrahydropyrimido [4',5':5,6][1,4]oxazino[2,3-*f*]isoindol-2(3*H*)-one (76 mg, 0.12 mmol, 1.0 eq) and NaOMe (33 mg, 0.62 mmol, 5.1 eq) were dissolved in MeOH (7 ml) and stirred for 4 h at room temperature. Dowex-H$^+$ (215 mg) was washed with MeOH and MeOH/water (1:1) and added to the reaction mixture. After 1 h the Dowex was filtered off, washed with MeOH and MeOH/water (1:1) and the solvent removed under reduced pressure. The product was obtained as a yellow solid (56 mg, 0.11 mmol, 94 %).

TLC (DCM/MeOH 9:1): R_f = 0.23.

^{1}H-NMR (300 MHz, CD$_3$OD): δ (ppm) = 0.90 (s$_{br}$), 3.79 (s$_{br}$), 3.89 (s$_{br}$), 4.02 (s$_{br}$), 4.15 (s$_{br}$), 5.91 (s$_{br}$), 7.69 (s$_{br}$).

HR-MS (ESI): calc. C$_{25}$H$_{33}$N$_4$NaO$_7$ ([M+Na]$^+$): 524.2241, found: 524.2247.

Bis(tetrabutylammonium) pyrophosphate
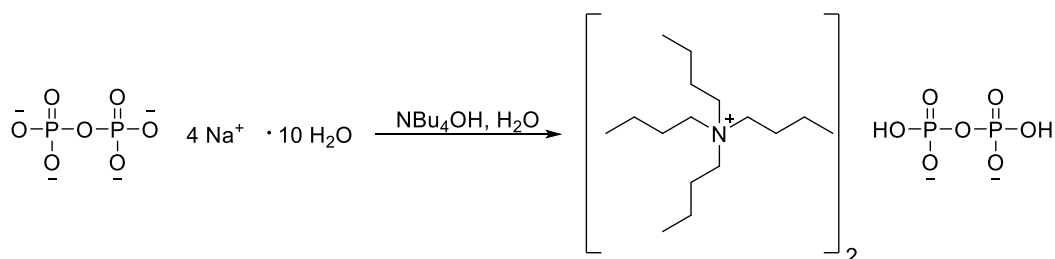
Dowex-H$^+$ (15 g) was filled into a column and washed with MeOH, until the eluate was colorless, then with water. Tetrasodium pyrophosphate decahydrate (1.02 g, 2.28 mmol, 1.0 eq) was dissolved in water, added to the column and eluted with water until the eluate was neutral. The resulting

solution was titrated with 40 % aq. NBu$_4$OH until a pH of 3.5 was reached. The solvent was removed under reduced pressure, the crude product (2.36 g) dried under high vacuum and used for the next step.

3-*N*-(5'-*O*-triphosphate-β-D-ribofuranosyl)-7,7,9,9-tetraethyl-8-oxyl-7,8,9,11-tetra-hydropyrimido[4',5':5,6][1,4]oxazino[2,3-*f*]isoindol-2-one (55)

3-*N*-(β-D-Ribofuranosyl)-7,7,9,9-tetraethyl-8-oxyl-7,8,9,11-tetrahydropyrimido[4',5':5,6][1,4]oxazino [2,3-*f*]isoindol-2-(3*H*)-one (25 mg, 0.05 mmol, 1.0 eq) and proton-sponge (15 mg, 0.07 mmol, 1.5 eq) were dried together under high vacuum, dissolved in PO$_4$Me$_3$ (0.9 ml) under inert atmosphere and cooled to -20 °C. POCl$_3$ (8 µl, 0.09 mmol, 1.8 eq) was added and the mixture stirred for 3 h at -20 °C. NBu$_3$ (83 µl, 0.35 mmol, 7.0 eq) and a solution of (NBu$_4$)$_2$PP$_i$ (223 mg, 0.34 mmol, 6.8 eq) in DMF (0.33 ml) were added and the mixture stirred for 1.5 h at 0 °C. TEAB buffer (1 M, pH 7.5, 6.6 ml) was added, the mixture allowed to warm to room temperature, washed with EtOAc and the aqueous phase concentrated under reduced pressure. The crude product was purified by ion exchange HPLC (0.1 M to 1 M TEAB buffer pH 7.5) to yield the product (5.6 µmol, 11 %) as a solution in TEAB buffer.

^{1}H-NMR (400 MHz, D$_2$O): δ (ppm) = 4.25 (s$_{br}$), 4.32 (s$_{br}$), 4.39 (s$_{br}$), 5.98 (s$_{br}$).

HR-MS (ESI): calc. C$_{25}$H$_{35}$N$_4$O$_{16}$P$_3$ ([M-H]$^-$): 740.1266, found: 740.1271.

5.4.4 Synthesis of benzimidazole nucleoside phosphoramidite 81

1-*N*-(2',3',5'-tri-*O*-benzoyl-β-D-ribofuranosyl)benzimidazole (77)

C₇H₆N₂ [118.14] + C₂₈H₂₄O₉ [504.49] → C₃₃H₂₆N₂O₇ [562.58]
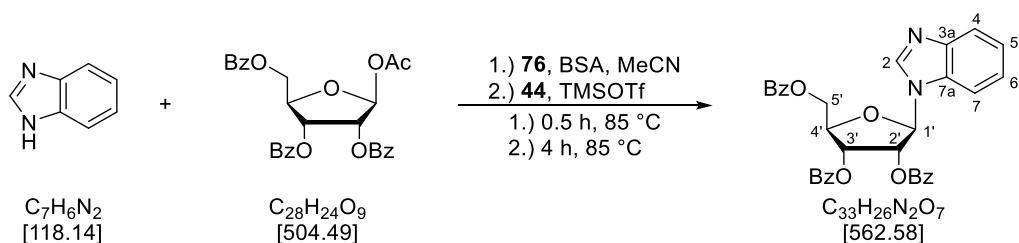
To a solution of benzimidazole (236 mg, 2.00 mmol, 2.0 eq.) in dry acetonitrile (7 ml) under inert atmosphere was added *N,O*-bis(trimethylsilyl)acetamide (0.5 ml, 1.98 mmol, 2.0 eq.) and the mixture stirred at 85 °C for 0.5 h. After cooling to room temperature, 1-*O*-acetyl-2,3,5-tri-*O*-benzoyl-β-D-ribofuranose (507 mg, 1.00 mmol, 1,0 eq.) and trimethylsilyl trifluoromethanesulfonate (0.22 ml, 1.24 mmol, 1.2 eq.) were added and the reaction mixture stirred at 85 °C for 4 h. After cooling to room temperature, sat. NaHCO₃ solution was added, extracted with DCM, the combined organic phases dried over Na₂SO₄, filtered and the solvent removed under reduced pressure. The residue was dissolved in DMF (25 ml) and stirred at 100 °C for 4 h to convert a side product and the solvent removed under reduced pressure. The crude product was purified by column chromatography (*n*-hexane/EtOAc 3:2). The product was obtained as a white solid (354 mg, 0.63 mmol, 63 %).
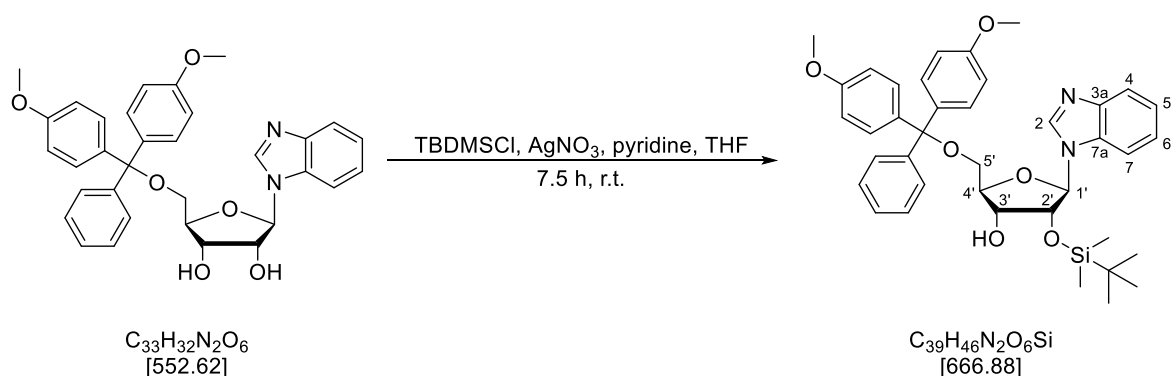
TLC (*n*-hexane/EtOAc 2:3): R_f = 0.45.

¹H-NMR (600 MHz, CDCl₃): δ (ppm) = 4.77 (dd, *J* = 12.3 Hz, *J* = 3.41 Hz, 1 H, 5'-H$_a$), 4.83 (dt, *J* = 4.4 Hz, *J* = 3.1 Hz, 1 H, 4'-H), 4.91 (dd, *J* = 12.3 Hz, *J* = 2.7 Hz, 1 H, 5'-H$_b$), 5.99 (dd, *J* = 5.8 Hz, *J* = 4.3 Hz, 1 H, 3'-H), 6.06 (t, *J* = 5.9 Hz, 1 H, 2'-H), 6.39 (d, *J* = 6.0 Hz, 1 H, 1'-H), 7.10-7.14 (m, 1 H, 6-H), 7.25-7.29 (m, 1 H, 5-H), 7.37-7.42 (m, 4 H, Bz-CH), 7.50 (t, *J* = 7.8 Hz, 2 H, Bz-CH), 7.55-7.59 (m, 2 H, Bz-CH), 7.60-7.65 (m, 2 H, Bz-CH, 4-H), 7.79-7.81 (m, 1 H, 7-H), 7.93-7.99 (m, 4 H, Bz-CH), 8.12-8.15 (m, 2 H, Bz-CH), 8.16 (s, 1 H, 2-H).
¹³C-NMR (125 MHz, CDCl₃): δ (ppm) = 63.78 (C-5'), 71.23 (C-3'), 73.72 (C-2'), 80.73 (C-4'), 87.67 (C-1'), 110.85 (C-4), 120.89 (C-7), 123.14 (C-5), 123.74 (C-6), 128.43 (*i*-Bz), 128.63 (Bz-CH), 128.64 (Bz-CH), 128.73 (*i*-Bz), 128.83 (Bz-CH), 129.32 (*i*-Bz), 129.81 (Bz-CH), 129.85 (Bz-CH), 129.87 (Bz-CH), 132.53 (C-7a), 133.65 (Bz-CH), 133.91 (Bz-CH), 140.84 (C-2), 144.47 (C-3a), 164.98 (Bz-CO), 165.30 (Bz-CO), 166.18 (Bz-CO).

HR-MS (ESI): calc. C₃₃H₂₇N₂O₇ ([M+H]⁺): 563.1813, found: 563.1813.

1-*N*-β-D-ribofuranosylbenzimidazole (78)

$$C_{33}H_{26}N_2O_7 \quad [562.58] \xrightarrow[\text{5 h, r.t.}]{\text{NaOMe, MeOH}} C_{12}H_{14}N_2O_4 \quad [250.25]$$
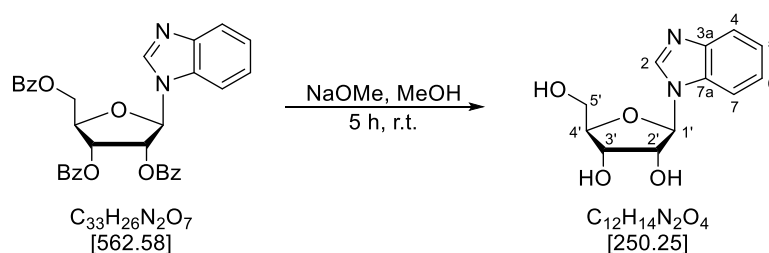
To a solution of 1-*N*-(2',3',5'-Tri-*O*-benzoyl-β-D-ribofuranosyl)benzimidazole (791 mg, 1.41 mmol, 1.0 eq.) in methanol (75 ml) was added sodium methanolate (381 mg, 7.05 mmol, 5.0 eq.) and the mixture stirred at room temperature for 4 h. Dowex-H⁺ (2.386 g) was washed with methanol and Methanol/water (1:1) and added to the reaction mixture. After stirring for 1 h, the Dowex was filtered off and the solvent removed under reduced pressure. The product was obtained as a white solid (333 mg, 1.33 mmol, 95 %) and used in the next step without further purification.

TLC (EtOAc/MeOH 2:3 + 1 % NEt₃): R_f = 0.44.

¹H-NMR (300 MHz, CD₃OD): δ (ppm) = 3.74-3.92 (m, 2 H, 5'-H), 4.13 (t, *J* = 3.4 Hz, 1 H, 4'-H), 4.28 (dd, *J* = 5.3 Hz, *J* = 3.5 Hz, 1 H, 3'-H), 4.44-4.49 (m, 1 H, 2'-H), 5.99 (dd, *J* = 5.8 Hz, *J* = 2.9 Hz, 1 H, 1'-H), 7.26-7.41 (m, 2 H, 5-H, 6-H), 7.66-7.70 (m, 1 H, 4-H), 7.72-7.77 (m, 1 H, 7-H), 8.50 (s, 1 H, 2-H).
¹³C-NMR (125 MHz, CD₃OD): δ (ppm) = 62.66 (C-5'), 71.68 (C-3'), 75.84 (C-2'), 86.84 (C-4'), 90.82 (C-1'), 112.35 (C-4), 120.06 (C-7), 123.89 (C-6), 124.44 (C-5), 134.10 (C-7a), 142.67 (C-2), 144.15 (C-3a).

HR-MS (ESI): calc. C₁₂H₁₅N₂O₄ ([M+H]⁺): 251.1026, found: 251.1027.

1-*N*-(5'-*O*-(4,4'-dimethoxytrityl)-β-D-ribofuranosyl)benzimidazole (79)

$$C_{12}H_{14}N_2O_4 \quad [250.25] \xrightarrow[\text{4 h, r.t.}]{\text{DMT-Cl, pyridine}} C_{33}H_{32}N_2O_6 \quad [552.62]$$
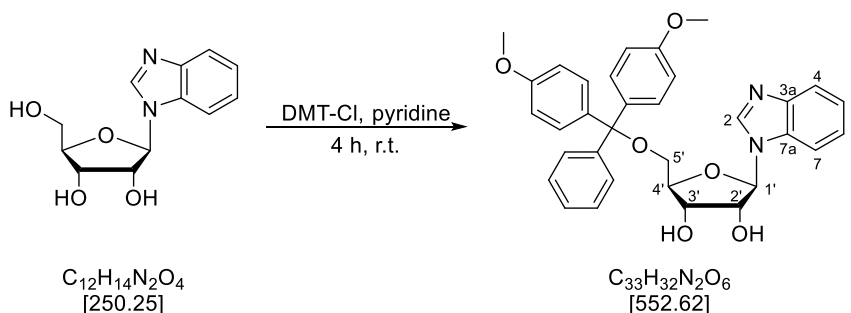
1-*N*-β-D-ribofuranosylbenzimidazole (103 mg, 0.41 mmol, 1.0 eq.) was coevaporated multiple times with dry pyridine and dissolved in dry pyridine (5.6 ml) under inert atmosphere. 4,4'-dimethoxytrityl chloride (177 mg, 0.52 mmol, 1.3 eq.) was added portionwise over 30 min and the mixture stirred at room temperature for 3 h. MeOH was added and the mixture stirred for 5 min, after which it was diluted with DCM and washed with cold water and sat. NaHCO₃ solution. The organic phase was

dried over Na₂SO₄, filtered and the solvent removed under reduced pressure. The crude product was purified by column chromatography (DCM/MeOH 95:5 + 1 % NEt₃). The product was obtained as a white solid (146 mg, 0.26 mmol, 64 %).

TLC (DCM/MeOH 95:5 + 1 % NEt₃): R_f = 0.39.

¹H-NMR (300 MHz, CDCl₃): δ (ppm) = 3.45 (qd, J = 10.5 Hz, J = 3.4 Hz, 2 H, 5'-H), 3.74, 3.75 (2 x s, 6 H, DMT-OMe), 4.26 (q, J = 3.4 Hz, 1 H, 4'-H), 4.43 (dd, J = 5.9 Hz, J = 3.5 Hz, 1 H, 3'-H), 4.63 (t, J = 6.0 Hz, 1 H, 2'-H), 5.84 (d, J = 6.1 Hz, 1 H, 1'-H), 6.74-6.79 (m, 4 H, DMT), 6.98 (ddd, J = 8.3 Hz, J = 7.2 Hz, J = 1.1 Hz, 1 H, 5-H), 7.14 (ddd, J = 8.2 Hz, J = 7.2 Hz, J = 1.1 Hz, 1 H, 6-H), 7.18-7.25 (m, 3 H, DMT), 7.29-7.33 (m, 4 H, DMT), 7.41-7.44 (m, 2 H, DMT), 7.59 (dd, J = 8.1 Hz, J = 0.9 Hz, 1 H, 7-H), 7.66 (dd, J = 8.2 Hz, J = 0.9 Hz, 1 H, 4-H), 7.87 (s, 1 H, 2-H).

¹³C-NMR (75 MHz, CDCl₃): δ (ppm) = 55.33 (DMT-OMe), 63.64 (C-5'), 70.86 (C-3'), 73.42 (C-2'), 84.34 (C-4'), 86.75 (DMT$_{quart}$), 90.43 (C-1'), 112.07 (C-7), 113.28 (DMT), 119.80 (C-4), 122.92 (C-6), 123.40 (C-5), 127.02, 128.00, 128.32, 130.26, 130.28 (DMT), 132.54 (C-7a), 135.60, 135.72 (DMT), 141.63 (C-2), 143.64 (C-3a), 144.62, 158.63 (DMT).

HR-MS (ESI): calc. für C₃₃H₃₃N₂O₆ ([M+H]⁺): 553.2333, found: 553.2329.

1-*N*-(2'-*O*-(*tert*-butyldimethylsilyl)-5'-*O*-(4,4'-dimethoxytrityl)-β-ᴅ-ribofuranosyl)benz-imidazole (80)

C₃₃H₃₂N₂O₆
[552.62]

TBDMSCl, AgNO₃, pyridine, THF
7.5 h, r.t.

C₃₉H₄₆N₂O₆Si
[666.88]

1-*N*-(5'-*O*-(4,4'-dimethoxytrityl)-β-ᴅ-ribofuranosyl)benzimidazole (115 mg, 0.21 mmol, 1.0 eq.) was dissolved in dry THF (2 ml) under inert atmosphere. Dry pyridine (37 mg, 0.47 mmol, 2.2 eq.), AgNO₃ (55 mg, 0.32 mmol, 1.5 eq.) and *tert*-butyldimethylsilyl chloride (58 mg, 0.38 mmol, 1.8 eq.) were added and the mixture stirred at room temperature for 7.5 h. The mixture was diluted with DCM, filtered over celite and the filtrate washed with sat. NaHCO₃ solution and sat. NaCl solution. The organic phase was dried over Na₂SO₄, filtered and the solvent removed under reduced pressure. The crude product was purified by column chromatography (toluene/acetone 4:1 + 1 % NEt₃ for packing the column). The product was obtained as a white solid (36 mg, 0.05 mmol, 26 %).

TLC (toluene/acetone 4:1 + 1 % NEt₃): R_f = 0.34.

¹H-NMR (300 MHz, CDCl₃): δ (ppm) = -0,39, -0.16 (2 x s, 6 H, TBDMS-Me), 0.81 (s, 9 H, TBDMS-*t*Bu), 3.45 (dd, *J* = 3.6 Hz, *J* = 10.8 Hz, 1 H, 5'-H_a), 3.55 (dd, *J* = 2.3 Hz, *J* = 10.7 Hz, 1 H, 5'-H_b), 3.78, 3.78 (2 x s, 6 H, DMT-OMe), 4.28-4.36 (m, 2 H, 3-'H, 4'-H), 4.77 (dd, *J* = 5.4 Hz, *J* = 7.0 Hz, 1 H, 2'-H), 5.85 (d, *J* = 7.2 Hz, 1 H, 1'-H), 6.82 (ddd, *J* = 1.0 Hz, *J* = 2.2 Hz, *J* = 8.9 Hz, 4 H, DMT), 7.00 (ddd, *J* = 1.1, *J* = 7.2 Hz, *J* = 8.3 Hz, 1 H, 5-H), 7.21-7.37 (m, 8 H, 6-H, DMT), 7.43-7.48 (m, 2 H, DMT), 7.64 (dd, *J* = 1.0 Hz, *J* = 8.2 Hz, 1 H, 7-H), 7.79 (dd, *J* = 0.9 Hz, *J* = 8.1 Hz, 1 H, 4-H), 8.08 (s, 1 H, 2-H).

¹³C-NMR (125 MHz, CDCl₃): δ (ppm) = -5.42, 18.48, 26.05, 55.29, 63.52, 64.02, 70.82, 85.36, 87.32, 88.02, 111.37, 113.45, 120.43, 122.74, 123.45, 127.35, 127.57, 128.15, 129.59, 129.83, 133.46, 134.69, 135.27, 142.00, 144.10, 158.83, 159.00.

HR-MS (ESI): calc. $C_{39}H_{47}N_2O_6Si$ ([M+H]⁺): 667.3198, found: 667.3191.

1-*N*-(2'-*O*-(*tert*-butyldimethylsilyl)-3'-*O*-(2-cyanoethyl-*N,N*-diisopropylphosphoramidite)-5'-*O*-(4,4'-dimethoxytrityl)-β-D-ribofuranosyl)benzimidazole (81)

C₃₉H₄₆N₂O₆Si
[666.88]

C₄₈H₆₃N₄O₇PSi
[866.42]
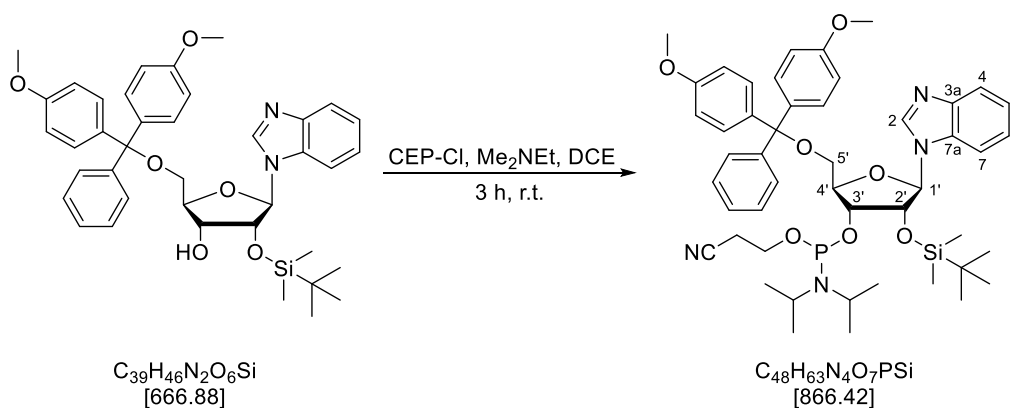
1-*N*-(2'-*O*-(*tert*-butyldimethylsilyl)-5'-*O*-(4,4'-dimethoxytrityl)-β-D-ribofuranosyl)benzimidazole (77 mg, 0.12 mmol, 1.0 eq.) was dissolved in dry DCE (2.5 ml) under inert atmosphere. Ethyldimethylamine (86 mg, 1.18 mmol, 10 eq.) and 2-cyanoethyl-*N,N*-diisopropylchloro-phosphoramidite (108 mg, 0.46 mmol, 3.9 eq.) were added and the mixture stirred for 3 h at room temperature. MeOH was added and the mixture stirred at room temperature for 5 min. The mixture was diluted with DCM and washed with sat. NaHCO₃ solution and water. The organic phase was dried over Na₂SO₄, filtered and the solvent removed under reduced pressure. The crude product was purified by column chromatography (*n*-hexane/EtOAc 7:3 + 1 % NEt₃ to 6:4 + 1 % NEt₃). The product was obtained as a white solid (67 mg, 0.08 mmol, 66 %) as a mixture of diastereomers.

TLC (*n*-hexane/EtOAc 1:1 + 1 % NEt₃): *R*_f = 0.34/0.45.

¹H-NMR (400 MHz, CDCl₃): δ (ppm) = -0.42, -0.41 (2 x s, 3 H, TBDMS-Me), -0.16, -0.15 (2 x s, 3 H, TBDMS-Me), 0.71,0.73 (2x s, 9 H, TBDMS-*t*Bu), 1.19, 1.25 (2 x m, 12 H, *i*Pr-CH₃), 2.27,2.68 (2 x q, *J* = 6.8 Hz, *J* = 6.6 Hz, 2 H, *i*Pr-CH), 3.46-3.55 (m, 2 H, 5'-H), 3.57-3.63 (m, 2 H, CE), 3.78 (2 x s, 6 H, DMT-OMe), 3.79 (2 x s, 6 H, DMT-OMe), 3.88-4.02 (m, 2 H, CE), 4.31-4.44 (m, 2 H, 3'-H, 4'-H), 4.72, 4.78 (2 x m, 1 H, 2'-H), 5.84, 5.93 (2 x d, *J* = 7.7 Hz, *J* = 7.6 Hz, 1 H, 1'-H), 6.79-6.85 (m, 4 H, DMT), 7.01 (t, *J* = 7.5 Hz, 1 H, 5-H), 7.21-7.25 (m, 2 H, 6-H, DMT), 7.27-7.32 (m, 2 H, DMT), 7.33-7.39 (m, 4 H,

DMT), 7.44-7.49 (m, 2 H, DMT), 7.62-7.69 (m, 1 H, 4-H), 7.76-7.78 (m, 1 H, 7-H), 8.12, 8.13 (2 x s, 1 H, 2-H).
^{31}P-NMR (300 MHz, CDCl$_3$): δ (ppm) = 148.75, 151.79.

HR-MS (ESI): ber. für C$_{48}$H$_{64}$N$_4$O$_7$PSi ([M+H]$^+$): 867.4276, gef.: 867.4276.

5.4.5 Various syntheses

2-Cyanoethyl-hex-5-yn-1-yl-*N,N*-diisopropylphosphoramidite (68)

C$_6$H$_{10}$O
[98.14]

C$_{15}$H$_{27}$N$_2$O$_2$P
[298.36]

5-Hexyn-1-ol (0.5 ml, 4.6 mmol, 1.0 eq.) and Me$_2$NEt (5.0 ml, 46 mmol, 10 eq.) were dissolved in dry DCM (6 ml) under inert atmosphere. CEP-Cl (1.22 g, 5.16 mmol, 1.1 eq.) was added and the mixture stirred for 2 h at room temperature, after which the solvent was removed under reduced pressure. The crude product was purified by column chromatography (*n*-hexane/EtOAc 9:1 + 1% NEt$_3$). The product was obtained as a colorless oil (1.19 g, 3.99 mmol, 87 %). The NMR data agree with literature data[179].

TLC (*n*-hexane/EtOAc 9:1 + 1% NEt$_3$): R_f = 0.30.

^{1}H-NMR (300 MHz, CDCl$_3$): δ (ppm) = 1.16, 1.18 (2 x d, *J* = 2.6 Hz, 12 H, *i*Pr-CH$_3$), 1.55-1.67 (m, 2 H, 3-H), 1.67-1.78 (m, 2 H, 2-H), 1.94 (t, *J* = 2.6 Hz, 1 H, 6-H), 2.22 (dt, *J* = 6.9 Hz, *J* = 2.6 Hz, 2 H, 4-H), 2.63 (t, *J* = 6.3 Hz, 2 H, 2'-H), 3.50-3.73 (m, 4 H, *i*Pr-CH, 1-H), 3.73-3.91 (m, 2 H, 1'-H).
^{13}C-NMR (125 MHz, CDCl$_3$): δ (ppm) = 18.30 (C-4), 20.55, 20.61 (C-2'), 24.73, 24.79, 24.81, 24.87 (*i*Pr-CH$_3$), 25.19 (C-3), 30.34, 30.39 (C-2), 43.15, 43.25 (*i*Pr-CH), 58.38, 58.53 (C-1'), 63.14, 63.27 (C-1), 68.58 (C-6), 84.33 (C-5), 117.66 (CN).
^{31}P-NMR (162 MHz, CDCl$_3$): δ (ppm) = 147.48.

HR-MS (ESI): calc. C$_{15}$H$_{27}$N$_2$NaO$_2$P ([M+Na]$^+$): 321.1702, found: 321.1702.

1-*O*-(4,4'-dimethoxytrityl)-2,2'-sulfonyldiethanol (83)

C$_4$H$_{10}$O$_4$S
[154.18]

C$_{25}$H$_{28}$O$_6$S
[456.55]
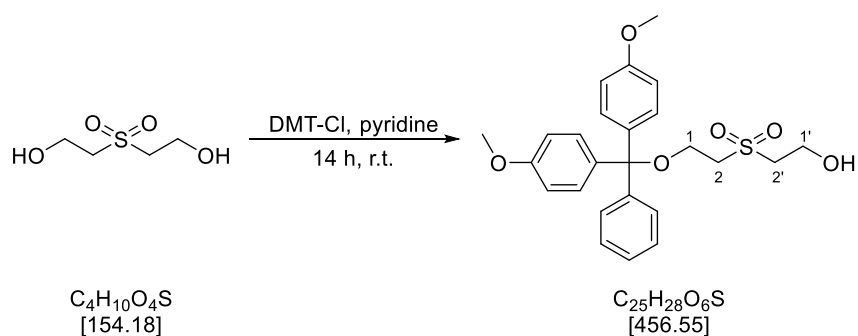
2,2'-sulfonyldiethanol (60-65 % in H$_2$O) (1.70 g, 6.5 mmol, 1.4 eq.) was coevaporated multiple times with dry pyridine and dissolved in dry pyridine (15 ml) under inert atmosphere. 4,4'-dimethoxytrityl chloride (1.54 g, 4.54 mmol, 1.0 eq.) was added portionwise over 60 min and the mixture stirred at room temperature for 14 h. The solvent was removed under reduced pressure, the residue dissolved in EtOAc and washed sat. NaHCO$_3$ solution and sat. NaCl solution. The organic phase was dried over Na$_2$SO$_4$, filtered, the solvent removed under reduced pressure and the product dried in high vacuum. The product was obtained as a colorless oil (1.10 g, 2.40 mmol, 52 %).

TLC (DCM/MeOH 99:1 + 1 % NEt$_3$): R_f = 0.24.

^{1}H-NMR (300 MHz, CDCl$_3$): δ (ppm) = 2.63 (s$_{br}$, 1 H, 1'-OH), 3.17 (t, *J* = 5.5 Hz, 2 H, 2-H), 3.34-3.38 (m, 2 H, 2'-H), 3.65 (dd, *J* = 6.0 Hz, *J* = 5.1, 2 H, 1-H), 3.77 (s, 6 H, DMT-OMe), 4.08 (d$_{br}$, *J* = 5.29 Hz, 2 H, 1'-H), 6.79-6.85 (m, 4 H, DMT), 7.17-7.31 (m, 7 H, DMT), 7.34-7.39 (m, 2 H, DMT).
^{13}C-NMR (125 MHz, CDCl$_3$): δ (ppm) = 55.31, 55.42, 56.62, 55.82, 57.79, 87.80, 113.47, 127.21, 128.03, 128.12, 130.00, 135.25, 144.16, 158.75.

HR-MS (ESI): ber. für C$_{25}$H$_{28}$O$_6$SNa ([M+Na]$^+$): 479.1499, gef.: 479.1490.

.

1-*O*-(2-cyanoethyl-*N*,*N*-diisopropylphosphoramidite)-1'-*O*-(4,4'-dimethoxytrityl)-2,2'-sulfonyldiethanol (84)

C$_{25}$H$_{28}$O$_6$S
[456.55]

C$_{34}$H$_{45}$N$_2$O$_7$PS
[656.77]
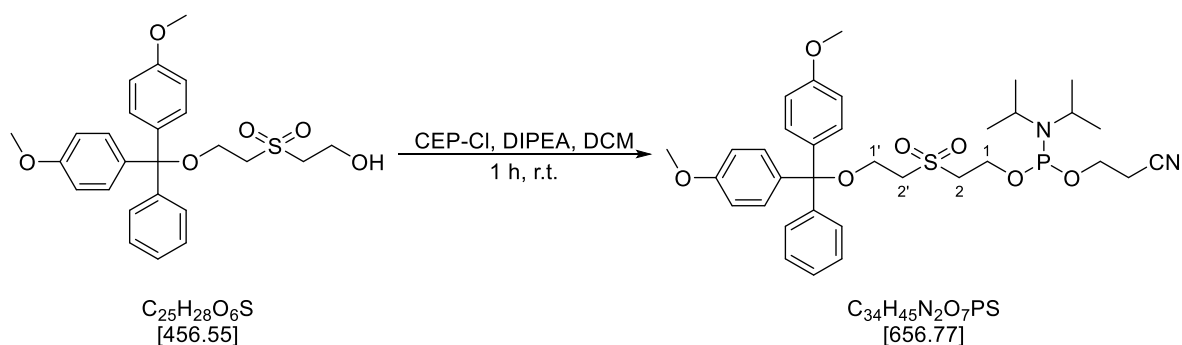
1-*O*-(4,4'-dimethoxytrityl)-2,2'-sulfonyldiethanol (1.10 g, 2.40 mmol, 1.0 eq.) was dissolved in dry DCM (6 ml) under inert atmosphere. Diisopropylethylamine (339 mg, 2.62 mmol, 1.1 eq.) and 2-cyanoethyl-*N*,*N*-diisopropylchlorophosphoramidite (584 mg, 2.47 mmol, 1.0 eq.) were added and the mixture stirred for 1 h at room temperature. The mixture was diluted with EtOAc and washed with sat. NaCl solution. The organic phase was dried over Na_2SO_4, filtered and the solvent removed under reduced pressure. The crude product was purified by column chromatography (*n*-hexane/EtOAc 2:1 + 1 % NEt_3). The product was obtained as a colorless oil (1.08 g, 1.65 mmol, 69 %).

TLC (*n*-hexane/EtOAc 2:1 + 1 % NEt_3): R_f = 0.27.

^{1}H-NMR (400 MHz, $CDCl_3$): δ (ppm) = 1.18 (d, *J* = 6.82 Hz, 6 H, *i*Pr-CH_3), 1.20 (d, *J* = 6.83 Hz, 6 H, *i*Pr-CH_3), 2.54-2.58 (m, 2 H, *i*Pr-CH), 3.23-3.34 (m, 2 H, 2'-H), 3.36-3.51 (m, 2 H, 2-H), 3.58-3.66 (m, 3 H, 1'-H, CE), 3.75-3.88 (m, 2 H, CE), 3.78 (s, 6 H, DMT-OMe), 4.01-4.09 (m, 1 H, CE), 4.09-4.15 (m, 2 H, 1-H), 6.82-6.86 (m, 4 H, DMT), 7.27-7.33 (m, 6 H, DMT), 7.40-7.43 (m, 2 H, DMT).
^{31}P-NMR (300 MHz, $CDCl_3$): δ (ppm) = 148.92.

HR-MS (ESI): ber. für $C_{34}H_{46}N_2O_7PS$ ([M+H]$^+$): 657.2758, gef.: 657.2748.

3',5'-Di-*O*-acetyldeoxyuridine (71)

$C_9H_{12}N_2O_5$
[228.20]

$C_{13}H_{16}N_2O_7$
[312.28]
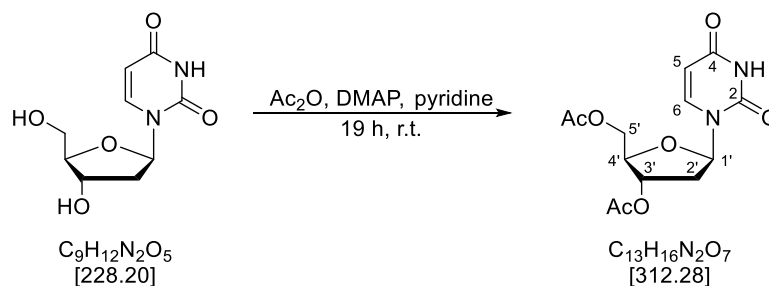
To a solution of deoxyuridine (6.85 g, 30.0 mmol, 1.0 eq.) in pyridine (20 ml) at 0 °C DMAP (644 mg, 5.44 mmol, 0.18 eq.) and Ac_2O (6.8 ml, 72.0 mmol, 2.4 eq.) were added. The mixture was stirred for 19 h at room temperature, after which the solvent was removed under reduced pressure, the residue dissolved in DCM, and washed with brine and water. The organic phase was dried over Na_2SO_4 and the solvent removed under reduced pressure. The crude product was purified by column chromatography (0 % to 10 % MeOH in DCM) and the product obtained as a colorless foam (7.97 g, 25.5 mmol, 85 %). The NMR data agree with literature data[189].

TLC (DCM/MeOH 98:2): R_f = 0.26.

^{1}H-NMR (400 MHz, $CDCl_3$): δ (ppm) = 2.11, 2.12 (2 x s, 6 H, Ac), 2.13-2.19 (m, 1 H, 2'-H_a), 2.53 (ddd, *J* = 14.2 Hz, *J* = 5.6 Hz, *J* = 2.0 Hz, 1 H, 2'-H_b), 4.27 (dt, *J* = 4.2 Hz, *J* = 3.1 Hz, 1 H, 5'-H_a), 4.29-4.40 (m,

2 H, 4'-H, 5'-H$_b$), 5.21 (dt, J = 6.3, J = 2.1 Hz, 1 H, 3'-H), 5.78 (ddd, J = 8.2 Hz, J = 2.4 Hz J = 0.8 Hz, 1 H, 5-H), 6.27 (dd, J = 8.4 Hz, J = 5.6 Hz, 1 H, 1'-H), 7.49 (d, J = 8.2 Hz, 1 H, 6-H).

13C-NMR (100 MHz, CDCl$_3$): δ (ppm) = 20.97, 21.05 (Ac-CH$_3$), 38.01 (C-2'), 63.95 (C-5'), 74.20 (C-3'), 82.51 (C-4'), 85.44 (C-1'), 103.10 (C-5), 138.90 (C-6), 150.19 (C-2), 162.85 (C-4), 170.34, 170.53 (Ac-CO).

HR-MS (ESI): calc. C$_{13}$H$_{16}$N$_2$NaO$_7$ ([M+Na]$^+$): 335.0850, found: 335.0843.

3',5'-Di-*O*-acetyl-5-bromodeoxyuridine (72)

$C_{13}H_{16}N_2O_7$
[312.28]

DBH, TMSOTf, DCM
1 h, 40 °C

$C_{13}H_{15}N_2O_7Br$
[391.17]
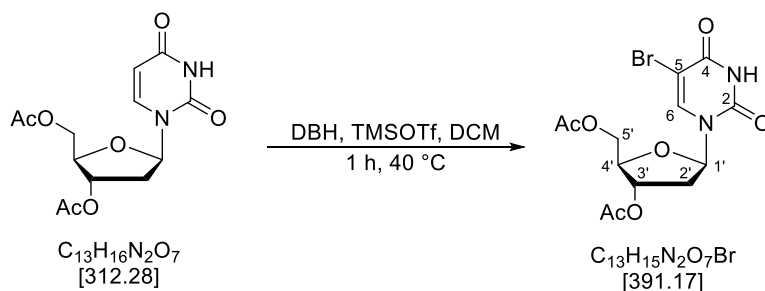
3',5'-Diacetyldeoxyuridine (7.97 g, 25.5 mmol, 1.0 eq.) was dissolved in dry DCM (100 ml) under inert atmosphere and TMSOTf (2.5 ml, 14 mmol, 0.6 eq.) was added. DBH (4.01 g, 14 mmol, 0.6 eq.) was added in portionwise over 5 min and the mixture stirred for 1 h at 40°C. After cooling to room temperature, sat. aq. Na$_2$HCO$_3$ was added and the mixture stirred overnight. The phases were separated and the organic phase washed with sat. aq. Na$_2$HCO$_3$ and H$_2$O. The combined aqueous phases were extracted with EtOAc and DCM, the combined organic phases dried over Na$_2$SO$_4$ and the solvent removed under reduced pressure. The residue was diluted with DCM and washed with H$_2$O. The combined aqueous phases were extracted with chloroform and the solvent removed under reduced pressure. The product was obtained as a colorless solid (7.89 g, 20.4 mmol, 80 %). The NMR data agree with literature data[190].

TLC (DCM/MeOH 10:1): R_f = 0.68.

1H-NMR (400 MHz, CDCl$_3$): δ (ppm) = 2.11, 2.20 (2 x s, 6 H, Ac), 2.15-2.23 (m, 1 H, 2'-H$_a$), 2.55 (ddd, J = 14.3 Hz, J = 5.8 Hz, J = 2.3 Hz, 1 H, 2'-H$_b$), 4.30 4.28-4.44 (m, 3 H, 4'-H, 5'-H), 5.23 (dt, J = 6.3, J = 2.3 Hz, 1 H, 3'-H), 6.30 (dd, J = 8.1 Hz, J = 5.7 Hz, 1 H, 1'-H), 7.90 (s, 1 H, 6-H).

13C-NMR (100 MHz, CDCl$_3$): δ (ppm) = 21.03, 21.08 (Ac-CH$_3$), 38.42 (C-2'), 63.95 (C-5'), 74.11 (C-3'), 82.83 (C-4'), 85.68 (C-1'), 97.52 (C-5), 138.71 (C-6), 149.39 (C-2), 158.60 (C-4), 170.24, 170.55 (Ac-CO).

HR-MS (ESI): calc. C$_{13}$H$_{15}$BrN$_2$NaO$_7$ ([M+Na]$^+$): 412.9955, found: 412.9949.

1-*N*-(2',3'-Di-*O*-acetyl-β-D-ribofuranosyl)-5-bromo-4-((1,1,3,3-tetraethyl-6-hydroxyisoindolin-5-yl)amino)pyrimidin-2-one (73)

$C_{13}H_{15}N_2O_7Br$	$C_{16}H_{26}N_2O$	$C_{29}H_{39}N_4O_7Br$
[391.17]	[262.40]	[635.56]
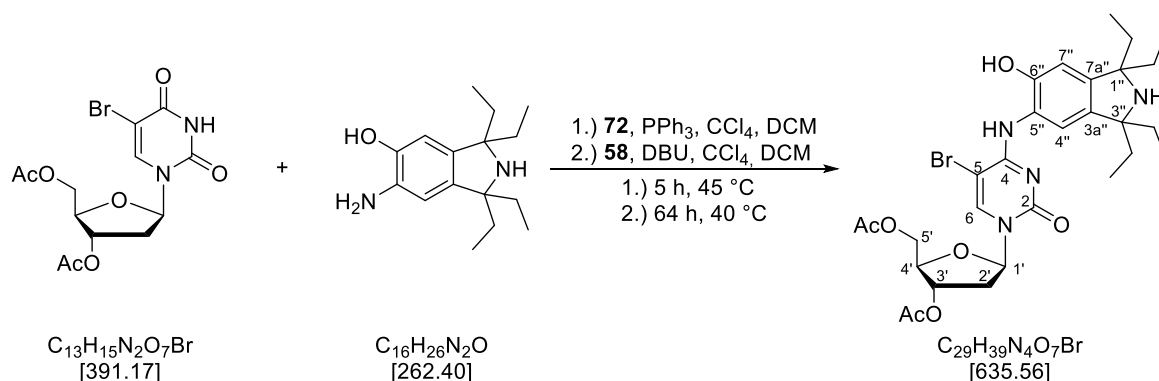
Triphenylphosphine (1.13, 4.31 mmol, 2.3 eq.) was dissolved in dry DCM (7.5 ml) and CCl₄ (7.5 ml) under inert atmosphere and the mixture stirred for 20 min at room temperature. 2',3'-Di-*O*-acetyl-5-bromodeoxyuridine (870 mg, 2.22 mmol, 1.2 eq) was added and the mixture stirred for 5 h at 45 °C. After cooling to room temperature, a solution of 6-amino-1,1,3,3-tetraethyl-5-hydroxyisoindoline (500 mg, 1.91 mmol, 1.0 eq) and DBU (350 µl, 2.0 mmol, 1.0 eq) in dry DCM (5 ml) and CCl₄ (5 ml) was added and the mixture was stirred for 64 h at 40 °C. The solvent was removed under reduced pressure and the residue purified by column chromatography (0 % to 35 % MeOH in DCM). After multiple attempts the product could not be fully purified (182 mg).

TLC (DCM/MeOH 10:1): R_f = 0.68.

¹H-NMR (400 MHz, CD₃OD): δ (ppm) = 1.03 (t, J = 7.4 Hz, 12 H, CH₂-C*H*₃), 1.96-2.05 (m, 8 H, C*H*₂-CH₃), 2.11, 2.14 (2 x s, 9 H, Ac), 2.31-2.39 (m, 1 H, 2'-Hₐ), 2.64 (dd, *J* = 5.9 Hz, *J* = 2.3 Hz, 1 H, 2'-H_b), 4.34-4.44 (m, 3 H, 4'-H, 5'-H), 5.25-5.31 (m, 1 H, 3'-H), 6.22 (dd, *J* = 7.6 Hz, *J* = 5.9 Hz, 1 H, 1'-H), 6.75 (s, 1 H, 7''-H), 8.17 (s, 1 H, 4''-H), 8.45 (s, 1 H, 6-H).

3-*N*-(2'-deoxy-β-D-Ribofuranosyl)-7,7,9,9-tetraethyl-7,8,9,11-tetrahydropyrimido[4',5':5,6][1,4]oxazino[2,3-*f*]isoindol-2-one (74)

$C_{29}H_{39}N_4O_7Br$	$C_{25}H_{34}N_4O_5$
[635.56]	[470.57]
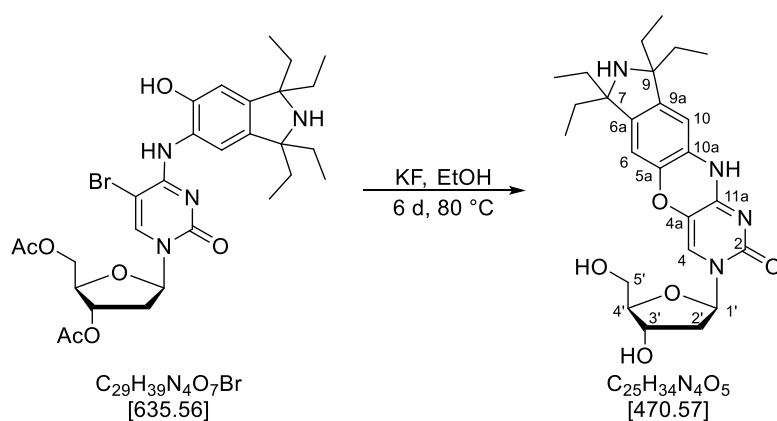
To a solution of 1-*N*-(2',3'-Di-*O*-acetyl-2'-deoxy-β-D-ribofuranosyl)-5-bromo-4-((1,1,3,3-tetraethyl-6-hydroxyisoindolin-5-yl)amino)pyrimidin-2-one (182 mg) in EtOH (15 ml), KF (167 mg, 2.87 mmol) was added and the mixture stirred for 5 d at 80 °C. After cooling to room temperature, the mixture was filtered and the solvent removed under reduced pressure. The crude product was purified by column chromatography (0 % to 35 % MeOH in DCM). After multiple attempts the product could not be fully purified (92 mg).

TLC (DCM/MeOH 5:1): R_f = 0.26.

¹H-NMR (400 MHz, CD₃OD): δ (ppm) = 0.85-0.95 (m, 12 H, CH₂-CH_3), 1.71-1.83 (m, 8 H, CH_2-CH₃), 2.15 (dt, *J* = 13.3 Hz, *J* = 6.5 Hz, 1 H, 2'-H$_a$), 2.33 (ddd, *J* = 13.5 Hz, *J* = 6.1 Hz, *J* = 3.8 Hz, 1 H, 2'-H$_b$), 3.72-3.84 (m, 2 H, 5'-H), 3.93 (q, *J* = 3.4 Hz, 1 H, 4'-H), 4.38 (dt, *J* = 6.6 Hz, *J* = 3.6 Hz, 1 H, 3'-H), 6.23 (t, *J* = 6.5 Hz, 1 H, 1'-H), 6.57, 6.59 (2 x s, 2 H, 6-H, 10-H), 7.71 (s, 1 H, 4-H).

N-Benzyl-1,1,3,3-tetramethylisoindoline (9)
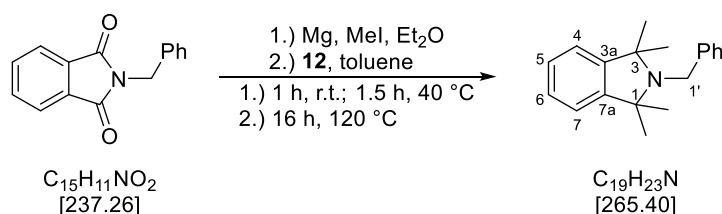
To a suspension of magnesium turnings (16.49 g, 678.5 mmol, 8.0 eq) in dry diethyl ether (60 ml) under inert atmosphere a solution of methyl iodide (38 ml, 602.8 mmol, 7.1 eq) in dry diethyl ether (80 ml) was added slowly and the mixture stirred for 1 h at room temperature and 1.5 h at 40 °C. After cooling to room temperature, a solution of *N*-benzylphthalimide (20.01 g, 84.34 mmol, 1.0 eq) in dry toluene (150 ml) was added dropwise, part of the solvent distilled off, and the mixture stirred for 16 h at 120 °C. After cooling to room temperature, *n*-hexane was added and the resulting mixture stirred for 7 h under air. The mixture was filtered over aluminium oxide 90 basic and the solvent removed under reduced pressure. The crude product was purified by column chromatography (*n*-hexane to *n*-hexane/EtOAc 3:1). The product was obtained as a colorless solid (6.21 g, 23.4 mmol, 31 %). The NMR data agree with literature data[119].

TLC (*n*-hexane): R_f = 0.19.

¹H-NMR (600 MHz, CDCl₃): δ (ppm) = 1.33 (s, 12 H, Me), 4.02 (s, 2 H, 1'-H), 7.15-7.18 (m, 2 H, 4-H, 7-H), 7.24 (dd, *J* = 6.7 Hz, *J* = 6.7 Hz, 1 H, 5'-H), 7.26-7.28 (m, 2 H, 5-H, 6-H), 7.32 (dd, *J* = 6.6 Hz, *J* = 6.6 Hz, 2 H, 3'-H, 7'-H), 7.50 (d, *J* = 7.5 Hz, 2 H, 4'-H, 6'-H).
¹³C-NMR (125 MHz, CDCl₃): δ (ppm) = 28.63 (Me), 46.45 (C-1'), 65.37 (C-1, C-3), 121.39 (C-5, C-6), 126.48 (C-5'), 126.83 (C-4, C-7), 127.98 (C-4', C-6'), 128.40 (C-3' C-7'), 143.50 (C-2'), 147.91 (C-3a, C-7a).

HR-MS (ESI): calc. $C_{19}H_{24}N$ ([M+H]$^+$): 266.1903, found: 266.1905.

1,1,3,3-Tetramethylisoindoline (13)

C$_{19}$H$_{23}$N
[265.40]

C$_{12}$H$_{17}$N
[175.28]
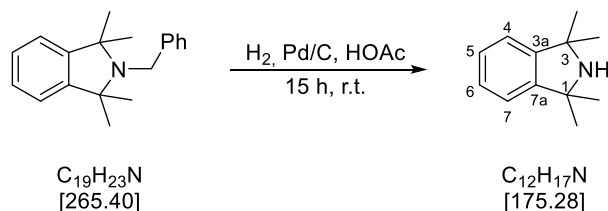
To a solution of *N*-benzyl-1,1,3,3-tetramethylisoindoline (10.3 g, 38.6 mmol, 1.0 eq) in acetic acid (50 ml) was added palladium (10 % on charcoal, 1.98 g, 1.93 mmol, 5 mol-%) and the mixture was stirred for 15 h at room temperature under hydrogen atmosphere. Afterwards, the mixture was filtered over Celite, the solvent removed under reduced pressure, the residue neutralized with aq. NaOH and the aqueous phase extracted with EtOAc. The combined organic phases were dried over Na$_2$SO$_4$, filtered, and the solvent removed under reduced pressure. The product was obtained as a colorless solid (8.33 g, quant.) and used in the next step without further purification. The NMR data agree with literature data[119].

TLC (DCM/MeOH 98:2): R_f = 0.13.

^{1}H-NMR (300 MHz, CDCl$_3$): δ (ppm) = 1.63 (s, 12 H, Me), 7.13 (dd, *J* = 5.7 Hz, *J* = 3.0 Hz, 2 H, 4-H, 7-H), 7.29 (dd, *J* = 5.7 Hz, *J* = 3.0 Hz, 2 H, 5-H, 6-H).
^{13}C-NMR (75 MHz, CDCl$_3$): δ (ppm) = 30.37 (Me), 65.32 (C-1, C-3), 121.54 (C-4, C-7), 128.30 (C-5, C-6), 145.73 (C-3a, C-7a).

HR-MS (ESI): calc. $C_{12}H_{18}N$ ([M+H]$^+$): 176.1434, found: 176.1434.

1,1,3,3-Tetramethyl-5-nitroisoindoline (14)

C$_{12}$H$_{17}$N
[175.28]

C$_{12}$H$_{16}$N$_2$O$_2$
[220.27]
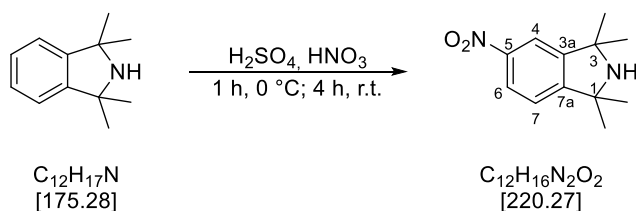
1,1,3,3-Tetramethylisoindoline (2.12 g, 9.78 mmol, 1.0 eq) was dissolved in conc. H$_2$SO$_4$ (20 ml). Conc. HNO$_3$ (5 ml) was added dropwise at 0 °C and the resulting mixture stirred for 1 h at 0 °C and 4 h at room temperature. It was then neutralized with aq. NaOH and extracted with EtOAc. The combined organic phases were dried over Na$_2$SO$_4$, filtered and the solvent removed under reduced pressure. The crude product was purified by column chromatography (2 % to 5 % MeOH in DCM).

The product was obtained as a yellow powder (2.11 g, 9.57 mmol, 98 %). The NMR data agree with literature data[168].

TLC (DCM/MeOH 98:2): R_f = 0.13.

^{1}H-NMR (300 MHz, CDCl$_3$): δ (ppm) = 1.49 (s, 6 H, Me), 1.51 (s, 6 H, Me), 7.24 (dd, J = 11.1 Hz, J = 0.6 Hz, 1 H, 7-H), 7.97 (dd, J = 2.8 Hz, J = 0.6 Hz, 1 H, 4-H), 8.14 (dd, J = 11.1 Hz, J = 2.8 Hz, 1 H, 6-H).
^{13}C-NMR (75 MHz, CDCl$_3$): δ (ppm) = 31.79, 31.93 (Me), 62.86 (C-3), 63.10 (C-1), 117.34 (C-4), 122.37 (C-7), 123.35 (C-6), 148.13 (C-5), 150.80 (C-7a), 156.18 (C-3a).

HR-MS (ESI): calc. C$_{12}$H$_{17}$N$_2$O$_2$ ([M+H]$^+$): 221.1286, found: 221.1295.

6-Amino-1,1,3,3-tetramethyl-5-nitroisoindoline (15)
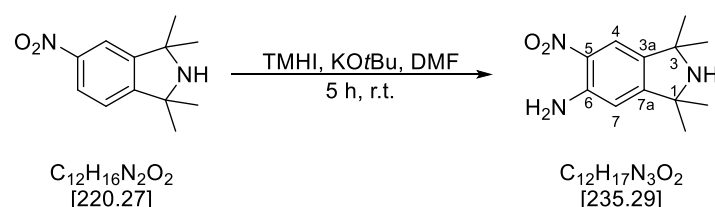
To a solution of 1,1,3,3-tetramethyl-5-nitroisoindoline (1.84 g, 8.36 mmol, 1.0 eq) in dry DMF (30 ml) under inert atmosphere was added 1,1,1-trimethylhydrazinium iodide (2.07 g, 9.25 mmol, 1.1 eq). After a clear solution was obtained, KOtBu (2.36 g, 20.2 mmol, 2.4 eq) was added and the mixture stirred for 5 h at room temperature. It was then poured on ice, neutralized with conc. HCl, and extracted with EtOAc and DCM. The combined organic phases were dried over Na$_2$SO$_4$, filtered and the solvent removed under reduced pressure. The crude product was purified by column chromatography (DCM/MeOH 97.5:2.5 + 1 % NEt$_3$). The product was obtained as a yellow powder (1.93 g, 8.20 mmol, 98 %). The NMR data agree with literature data[150].

TLC (DCM/MeOH 95:5 + 1 % NEt$_3$): R_f = 0.41.

^{1}H-NMR (400 MHz, CDCl$_3$): δ (ppm) = 1.43 (2 x s, 12 H, Me), 6.09 (s$_{br}$, 2 H, NH$_2$), 6.51 (s, 1 H, 7-H), 7.85 (s, 1 H, 4-H).
^{13}C-NMR (125 MHz, CDCl$_3$): δ (ppm) = 31.68, 32.18 (Me), 62.16 (C-3), 62.70 (C-1), 110.77 (C-7), 119.05 (C-4), 132.24 (C-6), 139.50 (C-7a), 144.94 (C-5), 158.45 (C-3a).

HR-MS (ESI): calc. C$_{12}$H$_{18}$N$_3$O$_2$ ([M+H]$^+$): 236.1394, found: 236.1396.

5,6-Diamino-1,1,3,3-tetramethylisoindoline (8)

C$_{12}$H$_{17}$N$_3$O$_2$
[235.29]

C$_{12}$H$_{19}$N$_3$
[205.31]
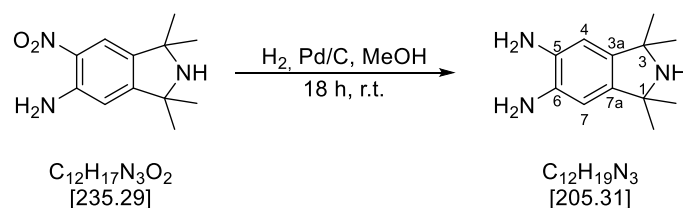
To a solution of 6-amino-1,1,3,3-tetramethyl-5-nitroisoindoline (1.93 g, 8.12 mmol, 1.0 eq) in MeOH (50 ml) palladium (10 % on charcoal, 1.12 g, 1.07 mmol, 13 mol-%) was added and the mixture stirred for 15 h under hydrogen atmosphere. Then the mixture was filtered over Celite and the solvent removed under reduced pressure. The product was obtained as a colorless solid (1.61 g, 7.84 mmol, 96 %) and used in the next step without further purification. The NMR data agree with literature data[150].

TLC (DCM/MeOH 95:5 + 1 % NEt$_3$): R_f = 0.37.

^{1}H-NMR (600 MHz, CDCl$_3$): δ (ppm) = 1.40 (s, 12 H, Me), 6.45 (s, 2 H, 4-H, 7-H).
^{13}C-NMR (125 MHz, CDCl$_3$): δ (ppm) = 32.26 (Me), 62.67 (C-1, C-3), 109.59 (C-4, C-7), 134.29 (C-5, C-6), 140.82 (C-3a, C-7a).

HR-MS (ESI): calc. C$_{12}$H$_{20}$N$_3$ ([M+H]$^+$): 206.1352, found: 206.1672.

5,5,7,7-tetramethyl-3,5,6,7-tetrahydroimidazo[4,5-*f*]isoindol-2-one (7)

C$_{12}$H$_{19}$N$_3$
[205.31]

C$_{13}$H$_{17}$N$_3$O
[231.30]
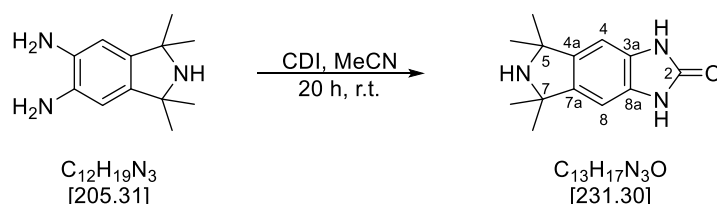
5,6-Diamino-1,1,3,3-tetramethylisoindoline (506 mg, 2.47 mmol, 1.0 eq) and 1,1'-carbonydiimidazole (810 mg, 4.91 mmol, 2.0 eq) were dissolved in dry MeCN (150 ml) under inert atmosphere and stirred for 20 h at room temperature. The solvent was removed under reduced pressure. The crude product was purified by column chromatography (2 % to 10 % MeOH in DCM + 1 % NEt$_3$). The product was obtained as a colorless solid (76 mg, 0.33 mmol, 13 %).

TLC (DCM/MeOH 9:1 + 1 % NEt$_3$): R_f = 0.33.

^{1}H-NMR (400 MHz, CD$_3$OD): δ (ppm) = 1.66 (s, 12 H, Me), 6.91 (s, 2 H, 4-H, 8-H).
^{13}C-NMR (125 MHz, CD$_3$OD): δ (ppm) = 30.31 (Me), 67.43 (C-5, C-7), 103.36 (C-4, C-8), 131.73 (C-3a, C-8a), 138.67 (C-4a, C-7a), 158.23 (C-2).

HR-MS (ESI): calc. $C_{13}H_{18}N_3O$ ([M+H]$^+$): 232.1444, found: 232.1448.

1-*N*-(3',5'-Di-*O*-toluoyl-2'-deoxy-β-ᴅ-ribofuranosyl)-5,5,7,7-tetramethyl-3,5,6,7-tetrahydro-imidazo[4,5-*f*]isoindol-2-one (6)

C$_{13}$H$_{17}$N$_3$O
[231.30]

C$_{21}$H$_{21}$O$_5$Cl
[388.84]

C$_{34}$H$_{37}$N$_3$O$_6$
[583.69]
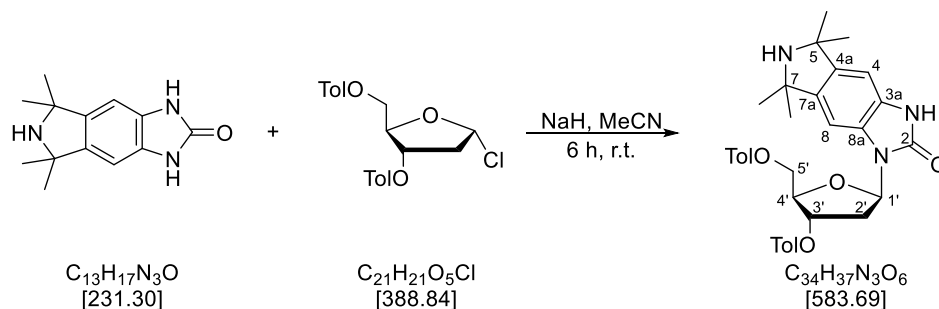
5,5,7,7-tetramethyl-3,5,6,7-tetrahydroimidazo[4,5-*f*]isoindol-2-one (214 mg, 0.93 mmol, 1.4 eq.) was dissolved in dry MeCN (60 ml) under inert atmosphere. NaH (48 mg, 1.20 mmol, 1.6 eq.) was added and the mixture stirred for 1 h at room temperature. Afterwards, 1-chloro-3,5-di-*O*-toluoyl-2-deoxy-α-ᴅ-ribofuranose (259 mg, 0.67 mmol, 1.0 eq.) was added and the mixture stirred for 5 h at room temperature. Sat. aq. NaHCO$_3$ and EtOAc were added and the organic phase washed with brine. The combined organic phases were dried over Na$_2$SO$_4$, filtered and the solvent removed under reduced pressure. The crude product was purified by column chromatography (5 % to 10 % MeOH in DCM). A mixture of α- and β-isomers was obtained (83 mg, 0.14 mmol, 21 %).

TLC (DCM/MeOH 9:1): R_f = 0.37.

^{1}H-NMR (400 MHz, CDCl$_3$): δ (ppm) = 1.41 (s, 3 H, Me), 1.46 (s, 3 H, Me), 1.58 (s, 6 H, Me), 2.36, 2.43 (2 x s, 6 H, Tol-Me), 2.52 (ddd, *J* = 14.0 Hz, *J* = 5.9 Hz, *J* = 2.0 Hz, 1 H, 2'-H$_a$), 3.26-3.35 (m, *J* = 14.1 Hz, 1 H, 2'-H$_b$), 4.53-4.56 (m, 1 H, 4'-H), 4.62 (dd, *J* = 11.9 Hz, *J* = 5.3 Hz, 1 H, 5'-H$_a$), 4.73 (dd, *J* = 11.8 Hz, *J* = 4.4 Hz, 1 H, 5'-H$_b$), 5.77 (ddd, *J* = 6.4 Hz, *J* = 2.4 Hz, *J* = 2.4 Hz, 1 H, 3'-H), 6.34 (dd, *J* = 8.4 Hz, *J* = 5.9 Hz, 1 H, 1'-H), 6.91 (s, 1 H, 4-H), 6.93 (s, 1 H, 8-H), 7.19 (d, *J* = 8.6 Hz, 1 H, Tol-CH), 7.27 (d, *J* = 8.6 Hz, 1 H, Tol-CH), 7.91 (d, *J* = 8.3 Hz, 1 H, Tol-CH), 7.97 (d, *J* = 8.2 Hz, 1 H, Tol-CH). (β-isomer)
^{13}C-NMR (100 MHz, CDCl$_3$): δ (ppm) = 21.80, 21.88 (Tol-Me), 31.10 (Me), 34.47 (C-2'), 64.52 (C-5'), 64.64 (C-5, C-7), 74.96 (C-3'), 81.69 (C-4'), 83.37 (C-1'), 102.76, 103.46 (C-4, C-8), 126.68, 126.96 (*i*-Tol), 128.36, 128.76 (C-3a, C-8a), 129.40, 129.43, 129.85, 129.94 (Tol-CH), 140.29 (C-4a, C-7a), 144.28, 144.57 (*p*-Tol), 154.98 (C-2), 166.21, 166.40 (Tol-CO). (β-isomer)

HR-MS (ESI): calc. $C_{34}H_{37}N_3NaO_6$ ([M+Na]$^+$): 606.2575, found: 606.2582.

2-Boc-1,1,3,3-tetramethyl-5-nitroisoindolin (21)

$C_{12}H_{16}N_2O_2$
[220.27]

$C_{17}H_{24}N_2O_4$
[320.39]
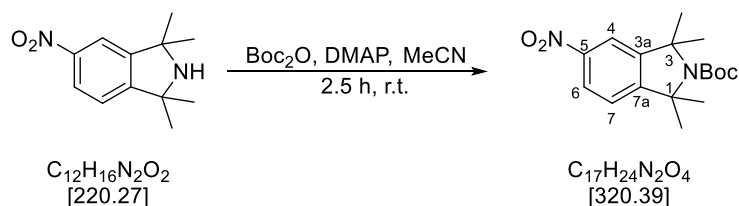
4-(Dimethylamino)pyridin (55 mg, 0.45 mmol, 1.0 eq) and di-*tert*-butyl dicarbonate (0.15 ml, 0.68 mmol, 1.4 eq) were dissolved in dry MeCN (100 ml) under inert atmosphere. 1,1,3,3-Tetramethyl-5-nitroisoindoline (105 mg, 0.47 mmol, 1.0 eq) was added and the mixture stirred for 4 h at room temperature. Water was added, the mixture extracted with EtOAc and the combined organic phases washed with 1 M HCl and brine, dried over Na_2SO_4 and the solvent removed under reduced pressure. The product was used in the next step without further purification (144 mg, 0.45 mmol, 96 %).

**TLC** (*n*-hexane/EtOAc 3:1): R_f = 0.46.

^{1}H-NMR (300 MHz, $CDCl_3$): δ (ppm) = 1.56, 1.57 (2 x s, 9 H, Boc), 1.73 (d, *J* = 7.2 Hz, 6 H, Me), 1.78 (d, *J* = 6.4 Hz, 6 H, Me), 7.31 (dd, *J* = 8.8 Hz, *J* = 8.8 Hz, 1 H, 7-H), 8.02 (dd, *J* = 6.0 Hz, *J* = 2.0 Hz, 1 H, 4-H), 8.21 (dd, *J* = 8.4 Hz, *J* = 2.4 Hz, 1 H, 6-H).
^{13}C-NMR (75 MHz, $CDCl_3$): δ (ppm) = 27.68 (Boc-CH_3) 29.72, 29.93 (Me), 67.17, 67.30, 67.77, 67.92 (C-1, C-3), 85.06 (Boc-quart), 117.42, 117.58 (C-4), 122.66, 122.81 (C-7), 123.92, 124.02 (C-6), 146.01, 146.12 (C-7a), 147.66 (Boc-CO), 148.54, 148.56 (C-5), 151.07, 151.21 (C-3a).

1,1,3,3-Tetramethyl-5-nitroisoindoline (14)

$C_{17}H_{24}N_2O_4$
[320.39]

$C_{12}H_{16}N_2O_2$
[220.27]
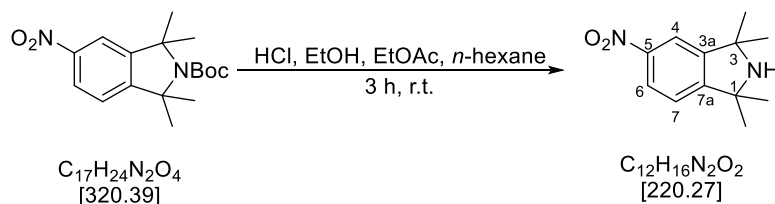
2-Boc-1,1,3,3-tetramethyl-5-nitroisoindoline (25 mg, 0.08 mmol, 1.0 eq) was dissolved in EtOH (7.5 ml) and conc. HCl (7.5 ml) with some drops of EtOAc and *n*-hexane for improved solubility. The mixture was stirred for another 3 h. It was neutralized with aq. NaOH and extracted with EtOAc. The combined organic phases were dried over Na_2SO_4, filtered and the solvent removed under reduced pressure. The product was obtained as a yellow solid (15 mg, 0.07 mmol, 88 %). The NMR data agree with literature data[168].

TLC (DCM/MeOH 95:5): R_f = 0.24.

¹H-NMR (300 MHz, CDCl₃): δ (ppm) = 1.49 (s, 6 H, Me), 1.51 (s, 6 H, Me), 7.24 (dd, *J* = 11.1 Hz, *J* = 0.6 Hz, 1 H, 7-H), 7.97 (dd, *J* = 2.8 Hz, *J* = 0.6 Hz, 1 H, 4-H), 8.14 (dd, *J* = 11.1 Hz, *J* = 2.8 Hz, 1 H, 6-H).
¹³C-NMR (75 MHz, CDCl₃): δ (ppm) = 31.79, 31.93 (Me), 62.86 (C-3), 63.10 (C-1), 117.34 (C-4), 122.37 (C-7), 123.35 (C-6), 148.13 (C-5), 150.80 (C-7a), 156.18 (C-3a).

HR-MS (ESI): calc. C₁₂H₁₇N₂O₂ ([M+H]⁺): 221.1286, found: 221.1295.

2,6-*N,N*-Di-Boc-6-amino-1,1,3,3-tetramethyl-5-nitroisoindoline (22)

$C_{12}H_{17}N_3O_2$
[235.29]

$C_{22}H_{33}N_3O_6$
[435.52]
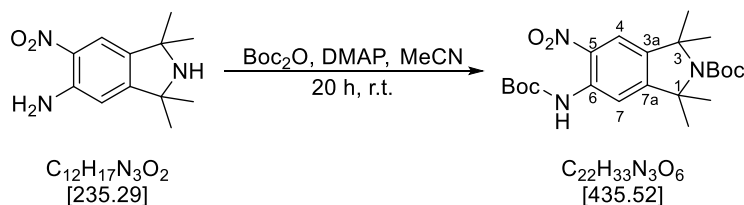
4-(Dimethylamino)pyridin (0.25 g, 2.00 mmol, 1.7 eq) and di-*tert*-butyl dicarbonate (0.76 ml, 3.45 mmol, 3.7 eq) were dissolved in dry MeCN (100 ml) under inert atmosphere. 6-Amino-1,1,3,3-tetramethyl-5-nitroisoindoline (0.27 g, 1.15 mmol, 1.0 eq) was added and the mixture stirred for 20 h at room temperature. Water was added, the mixture extracted with EtOAc and the combined organic phases washed with 1 M HCl and brine, dried over Na₂SO₄ and the solvent removed under reduced pressure. The product was used in the next step without further purification (0.162 g, 0.37 mmol, 32 %).

¹H-NMR (400 MHz, CDCl₃): δ (ppm) = 1.43 (s, 18 H, Boc-CH₃), 1.99, 2.01 (2 x s, 12 H, Me), 7.14 (s, 1 H, 7-H), 7.86 (s, 1 H, 4-H).
¹³C-NMR (100 MHz, CDCl₃): δ (ppm) = 27.97 (Boc-CH₃), 29.16, 29.31 (Me), 68.13 (C-1, C-3), 84.30 (Boc-quart), 118.82 (C-4), 125.06 (C-7), 134.82 (C-5), 143.58 (C-7a), 146.84 (C-6), 148.17 (C-3a) 150.36 (Boc-CO).

HR-MS (ESI): calc. C₂₂H₃₃N₃NaO₆ ([M+Na]⁺): 458.2262, found: 458.2253.

2,5-*N,N*-Di-Boc-5,6-diamino-1,1,3,3-tetramethyl-5-nitroisoindoline (23)

$C_{22}H_{33}N_3O_6$
[435.52]

$C_{22}H_{35}N_3O_4$
[405.54]
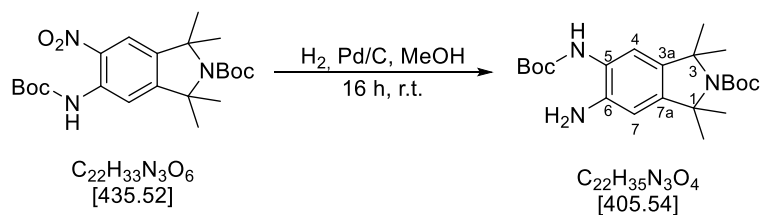
To a solution of 2,6-*N,N*-di-Boc-6-amino-1,1,3,3-tetramethyl-5-nitroisoindoline (0.16 g, 0.37 mmol, 1.0 eq) in MeOH (12 ml) palladium (10 % on charcoal, 40 mg, 0.04 mmol, 10 mol-%) was added and

the mixture stirred for 15 h under hydrogen atmosphere. Then the mixture was filtered over Celite and the solvent removed under reduced pressure. The product was obtained as a colorless solid (0.16 g, quant.) and used in the next step without further purification.

TLC (DCM/MeOH 95:5): R_f = 0.19.

^{1}H-NMR (400 MHz, CDCl$_3$): δ (ppm) = 1.43 (s, 18 H, Boc-CH$_3$), 1.99, 2.01 (2 x s, 12 H, Me), 7.14 (s, 1 H, 7-H), 7.86 (s, 1 H, 4-H).
^{13}C-NMR (100 MHz, CDCl$_3$): δ (ppm) = 27.97 (Boc-CH$_3$), 29.16, 29.31 (Me), 68.13 (C-1, C-3), 84.30 (Boc-quart), 118.82 (C-4), 125.06 (C-7), 134.82 (C-5), 143.58 (C-7a), 146.84 (C-6), 148.17 (C-3a) 150.36 (Boc-CO).

HR-MS (ESI): calc. C$_{22}$H$_{36}$N$_3$NaO$_4$ ([M+H]$^+$): 406.2700, found: 406.2686.

1,3-*N,N*-Di-Boc-5,5,7,7-tetraethyl-3,5,6,7-tetrahydroimidazo[4,5-*f*]isoindol-2-one (32)
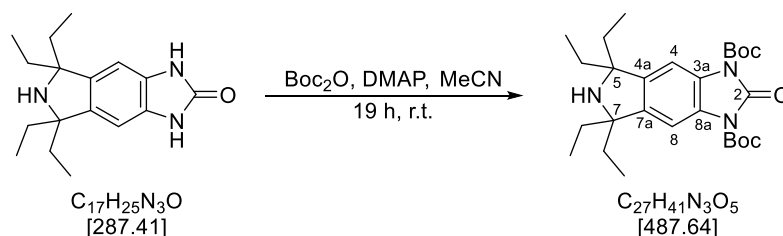
Di-*tert*-butyl dicarbonate (0.36 ml, 1.57 mmol, 4.5 eq) and DMAP (126 mg, 1.02 mmol, 2.9 eq) were dissolved in dry MeCN (30 ml) under inert atmosphere. 5,5,7,7-Tetraethyl-3,5,6,7-tetrahydroimidazo[4,5-*f*]isoindolo-2-one (101 mg, 0.35 mmol, 1.0 eq) was added and the mixture stirred for 19 h at room temperature. Water was added, the mixture extracted with EtOAc, the combined organic phases washed with 1 M HCl and brine, dried over Na$_2$SO$_4$, filtered and the solvent removed under reduced pressure. The crude product was purified by column chromatography (5 % to 10 % MeOH in DCM) and the product obtained as a light brown solid (121 mg, 0.25 mmol, 71 %).

^{1}H-NMR (400 MHz, CDCl$_3$): δ (ppm) = 0.88 (t, J = 7.4 Hz, 12 H, CH$_2$-CH_3), 1.65 (s, 18 H, Boc), 1.67-1.81 (m, 8 H, CH_2-CH$_3$), 7.56 (s, 2 H, 4-H, 8-H).

HR-MS (ESI): calc. C$_{27}$H$_{41}$N$_3$NaO$_5$ ([M+Na]$^+$): 510.2944, found: 510.2934.

7,7,9,9-Tetramethyl-7,8,9,11-tetrahydroisoindolo[5,6-*g*]pteridin-2,4-dione (42)
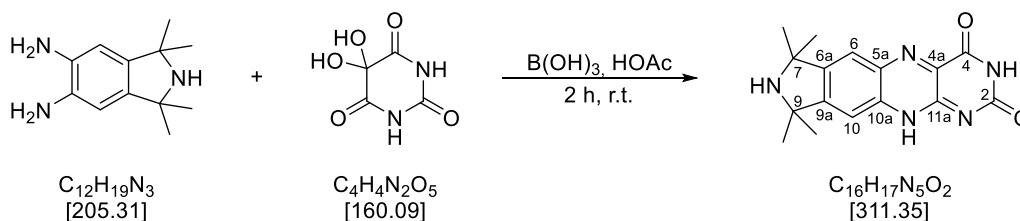
5,6-Diamino-1,1,3,3-tertramethylisoindoline (300 mg, 1.46 mmol, 1.0 eq) was dissolved in HOAc (20 ml) under inert atmosphere and boric acid (139 mg, 2.28 mmol, 1.6 eq) and alloxane hydrate (236 mg, 1.48 mmol, 1.0 eq) were added. After the mixture was stirred for 2 h at room temperature the solvent was removed under reduced pressure. The crude product was used in the next step without further purification.

TLC (DCM/MeOH 9:1 + 1 % NEt$_3$): R_f = 0.37.

^{1}H-NMR (400 MHz, CDCl$_3$ + <u>CD$_3$OD</u>): δ (ppm) = 1.86, 1.87 (2 x s, 12 H, Me), 7.84, 8.09 (2 x s, 2 H, 6-H, 10-H).

^{13}C-NMR (100 MHz, CDCl$_3$ + <u>CD$_3$OD</u>): δ (ppm) = 29.37, 29.49 (Me), 67.34, 67.55 (C-7, C-9), 121.12, 124.00 (C-6, C-10), 140.71, 144.66 (C-5a, C-10a), 145.50, 150.41 (C-6a, C-9a), 130.83, 147.03, 150.60, 161.22 (C-2, C-4, C-4a, C-11a).

HR-MS (ESI): calc. C$_{16}$H$_{18}$N$_5$O$_2$ ([M+H]$^+$): 312.1461, found: 312.1447.

1-*N*-(2',3',5'-Tri-*O*-benzoyl-β-D-ribofuranosyl)-7,7,9,9-tetramethyl-7,8,9,11-tetrahydroisoindolo[5,6-*g*]pteridin-2,4-dione (41)

$C_{16}H_{17}N_5O_2$ [311.35] $C_{28}H_{24}O_9$ [504.49] $C_{42}H_{37}N_5O_9$ [755.78]
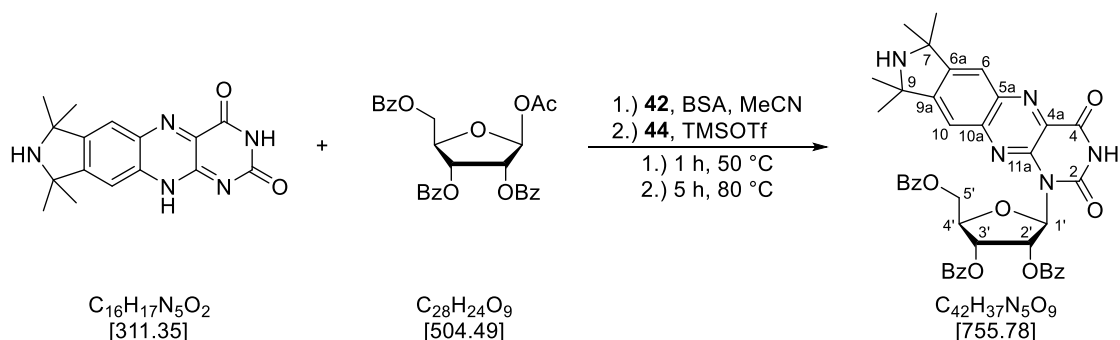
Under inert atmosphere 7,7,9,9-tetramethyl-7,8,9,11-tetrahydroisoindolo[5,6-*g*]pteridin-2,4-dione (767 mg, 2.46 mmol, 1.0 eq) was dissolved in dry MeCN (120 ml). *N*,*O*-Bis(trimethylsilyl)acetamide (4.9 ml, 8.9 mmol, 8.0 eq) was added and the mixture stirred for 1 h at 50 °C. After cooling to room temperature, 1-*O*-acetyl-2,3,5-tri-*O*-benzoyl-β-D-ribofuranose (1.74 g, 3.45 mmol, 1.4 eq) and trimethylsilyl trifluoromethanesulfonate (1.1 ml, 6.6 mmol, 2.7 eq) were added and the mixture stirred for 5 h at 80 °C. After cooling to room temperature, the mixture was poured into sat. aq. NaHCO$_3$, the organic phase washed with brine and the aqueous phases extracted with EtOAc. The combined organic phases were dried over Na$_2$SO$_4$, filtered and the solvent removed under reduced pressure. The crude product was purified by column chromatography (DCM/MeOH 95:5). The product was obtained as a yellow solid (1.02 g, 1.35 mmol, 51 % over 2 steps).

TLC (DCM/MeOH 95:5): R_f = 0.18.

¹H-NMR (400 MHz, CDCl₃): δ (ppm) = 1.86, 1.87 (2 x s, 12 H, Me), 4.60-4.69 (m, 1 H, 5'-Hₐ), 4.77-4.83 (m, 1 H, 4'-H, 5'-Hᵦ), 7.84, 8.09 (2 x s, 2 H, 6-H, 10-H).

¹³C-NMR (100 MHz, CDCl₃): δ (ppm) = 29.63, 29.73, 29.82, 29.94 (Me), 119.92, 124.70 (C-6, C-10), 128.53, 128.59, 129.90 (Bz-CH), 133.18, 133.62, 133.73 (*i*-Bz), 165.47, 165.66, 166.40 (Bz-CO).

HR-MS (ESI): calc. $C_{42}H_{38}N_5O_9$ ([M+H]⁺): 756.2664, found: 756.2675.

1-*N*-β-D-Ribofuranosyl-7,7,9,9-tetramethyl-7,8,9,11-tetrahydroisoindolo[5,6-*g*]pteridin-2,4-dione (45)
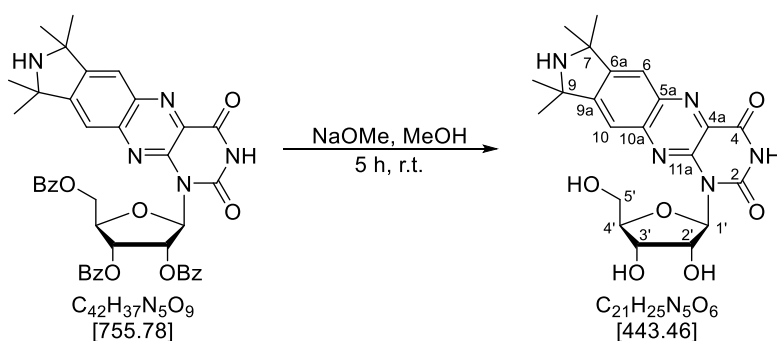
C₄₂H₃₇N₅O₉
[755.78]

C₂₁H₂₅N₅O₆
[443.46]

1-*N*-(2',3',5'-Tri-*O*-benzoyl-β-D-ribofuranosyl)-7,7,9,9-tetramethyl-7,8,9,11-tetrahydroisoindolo[5,6-*g*]pteridin-2,4-dione (276 mg, 0.35 mmol, 1.0 eq) and NaOMe (101 mg, 1.86 mmol, 5.4 eq) were dissolved in MeOH (30 ml) and stirred for 5 h at room temperature. Dowex-H⁺ (632 mg) was washed with MeOH and MeOH/water (1:1) and added to the reaction mixture. After 1 h the Dowex was filtered off, washed with MeOH and MeOH/water (1:1) and the solvent removed under reduced pressure. The product was obtained as a yellow solid (166 mg, quant.) and used for the next step without further purification.

TLC (EtOAc/MeOH 4:1): R_f = 0.19.

¹H-NMR (400 MHz, CD₃OD): δ (ppm) = 1.76 (s, 12 H, Me), 3.75 (dd, *J* = 12.0 Hz, *J* = 5.5 Hz, 1 H, 5'-Hₐ), 3.90 (dd, *J* = 12 Hz, *J* = 2.6 Hz, 1 H, 5'-Hᵦ), 3.94-3.99 (m, 1 H, 4'-H), 4.70 (sᵦᵣ, 1 H, 3'-H), 6.94 (sᵦᵣ, 1 H, 1'-H), 7.96, 8.11 (2 x s, 2 H, 6-H, 10-H).

¹³C-NMR (100 MHz, CD₃OD): δ (ppm) = 30.69 (Me), 63.48 (C-5'), 66.04, 66.28 (C-7, C-9), 71.18 (C-3'), 73.23 (C-2'), 85.54 (C-4'), 90.94 (C-1'), 121.38, 123.68 (C-6, C-10), 140.81, 144.05 (C-5a, C-10a), 150.51, 155.06 (C-6a, C-9a), 129.52, 147.32, 151.11, 161.65 (C-2, C-4, C-4a, C-11a).

HR-MS (ESI): calc. $C_{21}H_{26}N_5O_6$ ([M+H]⁺): 444.18776, found: 444.18845.

1-*N*-(5'-*O*-4,4'-Dimethoxytrityl-β-D-ribofuranosyl)-7,7,9,9-tetramethyl-7,8,9,11-tetrahydroisoindolo[5,6-*g*]pteridin-2,4-dione (46)

$C_{21}H_{25}N_5O_6$
[443.46]

$C_{42}H_{43}N_5O_8$
[745.83]
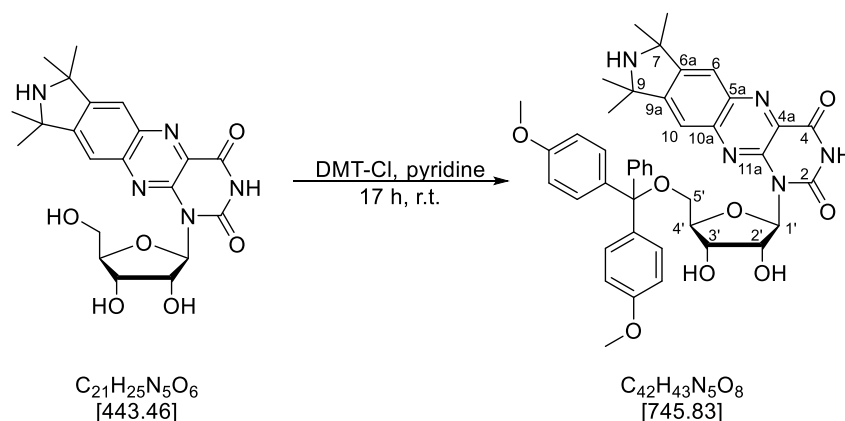
1-*N*-β-D-Ribofuranosyl-7,7,9,9-tetramethyl-7,8,9,11-tetrahydroisoindolo[5,6-*g*]pteridin-2,4-dione (338 mg, 0.76 mmol, 1.0 eq) was dissolved in dry pyridine (30 ml) under inert atmosphere. 4,4'-Dimethoxytrityl chloride (314 mg, 0.92 mmol, 1.2 eq) was added portionwise over 1.5 h and the mixture was stirred for 17 h at room temperature. MeOH was added, the mixture diluted with DCM and washed with cold water and sat. aq. $NaHCO_3$. The organic phase was dried over Na_2SO_4, filtered and the solvent removed under reduced pressure. The crude product was purified by column chromatography (DCM/MeOH 95:5 + 1 % NEt_3). The product was obtained as a yellow solid (386 mg, 0.52 mmol, 68 %).

TLC (DCM/MeOH 95:5 + 1 % NEt_3): R_f = 0.41.

¹H-NMR (400 MHz, $CDCl_3$): δ (ppm) = 1.40, 1.52, 1.52, 1.55 (4 x s, 12 H, Me), 3.42 (dd, *J* = 9.8 Hz, *J* = 4.0 Hz, 1 H, 5'-H$_a$), 3.50 (dd, *J* = 10.0 Hz, *J* = 6.8 Hz, 1 H, 5'-H$_b$), 3.69-3.70 (2 x s, 6 H, DMT-OMe), 4.08-4.14 (m, 1 H, 4'-H), 4.84 (dd, *J* = 7.2 Hz, *J* = 7.2 Hz, 1 H, 3'-H), 4.96 (dd, *J* = 6.8 Hz, *J* = 2.4 Hz, 1 H, 2'-H), 6.64 (dd, *J* = 8.8 Hz, *J* = 8.8 Hz, 4 H, DMT), 6.95 (s$_{br}$, 1 H, 1'-H), 7.03-7.09 (m, 3 H, DMT), 7.25 (dd, *J* = 9.0 Hz, *J* = 3.3 Hz, 3 H, DMT), 7.36 (dd, *J* = 8.0 Hz, *J* = 1.5 Hz, 2 H, DMT), 7.53, 7.96, (s, 2 H, 6-H, 10-H).
¹³C-NMR (100 MHz, $CDCl_3$): δ (ppm) = 31.78, 32.06, 32.09, 32.15 (Me), 45.90 (DMT-OMe), 62.45, 62.75 (C-7, C-9), 65.08 (C-5'), 71.28 (C-3'), 72.57 (C-2'), 82.79 (C-4'), 86.25 (DMT$_{quart}$), 90.30 (C-1'), 112.98 (DMT), 119.40, 122.42 (C-6, C-10), 126.71, 127.66, 128.33, 130.14, 130.23, 136.01, 136.21 (DMT), 139.88, 142.60 (C-5a, C-10a), 144.86 (DMT), 153.03, 157.76 (C-6a, C-9a), 158.41 (DMT), 129.72, 145.47, 151.47, 162.33 (C-2, C-4, C-4a, C-11a).

HR-MS (ESI): calc. $C_{42}H_{44}N_5O_8$ ([M+H]⁺): 746.3184, found: 746.3127.

1-*N*-(5'-*O*-4,4'-Dimethoxytrityl-2'-*O*-*tert*-butyldimethylsilyl-β-ᴅ-ribofuranosyl)-7,7,9,9-tetramethyl-7,8,9,11-tetrahydroisoindolo[5,6-*g*]pteridin-2,4-dione (47)
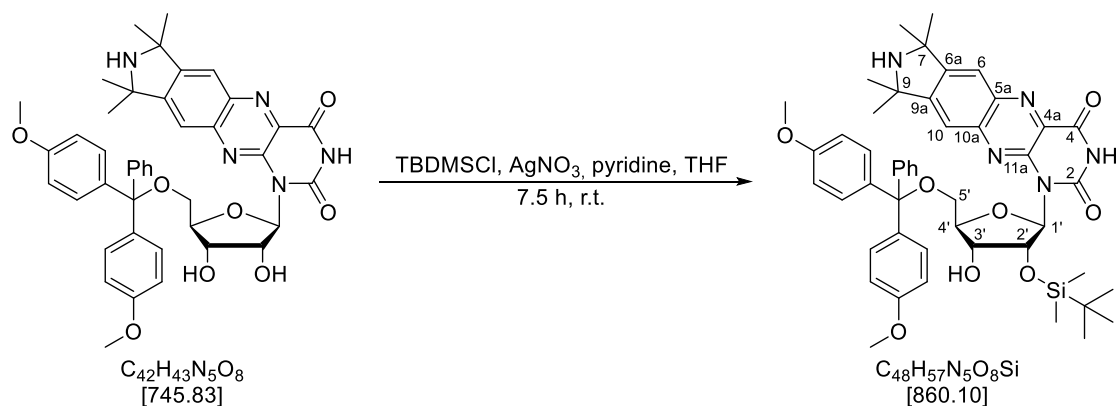
1-*N*-(5'-*O*-4,4'-Dimethoxytrityl-β-ᴅ-ribofuranosyl)-7,7,9,9-tetramethyl-7,8,9,11-tetrahydroisoindolo[5,6-*g*]pteridin-2,4-dione (151 mg, 0.20 mmol, 1.0 eq) was dissolved in dry THF (3 ml) under inert atmosphere. Pyridine (36 mg, 0.46 mmol, 2.3 eq), AgNO$_3$ (52 mg, 0.31 mmol, 1.5 eq) and TBDMSCl (59 mg, 0.40 mmol, 1.9 eq) were added and the mixture was stirred for 7.5 h at room temperature. The mixture was diluted with DCM, filtered over Celite and the filtrate washed with sat. aq. NaHCO$_3$ and brine. The organic phase was dried over Na$_2$SO$_4$, filtered and the solvent removed under reduced pressure. The crude product was purified by column chromatography (DCM/MeOH 98:2 + 1 % NEt$_3$). A mixture of 2'- and 3'-TBDMS isomers was obtained as a yellow solid (113 mg, 0.13 mmol, 65 %).

TLC (DCM/acetone 2:3 + 1 % NEt$_3$): R_f = 0.64 (2'-TBDMS isomer), 0.54 (3'-TBDMS isomer).

^{1}H-NMR (400 MHz, CDCl$_3$): δ (ppm) = 0.03, 0.07 (2 x s, 6 H, TBDMS-Me), 0.86 (s, 9 H, TBDMS-*t*Bu), 1.49, 1.57, 1.59, 1.60 (4 x s, 12 H, Me), 3.33 (dd, *J* = 10.2 Hz, *J* = 6.6 Hz, 1 H, 5'-H$_a$), 3.40 (dd, *J* = 10.4 Hz, *J* = 2.5 Hz, 1 H, 5'-H$_b$), 3.70 (s, 6 H, DMT-OMe), 4.10-4.14 (m, 1 H, 4'-H), 4.75 (s$_{br}$, 1 H, 2'-H), 4.88 (s$_{br}$, 1 H, 3'-H), 6.66 (s$_{br}$, 3 H, DMT), 7.08 (s$_{br}$, 3 H, DMT), 7.27-7.31 (m, 4 H, DMT), 7.37-7.41 (m, 2 H, DMT), 8.05, (s, 1 H, 6-H,).

^{13}C-NMR (100 MHz, CDCl$_3$): δ (ppm) = -4.73, -4.66 (TBDMS-Me), 18.11 (TBDMS$_{quart}$), 25.82 (TBDMS-*t*Bu), 31.86, 32.04, 32.08, 32.15 (Me), 55.26 (DMT-OMe), 62.63, 62.86 (C-7, C-9), 64.12 (C-5'), 71.67 (C-3'), 72.90 (C-2'), 82.88 (C-4'), 86.27 (DMT$_{quart}$), 113.00 (DMT), 122.62 (C-6), 126.70 (DMT), 127.69, 128.33, 130.14, 130.21 (DMT), 136.03, 136.13 (DMT), 142.75 (C-5a), 144.77 (DMT), 153.84 (C-6a), 158.41 (DMT), 158.70 (C-10a), 145.12, 159.30 (C-2, C-4, C-4a, C-11a).

HR-MS (ESI): calc. C$_{96}$H$_{114}$N$_{10}$NaO$_{16}$Si$_2$ ([2M+Na]$^+$): 1741.7845, found: 1741.7995.

5.5 Characterization of oligonucleotides

5.5.1 ESI-MS

Table 7: Mass of oligonucleotides I, III, V, VI, VII, XI and XIV calculated and measured by ESI-MS.

Name	5'-sequence-3'	calc. Mass [Da]	meas. mass [Da]
I	GACGTCGGAAGACGTCAGTA	6188.08110	6188.10978
III	GACGTB^{S}GGAAGACGTCAGTA	6379.22469	6379.25611
V	TACTGACGTCTTCCm^{6}GACGTC	6055.04361	6055.07142
VI	TACTGACGTCTTCCm^{6DA}PACGTC	6054.05959	6054.07929
VII	TACTGACGTCTTCCAACGTC	6025.03304	6025.06129
XI	FAM-Alk-CTGTAATACGACTCACTATA	6675.33015	6672.30726
XIV	FAM-Alk-UAAUACGACUCACUAUA	5955.00015	5954.97581

5.5.2 HPLC and HPLC-MS chromatograms
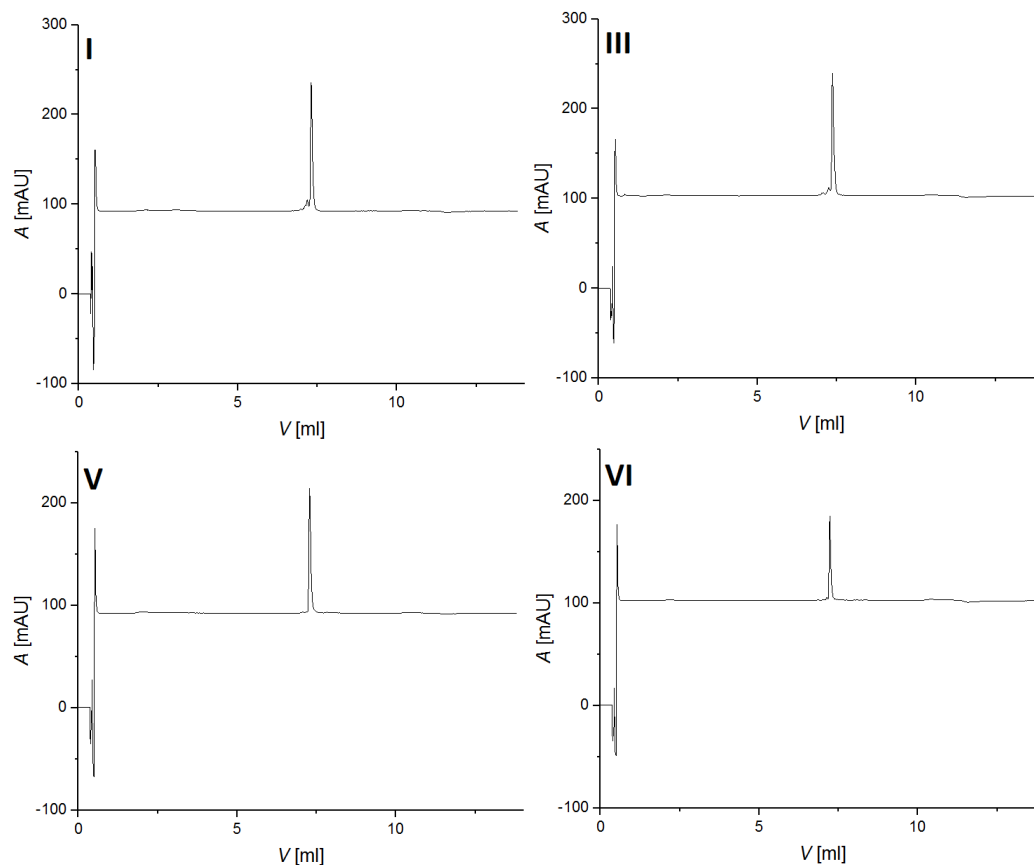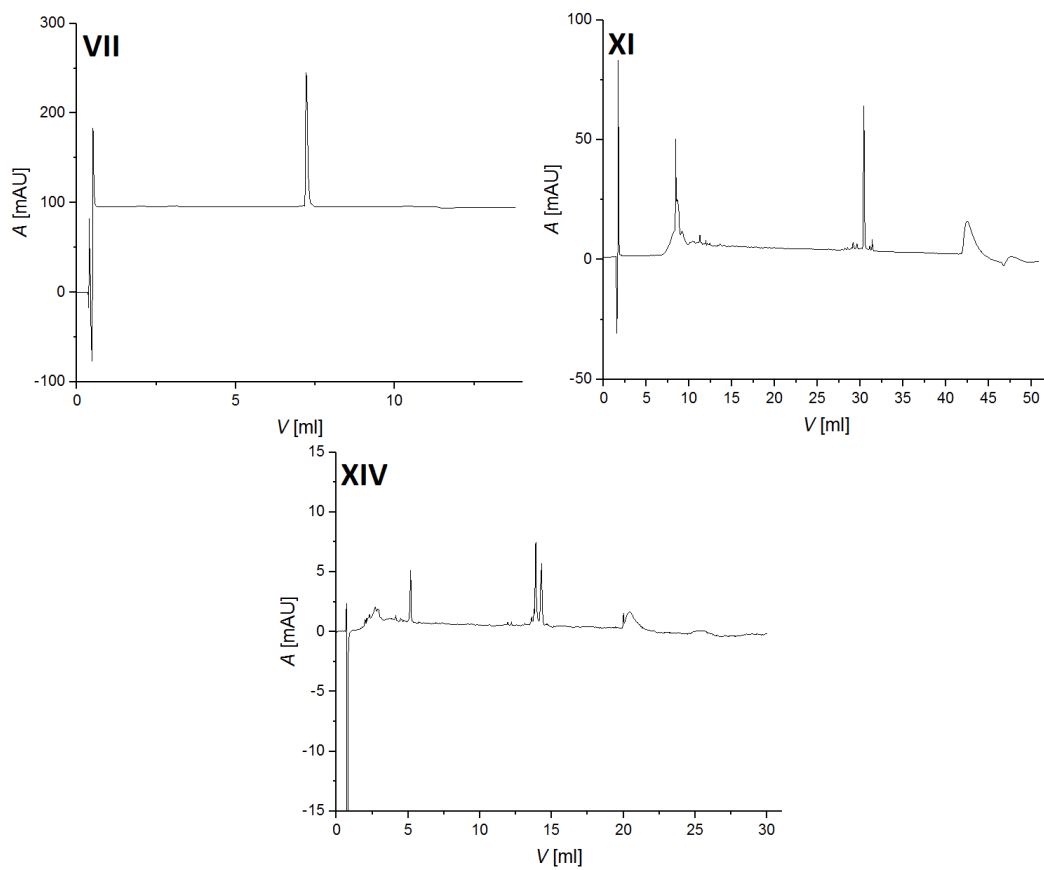
Fig. 135: HPLC chromatograms of oligonucleotides I, III, V, VI, VII, (2 x 250 mm column) and XI, XIV (4 x 250 mm column) (Buffer A: 25 mM Tris HCl, 6 M urea, pH 8.0; Buffer B: 25 mM Tris HCl, 6 M urea, 0.5 M NaClO₄, pH 8.0; 60 °C), 0 % to 48 % B in A in 12 CV.

5.6 EPR spectra with simulations
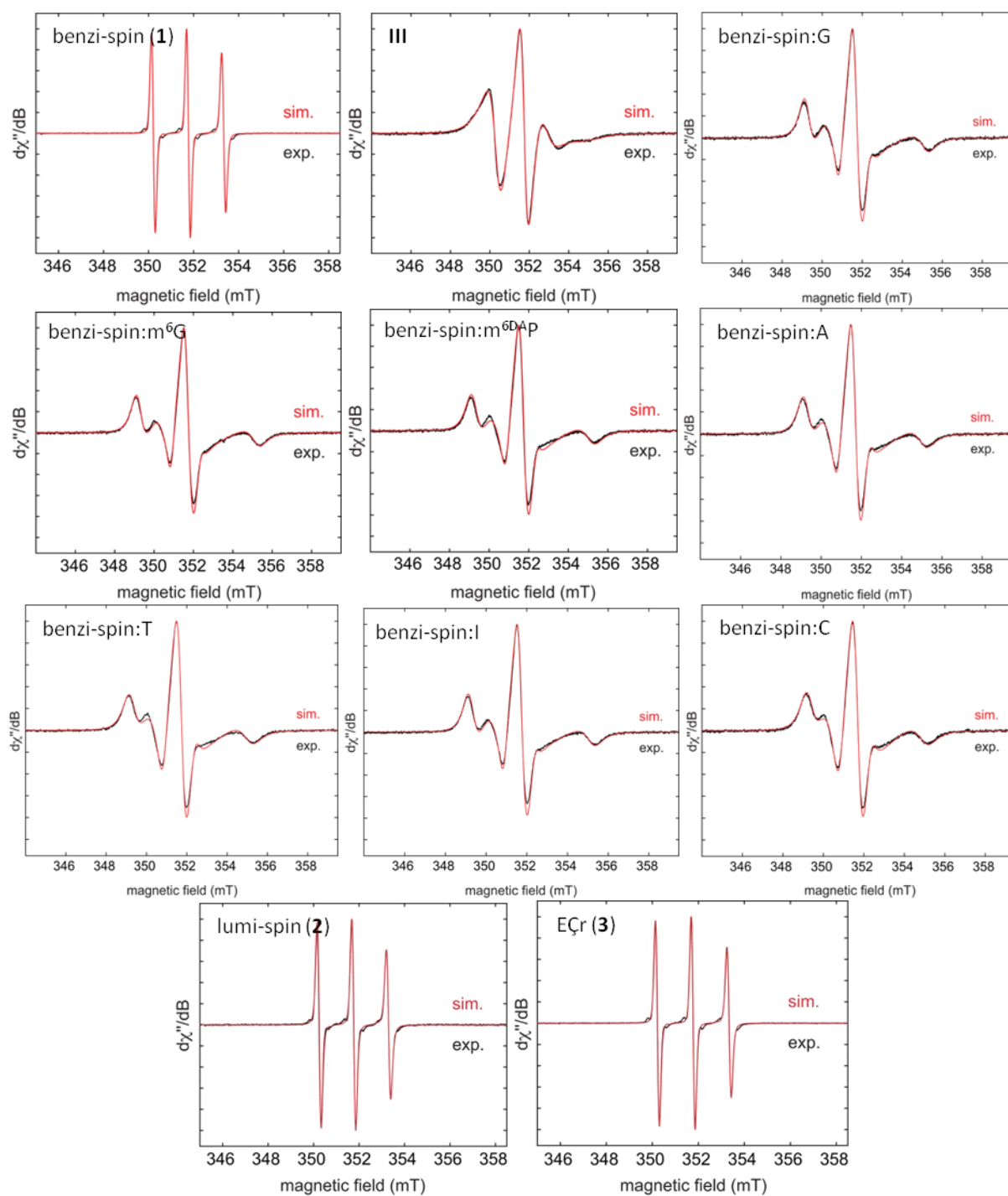
Fig. 136: Measured (black) and simulated (red) CW EPR spectra of benzi-spin (1) (g_{iso} = 2.0056, $a_{iso}(^{14}N)$ = 1.57 mT, $\tau_r \approx$ 100 ps), benzi-spin containing oligonucleotide III as a single strand and as double strands paired with IV-XI, lumi-spin (2) (g_{iso} = 2.0056, $a_{iso}(^{14}N)$ = 1.53 mT, $\tau_r \approx$ 100 ps) and EÇr (3) (g_{iso} = 2.0056, $a_{iso}(^{14}N)$ = 1.56 mT, $\tau_r \approx$ 100 ps).

5.7 EPR simulation parameters

Table 8: EPR simulation parameters (*g* values, hyperfine coupling constants, central line widths, spectral widths and rotational correlation times) for the spin labels and spin labeled oligonucleotides in phosphate buffer solution at 293 K.

Sample	*g* values	*A* [MHz]	$2A_{zz}$ [mT]	ΔH_0 [mT]	τ_r
Benzi-spin	$g_x = 2.0076$	$A_{xx} = 12$	7.7	0.17	93 ps
	$g_y = 2.0063$	$A_{yy} = 11$			
	$g_z = 2.0029$	$A_{zz} = 108$			
Flavi-spin	$g_x = 2.0090$	$A_{xx} = 10$	7.6	0.17	117 ps
	$g_y = 2.0056$	$A_{yy} = 12$			
	$g_z = 2.0023$	$A_{zz} = 106$			
EÇr	$g_x = 2.0083$	$A_{xx} = 11$	7.7	0.17	117 ps
	$g_y = 2.0061$	$A_{yy} = 13$			
	$g_z = 2.0024$	$A_{zz} = 107$			
III	$g_x = 2.0082$	$A_{xx} = 12$	7.5	0.43	3.1 ns
	$g_y = 2.0061$	$A_{yy} = 16$			
	$g_z = 2.0024$	$A_{zz} = 105$			
III:IV	$g_x = 2.0075$	$A_{xx} = 20$	7.0	0.49	12 ns
	$g_y = 2.0069$	$A_{yy} = 13$			
	$g_z = 2.0024$	$A_{zz} = 98$			
III:V	$g_x = 2.0078$	$A_{xx} = 20$	7.1	0.49	10 ns
	$g_y = 2.0068$	$A_{yy} = 10$			
	$g_z = 2.0023$	$A_{zz} = 100$			
III:VI	$g_x = 2.0076$	$A_{xx} = 21$	7.1	0.49	9.3 ns
	$g_y = 2.0068$	$A_{yy} = 9$			
	$g_z = 2.0023$	$A_{zz} = 100$			
III:VII	$g_x = 2.0075$	$A_{xx} = 21$	7.0	0.50	9.7 ns
	$g_y = 2.0069$	$A_{yy} = 11$			
	$g_z = 2.0023$	$A_{zz} = 98$			
III:VIII	$g_x = 2.0075$	$A_{xx} = 21$	7.1	0.51	8.5 ns
	$g_y = 2.0069$	$A_{yy} = 10$			
	$g_z = 2.0022$	$A_{zz} = 99$			
III:IX	$g_x = 2.0075$	$A_{xx} = 20$	7.0	0.50	11 ns
	$g_y = 2.0069$	$A_{yy} = 11$			
	$g_z = 2.0022$	$A_{zz} = 99$			
III:X	$g_x = 2.0074$	$A_{xx} = 22$	6.9	0.52	8.5 ns
	$g_y = 2.0070$	$A_{yy} = 10$			
	$g_z = 2.0023$	$A_{zz} = 97$			

5.8 HPLC-MS chromatograms of compound 1a
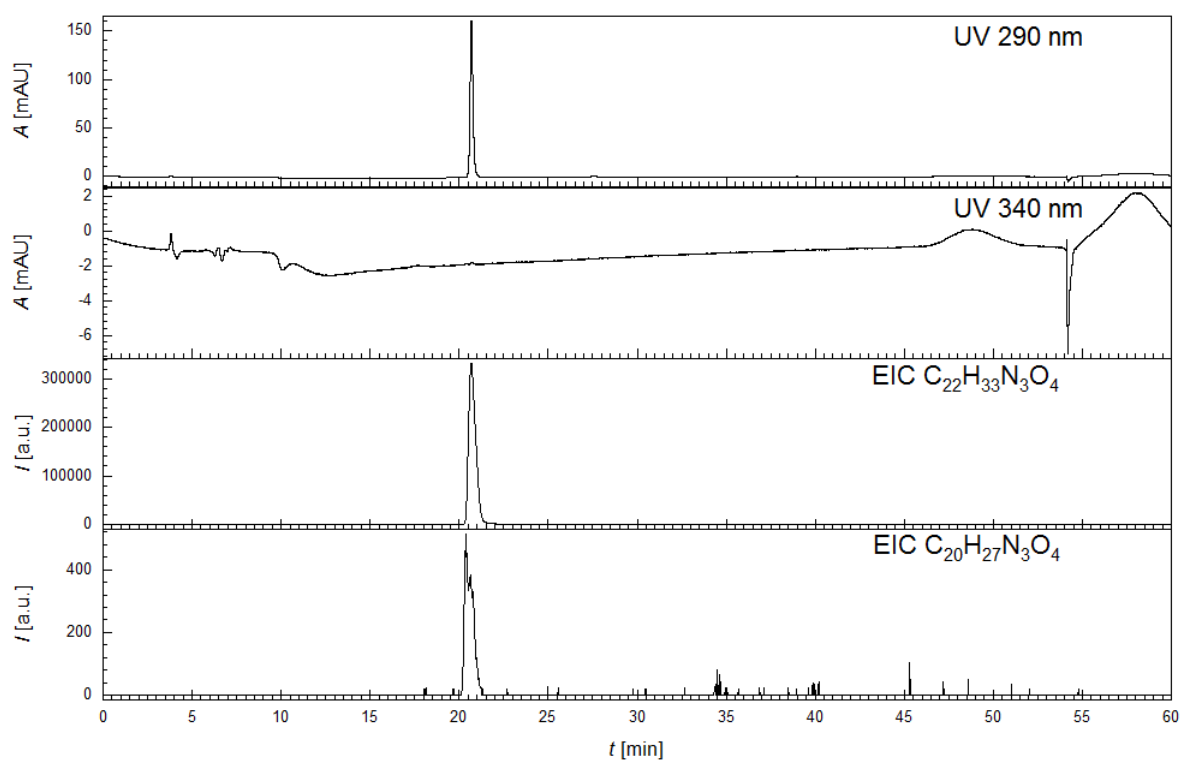
Fig. 137: HPLC-MS chromatograms of nucleoside 1a. Phenomenex Synergi 4 μm Fusion-RP 80 Å 2 x 25 mm column (Buffer A: 10 mM NH$_4$OAc pH 5.4; Buffer B: MeCN, 25 °C), 0 % to 70 % B in A in 35 min.
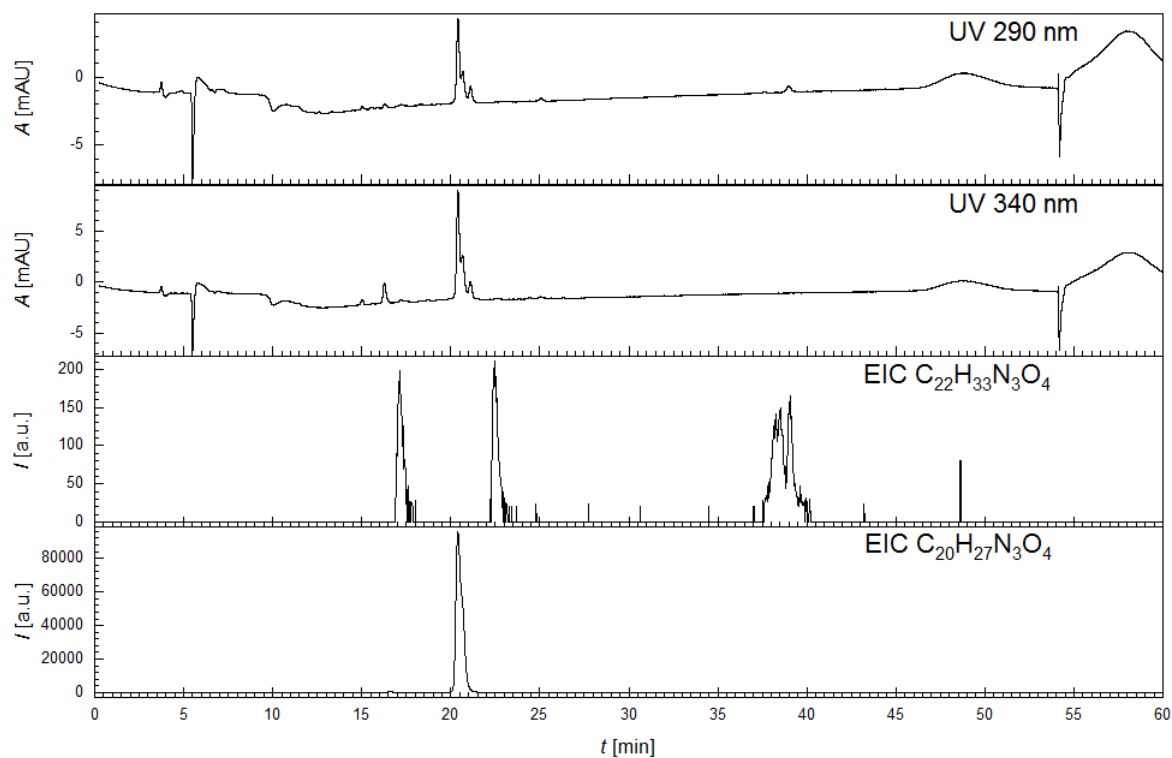
Fig. 138: HPLC-MS chromatograms of an irradiated sample (16 h, 290 nm) of nucleoside 1a. Phenomenex Synergi 4 μm Fusion-RP 80 Å 2 x 25 mm column (Buffer A: 10 mM NH$_4$OAc pH 5.4; Buffer B: MeCN, 25 °C), 0 % to 70 % B in A in 35 min.

6 Abbreviations

A	adenosine
A	hyperfine coupling constant
A	absorbance
Å	Ångström
A_{min}	minimal absorbance
Ac	acetyl
ac	acetyl
Ac_2O	acetic anhydride
a_{iso}	isotropic hyperfine coupling constant
Alk	alkyl linker
AP	apurinic/apyrimidinic
APE1	human apurinic/apyrimidinic endonuclease 1
aq.	aqueous
ASO	antisense oligonucleotide
ATP	adenosine triphosphate
AU	absorbance units
a.u.	arbitrary units
B	magnetic field
β_e	Bohr magneton
Boc	*tert*-butyloxycarbonyl
Boc_2O	di-*tert*-butyl dicarbonate
bp	base pairs
B^S	benzi-spin
BSA	*N,O*-bis(trimethylsilyl)acetamide
BTT	5-benzylthio-(1*H*)-tetrazole
Bu	butyl
Bz	benzoyl
bz	benzoyl
C	cytidine
°C	degrees Celsius
calc.	calculated
CEP	*O*-β-cyanoethyl-*N,N*-diisopropylphosphoramidite
CDI	1,1'-carbonyldiimidazole
cm	centimeters
conc.	concentrated
COSY	correlation spectroscopy
CPG	controlled pore glass
C^T	C^{TEMPO}
CTP	cytidine triphosphate
CuAAC	copper(I)-catalyzed azide-alkyne cycloaddition
CV	column volumes
CW	continuous wave
d	doublet
d	deoxy

δ	chemical shift
^{DA}P	diaminopurine ribonucleotide
dATP	deoxyadenosine triphosphate
DBH	1,3-dibromo-5,5-dimethylhydantoin
DCA	dichloroacetic acid
dCTP	deoxycytidine triphosphate
DCE	1,2-dichloroethane
$d\chi''/dB$	derivative of the imaginary part of the molecular magnetic susceptibility with respect to the external static magnetic field
DCM	dichloromethane
dd	doublet of doublets
DDQ	2,3-dichloro-5,6-dicano-1,4-benzoquinone
ΔE	energy difference
DEC	diethyl carbonate
DEER	double electron-electron resonance
dGTP	deoxyguanosine triphosphate
ΔH_0	peak-to-peak line width of the central line
DIPEA	diisopropylethylamine
dm	decimeters
DMAP	4-(dimetylamino)pyridine
DMF	dimethyl formamide
dmf	N,N-dimethylformamidine
DMHBI	dimethoxyhydroxybenzylidene imidazolone
DMSO	dimethyl sulfoxide
DMT	1,1'-dimethoxytrityl
DNA	deoxyribonucleic acid
DNAzyme	deoxyribozyme
dNTP	deoxynucleotide triphosphate
dq	doublet of quartets
dTTP	deoxythymidine triphosphate
ε	extinction coefficient
EDTA	ethylenediamine tetraacetic acid
EIC	extracted ion chromatogram
EPR	electron paramagnetic spectroscopy
eq	equivalents
em.	emission
ESI	electrospray ionization
Et	ethyl
EtOH	ethanol
Et_2O	diethyl ether
EtOAc	ethyl acetate
ETT	5-ethylthio-($1H$)-tetrazole
exc.	excitation
FAM	6-carboxyfluorescein
FRET	fluorescence resonance energy transfer/Förster resonance energy transfer
G	guanosine
G	Gauss
g	grams
g	g-factor

γ	gyromagnetic ratio
GFP	green fluorescent protein
GHz	gigahertz
g_{iso}	isotropic g-factor
GTP	guanosine triphosphate
h	hours
h	Planck constant
ℏ	reduced Planck constant
HBI	hydroxybenzylidene imidazolone
HIV	human immunodeficiency virus
HMBC	heteronuclear multiple bond correlation
HMDS	1,1,1,3,3,3-hexamethyldisilazane
HOAc	acetic acid
HPLC	high performance liquid chromatography
HPLC-MS	high performance liquid chromatography coupled with mass spectrometry
HR-MS	high resolution mass spectrometry
HSQC	heteronuclear single quantum correlation
Hyp	hyperchromicity
Hz	hertz
I	nuclear spin
I	intensity
i	ipso
i^6A	N^6-isopentenyladenosine
iEDDA	inverse electron demand Diels-Alder
J	coupling constant
K	Kelvin
kHz	kilohertz
KOtBu	potassium $tert$-butoxide
λ	wavelength
M	molecular ion peak
M	moles per liter
m	multiplet
m	meta
μ_0	vacuum permeability
mCPBA	metachloroperbenzoic acid
m6^{DA}P	N-6-methyldiaminopurine deoxyribonucleoside
Me	methyl
MeCN	acetonitrile
Me$_2$NEt	dimethylethylamine
MeOH	methanol
mg	milligrams
m^{6}A	N^6-methyladenosine
m^{6}G	O^6-methylguanosine
MHz	megahertz
min	minutes

ml	milliliters
μl	microliters
μm	micrometers
mM	millimoles per liter
mmol	millimoles
mRNA	messenger RNA
MS	mass spectrometry
ms	milliseconds
mT	millitesla
mW	milliwatt
m/z	mass/charge
ν	frequency
ν_{dd}	dipolar coupling frequency
NAM	naphthalene methoxide
NaOMe	sodium methoxide
NBu_3	tributylamine
*n*BuOH	*n*-butanol
NBu_4OH	tetrabutylammonium hydroxide
$(NBu_4)_2PP_i$	bis(tetrabutylammonium) pyrophosphate
NEt_3	triethylamine
nm	nanometers
NMI	1-methylimidazole
NMR	nuclear magnetic resonance
No.	number
NOESY	nuclear Overhauser enhancement and exchange spectroscopy
ns	nanoseconds
nt	nucleotides
NTP	nucleotide triphosphate
o	ortho
OTf	trifluoromethanesulfonate
p	para
PCR	polymerase chain reaction
PEG	polyethylene glykol
PELDOR	pulsed electron-electron double resonance
Ph	phenyl
pH	power of hydrogen
PP_i	pyrophosphate
ppm	parts per million
ps	picoseconds
quant.	quantitative
quart	quarternary
r_{AB}	interspin distance
R_f	retention factor
RBD	RNA-binding domain
RNA	ribonucleic acid

rRNA	ribosomal RNA
r.t.	room temperature
S	electron spin angular momentum
s	singlet
SAM	S-adenosyl methionine
sat.	saturated
s_{br}	broad singlet
SD	Shine-Dalgarno
SELEX	systematic evolution of ligands by exponential enrichment
S_N1	nucleophilic substitution of first order
S_N2	nucleophilic substitution of second order
SPS	solid-phase synthesis
ssNMR	solid-state NMR
T	thymidine
t	triplet
t	pump pulse time
ϑ	temperature
θ	angle between r_{AB} and B_0
τ	evolution time
TAM	tetrathiatriarylmethyl
TAR	trans-activation responsive
TBAF	tetrabutylammonium fluoride
TBDMS	$tert$-butyldimethylsilyl
TBE	Tris borate EDTA
tBu	$tert$-butyl
TCA	trichloroacetic acid
TEAB	triethylammonium bicarbonate
TEMPO	2,2,6,6-tetramethylpiperidin-1-yloxyl
TEMPOL	4-hydroxy-2,2,6,6-tetramethylpiperidin-1-yloxyl
TEN	Tris EDTA sodium chloride
THF	tetrahydrofurane
TLC	thin layer chromatography
T_m	melting temperature
T_m	phase memory time
TMHI	trimethylhydrazinium iodide
TMR	tetramethylrosamine
TMS	trimethylsilyl
TMSOTf	trimethylsilyl trifluoromethanesulfonate
TO	thiazole orange
Tol	toluoyl
TOM	tri-isoproplysilyl-oxymethyl
TPP	thiamine pyrophosphate
TPT	thienopyridinethione
τ_r	rotational correlation time
Tris	tris(hydroxymethyl)aminomethane
tRNA	transfer RNA
TTP	thymidine triphosphate
U	uridine
U	units

UV	ultraviolet
V	PELDOR signal amplitude
W	Watt
2A_{zz}	spectral width
4CI	4-cyanoindole
%	percent

7 Figures

8 Tables

9 References

1.   Mironov, A. S.; Gusarov, I.; Rafikov, R.; Lopez, L. E.; Shatalin, K.; Kreneva, R. A.; Perumov, D. A.; Nudler, E., Sensing small molecules by nascent RNA: a mechanism to control transcription in bacteria. *Cell* **2002,** *111* (5), 747-56.

2.   Nudler, E.; Gottesman, M. E., Transcription termination and anti-termination in E. coli. *Genes Cells* **2002,** *7* (8), 755-68.

3.   Winkler, W.; Nahvi, A.; Breaker, R. R., Thiamine derivatives bind messenger RNAs directly to regulate bacterial gene expression. *Nature* **2002,** *419* (6910), 952-6.

4.   Winkler, W. C.; Breaker, R. R., Genetic control by metabolite-binding riboswitches. *Chembiochem* **2003,** *4* (10), 1024-32.

5.   Sherwood, A. V.; Henkin, T. M., Riboswitch-Mediated Gene Regulation: Novel RNA Architectures Dictate Gene Expression Responses. *Annu Rev Microbiol* **2016,** *70*, 361-74.

6.   Roth, A.; Breaker, R. R., The structural and functional diversity of metabolite-binding riboswitches. *Annu Rev Biochem* **2009,** *78*, 305-34.

7.   McCown, P. J.; Corbino, K. A.; Stav, S.; Sherlock, M. E.; Breaker, R. R., Riboswitch diversity and distribution. *RNA* **2017,** *23* (7), 995-1011.

8.   Hallberg, Z. F.; Su, Y.; Kitto, R. Z.; Hammond, M. C., Engineering and In Vivo Applications of Riboswitches. *Annu Rev Biochem* **2017,** *86*, 515-39.

9.   Dixon, N.; Duncan, J. N.; Geerlings, T.; Dunstan, M. S.; McCarthy, J. E.; Leys, D.; Micklefield, J., Reengineering orthogonally selective riboswitches. *Proc Natl Acad Sci U S A* **2010,** *107* (7), 2830-5.

10.   Suess, B.; Fink, B.; Berens, C.; Stentz, R.; Hillen, W., A theophylline responsive riboswitch based on helix slipping controls gene expression in vivo. *Nucleic Acids Res* **2004,** *32* (4), 1610-4.

11.   Tuerk, C.; Gold, L., Systematic evolution of ligands by exponential enrichment: RNA ligands to bacteriophage T4 DNA polymerase. *Science* **1990,** *249* (4968), 505-10.

12.   Breuers, S.; Bryant, L. L.; Legen, T.; Mayer, G., Robotic assisted generation of 2'-deoxy-2'-fluoro-modifed RNA aptamers - High performance enabling strategies in aptamer selection. *Methods* **2019,** *161*, 3-9.

13.   Ni, S.; Zhuo, Z.; Pan, Y.; Yu, Y.; Li, F.; Liu, J.; Wang, L.; Wu, X.; Li, D.; Wan, Y.; Zhang, L.; Yang, Z.; Zhang, B. T.; Lu, A.; Zhang, G., Recent Progress in Aptamer Discoveries and Modifications for Therapeutic Applications. *ACS Appl Mater Interfaces* **2021,** *13* (8), 9500-19.

14.   Ng, E. W.; Shima, D. T.; Calias, P.; Cunningham, E. T., Jr.; Guyer, D. R.; Adamis, A. P., Pegaptanib, a targeted anti-VEGF aptamer for ocular vascular disease. *Nat Rev Drug Discov* **2006,** *5* (2), 123-32.

15.   He, F.; Wen, N.; Xiao, D.; Yan, J.; Xiong, H.; Cai, S.; Liu, Z.; Liu, Y., Aptamer-Based Targeted Drug Delivery Systems: Current Potential and Challenges. *Curr Med Chem* **2020,** *27* (13), 2189-219.

16.   Babendure, J. R.; Adams, S. R.; Tsien, R. Y., Aptamers switch on fluorescence of triphenylmethane dyes. *J Am Chem Soc* **2003,** *125* (48), 14716-7.

17.   Ellington, A. D.; Szostak, J. W., In vitro selection of RNA molecules that bind specific ligands. *Nature* **1990,** *346* (6287), 818-22.

18.   Holeman, L. A.; Robinson, S. L.; Szostak, J. W.; Wilson, C., Isolation and characterization of fluorophore-binding RNA aptamers. *Fold Des* **1998,** *3* (6), 423-31.

19.   Baugh, C.; Grate, D.; Wilson, C., 2.8 A crystal structure of the malachite green aptamer. *J Mol Biol* **2000,** *301* (1), 117-28.

20.   Dolgosheina, E. V.; Jeng, S. C.; Panchapakesan, S. S.; Cojocaru, R.; Chen, P. S.; Wilson, P. D.; Hawkins, N.; Wiggins, P. A.; Unrau, P. J., RNA mango aptamer-fluorophore: a bright, high-affinity complex for RNA labeling and tracking. *ACS Chem Biol* **2014,** *9* (10), 2412-20.

21.   Autour, A.; S, C. Y. J.; A, D. C.; Abdolahzadeh, A.; Galli, A.; Panchapakesan, S. S. S.; Rueda, D.; Ryckelynck, M.; Unrau, P. J., Fluorogenic RNA Mango aptamers for imaging small non-coding RNAs in mammalian cells. *Nat Commun* **2018,** *9* (1), 656-68.

22.   Paige, J. S.; Wu, K. Y.; Jaffrey, S. R., RNA mimics of green fluorescent protein. *Science* **2011,** *333* (6042), 642-6.

23.   Trachman, R. J.; Ferre-D'Amare, A. R., Tracking RNA with light: selection, structure, and design of fluorescence turn-on RNA aptamers. *Q Rev Biophys* **2019,** *52*, e8.

24.   Steinmetzger, C.; Palanisamy, N.; Gore, K. R.; Höbartner, C., A Multicolor Large Stokes Shift Fluorogen-Activating RNA Aptamer with Cationic Chromophores. *Chemistry* **2019,** *25* (8), 1931-5.

25.   Steinmetzger, C.; Bessi, I.; Lenz, A. K.; Höbartner, C., Structure-fluorescence activation relationships of a large Stokes shift fluorogenic RNA aptamer. *Nucleic Acids Res* **2019,** *47* (22), 11538-50.

26.   Kruger, K.; Grabowski, P. J.; Zaug, A. J.; Sands, J.; Gottschling, D. E.; Cech, T. R., Self-splicing RNA: autoexcision and autocyclization of the ribosomal RNA intervening sequence of Tetrahymena. *Cell* **1982,** *31* (1), 147-57.

27.   Guerrier-Takada, C.; Gardiner, K.; Marsh, T.; Pace, N.; Altman, S., The RNA moiety of ribonuclease P is the catalytic subunit of the enzyme. *Cell* **1983,** *35* (3 Pt 2), 849-57.

28.   Micura, R.; Höbartner, C., Fundamental studies of functional nucleic acids: aptamers, riboswitches, ribozymes and DNAzymes. *Chem Soc Rev* **2020,** *49* (20), 7331-53.

29.   Ban, N.; Nissen, P.; Hansen, J.; Moore, P. B.; Steitz, T. A., The complete atomic structure of the large ribosomal subunit at 2.4 A resolution. *Science* **2000,** *289* (5481), 905-20.

30.   Nissen, P.; Hansen, J.; Ban, N.; Moore, P. B.; Steitz, T. A., The structural basis of ribosome activity in peptide bond synthesis. *Science* **2000,** *289* (5481), 920-30.

31.   Ferre-D'Amare, A. R.; Scott, W. G., Small self-cleaving ribozymes. *Cold Spring Harb Perspect Biol* **2010,** *2* (10), a003574.

32.   Roth, A.; Weinberg, Z.; Chen, A. G.; Kim, P. B.; Ames, T. D.; Breaker, R. R., A widespread self-cleaving ribozyme class is revealed by bioinformatics. *Nat Chem Biol* **2014,** *10* (1), 56-60.

33.   Weinberg, Z.; Kim, P. B.; Chen, T. H.; Li, S.; Harris, K. A.; Lünse, C. E.; Breaker, R. R., New classes of self-cleaving ribozymes revealed by comparative genomics analysis. *Nat Chem Biol* **2015,** *11* (8), 606-10.

34.   Serganov, A.; Patel, D. J., Ribozymes, riboswitches and beyond: regulation of gene expression without proteins. *Nat Rev Genet* **2007,** *8* (10), 776-90.

35.   Kazantsev, A. V.; Rambo, R. P.; Karimpour, S.; Santalucia, J., Jr.; Tainer, J. A.; Pace, N. R., Solution structure of RNase P RNA. *RNA* **2011,** *17* (6), 1159-71.

36.   Breaker, R. R.; Emilsson, G. M.; Lazarev, D.; Nakamura, S.; Puskarz, I. J.; Roth, A.; Sudarsan, N., A common speed limit for RNA-cleaving ribozymes and deoxyribozymes. *RNA* **2003,** *9* (8), 949-57.

37.   Breaker, R. R.; Joyce, G. F., A DNA enzyme that cleaves RNA. *Chem Biol* **1994,** *1* (4), 223-9.

38.   Santoro, S. W.; Joyce, G. F., A general purpose RNA-cleaving DNA enzyme. *Proc Natl Acad Sci U S A* **1997,** *94* (9), 4262-6.

39.   Sednev, M. V.; Mykhailiuk, V.; Choudhury, P.; Halang, J.; Sloan, K. E.; Bohnsack, M. T.; Höbartner, C., N^6-Methyladenosine-Sensitive RNA-Cleaving Deoxyribozymes. *Angew Chem Int Ed Engl* **2018,** *57* (46), 15117-121.

40.   Liaqat, A.; Stiller, C.; Michel, M.; Sednev, M. V.; Höbartner, C., N^6-Isopentenyladenosine in RNA Determines the Cleavage Site of Endonuclease Deoxyribozymes. *Angew Chem Int Ed Engl* **2020,** *59* (42), 18627-31.

41.   Purtha, W. E.; Coppins, R. L.; Smalley, M. K.; Silverman, S. K., General deoxyribozyme-catalyzed synthesis of native 3'-5' RNA linkages. *J Am Chem Soc* **2005,** *127* (38), 13124-5.

42.   Büttner, L.; Javadi-Zarnaghi, F.; Höbartner, C., Site-specific labeling of RNA at internal ribose hydroxyl groups: terbium-assisted deoxyribozymes at work. *J Am Chem Soc* **2014,** *136* (22), 8131-7.

43.   Ghaem Maghami, M.; Dey, S.; Lenz, A. K.; Höbartner, C., Repurposing Antiviral Drugs for Orthogonal RNA-Catalyzed Labeling of RNA. *Angew Chem Int Ed Engl* **2020,** *59* (24), 9335-9.

44.   Ghaem Maghami, M.; Scheitl, C. P. M.; Höbartner, C., Direct in Vitro Selection of Trans-Acting Ribozymes for Posttranscriptional, Site-Specific, and Covalent Fluorescent Labeling of RNA. *J Am Chem Soc* **2019,** *141* (50), 19546-9.

45.   Trachman, R. J., 3rd; Abdolahzadeh, A.; Andreoni, A.; Cojocaru, R.; Knutson, J. R.; Ryckelynck, M.; Unrau, P. J.; Ferre-D'Amare, A. R., Crystal Structures of the Mango-II RNA Aptamer

Reveal Heterogeneous Fluorophore Binding and Guide Engineering of Variants with Improved Selectivity and Brightness. *Biochemistry* **2018,** *57* (26), 3544-8.

46.   Trachman, R. J., 3rd; Stagno, J. R.; Conrad, C.; Jones, C. P.; Fischer, P.; Meents, A.; Wang, Y. X.; Ferre-D'Amare, A. R., Co-crystal structure of the iMango-III fluorescent RNA aptamer using an X-ray free-electron laser. *Acta Crystallogr F Struct Biol Commun* **2019,** *75* (Pt 8), 547-51.

47.   Huang, H.; Suslov, N. B.; Li, N. S.; Shelke, S. A.; Evans, M. E.; Koldobskaya, Y.; Rice, P. A.; Piccirilli, J. A., A G-quadruplex-containing RNA activates fluorescence in a GFP-like fluorophore. *Nat Chem Biol* **2014,** *10* (8), 686-91.

48.   Warner, K. D.; Sjekloca, L.; Song, W.; Filonov, G. S.; Jaffrey, S. R.; Ferre-D'Amare, A. R., A homodimer interface without base pairs in an RNA mimic of red fluorescent protein. *Nat Chem Biol* **2017,** *13* (11), 1195-201.

49.   Ponce-Salvatierra, A.; Wawrzyniak-Turek, K.; Steuerwald, U.; Höbartner, C.; Pena, V., Crystal structure of a DNA catalyst. *Nature* **2016,** *529* (7585), 231-4.

50.   Borman, S., After Two Decades Of Trying, Scientists Report First Crystal Structure Of A DNAzyme. *Chemical & Engineering News* 7.1.2016, 2016, p 3.

51.   Ota, N.; Hirano, K.; Warashina, M.; Andrus, A.; Mullah, B.; Hatanaka, K.; Taira, K., Determination of interactions between structured nucleic acids by fluorescence resonance energy transfer (FRET): selection of target sites for functional nucleic acids. *Nucleic Acids Res* **1998,** *26* (3), 735-43.

52.   Bood, M.; Sarangamath, S.; Wranne, M. S.; Grotli, M.; Wilhelmsson, L. M., Fluorescent nucleobase analogues for base-base FRET in nucleic acids: synthesis, photophysics and applications. *Beilstein J Org Chem* **2018,** *14*, 114-29.

53.   Füchtbauer, A. F.; Wranne, M. S.; Bood, M.; Weis, E.; Pfeiffer, P.; Nilsson, J. R.; Dahlen, A.; Grotli, M.; Wilhelmsson, L. M., Interbase FRET in RNA: from A to Z. *Nucleic Acids Res* **2019,** *47* (19), 9990-7.

54.   Borjesson, K.; Preus, S.; El-Sagheer, A. H.; Brown, T.; Albinsson, B.; Wilhelmsson, L. M., Nucleic acid base analog FRET-pair facilitating detailed structural measurements in nucleic acid containing systems. *J Am Chem Soc* **2009,** *131* (12), 4288-93.

55.   Wranne, M. S.; Füchtbauer, A. F.; Dumat, B.; Bood, M.; El-Sagheer, A. H.; Brown, T.; Graden, H.; Grotli, M.; Wilhelmsson, L. M., Toward Complete Sequence Flexibility of Nucleic Acid Base Analogue FRET. *J Am Chem Soc* **2017,** *139* (27), 9271-80.

56.   Dumas, A.; Luedtke, N. W., Fluorescence properties of 8-(2-pyridyl)guanine "2PyG" as compared to 2-aminopurine in DNA. *Chembiochem* **2011,** *12* (13), 2044-51.

57.   Steinmetzger, C.; Bäuerlein, C.; Höbartner, C., Supramolecular Fluorescence Resonance Energy Transfer in Nucleobase-Modified Fluorogenic RNA Aptamers. *Angew Chem Int Ed Engl* **2020,** *59* (17), 6760-4.

58.   Barnwal, R. P.; Yang, F.; Varani, G., Applications of NMR to structure determination of RNAs large and small. *Arch Biochem Biophys* **2017,** *628*, 42-56.

59.   Cromsigt, J.; Schleucher, J.; Gustafsson, T.; Kihlberg, J.; Wijmenga, S., Preparation of partially 2H/13C-labelled RNA for NMR studies. Stereo-specific deuteration of the H5" in nucleotides. *Nucleic Acids Res* **2002,** *30* (7), 1639-45.

60.   Dayie, T. K.; Thakur, C. S., Site-specific labeling of nucleotides for making RNA for high resolution NMR studies using an E. coli strain disabled in the oxidative pentose phosphate pathway. *J Biomol NMR* **2010,** *47* (1), 19-31.

61.   Longhini, A. P.; LeBlanc, R. M.; Becette, O.; Salguero, C.; Wunderlich, C. H.; Johnson, B. A.; D'Souza, V. M.; Kreutz, C.; Dayie, T. K., Chemo-enzymatic synthesis of site-specific isotopically labeled nucleotides for use in NMR resonance assignment, dynamics and structural characterizations. *Nucleic Acids Res* **2016,** *44* (6), e52.

62.   Keane, S. C.; Heng, X.; Lu, K.; Kharytonchyk, S.; Ramakrishnan, V.; Carter, G.; Barton, S.; Hosic, A.; Florwick, A.; Santos, J.; Bolden, N. C.; McCowin, S.; Case, D. A.; Johnson, B. A.; Salemi, M.; Telesnitsky, A.; Summers, M. F., RNA structure. Structure of the HIV-1 RNA packaging signal. *Science* **2015,** *348* (6237), 917-21.

63.	Guo, F.; Li, Q.; Zhou, C., Synthesis and biological applications of fluoro-modified nucleic acids. *Org Biomol Chem* **2017,** *15* (45), 9552-65.

64.	Himmelstoß, M.; Erharter, K.; Renard, E.; Ennifar, E.; Kreutz, C.; Micura, R., 2'-O-Trifluoromethylated RNA – a powerful modification for RNA chemistry and NMR spectroscopy. *Chemical Science* **2020,** *11*, 11322-30.

65.	Viskova, P.; Krafcik, D.; Trantirek, L.; Foldynova-Trantirkova, S., In-Cell NMR Spectroscopy of Nucleic Acids in Human Cells. *Curr Protoc Nucleic Acid Chem* **2019,** *76* (1), e71.

66.	Hänsel, R.; Foldynova-Trantirkova, S.; Löhr, F.; Buck, J.; Bongartz, E.; Bamberg, E.; Schwalbe, H.; Dötsch, V.; Trantirek, L., Evaluation of parameters critical for observing nucleic acids inside living Xenopus laevis oocytes by in-cell NMR spectroscopy. *J Am Chem Soc* **2009,** *131* (43), 15761-8.

67.	Yamaoki, Y.; Kiyoishi, A.; Miyake, M.; Kano, F.; Murata, M.; Nagata, T.; Katahira, M., The first successful observation of in-cell NMR signals of DNA and RNA in living human cells. *Phys Chem Chem Phys* **2018,** *20* (5), 2982-5.

68.	Bao, H. L.; Liu, H. S.; Xu, Y., Hybrid-type and two-tetrad antiparallel telomere DNA G-quadruplex structures in living human cells. *Nucleic Acids Res* **2019,** *47* (10), 4940-7.

69.	Krafcikova, M.; Dzatko, S.; Caron, C.; Granzhan, A.; Fiala, R.; Loja, T.; Teulade-Fichou, M. P.; Fessl, T.; Hansel-Hertsch, R.; Mergny, J. L.; Foldynova-Trantirkova, S.; Trantirek, L., Monitoring DNA-Ligand Interactions in Living Human Cells Using NMR Spectroscopy. *J Am Chem Soc* **2019,** *141* (34), 13281-5.

70.	Dzatko, S.; Krafcikova, M.; Hänsel-Hertsch, R.; Fessl, T.; Fiala, R.; Loja, T.; Krafcik, D.; Mergny, J. L.; Foldynova-Trantirkova, S.; Trantirek, L., Evaluation of the Stability of DNA i-Motifs in the Nuclei of Living Mammalian Cells. *Angew Chem Int Ed Engl* **2018,** *57* (8), 2165-9.

71.	Yang, Y.; Wang, S., RNA Characterization by Solid-State NMR Spectroscopy. *Chemistry* **2018,** *24* (35), 8698-707.

72.	Dračínský, M.; Hodgkinson, P., Solid-state NMR studies of nucleic acid components. *RSC Advances* **2015,** *5*, 12300-10.

73.	Schlagnitweit, J.; Friebe Sandoz, S.; Jaworski, A.; Guzzetti, I.; Aussenac, F.; Carbajo, R. J.; Chiarparin, E.; Pell, A. J.; Petzold, K., Observing an Antisense Drug Complex in Intact Human Cells by in-Cell NMR Spectroscopy. *Chembiochem* **2019,** *20* (19), 2474-8.

74.	Yang, Y.; Xiang, S.; Liu, X.; Pei, X.; Wu, P.; Gong, Q.; Li, N.; Baldus, M.; Wang, S., Proton-detected solid-state NMR detects the inter-nucleotide correlations and architecture of dimeric RNA in microcrystals. *Chem Commun (Camb)* **2017,** *53* (96), 12886-9.

75.	Wiegand, T.; Schledorn, M.; Malar, A. A.; Cadalbert, R.; Dapp, A.; Terradot, L.; Meier, B. H.; Bockmann, A., Nucleotide Binding Modes in a Motor Protein Revealed by (31) P- and (1) H-Detected MAS Solid-State NMR Spectroscopy. *Chembiochem* **2020,** *21* (3), 324-30.

76.	Roessler, M. M.; Salvadori, E., Principles and applications of EPR spectroscopy in the chemical sciences. *Chem Soc Rev* **2018,** *47* (8), 2534-53.

77.	Goldfarb, D., Gd3+ spin labeling for distance measurements by pulse EPR spectroscopy. *Phys Chem Chem Phys* **2014,** *16* (21), 9685-99.

78.	Martorana, A.; Bellapadrona, G.; Feintuch, A.; Di Gregorio, E.; Aime, S.; Goldfarb, D., Probing protein conformation in cells by EPR distance measurements using Gd3+ spin labeling. *J Am Chem Soc* **2014,** *136* (38), 13458-65.

79.	Qi, M.; Gross, A.; Jeschke, G.; Godt, A.; Drescher, M., Gd(III)-PyMTA label is suitable for in-cell EPR. *J Am Chem Soc* **2014,** *136* (43), 15366-78.

80.	Yang, Y.; Yang, F.; Gong, Y. J.; Bahrenberg, T.; Feintuch, A.; Su, X. C.; Goldfarb, D., High Sensitivity In-Cell EPR Distance Measurements on Proteins using an Optimized Gd(III) Spin Label. *J Phys Chem Lett* **2018,** *9* (20), 6119-23.

81.	Yang, Y.; Yang, F.; Li, X. Y.; Su, X. C.; Goldfarb, D., In-Cell EPR Distance Measurements on Ubiquitin Labeled with a Rigid PyMTA-Gd(III) Tag. *J Phys Chem B* **2019,** *123* (5), 1050-9.

82.	Shah, A.; Roux, A.; Starck, M.; Mosely, J. A.; Stevens, M.; Norman, D. G.; Hunter, R. I.; El Mkami, H.; Smith, G. M.; Parker, D.; Lovett, J. E., A Gadolinium Spin Label with Both a Narrow

Central Transition and Short Tether for Use in Double Electron Electron Resonance Distance Measurements. *Inorg Chem* **2019,** *58* (5), 3015-25.

83.   Song, Y.; Meade, T. J.; Astashkin, A. V.; Klein, E. L.; Enemark, J. H.; Raitsimring, A., Pulsed dipolar spectroscopy distance measurements in biomacromolecules labeled with Gd(III) markers. *J Magn Reson* **2011,** *210* (1), 59-68.

84.   Fielding, A. J.; Carl, P. J.; Eaton, G. R.; Eaton, S. S., Multifrequency EPR of Four Triarylmethyl Radicals. *Applied Magnetic Resonance* **2005,** *28*, 231-8.

85.   Owenius, R.; Eaton, G. R.; Eaton, S. S., Frequency (250 MHz to 9.2 GHz) and viscosity dependence of electron spin relaxation of triarylmethyl radicals at room temperature. *J Magn Reson* **2005,** *172* (1), 168-75.

86.   Ardenkjaer-Larsen, J. H.; Laursen, I.; Leunbach, I.; Ehnholm, G.; Wistrand, L. G.; Petersson, J. S.; Golman, K., EPR and DNP properties of certain novel single electron contrast agents intended for oximetric imaging. *J Magn Reson* **1998,** *133* (1), 1-12.

87.   Baber, J. L.; Louis, J. M.; Clore, G. M., Dependence of distance distributions derived from double electron-electron resonance pulsed EPR spectroscopy on pulse-sequence time. *Angew Chem Int Ed Engl* **2015,** *54* (18), 5336-9.

88.   Shevelev, G. Y.; Krumkacheva, O. A.; Lomzov, A. A.; Kuzhelev, A. A.; Rogozhnikova, O. Y.; Trukhin, D. V.; Troitskaya, T. I.; Tormyshev, V. M.; Fedin, M. V.; Pyshnyi, D. V.; Bagryanskaya, E. G., Physiological-temperature distance measurement in nucleic acid using triarylmethyl-based spin labels and pulsed dipolar EPR spectroscopy. *J Am Chem Soc* **2014,** *136* (28), 9874-7.

89.   Shevelev, G. Y.; Gulyak, E. L.; Lomzov, A. A.; Kuzhelev, A. A.; Krumkacheva, O. A.; Kupryushkin, M. S.; Tormyshev, V. M.; Fedin, M. V.; Bagryanskaya, E. G.; Pyshnyi, D. V., A Versatile Approach to Attachment of Triarylmethyl Labels to DNA for Nanoscale Structural EPR Studies at Physiological Temperatures. *J Phys Chem B* **2018,** *122* (1), 137-43.

90.   Hintz, H.; Vanas, A.; Klose, D.; Jeschke, G.; Godt, A., Trityl Radicals with a Combination of the Orthogonal Functional Groups Ethyne and Carboxyl: Synthesis without a Statistical Step and EPR Characterization. *J Org Chem* **2019,** *84* (6), 3304-20.

91.   Nilsen, A.; Braslau, R., Nitroxide Decomposition: Implications toward Nitroxide Design for Applications in Living Free-Radical Polymerization. *Journal of Polymer Science: Part A: Polymer Chemistry* **2006,** *44*, 697-717.

92.   Bowman, D. F.; Gillan, T.; Ingold, K. U., Kinetic Applications of Electron Paramagnetic Resonance Spectroscopy. III. Self-Reactions of Dialkyl Nitroxide Radicals. *Journal of the American Chemical Society* **1971,** *93* (24), 6555-561.

93.   Bobko, A. A.; Kirilyuk, I. A.; Grigor'ev, I. A.; Zweier, J. L.; Khramtsov, V. V., Reversible reduction of nitroxides to hydroxylamines: roles for ascorbate and glutathione. *Free Radic Biol Med* **2007,** *42* (3), 404-12.

94.   Paletta, J. T.; Pink, M.; Foley, B.; Rajca, S.; Rajca, A., Synthesis and reduction kinetics of sterically shielded pyrrolidine nitroxides. *Org Lett* **2012,** *14* (20), 5322-5.

95.   Sato, H.; Kathirvelu, V.; Fielding, A.; Blinco, J. P.; Micallef, A. S.; Bottle, S. E.; Eaton, S. S.; Eaton, G. R., Impact of molecular size on electron spin relaxation rates of nitroxyl radicals in glassy solvents between 100 and 300 K. *Molecular Physics* **2007,** *105*, 2137-51.

96.   Nakagawa, K.; Candelaria, M. B.; Chik, W. W. C.; Eaton, S. S.; Eaton, G. R., Electron-Spin Relaxation Times of Chromium(V). *Journal of Magnetic Resonance* **1992,** *98*, 81-91.

97.   Meyer, V.; Swanson, M. A.; Clouston, L. J.; Boratynski, P. J.; Stein, R. A.; McHaourab, H. S.; Rajca, A.; Eaton, S. S.; Eaton, G. R., Room-temperature distance measurements of immobilized spin-labeled protein by DEER/PELDOR. *Biophys J* **2015,** *108* (5), 1213-9.

98.   Huang, S.; Paletta, J. T.; Elajaili, H.; Huber, K.; Pink, M.; Rajca, S.; Eaton, G. R.; Eaton, S. S.; Rajca, A., Synthesis and Electron Spin Relaxation of Tetracarboxylate Pyrroline Nitroxides. *J Org Chem* **2017,** *82* (3), 1538-44.

99.   Qin, P. Z.; Butcher, S. E.; Feigon, J.; Hubbell, W. L., Quantitative analysis of the isolated GAAA tetraloop/receptor interaction in solution: a site-directed spin labeling study. *Biochemistry* **2001,** *40* (23), 6929-36.

100.   Nguyen, P. H.; Popova, A. M.; Hideg, K.; Qin, P. Z., A nucleotide-independent cyclic nitroxide label for monitoring segmental motions in nucleic acids. *BMC Biophys* **2015,** *8*, 6-14.

101.   Hara, H.; Horiuchi, T., 4-Thiouridin-Specific Spin-Labeling of E. coli Transfer RNA. *Biochemical and Biophysical Research Communications* **1970,** *38* (2), 305-11.

102.   Kim, N. K.; Murali, A.; DeRose, V. J., A distance ruler for RNA using EPR and site-directed spin labeling. *Chem Biol* **2004,** *11* (7), 939-48.

103.   Edwards, T. E.; Okonogi, T. M.; Robinson, B. H.; Sigurdsson, S. T., Site-specific incorporation of nitroxide spin-labels into internal sites of the TAR RNA; structure-dependent dynamics of RNA by EPR spectroscopy. *J Am Chem Soc* **2001,** *123* (7), 1527-8.

104.   Saha, S.; Jagtap, A. P.; Sigurdsson, S. T., Site-directed spin labeling of 2'-amino groups in RNA with isoindoline nitroxides that are resistant to reduction. *Chem Commun (Camb)* **2015,** *51* (66), 13142-5.

105.   Kuznetsov, N. A.; Milov, A. D.; Koval, V. V.; Samoilova, R. I.; Grishin, Y. A.; Knorre, D. G.; Tsvetkov, Y. D.; Fedorova, O. S.; Dzuba, S. A., PELDOR study of conformations of double-spin-labeled single- and double-stranded DNA with non-nucleotide inserts. *Phys Chem Chem Phys* **2009,** *11* (31), 6826-32.

106.   Sicoli, G.; Wachowius, F.; Bennati, M.; Höbartner, C., Probing secondary structures of spin-labeled RNA by pulsed EPR spectroscopy. *Angew Chem Int Ed Engl* **2010,** *49* (36), 6443-7.

107.   Flaender, M.; Sicoli, G.; Fontecave, T.; Mathis, G.; Saint-Pierre, C.; Boulard, Y.; Gambarelli, S.; Gasparutto, D., Site-specific insertion of nitroxide-spin labels into DNA probes by click chemistry for structural analyses by ELDOR spectroscopy. *Nucleic Acids Symp Ser (Oxf)* **2008,** (52), 147-8.

108.   Ding, P.; Wunnicke, D.; Steinhoff, H. J.; Seela, F., Site-directed spin-labeling of DNA by the azide-alkyne 'click' reaction: nanometer distance measurements on 7-deaza-2'-deoxyadenosine and 2'-deoxyuridine nitroxide conjugates spatially separated or linked to a 'dA-dT' base pair. *Chemistry* **2010,** *16* (48), 14385-96.

109.   Wuebben, C.; Blume, S.; Abdullin, D.; Brajtenbach, D.; Haege, F.; Kath-Schorr, S.; Schiemann, O., Site-Directed Spin Labeling of RNA with a Gem-Diethylisoindoline Spin Label: PELDOR, Relaxation, and Reduction Stability. *Molecules* **2019,** *24* (24).

110.   Schiemann, O.; Piton, N.; Mu, Y.; Stock, G.; Engels, J. W.; Prisner, T. F., A PELDOR-based nanometer distance ruler for oligonucleotides. *J Am Chem Soc* **2004,** *126* (18), 5722-9.

111.   Gophane, D. B.; Sigurdsson, S. T., Hydrogen-bonding controlled rigidity of an isoindoline-derived nitroxide spin label for nucleic acids. *Chem Commun (Camb)* **2013,** *49* (10), 999-1001.

112.   Gophane, D. B.; Endeward, B.; Prisner, T. F.; Sigurdsson, S. T., A semi-rigid isoindoline-derived nitroxide spin label for RNA. *Org Biomol Chem* **2018,** *16* (5), 816-24.

113.   Gophane, D. B.; Endeward, B.; Prisner, T. F.; Sigurdsson, S. T., Conformationally restricted isoindoline-derived spin labels in duplex DNA: distances and rotational flexibility by pulsed electron-electron double resonance spectroscopy. *Chemistry* **2014,** *20* (48), 15913-9.

114.   Miller, T. R.; Hopkins, P. B., Toward the Synthesis of a Second-Generation Nitroxide Spin Probe for DNA Dynamics Studies. *Bioorganic & Medicinal Chemistry Letters* **1994,** *4* (8), 981-6.

115.   Barhate, N.; Cekan, P.; Massey, A. P.; Sigurdsson, S. T., A nucleoside that contains a rigid nitroxide spin label: a fluorophore in disguise. *Angew Chem Int Ed Engl* **2007,** *46* (15), 2655-8.

116.   Cekan, P.; Smith, A. L.; Barhate, N.; Robinson, B. H.; Sigurdsson, S. T., Rigid spin-labeled nucleoside C: a nonperturbing EPR probe of nucleic acid conformation. *Nucleic Acids Res* **2008,** *36* (18), 5946-54.

117.   Höbartner, C.; Sicoli, G.; Wachowius, F.; Gophane, D. B.; Sigurdsson, S. T., Synthesis and characterization of RNA containing a rigid and nonperturbing cytidine-derived spin label. *J Org Chem* **2012,** *77* (17), 7749-54.

118.   Juliusson, H. Y.; Sigurdsson, S. T., Reduction Resistant and Rigid Nitroxide Spin-Labels for DNA and RNA. *J Org Chem* **2020,** *85* (6), 4036-46.

119.   Bartels, A. Rigid Spin Labels for Purine Nucleosides in RNA and DNA. Georg-August-Universität Göttingen, Sierke Verlag, 2016.

120.   Caruthers, M. H., Gene synthesis machines: DNA chemistry and its uses. *Science* **1985,** *230* (4723), 281-5.

121.   Caruthers, M. H., Chemical Synthesis of DNA and DNA Analogues. *Accounts of Chemical Research* **1991,** *24*, 278-84.

122.   Huynh, V.; McCollum, C.; Jacobson, K.; Theisen, P.; Vinayak, R.; Spiess, E.; Andrus, A., Fast Oligonucleotide Deprotection Phosphoramidite Chemistry for DNA Synthesis. *Tetrahedron Letters* **1990,** *31* (50), 7269-72.

123.   Usman, N.; Ogilvie, K. K.; Jiang, M.-J.; Cedergren, R. J., Automated Chemical Synthesis of Long Oligoribonucleotides Using 2'-O-Silylated Ribonucleoside 3'-O-Phosphoramidites on a Controlled-Pore Glass Support: Synthesis of a 43-Nucleotide Sequence Similar to the 3'-Half Molecule of an Escherichia coli Formylmethionine tRNA. *Journal of the American Chemical Society* **1987,** *109* (25), 7845-54.

124.   Pitsch, S.; Weiss, P. A.; Jenny, L.; Stutz, A.; Wua, X., Reliable Chemical Synthesis of Oligoribonucleotides (RNA) with 2'-O-[(Triisopropylsilyl)oxy]methyl(2'-O-tom)-Protected Phosphoramidites. *Helvetica Chimica Acta* **2001,** *84*, 3773-95.

125.   Beaucage, S. L.; Caruthers, M. H., Synthetic strategies and parameters involved in the synthesis of oligodeoxyribonucleotides according to the phosphoramidite method. *Curr Protoc Nucleic Acid Chem* **2001,** *Chapter 3*, Unit 3 3.

126.   Seven, I.; Weinrich, T.; Gränz, M.; Grünewald, C.; Brüß, S.; Krstić, I.; Prisner, T. F.; Heckel, A.; Göbel, M. W., Photolabile Protecting Groups for Nitroxide Spin Labels. *European Journal of Organic Chemistry* **2014**, 4037-43.

127.   Weinrich, T.; Gränz, M.; Grünewald, C.; Prisner, T. F.; Göbel, M. W., Synthesis of a Cytidine Phosphoramidite with Protected Nitroxide Spin Label for EPR Experiments with RNA. *European Journal of Organic Chemistry* **2017**, 491-6.

128.   Weinrich, T.; Jaumann, E. A.; Scheffer, U. M.; Prisner, T. F.; Göbel, M. W., Phosphoramidite building blocks with protected nitroxides for the synthesis of spin-labeled DNA and RNA. *Beilstein J Org Chem* **2018,** *14*, 1563-9.

129.   Juliusson, H. Y.; Segler, A.-L. J.; Sigurdsson, S. T., Benzoyl-Protected Hydroxylamines for Improved Chemical Synthesis of Oligonucleotides Containing Nitroxide Spin Labels. *European Journal of Organic Chemistry* **2019**, 3799-805.

130.   Büttner, L.; Seikowski, J.; Wawrzyniak, K.; Ochmann, A.; Höbartner, C., Synthesis of spin-labeled riboswitch RNAs using convertible nucleosides and DNA-catalyzed RNA ligation. *Bioorg Med Chem* **2013,** *21* (20), 6171-80.

131.   Kerzhner, M.; Matsuoka, H.; Wuebben, C.; Famulok, M.; Schiemann, O., High-Yield Spin Labeling of Long RNAs for Electron Paramagnetic Resonance Spectroscopy. *Biochemistry* **2018,** *57* (20), 2923-31.

132.   Obeid, S.; Yulikov, M.; Jeschke, G.; Marx, A., Enzymatic synthesis of multiple spin-labeled DNA. *Angew Chem Int Ed Engl* **2008,** *47* (36), 6782-5.

133.   Obeid, S.; Yulikov, M.; Jeschke, G.; Marx, A., Enzymatic synthesis of multi spin-labeled DNA. *Nucleic Acids Symp Ser (Oxf)* **2008,** (52), 373-4.

134.   Domnick, C.; Hagelueken, G.; Eggert, F.; Schiemann, O.; Kath-Schorr, S., Posttranscriptional spin labeling of RNA by tetrazine-based cycloaddition. *Org Biomol Chem* **2019,** *17* (7), 1805-8.

135.   Domnick, C.; Eggert, F.; Wuebben, C.; Bornewasser, L.; Hagelueken, G.; Schiemann, O.; Kath-Schorr, S., EPR Distance Measurements on Long Non-coding RNAs Empowered by Genetic Alphabet Expansion Transcription. *Angew Chem Int Ed Engl* **2020,** *59* (20), 7891-6.

136.   Thomas, F.; Michon, J.; Lhomme, J., Interaction of a spin-labeled adenine-acridine conjugate with a DNA duplex containing an abasic site model. *Biochemistry* **1999,** *38* (6), 1930-7.

137.   Belmont, P.; Chapelle, C.; Demeunynck, M.; Michon, J.; Michon, P.; Lhomme, J., Introduction of a nitroxide group on position 2 of 9-phenoxyacridine: easy access to spin labelled DNA-binding conjugates. *Bioorg Med Chem Lett* **1998,** *8* (6), 669-74.

138.   Kamble, N. R.; Gränz, M.; Prisner, T. F.; Sigurdsson, S. T., Noncovalent and site-directed spin labeling of duplex RNA. *Chem Commun (Camb)* **2016,** *52* (100), 14442-5.

139. Kamble, N. R.; Sigurdsson, S. T., Purine-Derived Nitroxides for Noncovalent Spin-Labeling of Abasic Sites in Duplex Nucleic Acids. *Chemistry* **2018,** *24* (16), 4157-64.

140. Heinz, M.; Erlenbach, N.; Stelzl, L. S.; Thierolf, G.; Kamble, N. R.; Sigurdsson, S. T.; Prisner, T. F.; Hummer, G., High-resolution EPR distance measurements on RNA and DNA with the non-covalent G spin label. *Nucleic Acids Res* **2020,** *48* (2), 924-33.

141. Shelke, S. A.; Sigurdsson, S. T., Effect of N3 modifications on the affinity of spin label ç for abasic sites in duplex DNA. *Chembiochem* **2012,** *13* (5), 684-90.

142. Shelke, S. A.; Sigurdsson, S. T., Structural changes of an abasic site in duplex DNA affect noncovalent binding of the spin label ç. *Nucleic Acids Res* **2012,** *40* (8), 3732-40.

143. Shelke, S. A.; Sigurdsson, S. T., Noncovalent and site-directed spin labeling of nucleic acids. *Angew Chem Int Ed Engl* **2010,** *49* (43), 7984-6.

144. Juliusson, H. Y.; Sigurdsson, S. T., Nitroxide-Derived N-Oxide Phenazines for Noncovalent Spin-Labeling of DNA. *Chembiochem* **2020,** *21* (18), 2635-42.

145. Saha, S.; Hetzke, T.; Prisner, T. F.; Sigurdsson, S. T., Noncovalent spin-labeling of RNA: the aptamer approach. *Chem Commun (Camb)* **2018,** *54* (83), 11749-52.

146. Gannett, P. M.; Darian, E.; Powell, J.; Johnson, E. M., 2nd; Mundoma, C.; Greenbaum, N. L.; Ramsey, C. M.; Dalal, N. S.; Budil, D. E., Probing triplex formation by EPR spectroscopy using a newly synthesized spin label for oligonucleotides. *Nucleic Acids Res* **2002,** *30* (23), 5328-37.

147. Schiemann, O., Mapping global folds of oligonucleotides by pulsed electron-electron double resonance. *Methods Enzymol* **2009,** *469*, 329-51.

148. Fedorova, O. S.; Tsvetkov, Y. D., Pulsed electron double resonance in structural studies of spin-labeled nucleic acids. *Acta Naturae* **2013,** *5* (1), 9-32.

149. Halbmair, K.; Seikowski, J.; Tkach, I.; Höbartner, C.; Sezer, D.; Bennati, M., High-resolution measurement of long-range distances in RNA: pulse EPR spectroscopy with TEMPO-labeled nucleotides. *Chem Sci* **2016,** *7* (5), 3172-80.

150. Schiemann, O.; Cekan, P.; Margraf, D.; Prisner, T. F.; Sigurdsson, S. T., Relative orientation of rigid nitroxides by PELDOR: beyond distance measurements in nucleic acids. *Angew Chem Int Ed Engl* **2009,** *48* (18), 3292-5.

151. Martin, R. E.; Pannier, M.; Diederich, F.; Gramlich, V.; Hubrich, M.; Spiess, H. W., Determination of End-to-End Distances in a Series of TEMPO Diradicals of up to 2.8 nm Length with a New Four-Pulse Double Electron Electron Resonance Experiment. *Angew Chem Int Ed Engl* **1998,** *37* (20), 2833-7.

152. Pannier, M.; Veit, S.; Godt, A.; Jeschke, G.; Spiess, H. W., Dead-time free measurement of dipole-dipole interactions between electron spins. 2000. *J Magn Reson* **2011,** *213* (2), 316-25.

153. Jeschke, G.; Chechik, V.; Ionita, P.; Godt, A.; Zimmermann, H.; Banham, J.; Timmel, C. R.; Hilger, D.; Jung, H., DeerAnalysis2006 - a Comprehensive Software Package for Analyzing Pulsed ELDOR Data. *Applied Magnetic Resonance* **2006,** *30*, 473-98.

154. Spindler, P. E.; Waclawska, I.; Endeward, B.; Plackmeyer, J.; Ziegler, C.; Prisner, T. F., Carr-Purcell Pulsed Electron Double Resonance with Shaped Inversion Pulses. *J Phys Chem Lett* **2015,** *6* (21), 4331-5.

155. Stelzl, L. S.; Erlenbach, N.; Heinz, M.; Prisner, T. F.; Hummer, G., Resolving the Conformational Dynamics of DNA with Angstrom Resolution by Pulsed Electron-Electron Double Resonance and Molecular Dynamics. *J Am Chem Soc* **2017,** *139* (34), 11674-77.

156. Gränz, M.; Erlenbach, N.; Spindler, P.; Gophane, D. B.; Stelzl, L. S.; Sigurdsson, S. T.; Prisner, T. F., Dynamics of Nucleic Acids at Room Temperature Revealed by Pulsed EPR Spectroscopy. *Angew Chem Int Ed Engl* **2018,** *57* (33), 10540-3.

157. Collauto, A.; von Bülow, S.; Gophane, D. B.; Saha, S.; Stelzl, L. S.; Hummer, G.; Sigurdsson, S. T.; Prisner, T. F., Compaction of RNA Duplexes in the Cell*. *Angew Chem Int Ed Engl* **2020,** *59* (51), 23025-29.

158. Gmeiner, C.; Dorn, G.; Allain, F. H. T.; Jeschke, G.; Yulikov, M., Spin labelling for integrative structure modelling: a case study of the polypyrimidine-tract binding protein 1 domains in complexes with short RNAs. *Phys Chem Chem Phys* **2017,** *19* (41), 28360-80.

159.   Wu, Z.; Feintuch, A.; Collauto, A.; Adams, L. A.; Aurelio, L.; Graham, B.; Otting, G.; Goldfarb, D., Selective Distance Measurements Using Triple Spin Labeling with Gd(3+), Mn(2+), and a Nitroxide. *J Phys Chem Lett* **2017,** *8* (21), 5277-82.

160.   Krumkacheva, O. A.; Shevelev, G. Y.; Lomzov, A. A.; Dyrkheeva, N. S.; Kuzhelev, A. A.; Koval, V. V.; Tormyshev, V. M.; Polienko, Y. F.; Fedin, M. V.; Pyshnyi, D. V.; Lavrik, O. I.; Bagryanskaya, E. G., DNA complexes with human apurinic/apyrimidinic endonuclease 1: structural insights revealed by pulsed dipolar EPR with orthogonal spin labeling. *Nucleic Acids Res* **2019,** *47* (15), 7767-80.

161.   Malygin, A. A.; Krumkacheva, O. A.; Graifer, D. M.; Timofeev, I. O.; Ochkasova, A. S.; Meschaninova, M. I.; Venyaminova, A. G.; Fedin, M. V.; Bowman, M.; Karpova, G. G.; Bagryanskaya, E. G., Exploring the interactions of short RNAs with the human 40S ribosomal subunit near the mRNA entry site by EPR spectroscopy. *Nucleic Acids Res* **2019,** *47* (22), 11850-60.

162.   Wuebben, C.; Vicino, M. F.; Mueller, M.; Schiemann, O., Do the P1 and P2 hairpins of the Guanidine-II riboswitch interact? *Nucleic Acids Res* **2020,** *48* (18), 10518-26.

163.   Aloisi, C. M. N.; Sturla, S. J.; Gahlon, H. L., A gene-targeted polymerase-mediated strategy to identify O(6)-methylguanine damage. *Chem Commun (Camb)* **2019,** *55* (27), 3895-8.

164.   Loakes, D., Survey and summary: The applications of universal DNA base analogues. *Nucleic Acids Res* **2001,** *29* (12), 2437-47.

165.   Johnson, J.; Okyere, R.; Joseph, A.; Musier-Forsyth, K.; Kankia, B., Quadruplex formation as a molecular switch to turn on intrinsically fluorescent nucleotide analogs. *Nucleic Acids Res* **2013,** *41* (1), 220-8.

166.   Gahlon, H. L.; Sturla, S. J., Hydrogen bonding or stacking interactions in differentiating duplex stability in oligonucleotides containing synthetic nucleoside probes for alkylated DNA. *Chemistry* **2013,** *19* (33), 11062-7.

167.   de Oliveira, K. N.; Costa, P.; Santin, J. R.; Mazzambani, L.; Bürger, C.; Mora, C.; Nunes, R. J.; de Souza, M. M., Synthesis and antidepressant-like activity evaluation of sulphonamides and sulphonyl-hydrazones. *Bioorg Med Chem* **2011,** *19* (14), 4295-306.

168.   Haugland, M. M.; El-Sagheer, A. H.; Porter, R. J.; Pena, J.; Brown, T.; Anderson, E. A.; Lovett, J. E., 2'-Alkynylnucleotides: A Sequence- and Spin Label-Flexible Strategy for EPR Spectroscopy in DNA. *J Am Chem Soc* **2016,** *138* (29), 9069-72.

169.   Grzegozek, M., Vicarious Nucleophilic Amination of Nitroquinolines by 1,1,1-Trimethylhydrazinium Iodide. *Journal of Heterocyclic Chemistry* **2008,** *45*, 1879-82.

170.   Englund, E. A.; Gopi, H. N.; Appella, D. H., An efficient synthesis of a probe for protein function: 2,3-diaminopropionic acid with orthogonal protecting groups. *Org Lett* **2004,** *6* (2), 213-5.

171.   Jayavardena, V. C.; Fairfull-Smith, K. E.; Bottle, S. E., Improving the Yield of the Exhaustive Grignard Alkylation of N-Benzylphthalimide. *Aust. J. Chem.* **2013,** *66* (6), 619-25.

172.   de Gonzalo, G.; Smit, C.; Jin, J.; Minnaard, A. J.; Fraaije, M. W., Turning a riboflavin-binding protein into a self-sufficient monooxygenase by cofactor redesign. *Chem Commun (Camb)* **2011,** *47* (39), 11050-2.

173.   Vorbrüggen, H.; Höfle, G., On the Mechanism of Nucleoside Synthesis. *Chem. Ber.* **1981,** *114*, 1256-68.

174.   Ritzmann, G.; Harzer, K.; Pleiderer, W., Synthese von Lumazin- und Isopterin-N-1-β-D-ribofuranosiden und -(2-desoxyribofuranosiden) - Strukturanaloga des Uridins, Cytidins und Thymidins. *Angewandte Chemie* **1971,** *83* (23), 975-7.

175.   Hakimelahi, G. H.; Proba, Z. A.; Ogilvie, K. K., Nitrate Ion as Catalyst for Selective Silylations of Nucleosides. *Tetrahedron Letters* **1981,** *22* (48), 4775-8.

176.   Sikorska, E.; Khmelinskii, I. V.; Worrall, D. R.; Koput, J.; Sikorski, M., Spectroscopy and photophysics of iso- and alloxazines: experimental and theoretical study. *J Fluoresc* **2004,** *14* (1), 57-64.

177.   Rayala, R.; Wnuk, S. F., Bromination at C-5 of Pyrimidine and C-8 of Purine Nucleosides with 1,3-Dibromo-5,5-dimethylhydantoin. *Tetrahedron Lett* **2012,** *53* (26), 3333-6.

178. Nawale, G. N.; Gore, K. R.; Höbartner, C.; Pradeepkumar, P. I., Incorporation of 4'-C-aminomethyl-2'-O-methylthymidine into DNA by thermophilic DNA polymerases. *Chem. Commun.* **2012,** *48*, 9619-21.

179. El-Sagheer, A. H.; Kumar, R.; Findlow, S.; Werner, J. M.; Lane, A. N.; Brown, T., A very stable cyclic DNA miniduplex with just two base pairs. *Chembiochem* **2008,** *9* (1), 50-2.

180. Dallmann, A.; Beribisky, A. V.; Gnerlich, F.; Rübbelke, M.; Schiesser, S.; Carell, T.; Sattler, M., Site-Specific Isotope-Labeling of Inosine Phosphoramidites and NMR Analysis of an Inosine-Containing RNA Duplex. *Chemistry* **2016,** *22* (43), 15350-9.

181. Blaisdell, T. P.; Lee, S.; Kasaplar, P.; Sun, X.; Tan, K. L., Practical silyl protection of ribonucleosides. *Org Lett* **2013,** *15* (18), 4710-3.

182. Cheong, V. V.; Heddi, B.; Lech, C. J.; Phan, A. T., Xanthine and 8-oxoguanine in G-quadruplexes: formation of a G.G.X.O tetrad. *Nucleic Acids Res* **2015,** *43* (21), 10506-14.

183. Scheitl, C. P. M.; Ghaem Maghami, M.; Lenz, A. K.; Höbartner, C., Site-specific RNA methylation by a methyltransferase ribozyme. *Nature* **2020,** *587* (7835), 663-7.

184. Parsch, J.; Engels, J. W., C-F...H-C hydrogen bonds in ribonucleic acids. *J Am Chem Soc* **2002,** *124* (20), 5664-72.

185. Horn, T.; Urdea, M. S., A Chemical 5'-Phosphorylation of Oligodeoxyribonucleotides that can be Monitored by Trityl Cation Release. *Tetrahedron Letters* **1986,** *27* (39), 4705-8.

186. Stoll, S.; Schweiger, A., EasySpin, a comprehensive software package for spectral simulation and analysis in EPR. *J Magn Reson* **2006,** *178* (1), 42-55.

187. Shi, L.; Zhang, G.; Pan, F., Fe2(SO4)3·xH2O-catalyzed per-O-acetylation of sugars compatible with acid-labile protecting groups adopted in carbohydrate chemistry. *Tetrahedron* **2008,** *64*, 2572-5.

188. Fu, Y.; Dai, Q.; Zhang, W.; Ren, J.; Pan, T.; He, C., The AlkB domain of mammalian ABH8 catalyzes hydroxylation of 5-methoxycarbonylmethyluridine at the wobble position of tRNA. *Angew Chem Int Ed Engl* **2010,** *49* (47), 8885-8.

189. Kumar, V.; Malhotra, S. V., Synthesis of nucleoside-based antiviral drugs in ionic liquids. *Bioorg Med Chem Lett* **2008,** *18* (20), 5640-2.

190. Asakura, J.; Robins, M. J., Cerium(IV)-Mediated Halogenation at C-5 of Uracil Derivatives. *J. Org. Chem.* **1990,** *55* (16), 4928-33.